

1N-44  
84783  
P. 222

NASA Contractor Report 189045

(NASA-CR-189045) ANALYSIS, DESIGN, AND  
EXPERIMENTAL RESULTS FOR LIGHTWEIGHT SPACE  
HEAT RECEIVER CANISTERS, PHASE I Interim  
Report, Jul. 1989 - Jul. 1991 (Sundstrand  
Corp.) 222 p

N92-22964

Unclas  
0084783

CSSL 10B G3/44

# Analysis, Design, and Experimental Results for Lightweight Space Heat Receiver Canisters

## Phase I Interim Report

Michael G. Schneider, Mark A. Brege, and Gary R. Heidenreich  
*Sundstrand Corporation*  
*Rockford, Illinois*

July 30, 1991

Prepared for  
Lewis Research Center  
Under Contract NAS3-25554



National Aeronautics and  
Space Administration

**Lewis Research Center**  
Cleveland, Ohio 44135  
AC 216 433-4000

## Table of Contents

	<u>Page Number</u>	
1.0	SUMMARY	1
2.0	INTRODUCTION	1
3.0	DESIGN OF CRITICAL TECHNOLOGY EXPERIMENTS	2
3.1	Program Summary	2
3.1.1	Objectives and Requirements	2
3.1.2	Critical Issues	7
3.1.3	Schedule	8
3.2	Task I, Subtask A Description	8
3.2.1	Evaluation of Critical Technology Status	8
3.2.2	Methodology Development	14
3.2.2.1	Thermal Conductivity Enhancement	14
3.2.2.2	Void Control	17
3.2.2.3	Test Facility Selection	19
3.2.2.4	Salt Purification/Filling Procedure	24
3.2.3	Design of Apparatus	25
3.2.3.1	Test Facility Design	25
3.2.3.2	Test Canister Design	33
3.2.4	Initial Safety Assessment	42
4.0	HARDWARE FABRICATION	42
4.1	Canister Fabrication	42
4.2	Procurement of Nickel Foam	42
4.3	Reduction of Nickel Foam	42
4.4	Filling Canisters	55
4.5	Welding the Closure Caps	61
4.6	Canister Insulation	63
4.7	Thermocouple Attachment	63
5.0	EXPERIMENTAL TEST PROGRAM	73
5.1	Test Facilities	73
5.2	Test Plan	79
5.3	Test Results	82
5.3.1	Wicking Test	82
5.3.2	Thermal Cycle Tests	82
5.3.3	Dimension Data	121
5.3.4	X-ray Data	131



## Table of Contents

	<u>Page Number</u>
6.0 SUMMARY OF RESULTS	131
7.0 RECOMMENDED STUDY AND DEVELOPMENT PLAN	139
7.1 Critical Technology Experiments	139
7.2 Brayton Heat Receiver Preliminary Design	140
7.2.1 Preliminary Thermal Analysis	140
7.2.2 Preliminary Structural Analysis	140
7.2.3 Preliminary Fabrication Plan	140
REFERENCES	141
Appendix A Safety Information	143
Appendix B Reduction and Filling Procedure Specifics	153
Appendix C Test Data	176

## 1.0 SUMMARY

Critical technology experiments have been performed on thermal energy storage modules in support of the Brayton Advanced Heat Receiver program. The modules are wedge-shaped canisters designed to minimize the mechanical stresses in the canisters that occur during the phase change of the lithium fluoride phase change material. Nickel foam inserts in some of the canisters were used to provide thermal conductivity enhancement and to see if it would distribute the void volume throughout the canister. A procedure was developed for reducing the nickel oxides on the nickel foam to enhance the wicking ability of the foam. The canisters were filled with lithium fluoride and closure welded at NASA Lewis Research Center. Two canisters, one with a nickel foam insert, the other without an insert, were thermally cycled in various orientations in a fluidized bed furnace at Sundstrand. The only measurable impact of the nickel foam was seen when the back and short sides of the canister were insulated to simulate operation in the advanced receiver design. In tests with insulation, the furnace to back side  $\Delta T$  was larger in the canister with the nickel foam insert, probably due to the radiant absorptivity of the nickel. However, the differences in the temperature profiles of the two canisters were small, and in many cases the profiles matched each other fairly well. Computed Tomography (CT) was successfully used to non-destructively demarcate void locations in the canisters. Finally, canister dimensional stability was measured throughout the thermal cycling test program with an inspection fixture, and dimensions changed by only 0.178 to 0.203 mm (.007 to .008 inch) on average for both canisters with a maximum change of 0.635 mm (.025 inch). This report will describe the results of the in-depth analysis, the design and development approaches, and the results of the thermal cycling tests and the non-destructive inspections.

## 2.0 INTRODUCTION

This study is part of an OAET program for development of advanced technology for future space power systems. It consists of two phases which are intended to lead to the design and fabrication of a heat receiver/thermal energy storage subsystem for a 7 kWe Brayton or a 7 kWe Stirling solar dynamic space power system.

Solar dynamic electric power generation is currently being considered for future space applications. A space solar dynamic power system uses reflective surfaces to collect and concentrate solar thermal energy into a heat receiver for ultimate conversion to electricity in a dynamic power conversion subsystem. Excess energy is collected during the sunlight portion of each orbit and stored in the heat transfer medium of a thermal energy storage unit to provide continuous thermal energy input to the power conversion subsystem, and therefore, continuous electricity, during both the sunlight and eclipse portion of each orbit.

Phase I consisted of two tasks and Phase II will consist of three tasks. Initially, only Phase I will be funded and continuation from Phase I to Phase II will be based on options exercised by NASA.

## 3.0 DESIGN OF CRITICAL TECHNOLOGY EXPERIMENTS

### 3.1 Program Summary

#### 3.1.1 Program Objectives and Requirements

The objective of the Advanced Solar Dynamic (ASD) program at NASA Lewis is to develop small and lightweight systems which show improved efficiency and specific weight over the current state-of-the-art (SOA), i.e., Space Station solar dynamic technology. Figure 1 summarizes a comparison of NASA goals with Space Station design. Since the heat receiver/thermal energy storage subsystem is the heaviest component in the solar dynamic power system, innovative concepts were generated in order to meet the greatly reduced mass requirements (one half of Space Station specific weight) set forth in the ASD program goals. In generating these innovative concepts, the Contractor considered high risk designs which have high technical payoffs. The primary effort focused on (1) minimizing the mass and size of the heat receiver/thermal energy storage unit, (2) maximizing thermal efficiency, and (3) maximizing reliability.

The specific objective of Phase I, Task 1 was to design experiments to evaluate the impact of critical technology issues identified by the contractor on overall heat receiver performance. The objective of Task 2 was to conduct the critical technology experiments identified and designed in Task 1. The overall objectives of Phase I as applied to the Sundstrand receiver concept are summarized in Table I.

The requirements for the design of the advanced receiver are:

- 7-10 years life with 90 minutes thermal cycle periods
- Scalable to 25 kWe and above
- Designed to accommodate launch by Shuttle Transport System (STS) or Expendable Launch Vehicle (ELV)
- Tolerance to non-axisymmetric flux due to concentrator design or degradation or pointing and tracking errors
- Performance verifiable by terrestrial testing
- Ability to interface appropriately with Brayton engine

In Task 1, a trade study was performed to select the best Brayton cycle heat receiver design based on the efficiency, specific mass and reliability goals that had been set forth. The annular heat pipe design, shown in Figure 2 was selected because it is the most reliable and efficient and has a specific mass of 20.6 kg/kWe, well within design goals. The integral heat pipe provides nearly isothermal heat addition to the thermal energy storage canisters. To improve survivability, in the event of a micrometeoroid penetration, and to reduce heat pipe wicking height for ground testing, the annulus is divided into eight sectors. Heat pipe operation modes for insolation and eclipse portions of an orbit are shown in Figure 3a and b.



ADDRESS FOR MAILING ONLY QUARTERMASTER

# POWER TECHNOLOGY DIVISION



Lewis Research Center

## SOLAR DYNAMIC SYSTEM TECHNOLOGY COMPARISON

TECHNOLOGY	SPACE STATION SOA			LDR JPL	ASD GOALS
	DESIGN (HARRIS)	FLIGHT (ROCKET)	DEV.		
CONCENTRATOR Sp. Wt. kg/M	4	5	5		1
HEAT RECEIVER Sp. Wt. kg/kWe	DESIGN	FAB. & TEST	---		TECH. DEV.
	AIR-RESEARCH 66 <sup>1</sup> 53 <sup>2</sup>	BOEING *91 **64	N/A	STIRLING BRAYTON	27 19

\*TEST

\*\*FLIGHT

1 Based upon 25 kWe to user  
 2 Based upon 31 kWe capability

Notes added  
 by Sundstrand 2/20/90

MW98-55TAC.06

**Table I - PHASE I OBJECTIVES**

- 
- **EVALUATE CAPABILITIES OF WEDGE CANISTER DESIGNS**
    - **PREVENTION OF THERMAL RATCHETING**
    - **PERFORMANCE WITH INSULATED SURFACES**
    - **EFFECTIVENESS OF THE THERMAL CONDUCTIVITY ENHANCEMENT (TCE)**
    - **EFFECTIVENESS/NEED OF VOID CONTROL**
      - **ONE G VERSUS ZERO G OPERATION**
    - **WEIGHT MINIMIZATION**
  - **DEMONSTRATION TECHNIQUES**
    - **SEVERAL CYCLES IN VARIOUS ORIENTATIONS**
    - **MONITOR CHANGE**
      - **DEFORMATION**
      - **T/C DATA**
      - **X-RAY (AND/OR COMPUTED TOMOGRAPHY)**
- 



Figure 2 - BRAYTON ADVANCED HEAT RECEIVER - SELECTED CONCEPT

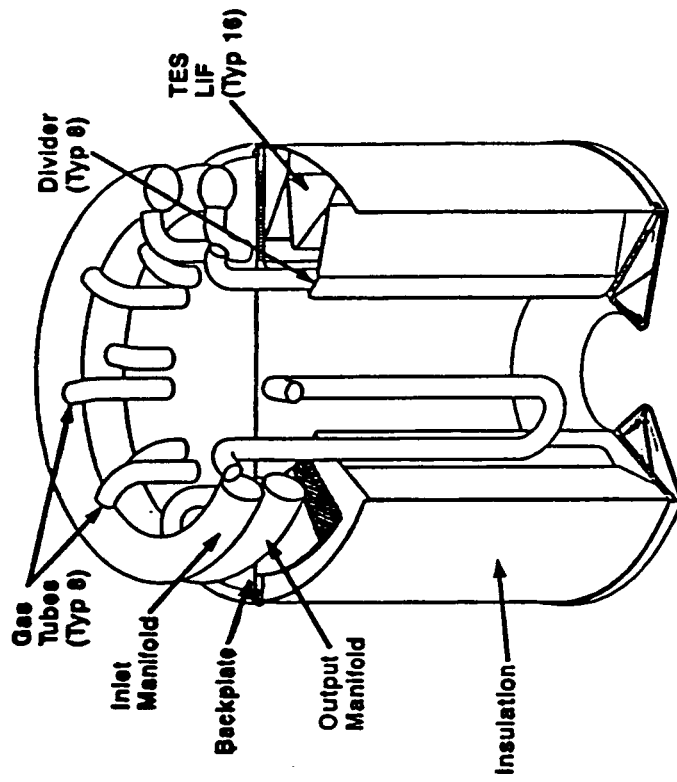
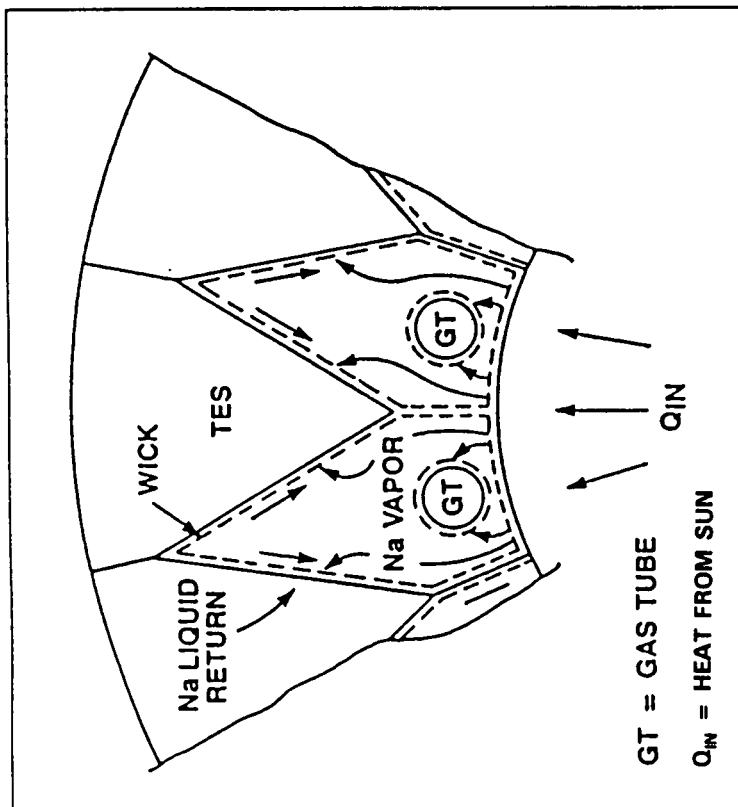
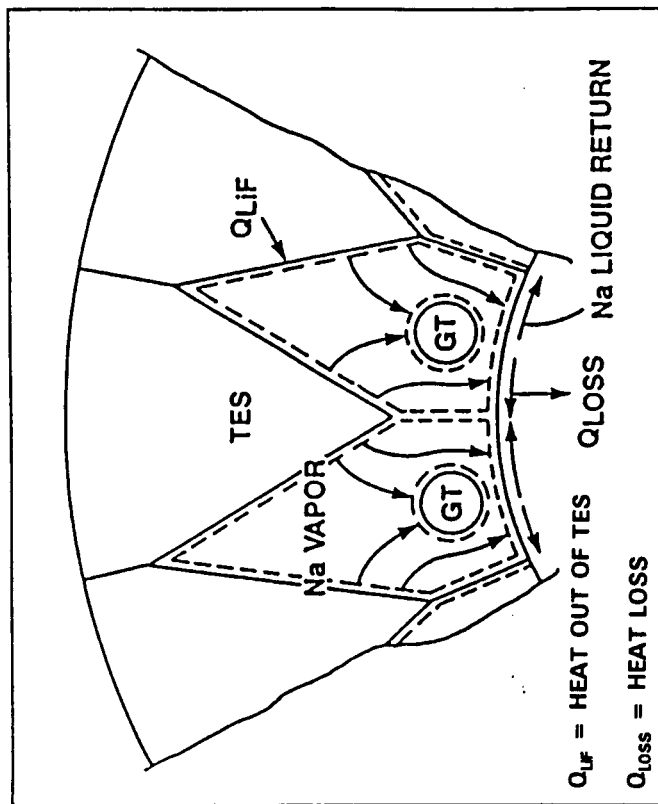


Figure 3 - HEAT PIPE OPERATION MODES



a) During Insolation



b) During Eclipse

Experiments designed to address the critical issues identified during Task 1 were performed in Task 2. The main objectives of these experiments were to learn about void control, thermal conductivity enhancement, and containment mechanical integrity of the thermal energy storage canisters. Two canisters were subjected to simulated orbital thermal cycles to learn about these critical issues.

### 3.1.2 Critical Issues

Several critical issues that were identified in the design and development of an advanced lightweight Brayton heat receiver using lithium fluoride (LiF) as the phase change energy storage medium. The first was associated with long term compatibility of the LiF salt with its containment material. Many inorganic salts used for Thermal Energy Storage (TES) react with their containers causing changes in thermophysical properties such as latent heat and conductivity. In the extreme case, the salt can corrode through the container and cause significant secondary failures. In the case of a heat pipe design such as proposed by Sundstrand, another consideration is introduced, namely the need for compatibility between the container and the heat pipe working fluid, in this case sodium (Na) liquid metal which itself is quite corrosive.

The second issue of major concern for LiF is the question of void control in zero gravity. Since LiF expands by about 30 percent on melting, its container has to be sized for the liquid volume to be expected at the maximum operating temperature. When the salt freezes, a void forms as a result of the reduction in volume. In a 1 g environment, the void tends to form at the top, though the salt will freeze on the surface from which heat is extracted. In zero g, the location of the void will be affected both by the cooling process and from where the heat is extracted and also by the surface tension of the liquid salt since the surface will tend towards a minimum energy condition.

The concern about void control is two fold; if the void forms adjacent to a surface which is later exposed to high fluxes, such as in a direct insolation type receiver, then the container material can burn through; alternatively if the void moves to a location a long way from the heat source it is possible that the hydrostatic pressures formed by the melting salt that cannot access the void will stress the container walls beyond the yield point. This process repeated over a period of time, called thermal ratcheting, will ultimately cause failure of the container.

The third design issue can be related to void control in that it can be of assistance in its control. This is the need for thermal conductivity enhancement. Typical TES salts such as LiF have relatively low thermal conductivity. Since the controlling temperature in the container is the melting point of the salt, it is necessary for the surface temperature of the container to be higher than the melting point during charge and lower during discharge. The temperature difference is a function of the size and shape of the container and conductive path length of the Phase Change Material (PCM). For large containers, the variation in temperature can be significant (hundreds of degrees Celsius) during an orbit, greatly impacting the performance of the power conversion system.

Various materials can be added to the container to increase its effective conductivity and reduce cycle temperature variation. A similar effect can be obtained by reducing the size of the container and increasing the number of containers. The effect of this conductivity increase is an increase in receiver weight since the amount of energy storage material does



not change. The preferred solution is to select the amount of conductivity enhancement to minimize system weight, whereby a trade-off is made between receiver weight and cycle  $\Delta T$  and hence concentrator and radiator weights. This is seen clearly by reference to Figure 4.

### 3.1.3 Schedule

Detailed schedules for Task 1 and Task 2 are presented in Figures 5 and 6.

## 3.2 Task 1, Subtask A Description

### 3.2.1 Evaluation of Critical Technology Status

The solar dynamic heat receiver technology monthly reports from Boeing Aerospace were reviewed. Their difficulty in establishing a repeatable liquid salt filling procedure emphasizes the need for careful analysis during the Fabrication Plan.

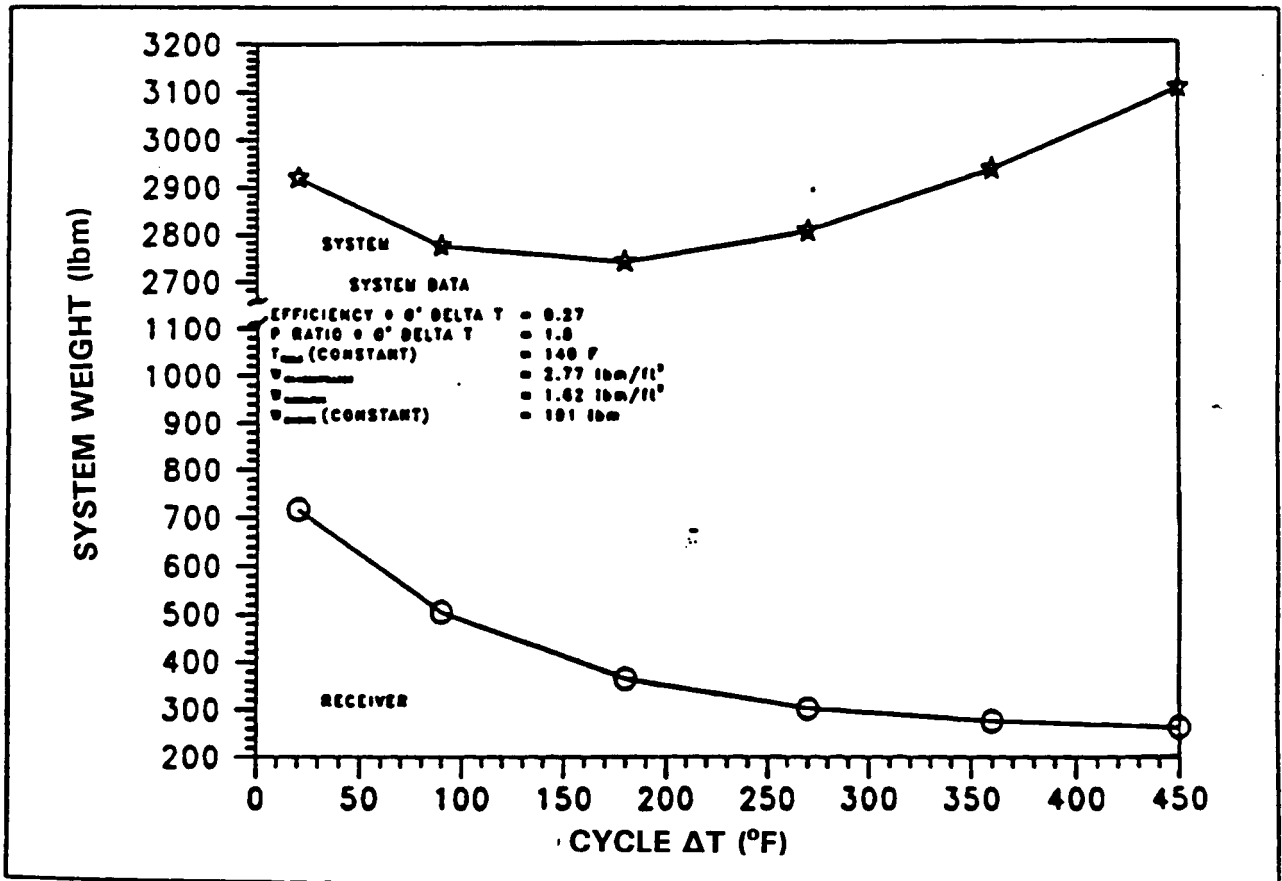
Two reports on the mechanical properties of salts at elevated temperatures were reviewed. Olszewski, et. al., used acoustic emission monitoring of LiH during thermal cycling to determine that repeatable cracking of the salt occurred [1]. The test data showed a strong dependence between the initiation of cracking and the cooling rate. The faster the material cooled, the higher the temperature at which cracking began. For the particular application under consideration, cracking initiated at about 750K, above the minimum storage temperature of 700K. It was questioned whether a similar type of cracking would occur in a fluoride salt.

Raj and Whittenberger described deformation behavior of single crystal LiF and  $\text{CaF}_2$  and polycrystalline LiF-22 (mol percent)/ $\text{CaF}_2$  in the temperature range of 300 to 1275K [2]. While cracks were evident in the polycrystalline eutectic at room temperature, no sudden drops in load were observed in tests conducted above 500K. Thus it does not appear that predictable stress relief cracks that communicate with the void will be present. However, the salt strength at temperatures near the melting point is quite low compared to that at room temperature. Performance during start-up from room temperature is an important design and reliability driver.

Three reports concerning evaporation of super-alloy materials in high vacuum and high temperatures were reviewed [3, 4, and 5]. All express concern about degradation of elements such as Cr and Mn. The ongoing testing of LiF-Hastelloy B-2 compatibility and vacuum exposure of the B-2 material at NASA-LeRC (Whittenberger) will be closely followed.

System performance considerations have an important role in the optimization of components. A NASA paper discussing the thermal evaluation of cavity heat pipe receivers was obtained [6]. The report indicates the number of canisters to be a primary factor in determining the magnitude of cavity temperature variation. It also shows the importance of incorporating high thermal conductivity materials such as boron nitride or pyrolytic graphite to achieve reduction of cavity temperature variations and thus achieve overall system performance gains. This work, or extensions of it, can be utilized throughout the Phase I effort to evaluate system effects. However, this will be less

Figure 4 - SYSTEM WEIGHT VS. CYCLE  $\Delta T$



**TASK I ADV HEAT RECEIVER**

TASK DESCRIPTION	1989												1990						
	JUNE	JULY	AUGUST	SEPTEMBER	OCTOBER	NOVEMBER	DECEMBER	JANUARY	FEBRUARY	JUNE	JULY	AUGUST	SEPTEMBER	OCTOBER	NOVEMBER	DECEMBER	JANUARY	FEBRUARY	
CONTRACT START DATE 6/5/89	✓																		
UPDATE PRG PLAN		✓																	
TASK I																			
SUBTASK A																			
DESIGN CRIT TECH EXPERIMENTS																			
EVALUATE CRITICAL TECHNOLOGY STATUS																			
- REVIEW NASA, BOEING, ETC.																			
METHODOLOGY DEVELOPMENT																			
-VENDOR INFORMATION																			
-POC TEST EVALUATION																			
-LONG LEAD ITEMS DETERM																			
INTERIM REVIEW AT NASA																			
-TEST PLAN																			
-INSTRUMENTATION PLAN																			
A3 DESIGN OF APPARATUS																			
-CANISTER DESIGN																			
-CAPSULE DESIGN																			
-TEST FACILITIES DESIGN																			
INITIAL SAFETY ASSESSMENT																			
SUBMIT AGENDA FOR REVIEW																			
SUB-TASK A REVIEW																			
SUBTASK B																			
B1 STUDY AND DEVELOPMENT PLAN																			
END OF TASK I																			
MONTHLY REPORTS																			
TASK I FINAL REPORT																			
DRAFT TO NASA																			



**Sundstrand Aviation**  
 Rockford, Illinois  
 a unit of Sundstrand Corp.

ACTUALS	PLANNED	ESTIMATED	MILESTONE	DEPENDENT	CRITICAL	TASKS	AUTHOR	RUN DATE	VERSION	PAGE
			✓	0	◆	28	HEIDENREIC	12/22/89	v1.23	1 of 1

NASA BRAYTON RECEIVER TASK II

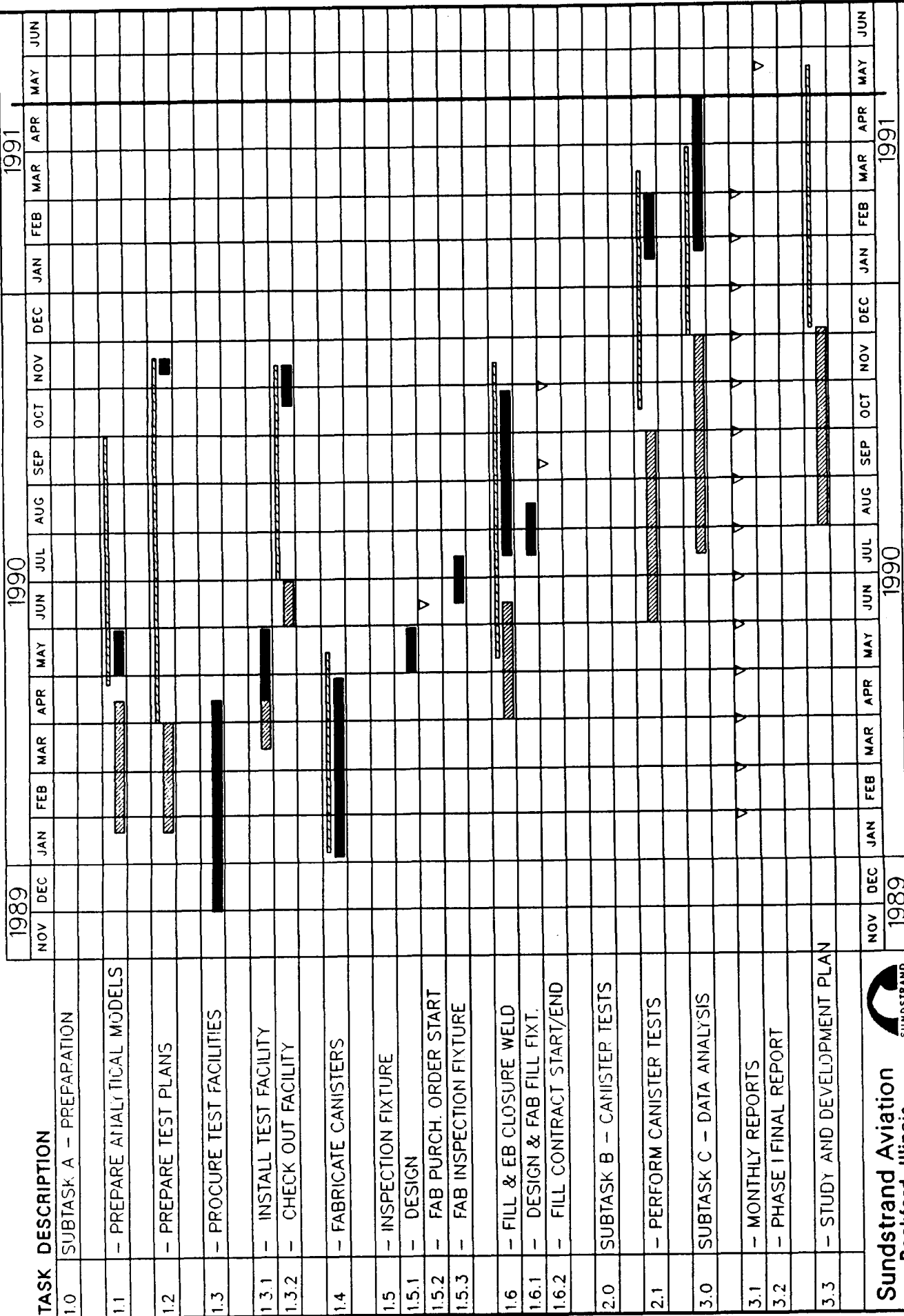


Figure 6 - TASK II SCHEDULE

important for a heat pipe receiver which provides for integration of these effects by virtue of the high conductance of the heat pipe.

When thermal conductivity enhancement (TCE) is added to the phase change material, the question of how to estimate the effective thermal conductivity of the matrix is important for the determination of both performance (cycle temperature variation) and mass. A number of models and various empirical data are found in the literature. The simple parallel model:

$$k_e = \epsilon k_f + (1 - \epsilon) k_s \quad (1)$$

where:  $k_e$  = effective thermal conductivity  
 $\epsilon$  = porosity, i.e. volume fraction of PCM  
 $k_f$  = Phase Change Material (PCM) thermal conductivity  
 $k_s$  = thermal conductivity of enhancement material

gives an upper limit for the effective conductivity and was used in Sundstrand's proposal analyses. A lower limit would be to assume that the materials are in series. A paper presented at the 1989 IECEC discussed numerous models for determining the effective conductivity of sintered metal fibers [7]. Using Equation (14) from Reference 7:

$$\frac{k_e}{k_s} = 1 + \frac{\epsilon}{\frac{1 - \epsilon}{m} - \frac{k_s}{k_f - k_s}} \quad (2)$$

where:  $m = [1.19 - 29.9 (d/\ell) (.82 - \epsilon)^2 + (1.09 - 2.64 (d/\ell))]$   
 (Equation 15 of Reference 7)  
 $d/\ell$  = aspect ratio, diameter/fiber length

When the following property values are inserted into Equation (2):

$k_f = 1.73 \text{ W/m-K (1.0 B/ft-hr-F (LiF))}$   
 $k_s = 73.39 \text{ W/m-K (42.4 B/ft-hr-F (Ni))}$   
 $\epsilon = .95$   
 $d/\ell = .01$

we get:

$$k_e = 3.16 \text{ W/m-K (1.823 B/ft-hr-F)}$$

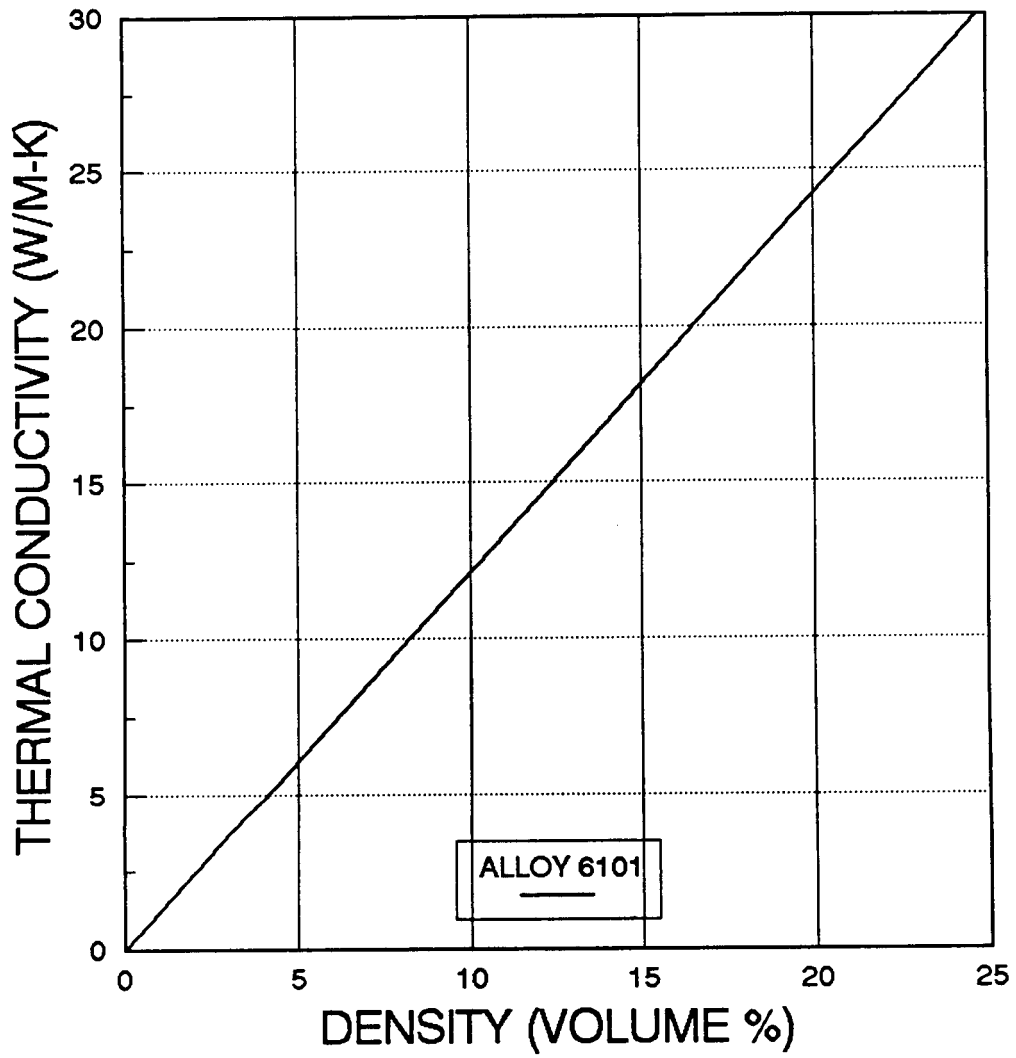
This is only 60 percent of the value calculated from the parallel model, i.e.

$$k_e = (.95) (1.73) + (.05) (73.39) = 5.31 \text{ W/m-K (3.07 B/ft-hr-F)}$$

Duocel foam was being investigated as a potential TCE. The thermal conductivity of Duocel aluminum foam as a function of density (volume percentage) is shown in Figure 7. Converting this curve to the conductivity of nickel, we obtain

$$k_{s, \text{Ni Foam}} = 25.3 (1 - \epsilon) \text{ B/ft-hr-F} = 2.20 \text{ W/m-K (1.27 Btu/ft-hr-F)} \quad (3)$$

Figure 7 - AL DUOCEL FOAM THERMAL CONDUCTIVITY



R. L. Gay, et. al., showed data that indicated that the enhancement with nickel fins is only about 31 percent of that calculated [8]. This lower than predicted enhancement is in accordance with the theory of Knowles at Energy Science which suggests that very fine and uniform dispersement of the TCE is required to approach the conductivity enhancement given by Equation (1) [9].

The preceding investigation indicates that caution needs to be used to prevent errors in performance and weight estimates. Future receiver analysis will be performed using the parallel model modified with the TCE conductivity as given in Equation (3) to calculate the effective conductivity of Ni foam.

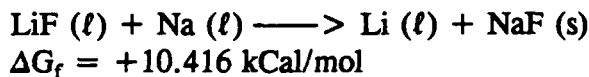
Other efforts in the technology review included review of both the Sanders and Garrett conceptual design final reports and visits to Oak Ridge and Los Alamos National Laboratories as well as visits and discussions with Dynatherm and Thermacore.

### 3.2.2 Methodology Development

Table II summarizes the elements of the study effort of this subtask. Evaluations of material compatibility performed early in Task 1, as well as work done by Oak Ridge, NASA, and Boeing, indicated that Sundstrand should devote its efforts to canister experiments rather than additional compatibility tests.

#### 3.2.2.1 Thermal Conductivity Enhancement

The enhancement of thermal conductivity by use of a slurry as proposed by Phillips of JPL was investigated. The reactivity of lithium fluoride and sodium was examined at 1200K, 79K above the melting point of lithium fluoride.



The positive value of the Gibbs free energy indicates that no reaction would be expected.

The addition of sodium could serve two purposes. First, the high conductivity of the liquid metal would enhance the overall conductivity, minimizing cycle temperature variation and secondly the internal vapor pressure of the canister would match the heat pipe pressure and minimize pressure generated stresses on the canister wall. However, there is concern about segregation of the sodium and liquid salt, especially during 1 g tests.

A series of experiments could be performed to evaluate this potential approach. An inexpensive annular heat pipe, such as those manufactured by Dynatherm, could be filled with only LiF salt. Another could be filled with the salt and the heat pipe working fluid (Na). Figure 8a shows a potential charge cycle test. Heat input  $Q_{in}$  would be from the inside diameter. Thermocouples around the circumference would monitor the uniformity of the temperature gradient as a function of angular orientation. A gas gap calorimeter could be mounted on the outer diameter. Other TCE materials could be installed in place

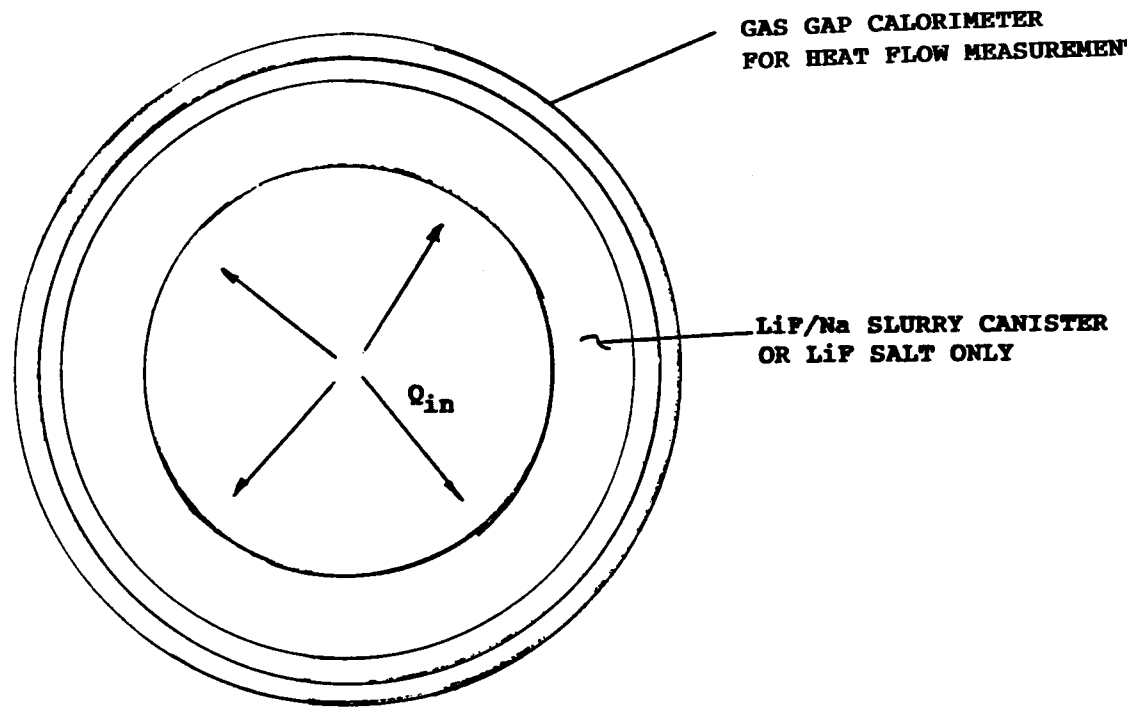
Table II - ELEMENTS OF STUDY FOR SUBTASK A

- 
- MATERIALS
  - COMPATIBILITY (PCM, TCE, CONTAINMENT, Na, PROCESSING)
  - PROPERTIES (k, WICKING HT)
  - AVAILABILITY
  - PERFORMANCE (MASS, AT)
  - COST
  - VOID CONTROL
  - OVERALL TEST PHILOSOPHY
  - TEST FACILITIES
  - CANISTER VERSUS CAPSULE TESTS
  - POTENTIAL PROOF OF CONCEPT (POC) TESTS
- 

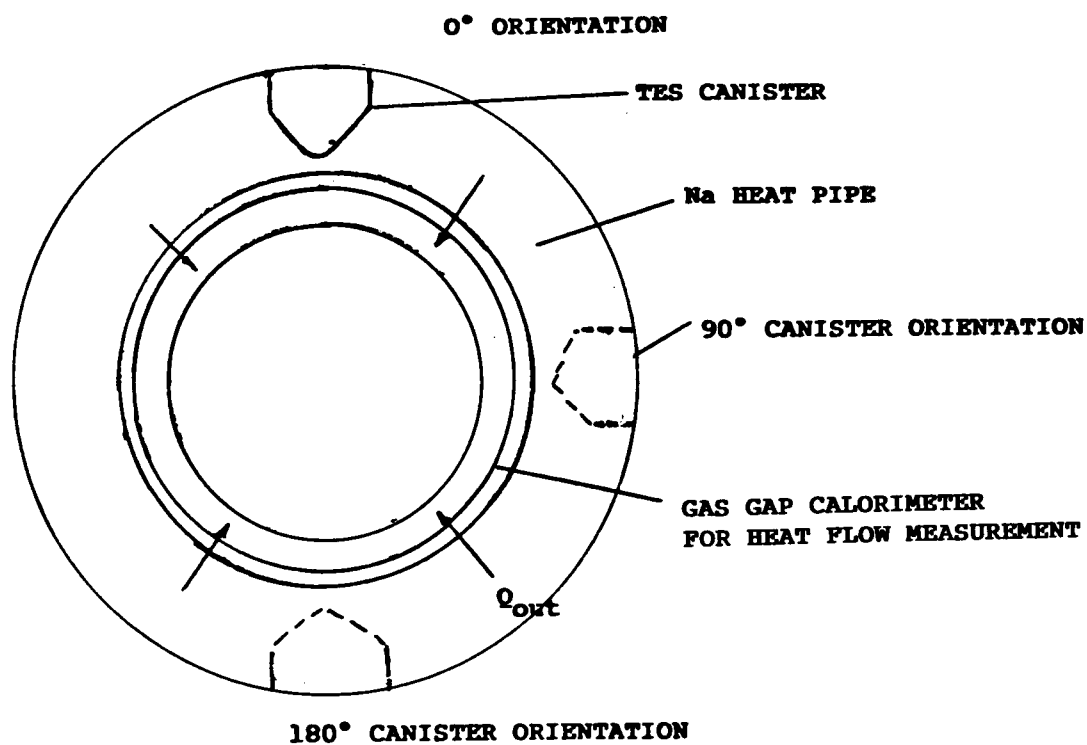




Figure 8 - EXPERIMENTS FOR EVALUATION OF SODIUM CONDUCTIVITY ENHANCEMENTS



(a) TES CHARGE TEST



(b) TES DISCHARGE TEST

of liquid sodium. At a later time, a wedge shaped canister could be installed in the heatpipe. In Figure 8b, heat flow during a discharge cycle,  $Q_{out}$ , is shown. Energy flows radially inward from a TES canister through a heat pipe to a gas gap calorimeter. The dotted canisters represent tests with the canister in various angular orientations. These experiments were not included in the plans for Task 2, but could be considered for future experiments.

One of the major concerns with the use of TCE materials is their wicking ability with the salt. This is an important factor in both void control and proper use of TCE. Various materials were considered for use as TCE. Preliminary experiments were performed to evaluate their suitability, and work done by other contractors such as Boeing was reviewed.

Two vendors were contacted for information on SiC. They were ERG Corporation in Oakland, California and American Matrix, Inc. in Knoxville, Tennessee. Samples were requested. The American Matrix material comes in whisker and platelet preforms. They contain 1000 ppm of Fe, Ca, Mn, K oxides plus < 1.1 percent  $SiO_2$  which is on the surface.

The material properties of potential Thermal Conductivity Enhancement (TCE) materials are shown in Table III. In order to select the TCE material(s) to use in the critical technology experiments, several simple wicking experiments were performed. These tests consisted of melting a LiF/KF eutectic salt in a Ni-201 crucible in an argon atmosphere glove box, inserting a TCE sample into the molten salt, holding the system for 15 minutes, and then turning the tube furnace off and allowing the system to cool. The wicking height was estimated by caliper measurement. LiF/KF eutectic was chosen as the test material for this experiment because it had been used in former tests at Sundstrand. Two TCE materials were tested: 2.6 pores per mm (65 pores per inch (ppi)) Nickel foam (from Astromet Corporation) and 3.1 pores per mm (80 ppi) SiC foam (from ERG Corporation). The wicking heights were approximately 1.5 cm for the nickel and 1.85 cm for the SiC. The salt was then remelted to remove the TCE sample from the crucible. When the SiC foam was removed using tweezers, it crumbled into powder.

The tests were subsequently repeated with LiF. There was no wicking evident in the test performed with the nickel foam. The LiF salt wicked all the way to the top of the SiC foam, a distance of 2.1 cm. However, when the salt was remelted, the foam, broke up and was destroyed.

Based upon these tests, the SiC foam from ERG Corporation was not pursued further. With regard to the nickel foam, several options were investigated. One alternative was to use the foam as is, realizing that the nickel oxide would prevent wetting. Another was to process the material to remove the oxide, such as Boeing reported [5].

### 3.2.2.2 Void Control

Of greatest concern in the use of a PCM like LiF is the high volume change on melting. If the void location is not adequately controlled, the canister could rupture due to thermal ratcheting. The wedge shaped canisters of the Sundstrand preliminary design were intended to help in this regard, by allowing the void to form on the adiabatic back surfaces

Table III - POTENTIAL THERMAL CONDUCTIVITY ENHANCEMENT MATERIALS

	(ERG) RVC	(ERG) Electroless Ni on RVC	(Astromet) Tungsten PM	(Ultramet) Tungsten-CVT onto RVC	(Astromet) Nickel PM	(ERG) SiC
Pores Per Inch (PPI)	100	100	?	100	? 65	100
Cost per 10" Canister	\$158	\$335	?	\$4060	?	\$860
Density (lb/ft <sup>3</sup> )	3.1	95.6 (~.001 NI)	?	31.2	? 35	16 (~81.)
TCE Mass/Receiver						
Survivability						
Compatibility						
1. LiF	Good	Good	Good	Good	Good	Good
2. Na	Fair	Good	Questionable	Questionable	Good	
3. Li	Bad	Good	Questionable	Questionable	Good	
4. Inconel 617	Good	Good	Questionable	Questionable	Good	Good
Delivery	4-6 wks	4-6 wks		4 wks		8-10 wks
Wetability	Poor					
Thermal Conductivity						

and using the wedge shape to break the solid bridge of salt on a remelt. Potential void location in one g and zero g for different orientations is shown in Figure 9. These locations are only valid for short or segmented canisters, since with a long narrow canister the void probably forms towards one end due to the surface tension effects.

Table IV presents a list of preliminary test configurations that were considered for different canisters. Test configurations 5 and 6 were considered optional tests.

The intent of Configuration 1 was to test potential TCE or void control materials. Reference 1 indicated that the contact angle values from a substrate such as tungsten and tantalum are below 30 degrees after repeated LiF exposure. Thus these materials have acceptable wettability to lithium fluoride and are candidates for Thermal Conductivity Enhancement (TCE) or void control. One drawback is their high density. The weight of a canister with these materials will increase rapidly.

However, if the wetting material can be deposited on a lightweight porous substrate, the composite material may be useful as a void control mechanism.

Several vendors were contacted for information. ASTROMET makes tungsten foam by the powder metallurgy process. They have made foam with 1.8 pores per mm (45 ppi). This may not be sufficient to enable wicking the entire canister radial length. Further information was requested on the possibility of obtaining smaller pores. The question of whether the void could position itself at one axial end in zero g was investigated, and it appears this is possible.

ULTRAMET Corporation produces a composite material of tungsten Chemical Vapor Infiltrated (CVI) onto a reticulated vitreous carbon substrate. They have demonstrated their capability to produce a foam with 3.9 pores per mm (100 ppi) at 2.63 percent of theoretical density. This process is expensive. An estimated cost to produce a contoured insert for a 2.54 cm (10 inch) long canister is \$4060. If a powdered metal foam with approximately 3.9 pores per mm (100 ppi) could be obtained and was substantially lower in cost than the CVI process, it might be cost effective to experiment with the higher density material initially. If the foam provides good void control, the lower density material could be tested later in Phase II.

### 3.2.2.3 Test Facility Selection

The baseline thermal cycling test concept that was originally proposed for canisters and/or capsules is shown in Figure 10. The use of high temperature sodium in the Sundstrand Materials Science Lab does not meet safety requirements, so this approach was reevaluated. A preliminary comparison of an "inert" vessel (one filled with GN<sub>2</sub> or Argon) and one filled with a sodium bath is summarized in Table V. This preliminary analysis indicated that the sodium bath vessel presents a number of difficulties that make its use less attractive than originally believed. The major problems are:

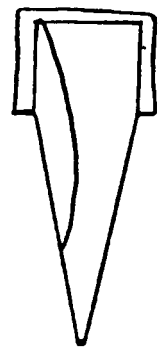
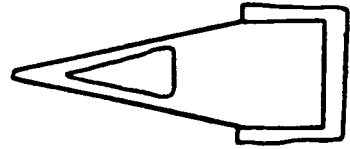
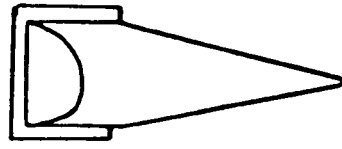
1. The sodium vessel cannot be used in the Sundstrand Material Science and Engineering Lab (MS&E) because of safety considerations. In addition, a glove box and associated apparatus are required to remove the test hardware. Cost per test would be significantly increased.

Figure 9 - ANTICIPATED VOID LOCATIONS WITHOUT VOID CONTROL

WITH ADIABATIC SURFACES

WITHOUT ADIABATIC SURFACES

1 G



0 G

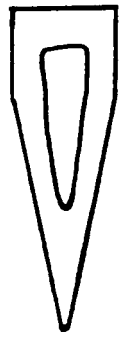
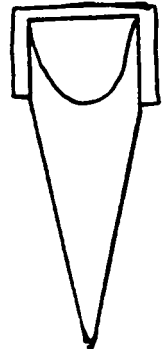
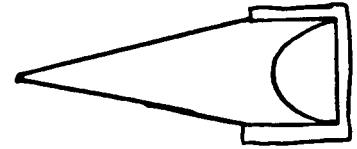
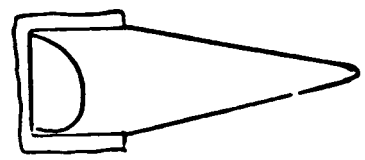
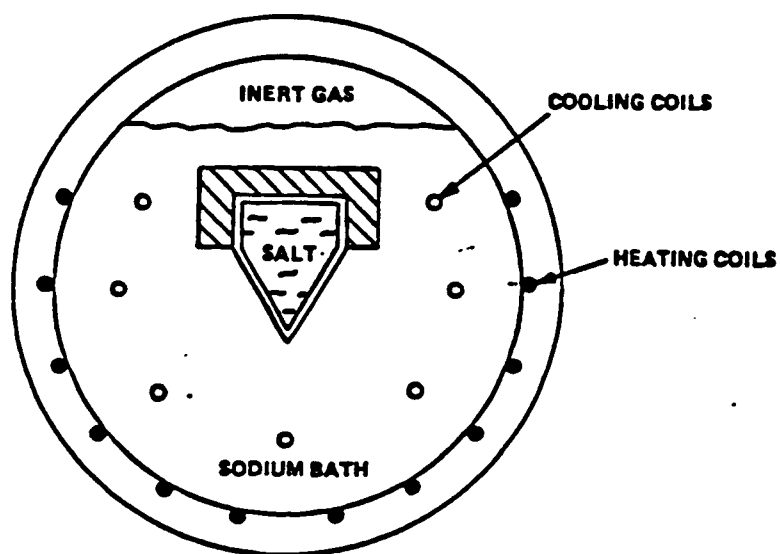


Table IV - PRELIMINARY TEST CONFIGURATIONS

CONFIGURATION NO.	TEST DESCRIPTION
1	Fill procedure checkout and LiF wicking test with proposed TCE material.
2	Performance tests with no TCE, various orientations.
3	Wicking test with TCE material. Does the void migrate to hot (insulated) end against gravity?
4	Upon successful completion of test with configuration 3, performance tests with TCE installed.
5	Performance tests with 10% by volume Li added to LiF, I.D. of canister to be wicked, various orientations.
6	Compatibility/performance tests with 10% by volume sodium added to LiF.

**Figure 10 - TES CANISTER THERMAL CYCLING TEST BASELINE CONCEPT**



**Table V - COMPARISON BETWEEN INERT TEST VESSEL AND SODIUM VESSEL**

	INERT VESSEL	SODIUM VESSEL
1. COST	≈ \$40K	≈ \$50K
2. MATERIALS	316 SS	INCONEL 625, FORGING REQUIRED
3. SAFETY	USE IN MS&E LAB	OUTSIDE MS&E TEST LAB BECAUSE OF Na AND PRESSURE RATING
4. DESIGN	HEATERS INTERNAL	HEATERS EXTERNAL
5. HANDLING	NO SPECIAL REQUIREMENTS	GLOVE BOX TO OPEN VESSEL - POTENTIAL PROBLEMS OF OXIDATION AND CREEP
6. CORROSION	NONE	NEED PURIFIED Na; WILL BECOME CONTAMINATED WHEN OPENED
7. TEMPERATURE UNIFORMITY	ADEQUATE	EXCELLENT
8. INDUCED ΔT	WITH SEPARATE HEATING ZONES	DIFFICULT - VERTICAL ORIENTATION ONLY
9. OTHER	EASY TO CHANGE ORIENTATION	VERTICAL ORIENTATION ONLY BECAUSE OF SEALS



2. It is believed that the sodium would become contaminated with trace impurity oxygen each time the vessel is opened. This in turn would require cleaning the vessel internal surfaces as well as replenishing the sodium.
3. There is concern that the vessel-to-head seals could leak if exposed to liquid sodium, especially after numerous thermal cycles and openings. To reduce this possibility, the vessel would be oriented vertically. This would limit the canister size or orientation options.
4. A sodium filled vessel must be heated externally, increasing the external surface temperature, providing greater chance of oxidation and galling of the fasteners.
5. One suggested test was to induce an axial  $\Delta T$  on the canister/capsule to investigate mass transfer effects. This would be very difficult to implement in a sodium filled vessel because of the excellent heat transfer properties of sodium.

There appeared to be no real technical advantages and numerous cost disadvantages to the use of a sodium vessel. Any sodium compatibility tests could be performed in another manner, such as with small capsules or heat pipes filled with sodium. A detailed description of the test facilities selected is presented in Section 3.2.3.

#### 3.2.2.4 Salt Purification/Filling Procedure

The purity of LiF and the filling techniques used in processing a TES canister have significant effects on corrosion, performance and life. LiF as received, contains  $H_2O$ ,  $O_2$ , metal oxides, metal fluorides, and other contaminants. Corrosion rates will depend on the concentration of these impurities.

The following salt purification techniques and filling procedures were evaluated.

1. Procure anhydrous, reagent grade LiF in granular form. Cast in canisters in a purified argon glove box. Super heating LiF to 1223K during filling has been reported [10] to remove  $H_2O$  and HF and thus would be part of the process.
2. Same as (1) above and draw vacuum on molten salt prior to final solidification. Vacuum melting LiF following filling will also remove  $H_2O$ ,  $O_2$  and trapped gases [10].
3. Prior to filling, purify LiF by spraying the molten salt with 20 HF/80  $H_2$  at 923K until HF is constant, then with  $H_2$  at 973K until HF content is low. Freeze, granulate and cast into canister per (1) or (2) above. Purification of LiF by spraying will not only remove  $H_2O$  and  $O_2$ , but will reduce metal oxides and metal fluorides to their respective metals. This technique is discussed in an Oak Ridge report performed for NASA [10].
4. Use of LiF reservoir and transfer lines to perform a liquid fill. Prior to filling, purify LiF in the reservoir by spraying as in (3) above, then transfer molten salt to the canister. Such a closed system filling technique was developed by Boeing under NASA contract [5].

Los Alamos National Laboratories proposed a relatively simple canister filling approach that had been considered for Task 2. Figure 11 shows a schematic representation of this scheme. This was a liquid fill technique using RF heating in a vacuum chamber.

Potential proof of concept tests were considered in Task I using paraffins to simulate salt void generation. Detailed evaluation concluded that material property differences would limit the applicability.

### 3.2.3 Design of Apparatus

#### 3.2.3.1 Test Facility Design

During a visit to Parr Corporation (a vendor of liquid metal furnaces) to discuss a sodium filled test facility, information was provided concerning the canister size, heat load, cycle times, and orientations required to thermal cycle a canister. Parr expressed concern in meeting the cool down time requirement.  $\text{GN}_2$  cooling coils, forced convection cooling of the vessel, and water cooling were evaluated. However, it was decided that the use of sodium was unacceptable as reported in Section 3.2.2.

A pressure vessel filled with helium was therefore analyzed for its ability to be adequately cooled during the simulated eclipse portion of an orbital cycle. Initial analysis indicated forced convection would be required. This would pose problems in that a fan inside the vessel that could tolerate high temperatures is not normally provided. The initial analysis was for a full scale canister with a heat flow of 1.7 kW during cooling. Smaller canister designs were also investigated. For smaller cross-section and subscale length canisters, the cooling requirements drop to 351 watts. Analysis indicated that natural convection would transfer the heat from the canister to the helium.

NASA expressed concern about isothermality across the canister surface using this technique. Non-uniformity would not provide an adequate representation of a heat pipe heat addition process.

Thus other facility types were added for investigation. An evaluation matrix of potential test apparatus, shown in Table VI, was developed. The first apparatus investigated was the liquid metal pressurized vessel shown schematically in Figure 12 and discussed earlier. This type of apparatus would be most useful for long duration tests and compatibility tests which are not the objectives of this phase.

A somewhat less expensive version of the pressurized liquid metal vessel is one filled with an inert gas shown schematically in Figure 13 and pictorially in Figure 14. An even less expensive inert gas filled retort with a tube furnace is shown in Figure 15. Two concerns about these systems are whether they can remove the heat in the required time to simulate the low earth orbit eclipse and secondly how uniform the canister surface temperature would be with natural convection circulation. A fourth concept is the fluidized bed furnace shown in Figure 16. An advantage of this type of equipment is the bed temperature uniformity, a result of the high heat transfer coefficient caused by the fluidizing gas flow. The heat transfer coefficient should be approximately  $320 \text{ W/m}^2\text{K}$  for a bed at  $1173\text{K}$  [11]. Analysis indicated that gaseous nitrogen flowing through a coiled tube inserted into the bed during the simulated eclipse cycle should be able to remove the bed heat in the required time.

Figure 11 - LOS ALAMOS PROPOSED LiF FILLING APPARATUS

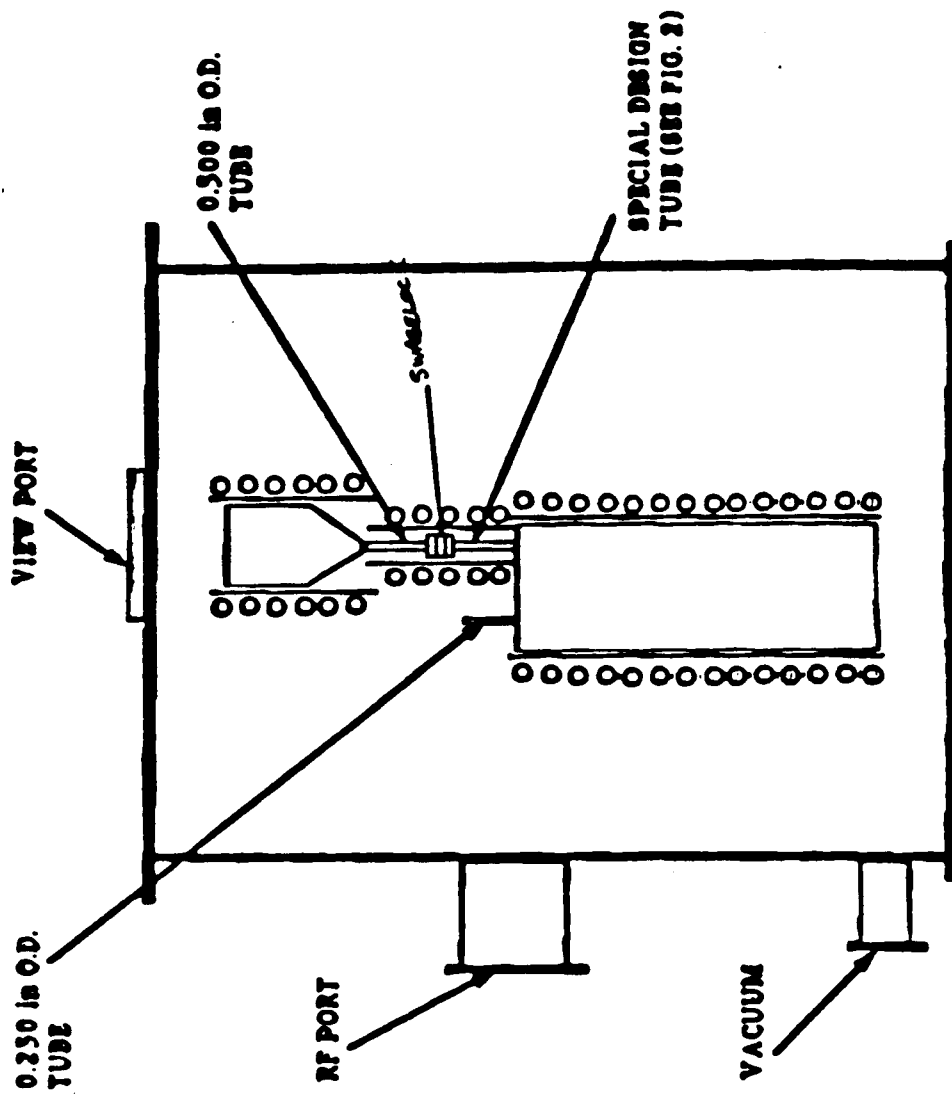


Table VI - TEST FACILITY EVALUATION MATRIX

	LIQUID METAL VESSEL	INERT GAS FILLED VESSEL	TUBE FURNACE WITH INERT GAS RETORT	FLUIDIZED BED FURNACE	LANL TWO-STAGE HEAT PIPE	THERMOCORE		UNIVERSITY OF KENTUCKY LIQUID METAL PUMPED LOOP
						RADIATOR COUPLED	INDIVIDUAL HEAT PIPE	
FACILITY COST	50 K <sup>+</sup>	35 K	13 K	15 K	35	15	22	N/A
ISOTHERMALITY	GOOD	FAIR	FAIR	GOOD	FAIR	FAIR	GOOD	GOOD
LEO CYCLE TIME	YES	YES	POSSIBLE, EXTRA COST	YES W/ COOLING COIL	YES	YES	YES	YES
EASE OF TEST	VERY DIFFICULT	GOOD	FAIR	GOOD	DIFFICULT	FAIR	FAIR	DIFFICULT
LONG DURATION CAPABILITY	YES	YES	NO	YES	NO	YES	YES	NO
RUN COST	HIGH	LOW	MEDIUM	LOW	HIGH	MEDIUM	MEDIUM	N/A



Figure 12 - LIQUID METAL VESSEL

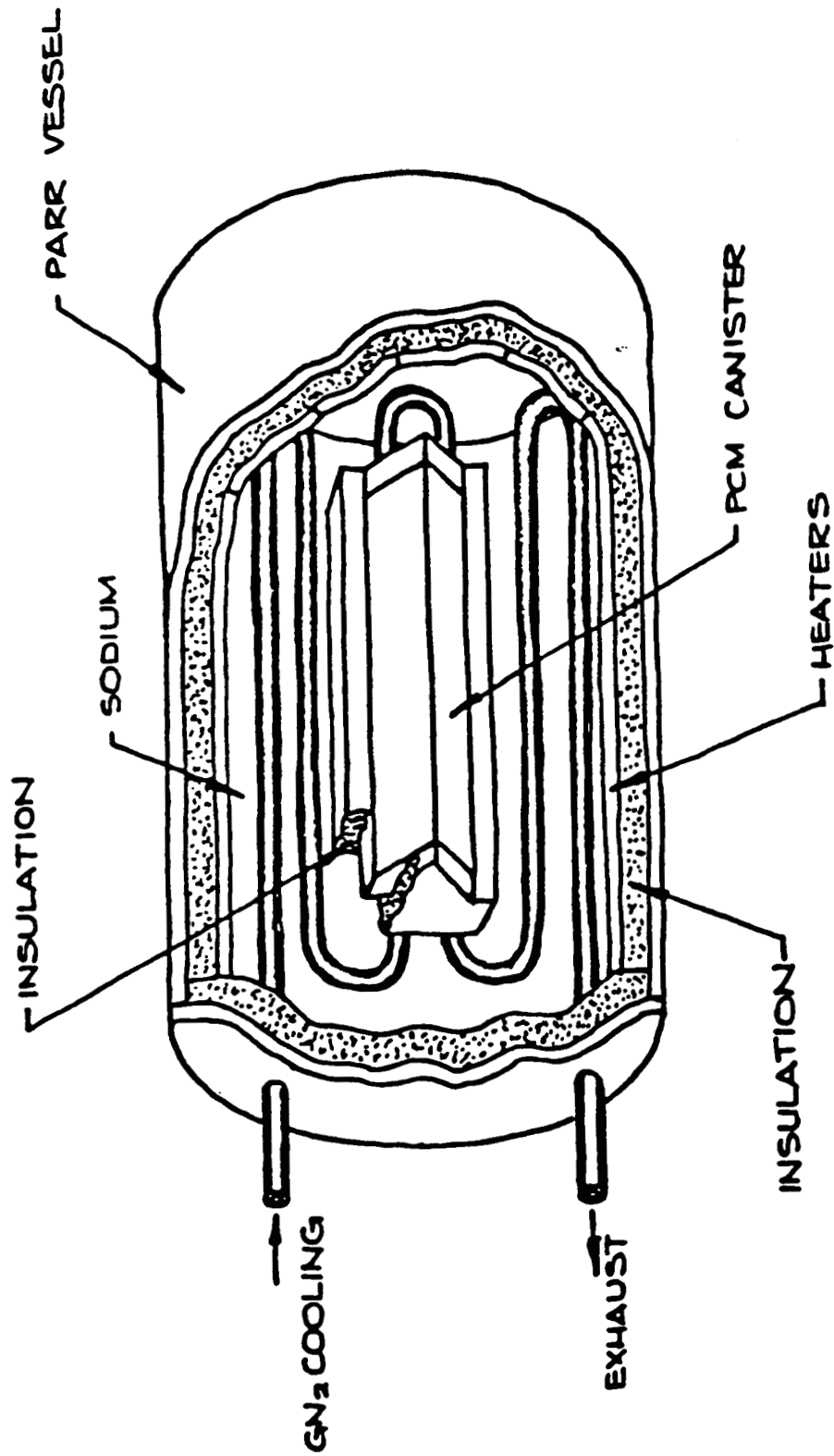


Figure 13 - INERT GAS FILLED VESSEL

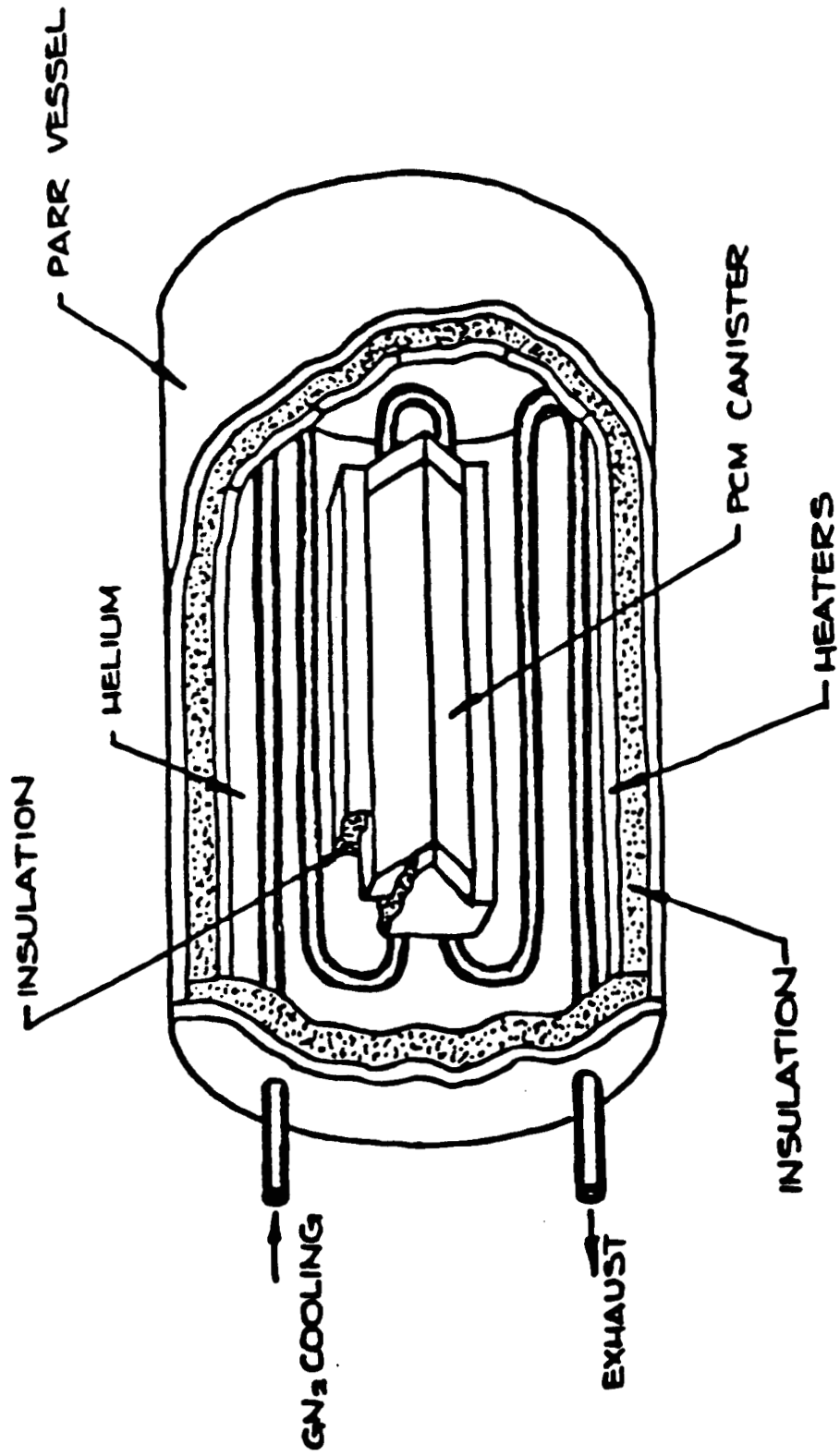


Figure 14 - INERT GAS FILLED VESSEL

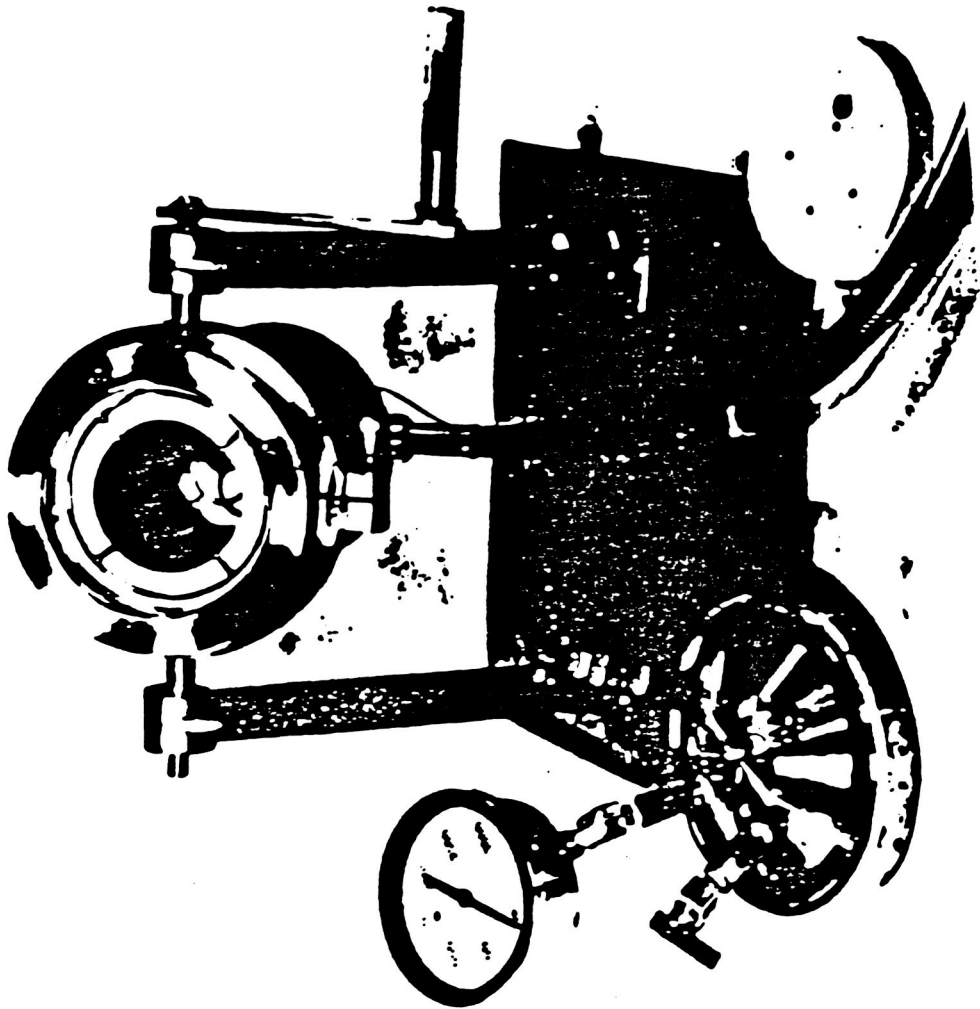


Figure 15 - INERT GAS FILLED VESSEL

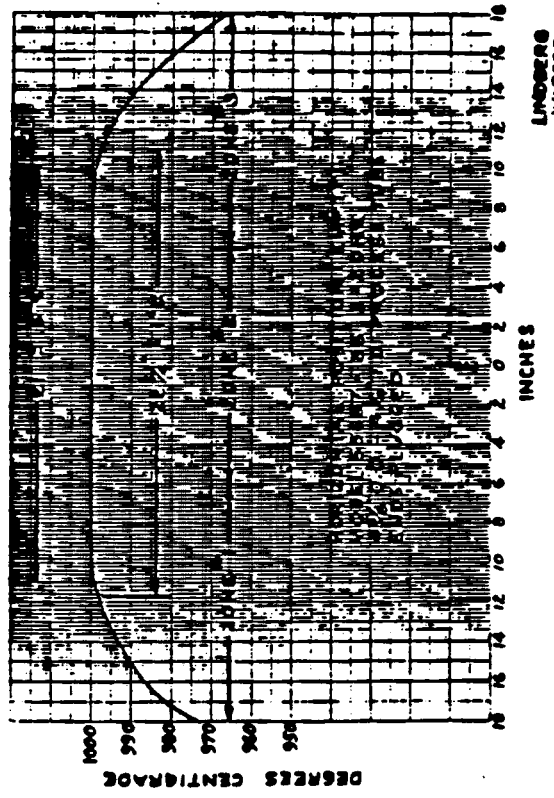
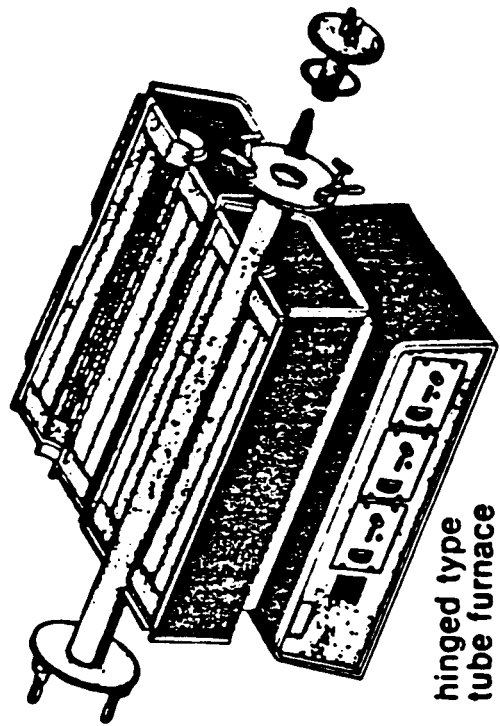
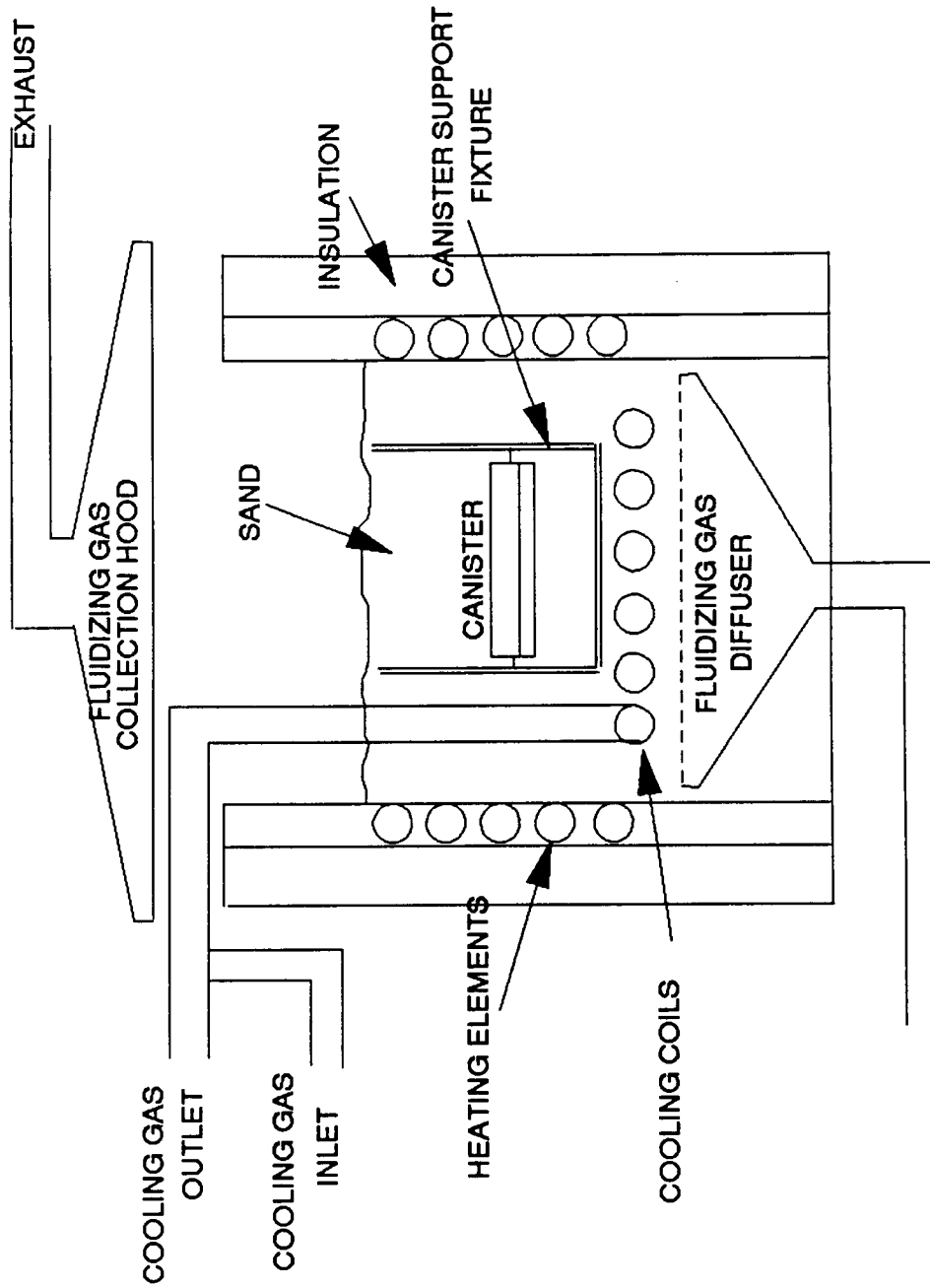




Figure 16 - FLUIDIZED BED FURNACE



Los Alamos National Laboratories proposed a two-stage radiation coupled heat pipe furnace. The canister would be enclosed inside an annular heat pipe for ease of test article changeover. This is shown in Figure 17. While eliminating unknown convection currents, this concept is radiation coupled, and thus does not truly simulate the heat pipe. In addition, the testing is mechanically complex because the canister must be physically moved from the hot furnace to the cold furnace to simulate the orbital cycle.

Figure 18 shows an annular heat pipe proposed by Thermacore. Their proposal would utilize a water cooled jacket to remove the heat and provide calorimetry. The heat transfer would also be by radiation. Another version is shown in Figure 19. In this version, each canister would be enclosed in a heat pipe with a single water cooled jacket.

The fluidized bed furnace was finally selected as the test apparatus for the canister experiments. A  $\text{GN}_2$  cooling coil was designed to enable removal of heat from the bed and canister in the required cycle time of 30 minutes. The final design uses a coil 1.27 cm (0.500 inch) outside diameter by 4.06 m (160 inch) length. The cooling coil requirements were added to the specification for the fluidized bed.

### 3.2.3.2 Test Canister Design

The lowest weight receiver presented in the Sundstrand proposal results in an overall cycle  $\Delta T$  of approximately 723K (450°F). This large swing in temperature requires the engine to run off-design much of the time. Thus the system weight will increase due to increased radiator and concentrator sizes required at the lower overall system efficiency. A preliminary system weight trade study showed minimum system weight in the range of 41.7-111.1K (75-200°F) total cycle  $\Delta T$  (see Figure 4). A number of SINDA thermal analysis computer runs were made with different canister sizes. Results are shown in Table VII. The receiver specific weights were calculated with the conservative assumption that the canisters had separate walls from the heat pipe. Substantial reduction in cycle  $\Delta T$  can be achieved with modest increases in weight.

Particular attention was paid to two areas of the canister design; 1) the closure weld design and 2) deformation.

There was concern that the fill tube and pinch-off tube internal volumes could become filled with solidified salt. If this salt did not have a pathway to the void upon remelting, excessive local stresses and failure could result. The fill-tube cap was designed to eliminate the fill tube internal volume and to be EB welded. With an EB weld design, there is no necessity for a pinch-off tube. The design is shown in Figures 20 and 21.

A 2-D finite element ANSYS analysis of the canister was generated. Uniform pressure loading was imposed to simulate operation either inside a heat pipe or at ambient pressure during component testing. A typical plot of the nodes showing the pressure loading (solid line) and boundary constraints is shown in Figure 22, and one showing the nodal elements is shown in Figure 23. Initial results with thin wall material 0.838 mm (.033 inch), thick and a small top radius 3.175 mm (0.125 inch), predicted maximum equivalent stress significantly greater than the yield strength of Inconel 617 sheet. Therefore, a parametric study of wall thickness and top radius versus stress and

Figure 17 - LANL TWO-STAGE HEAT PIPE FURNACE

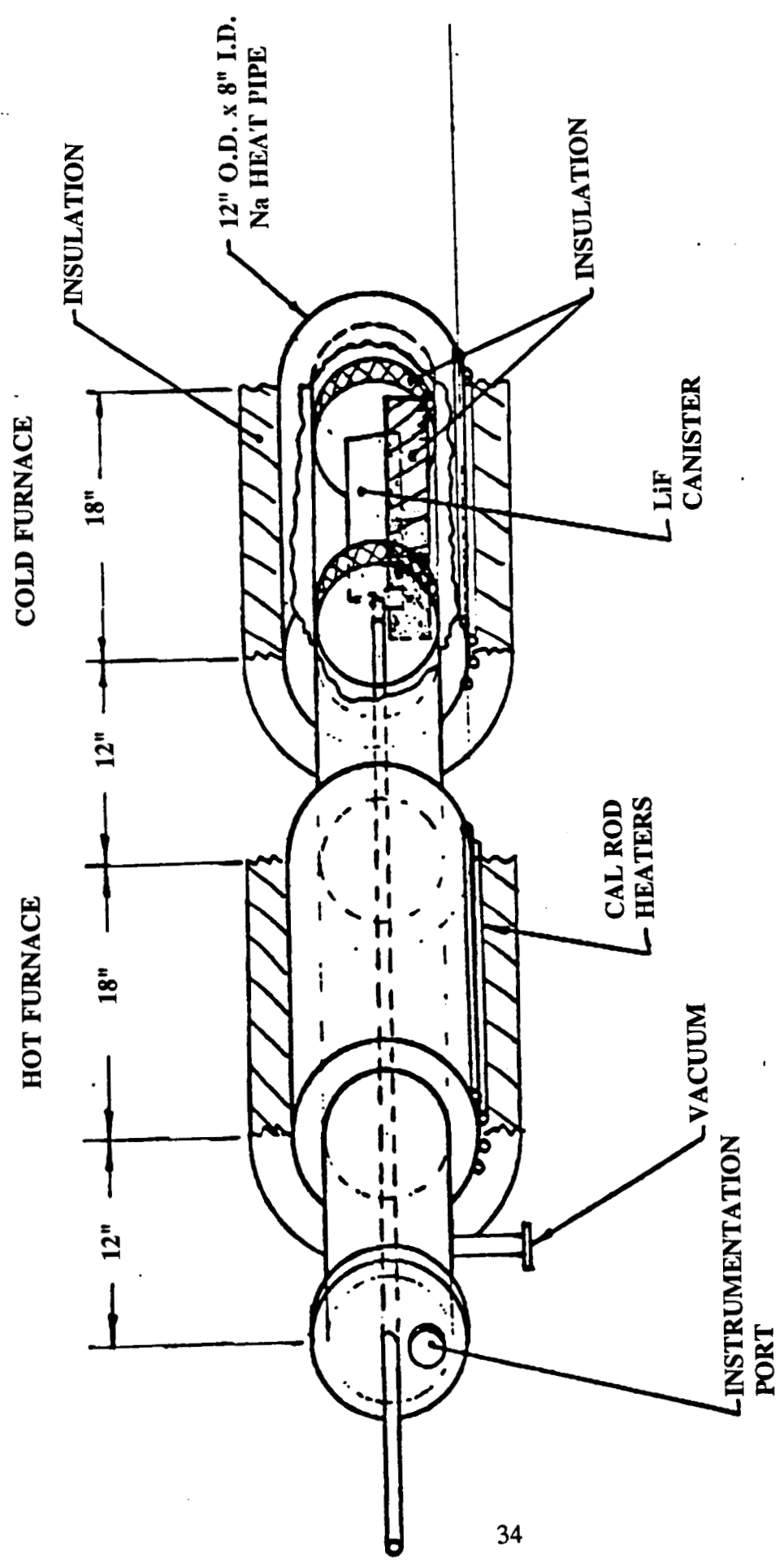


Figure 18 - ANNULAR HEAT PIPE FURNACE

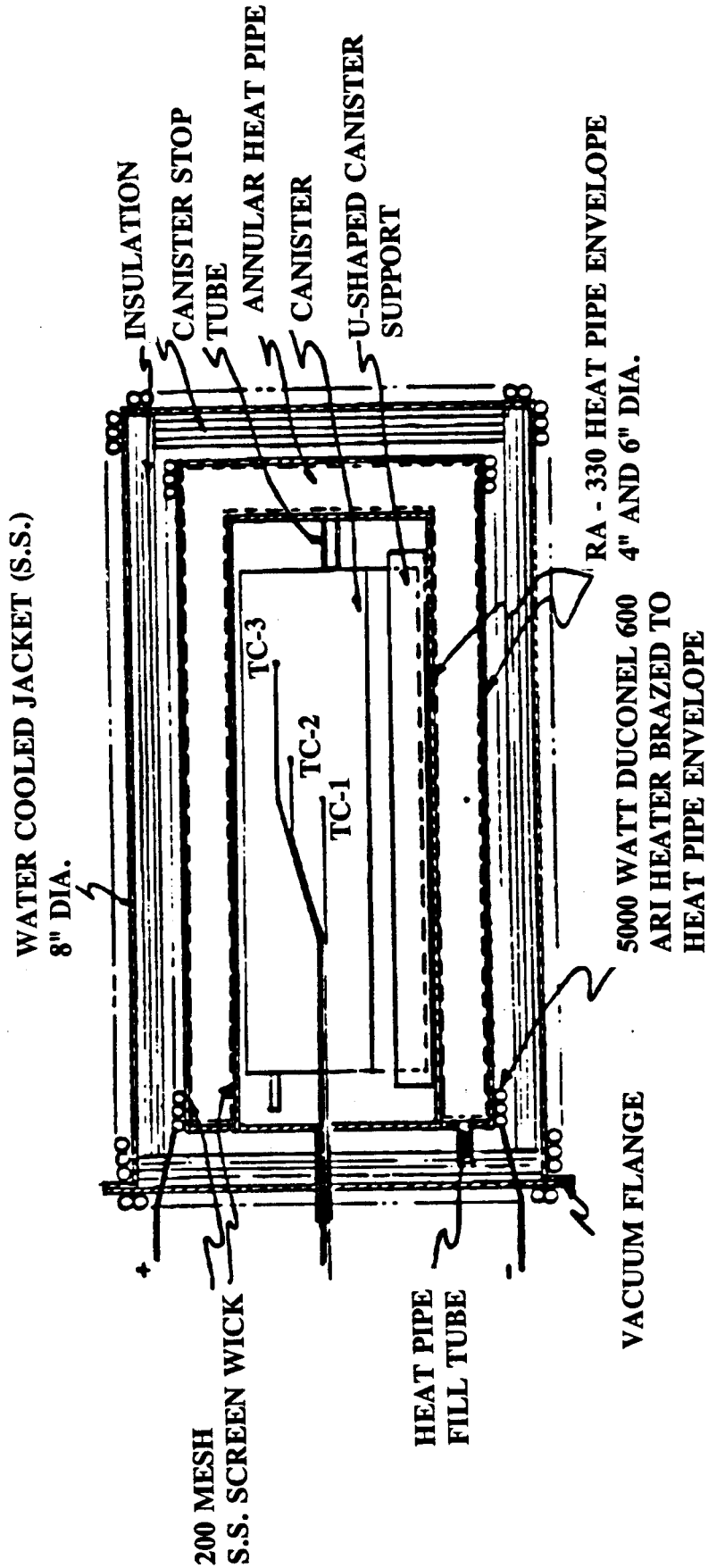


Figure 19 - CANISTER IN HP VAPOR SPACE

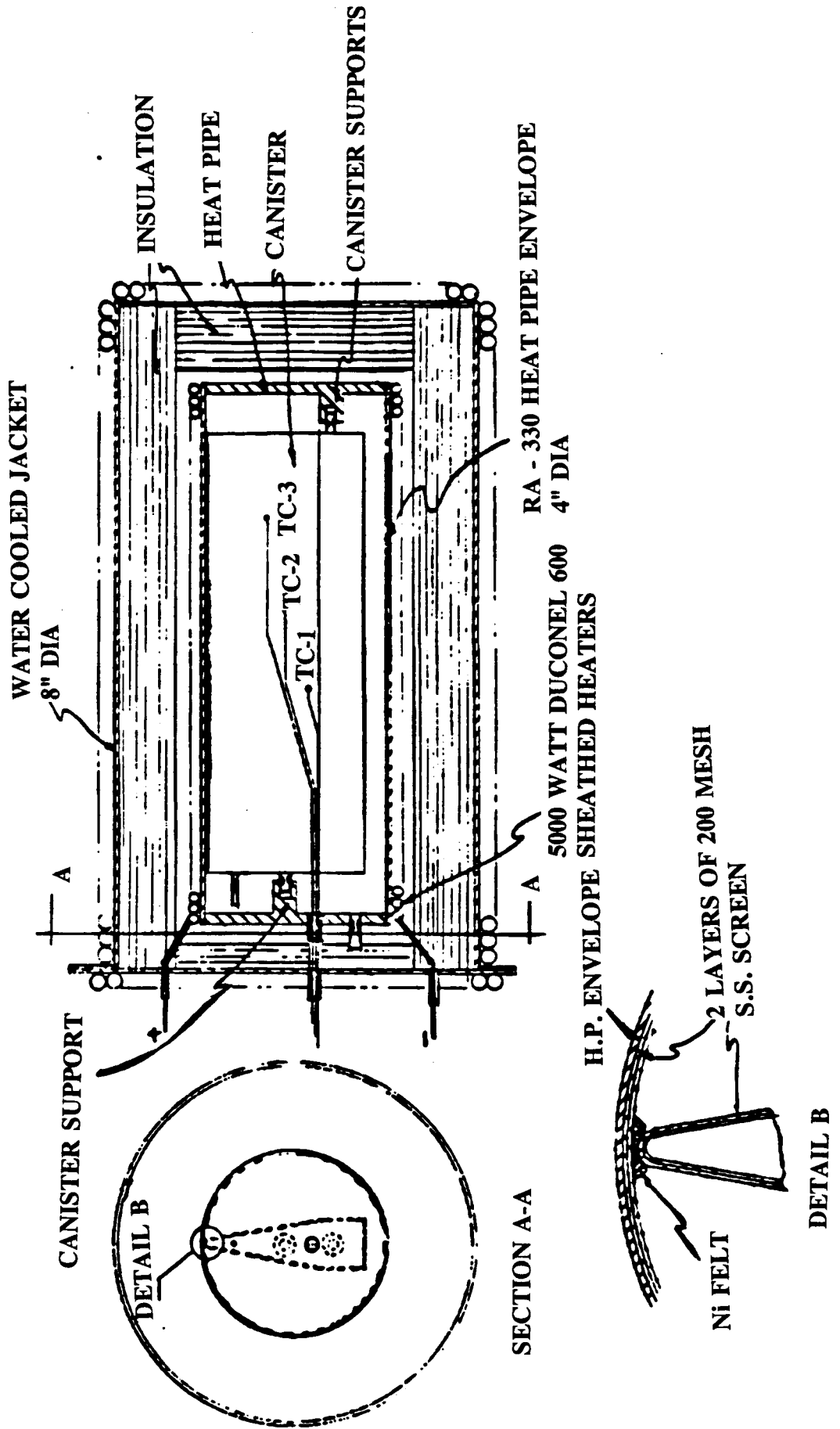
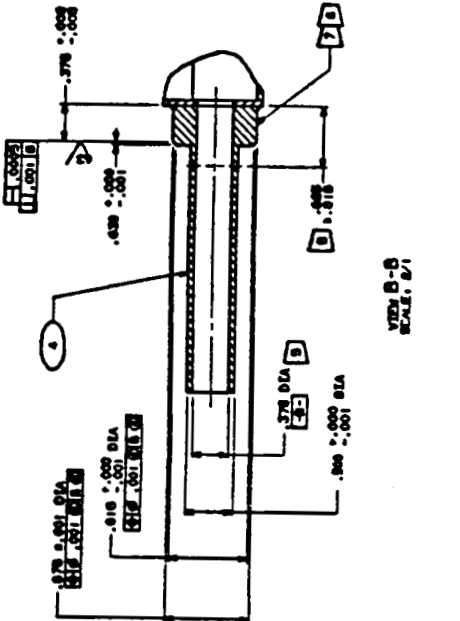


Table VII - CANISTER DESIGN AND ANALYSIS

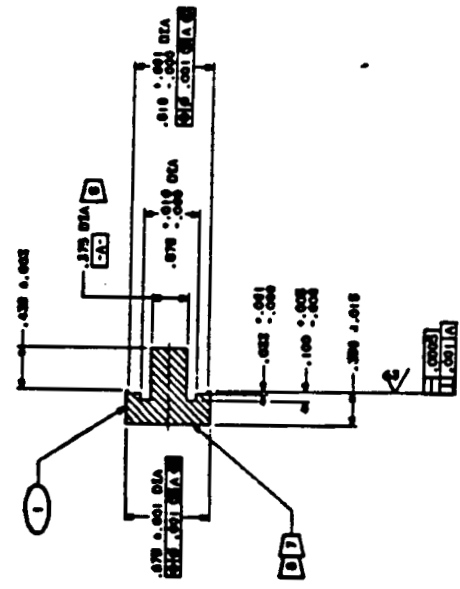
CASE	QTY CANISTERS	SIZE INCHES	RECEIVER SPECIFIC WT, KG/KWE	PREDICTED DELTA-T, °F
1	16	INTEGRAL (PROPOSAL) 3.56 x 4.16 x 15.9	13.2	458
2	24	SEPARATE 2.25 x 3.77 x 15.9	15.1	267
3	32	SEPARATE 1.4 x 3.44 x 19.5	16.6	213
4	32	SEPARATE 1.1 x 3.5 x 24	18.1	173
5	32	SEPARATE 1.1 x 3.5 x 24 NO INSULATION	18.1	81
6	32	SEPARATE 1.4 x 2.2 x 24	20.6	186



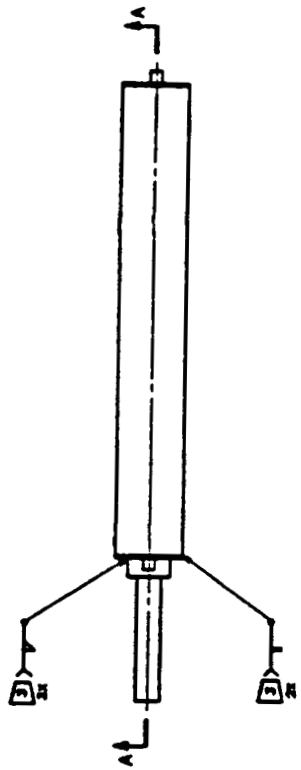
- 1 INTERPRET DIMENSIONS PER ASME Y14.5-1993 AND UNLESS OTHERWISE SPECIFIED
- 2 ALL DIMENSIONS ARE IN INCHES
- 3 SURFACES UNLESS OTHERWISE SPECIFIED ARE TO BE FINISHED TO A 32 RMS SURFACE FINISH UNLESS OTHERWISE SPECIFIED
- 4 MATERIALS ARE TO BE 1515 CLASS II, 0
- 5 SURFACES TO BE FINISHED TO A 32 RMS SURFACE FINISH UNLESS OTHERWISE SPECIFIED
- 6 DIMENSIONS ARE TO BE AS SHOWN UNLESS OTHERWISE SPECIFIED
- 7 DIMENSIONS ARE TO BE AS SHOWN UNLESS OTHERWISE SPECIFIED
- 8 DIMENSIONS ARE TO BE AS SHOWN UNLESS OTHERWISE SPECIFIED
- 9 DIMENSIONS ARE TO BE AS SHOWN UNLESS OTHERWISE SPECIFIED



END CAP  
SCALE: 2/1



END CAP  
SCALE: 2/1



SECTION A-A

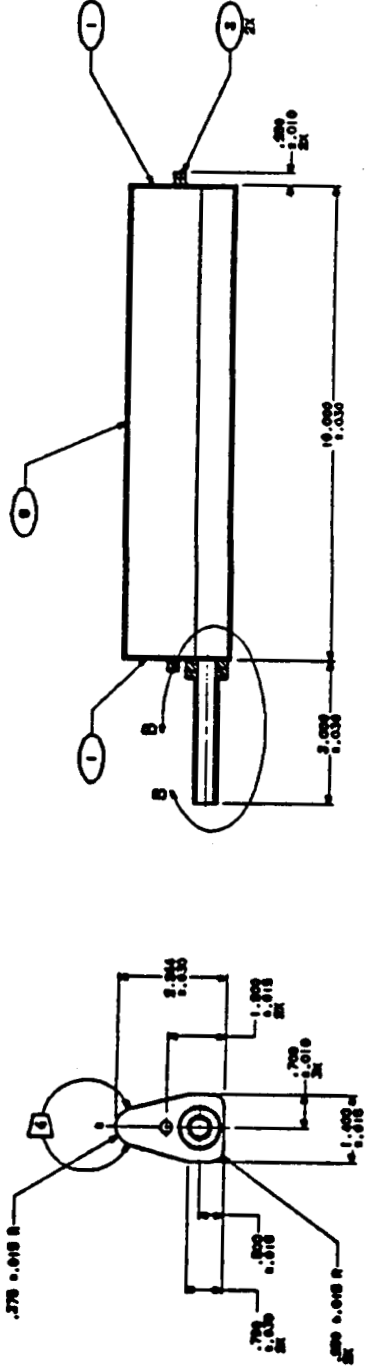


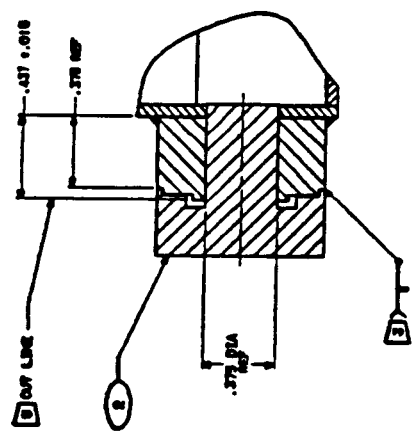
Figure 20 - TEST CANISTER DESIGN

QTY	QTY	PART NUMBER	MATERIAL
1	1	EP2000-711-1	INCOEL 600
2	2	EP2000-711-2	INCOEL 617
2	2	EP2000-711-3	INCOEL 600
1	1	EP2000-711-4	INCOEL 600

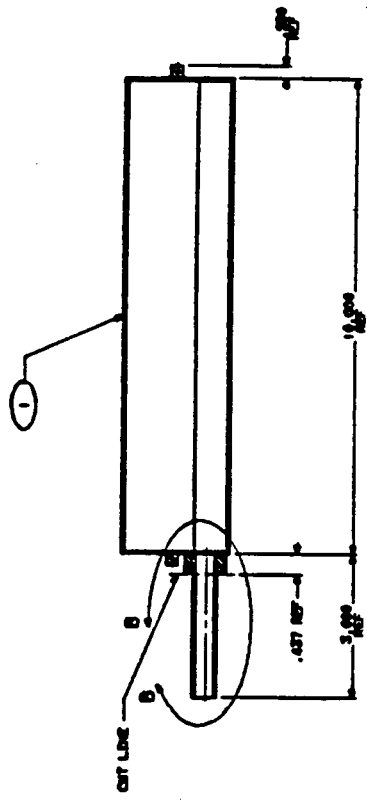
PARTS LIST			
1	END CAP, .375 DIA, .130 TH, .015 DIA HOLE	INCOEL 600	END CAP, .375 DIA, .130 TH, .015 DIA HOLE
2	END COVER, .375 DIA, .015 DIA HOLE	INCOEL 617	END COVER, .375 DIA, .015 DIA HOLE
2	SUPPORTS, .375 DIA, .015 DIA HOLE	INCOEL 600	SUPPORTS, .375 DIA, .015 DIA HOLE
1	PELL TUBE, .375 DIA, .015 DIA HOLE	INCOEL 600	PELL TUBE, .375 DIA, .015 DIA HOLE

TEST CANISTER FABRICATION			
DATE	BY	CHKD	APP'D

UNLESS OTHERWISE SPECIFIED:  
 1. INTERPRET DIMENSIONS PER ASME Y14.5M-1993.  
 2. ALL DIMENSIONS ARE IN INCHES.  
 3. DIMENSIONS SHOWN ARE PER UNLESS OTHERWISE SPECIFIED PER FIG. 11, Q. II.  
 4. 100% INSPECTION.  
 5. PHOTOGRAPHIC PROOF REQUIRED FOR ACCEPTANCE PER FIG. 11, Q. II.  
 6. DISCONTINUITIES PER FIG. 10114 CLASS II, (C).  
 7. FINISH: SURFACE TO BE AS SHOWN.  
 8. DIMENSIONS TO CENTER UNLESS OTHERWISE SPECIFIED.  
 9. DIMENSIONS TO CENTER UNLESS OTHERWISE SPECIFIED.  
 10. DIMENSIONS TO CENTER UNLESS OTHERWISE SPECIFIED.  
 11. DIMENSIONS TO CENTER UNLESS OTHERWISE SPECIFIED.  
 12. DIMENSIONS TO CENTER UNLESS OTHERWISE SPECIFIED.  
 13. DIMENSIONS TO CENTER UNLESS OTHERWISE SPECIFIED.  
 14. DIMENSIONS TO CENTER UNLESS OTHERWISE SPECIFIED.  
 15. DIMENSIONS TO CENTER UNLESS OTHERWISE SPECIFIED.  
 16. DIMENSIONS TO CENTER UNLESS OTHERWISE SPECIFIED.  
 17. DIMENSIONS TO CENTER UNLESS OTHERWISE SPECIFIED.  
 18. DIMENSIONS TO CENTER UNLESS OTHERWISE SPECIFIED.  
 19. DIMENSIONS TO CENTER UNLESS OTHERWISE SPECIFIED.  
 20. DIMENSIONS TO CENTER UNLESS OTHERWISE SPECIFIED.  
 21. DIMENSIONS TO CENTER UNLESS OTHERWISE SPECIFIED.  
 22. DIMENSIONS TO CENTER UNLESS OTHERWISE SPECIFIED.  
 23. DIMENSIONS TO CENTER UNLESS OTHERWISE SPECIFIED.  
 24. DIMENSIONS TO CENTER UNLESS OTHERWISE SPECIFIED.  
 25. DIMENSIONS TO CENTER UNLESS OTHERWISE SPECIFIED.  
 26. DIMENSIONS TO CENTER UNLESS OTHERWISE SPECIFIED.  
 27. DIMENSIONS TO CENTER UNLESS OTHERWISE SPECIFIED.  
 28. DIMENSIONS TO CENTER UNLESS OTHERWISE SPECIFIED.  
 29. DIMENSIONS TO CENTER UNLESS OTHERWISE SPECIFIED.  
 30. DIMENSIONS TO CENTER UNLESS OTHERWISE SPECIFIED.  
 31. DIMENSIONS TO CENTER UNLESS OTHERWISE SPECIFIED.  
 32. DIMENSIONS TO CENTER UNLESS OTHERWISE SPECIFIED.  
 33. DIMENSIONS TO CENTER UNLESS OTHERWISE SPECIFIED.  
 34. DIMENSIONS TO CENTER UNLESS OTHERWISE SPECIFIED.  
 35. DIMENSIONS TO CENTER UNLESS OTHERWISE SPECIFIED.  
 36. DIMENSIONS TO CENTER UNLESS OTHERWISE SPECIFIED.  
 37. DIMENSIONS TO CENTER UNLESS OTHERWISE SPECIFIED.  
 38. DIMENSIONS TO CENTER UNLESS OTHERWISE SPECIFIED.  
 39. DIMENSIONS TO CENTER UNLESS OTHERWISE SPECIFIED.  
 40. DIMENSIONS TO CENTER UNLESS OTHERWISE SPECIFIED.  
 41. DIMENSIONS TO CENTER UNLESS OTHERWISE SPECIFIED.  
 42. DIMENSIONS TO CENTER UNLESS OTHERWISE SPECIFIED.  
 43. DIMENSIONS TO CENTER UNLESS OTHERWISE SPECIFIED.  
 44. DIMENSIONS TO CENTER UNLESS OTHERWISE SPECIFIED.  
 45. DIMENSIONS TO CENTER UNLESS OTHERWISE SPECIFIED.  
 46. DIMENSIONS TO CENTER UNLESS OTHERWISE SPECIFIED.  
 47. DIMENSIONS TO CENTER UNLESS OTHERWISE SPECIFIED.  
 48. DIMENSIONS TO CENTER UNLESS OTHERWISE SPECIFIED.  
 49. DIMENSIONS TO CENTER UNLESS OTHERWISE SPECIFIED.  
 50. DIMENSIONS TO CENTER UNLESS OTHERWISE SPECIFIED.  
 51. DIMENSIONS TO CENTER UNLESS OTHERWISE SPECIFIED.  
 52. DIMENSIONS TO CENTER UNLESS OTHERWISE SPECIFIED.  
 53. DIMENSIONS TO CENTER UNLESS OTHERWISE SPECIFIED.  
 54. DIMENSIONS TO CENTER UNLESS OTHERWISE SPECIFIED.  
 55. DIMENSIONS TO CENTER UNLESS OTHERWISE SPECIFIED.  
 56. DIMENSIONS TO CENTER UNLESS OTHERWISE SPECIFIED.  
 57. DIMENSIONS TO CENTER UNLESS OTHERWISE SPECIFIED.  
 58. DIMENSIONS TO CENTER UNLESS OTHERWISE SPECIFIED.  
 59. DIMENSIONS TO CENTER UNLESS OTHERWISE SPECIFIED.  
 60. DIMENSIONS TO CENTER UNLESS OTHERWISE SPECIFIED.  
 61. DIMENSIONS TO CENTER UNLESS OTHERWISE SPECIFIED.  
 62. DIMENSIONS TO CENTER UNLESS OTHERWISE SPECIFIED.  
 63. DIMENSIONS TO CENTER UNLESS OTHERWISE SPECIFIED.  
 64. DIMENSIONS TO CENTER UNLESS OTHERWISE SPECIFIED.  
 65. DIMENSIONS TO CENTER UNLESS OTHERWISE SPECIFIED.  
 66. DIMENSIONS TO CENTER UNLESS OTHERWISE SPECIFIED.  
 67. DIMENSIONS TO CENTER UNLESS OTHERWISE SPECIFIED.  
 68. DIMENSIONS TO CENTER UNLESS OTHERWISE SPECIFIED.  
 69. DIMENSIONS TO CENTER UNLESS OTHERWISE SPECIFIED.  
 70. DIMENSIONS TO CENTER UNLESS OTHERWISE SPECIFIED.  
 71. DIMENSIONS TO CENTER UNLESS OTHERWISE SPECIFIED.  
 72. DIMENSIONS TO CENTER UNLESS OTHERWISE SPECIFIED.  
 73. DIMENSIONS TO CENTER UNLESS OTHERWISE SPECIFIED.  
 74. DIMENSIONS TO CENTER UNLESS OTHERWISE SPECIFIED.  
 75. DIMENSIONS TO CENTER UNLESS OTHERWISE SPECIFIED.  
 76. DIMENSIONS TO CENTER UNLESS OTHERWISE SPECIFIED.  
 77. DIMENSIONS TO CENTER UNLESS OTHERWISE SPECIFIED.  
 78. DIMENSIONS TO CENTER UNLESS OTHERWISE SPECIFIED.  
 79. DIMENSIONS TO CENTER UNLESS OTHERWISE SPECIFIED.  
 80. DIMENSIONS TO CENTER UNLESS OTHERWISE SPECIFIED.  
 81. DIMENSIONS TO CENTER UNLESS OTHERWISE SPECIFIED.  
 82. DIMENSIONS TO CENTER UNLESS OTHERWISE SPECIFIED.  
 83. DIMENSIONS TO CENTER UNLESS OTHERWISE SPECIFIED.  
 84. DIMENSIONS TO CENTER UNLESS OTHERWISE SPECIFIED.  
 85. DIMENSIONS TO CENTER UNLESS OTHERWISE SPECIFIED.  
 86. DIMENSIONS TO CENTER UNLESS OTHERWISE SPECIFIED.  
 87. DIMENSIONS TO CENTER UNLESS OTHERWISE SPECIFIED.  
 88. DIMENSIONS TO CENTER UNLESS OTHERWISE SPECIFIED.  
 89. DIMENSIONS TO CENTER UNLESS OTHERWISE SPECIFIED.  
 90. DIMENSIONS TO CENTER UNLESS OTHERWISE SPECIFIED.  
 91. DIMENSIONS TO CENTER UNLESS OTHERWISE SPECIFIED.  
 92. DIMENSIONS TO CENTER UNLESS OTHERWISE SPECIFIED.  
 93. DIMENSIONS TO CENTER UNLESS OTHERWISE SPECIFIED.  
 94. DIMENSIONS TO CENTER UNLESS OTHERWISE SPECIFIED.  
 95. DIMENSIONS TO CENTER UNLESS OTHERWISE SPECIFIED.  
 96. DIMENSIONS TO CENTER UNLESS OTHERWISE SPECIFIED.  
 97. DIMENSIONS TO CENTER UNLESS OTHERWISE SPECIFIED.  
 98. DIMENSIONS TO CENTER UNLESS OTHERWISE SPECIFIED.  
 99. DIMENSIONS TO CENTER UNLESS OTHERWISE SPECIFIED.  
 100. DIMENSIONS TO CENTER UNLESS OTHERWISE SPECIFIED.



SEE FIG. 11  
 (80% OF TOTAL)



SECTION A-A

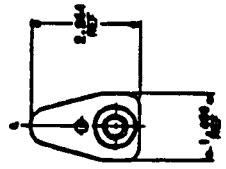


Figure 21 - TEST CANISTER CLOSURE DESIGN

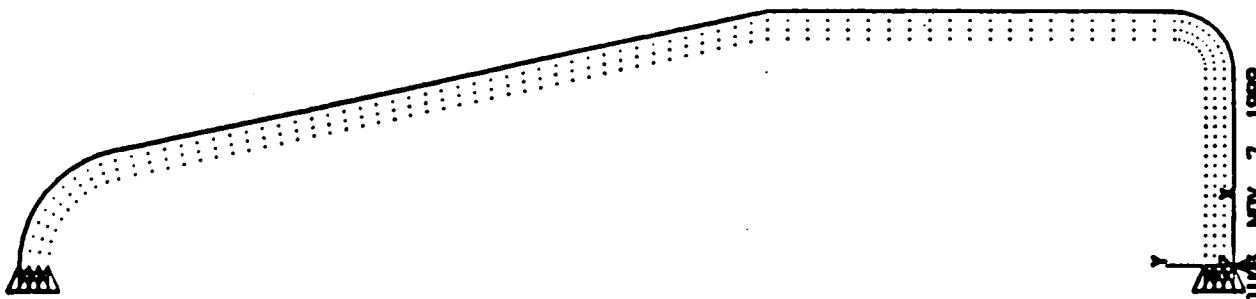
NO	QTY	PART NUMBER	MATERIAL	PARTS LIST
1	1	EP2809-711-2	INCONEL	CANISTER, PARTICULATE
2	1	EP2809-711-1	INCONEL	END CAP

REV	DATE	BY	CHKD
1			
2			
3			
4			
5			
6			
7			
8			
9			
10			
11			
12			
13			
14			
15			
16			
17			
18			
19			
20			
21			
22			
23			
24			
25			
26			
27			
28			
29			
30			
31			
32			
33			
34			
35			
36			
37			
38			
39			
40			
41			
42			
43			
44			
45			
46			
47			
48			
49			
50			
51			
52			
53			
54			
55			
56			
57			
58			
59			
60			
61			
62			
63			
64			
65			
66			
67			
68			
69			
70			
71			
72			
73			
74			
75			
76			
77			
78			
79			
80			
81			
82			
83			
84			
85			
86			
87			
88			
89			
90			
91			
92			
93			
94			
95			
96			
97			
98			
99			
100			

EP2809-712  
 CANISTER, CLOSURE  
 LITHIUM FLUORIDE  
 EP 99167/EP2809-712

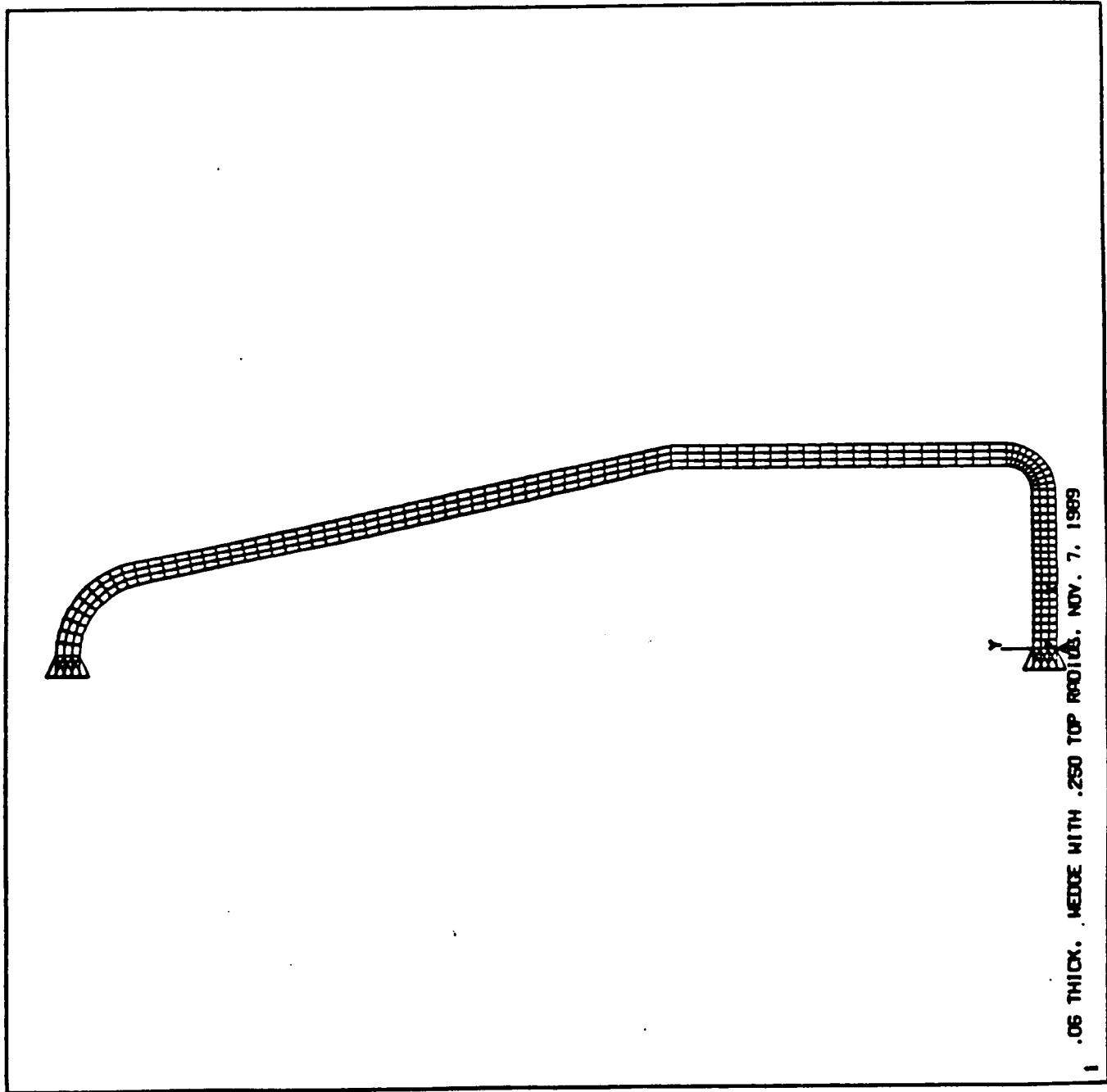


RMSYS 4.3  
NOV 7 1969  
17.51.36  
PLOT NO. 3  
PREP7 NODES  
TD15 BC  
PRES BC  
ZV=1  
DIST=1.43  
XF=.276  
YF=1.3  
MX=15  
MY=15  
NCON=18  
VMIN=15



1  
.06 THICK. WEDGE WITH .250 TOP RADIUS. NOV. 7, 1969

ANSYS 4.3  
NOV 7 1989  
17:51:33  
PLOT NO. 2  
PREP7 ELEMENTS  
T01S BC  
PRES BC  
ZV=1  
DIST=1.43  
XF=.275  
YF=1.3  
MX=15  
MY=15  
NCON=18  
VMIN=15



.06 THICK. WEDGE WITH .250 TOP RADIUS. NOV. 7, 1989

Figure 23 - TYPICAL CANISTER FINITE ELEMENT PLOT

weight was performed. Results are shown in Table VIII. Also shown are results of an alternate canister geometry, namely, a triangular shape. This shape was presented in the Sundstrand proposal as a simpler design to fabricate, but one that could present some packaging problems. An elemental plot of a typical triangular geometry is shown in Figure 24.

### 3.2.4 Initial Safety Assessment

A safety assessment per the reliability and quality requirements of the contract was completed. Appendix A contains two memos generated from this safety assessment. The testing was performed in a hazardous laboratory with proper safeguards for both personnel and equipment. No special problems were found during the assessment. A final safety walk-through was conducted with the test apparatus and test article in place prior to the commencement of testing.

## 4.0 HARDWARE FABRICATION

### 4.1 Canister Fabrication

Tempe Precision, Tempe, Arizona was selected to fabricate the four canisters. The canisters are Tungsten Inert Gas (TIG) arc weldments, fabricated from 1.524 mm (0.060 inch) thick Inconel 617 sheet stock. Two axial weld lines were used to minimize the bending tooling costs. Figures 25a, b and c show photographs of the canisters before the end plates were welded. Note that two of the canisters contain nickel foam inserts.

### 4.2 Procurement of Nickel Foam

Analysis had indicated that the nickel foam should fill at least 10 percent of the volume in order to appreciably enhance the thermal conductivity. A foam with 3.94 pores per mm (100 ppi) was specified to meet this requirement. However, difficulties were encountered procuring a foam of this density because of cost and lead time constraints. A revision was made to the foam density requirements to allow a foam density of 2.362 pores per mm (60 ppi). The foam was procured from Astromet Corporation in a rough cut form. Final sizing of the foam was performed by Tempe Precision.

### 4.3 Reduction of Nickel Foam

Tests performed by Boeing researchers indicated that metal oxides on the nickel foam adversely affect the wicking ability of the matrix [5]. In order to improve the wicking ability of the nickel foam, a hydrogen reduction process was used to remove oxides on the foam surface. This process was performed in a modified vacuum furnace at Progressive Steel Treating, Inc., Loves Park, Illinois. The process served both to reduce oxides and to anneal the canisters.

The furnace was vacuum-baked for one day to remove impurities, and was plumbed with a gas inlet line to allow introduction of an ultra-high purity 95 percent argon, 5 percent hydrogen mixture for the reduction process. The plumbing schematic is shown in Figure 26. Figure 27 shows the gas inlet line complete with venturi flow meter, pressure gauges, oxygen-consuming material capsule (called an oxygen getter), and shut-off valve. In Figure 28, a view into the vacuum furnace, one can see the gas inlet line as it feeds

Table VIII - RESULTS OF ANSYS STRESS ANALYSIS

CONFIGURATION	SHAPE	WALL THICKNESS		NOSE RADIUS		PRESSURE LOADING		MAX STRESS	
		MM	(INCH)	MM	(INCH)	kPa	(PSID)	MPa	(PSI)
1	Wedge	0.838	.033	3.175	.125	103.4	15	487.9	70,770
2	Wedge	1.524	.060	3.175	.125	103.4	15	172.7	25,053
3	Wedge	1.524	.060	6.350	.250	103.4	15	101.8	14,763
4	Triangular	0.838	.033	3.175	.125	103.4	15	216.5	31,394
5	Triangular	1.524	.060	3.175	.125	103.4	15	72.5	10,514
6	Wedge	1.524	.060	9.525	.375	103.4	15	61.0	8,854

Inconel 617

1255K (1800°F)  $F_y = 96.5 \text{ MPa (14 ksi) x .95 factor} = 91.7 \text{ MPa (13.3 ksi)}$

1144K (1600°F)  $F_y = 172.4 \text{ MPa (25 ksi) x .95 factor} = 163.8 \text{ MPa (23.8 ksi)}$

$F_y =$  yield strength

ANSYS 4.3

NOV 3 1989

14.47.27

PLOT NO. 1

PREP7 ELEMENTS

T01S BC

PRES BC

ZV=1

DIST=.107

XF=.554

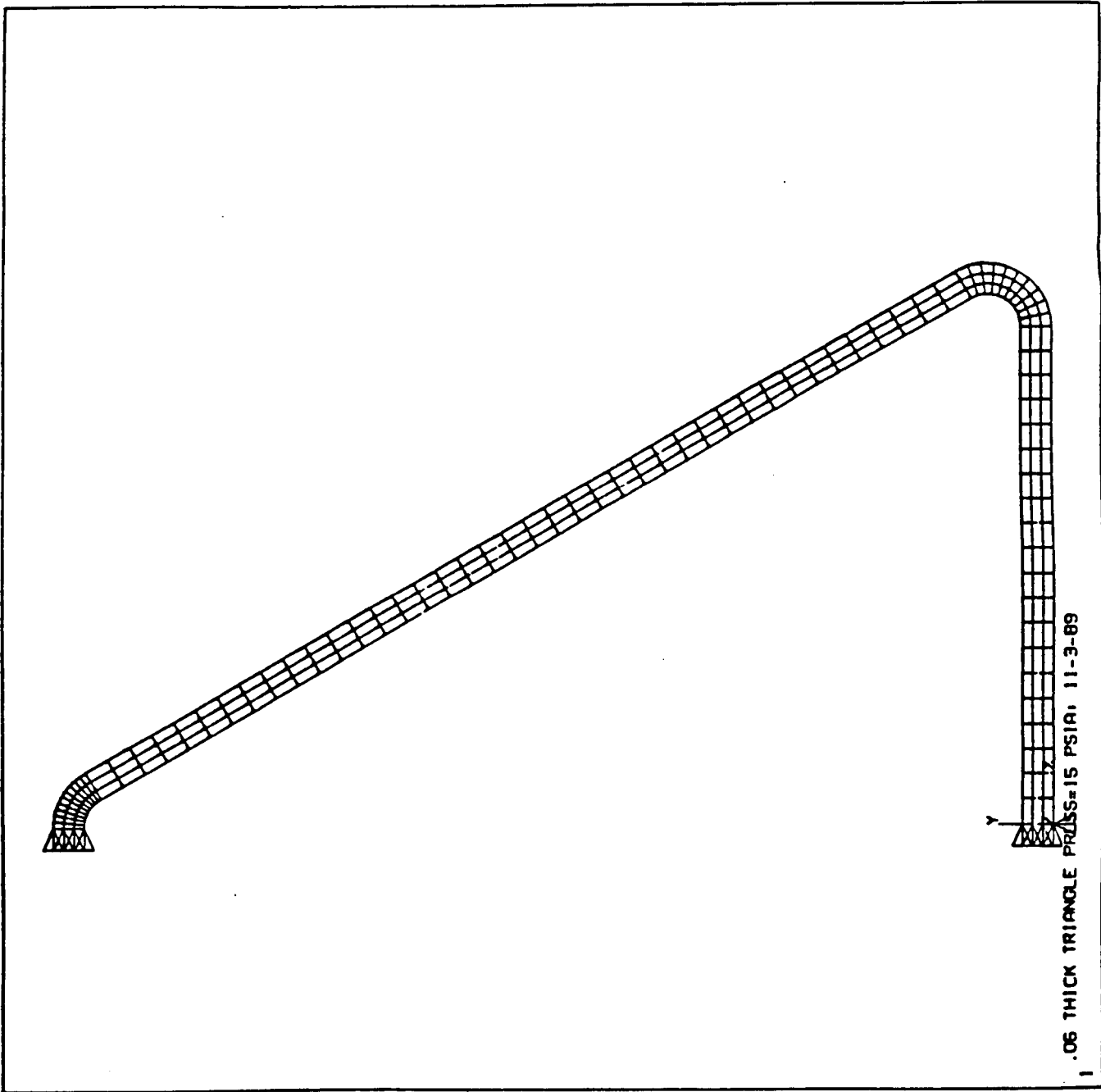
YF=.976

MX=15

MN=15

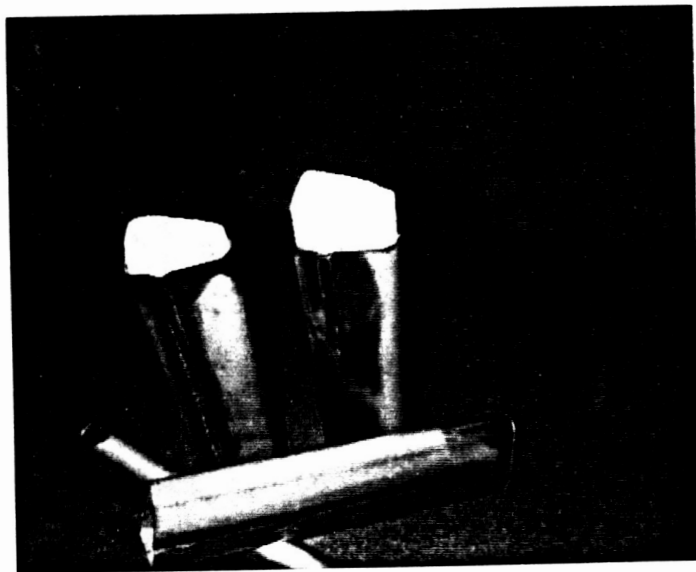
NCON=18

VMIN=15

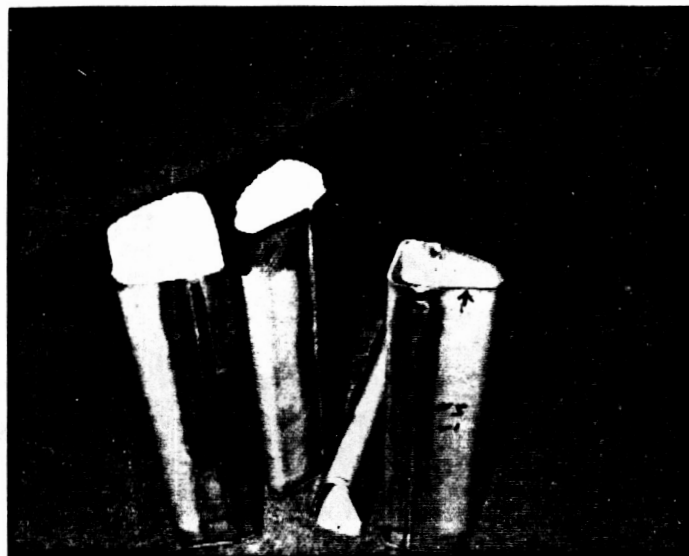


.06 THICK TRIANGLE PRSS=15 PSIA: 11-3-89

ORIGINAL PAGE  
BLACK AND WHITE PHOTOGRAPH



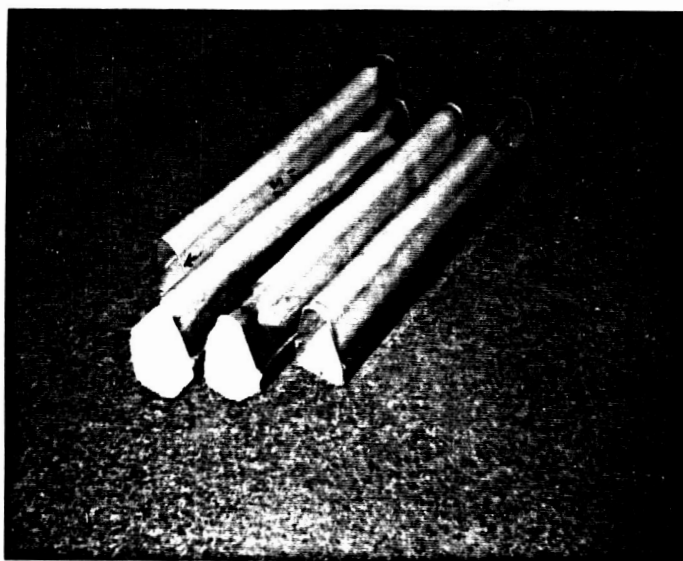
(a)



(b)

Figure 25 - INCONEL 617 CANISTERS BEING PROCESSED AT  
TEMPE PRECISION, TWO WITH Ni FOAM AND TWO WITHOUT

ORIGINAL PAGE  
BLACK AND WHITE PHOTOGRAPH



(c)

**Figure 25 (Continued)**

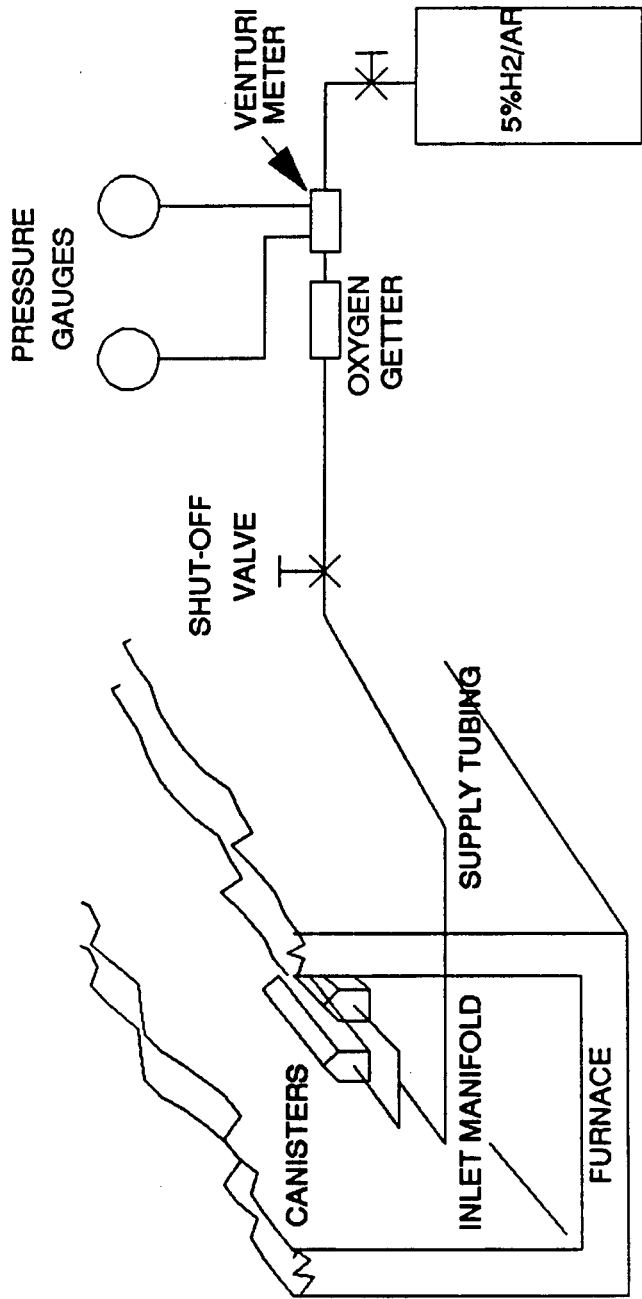


Figure 26 - HEAT TREAT/REDUCTION LAYOUT



ORIGINAL PAGE  
BLACK AND WHITE PHOTOGRAPH

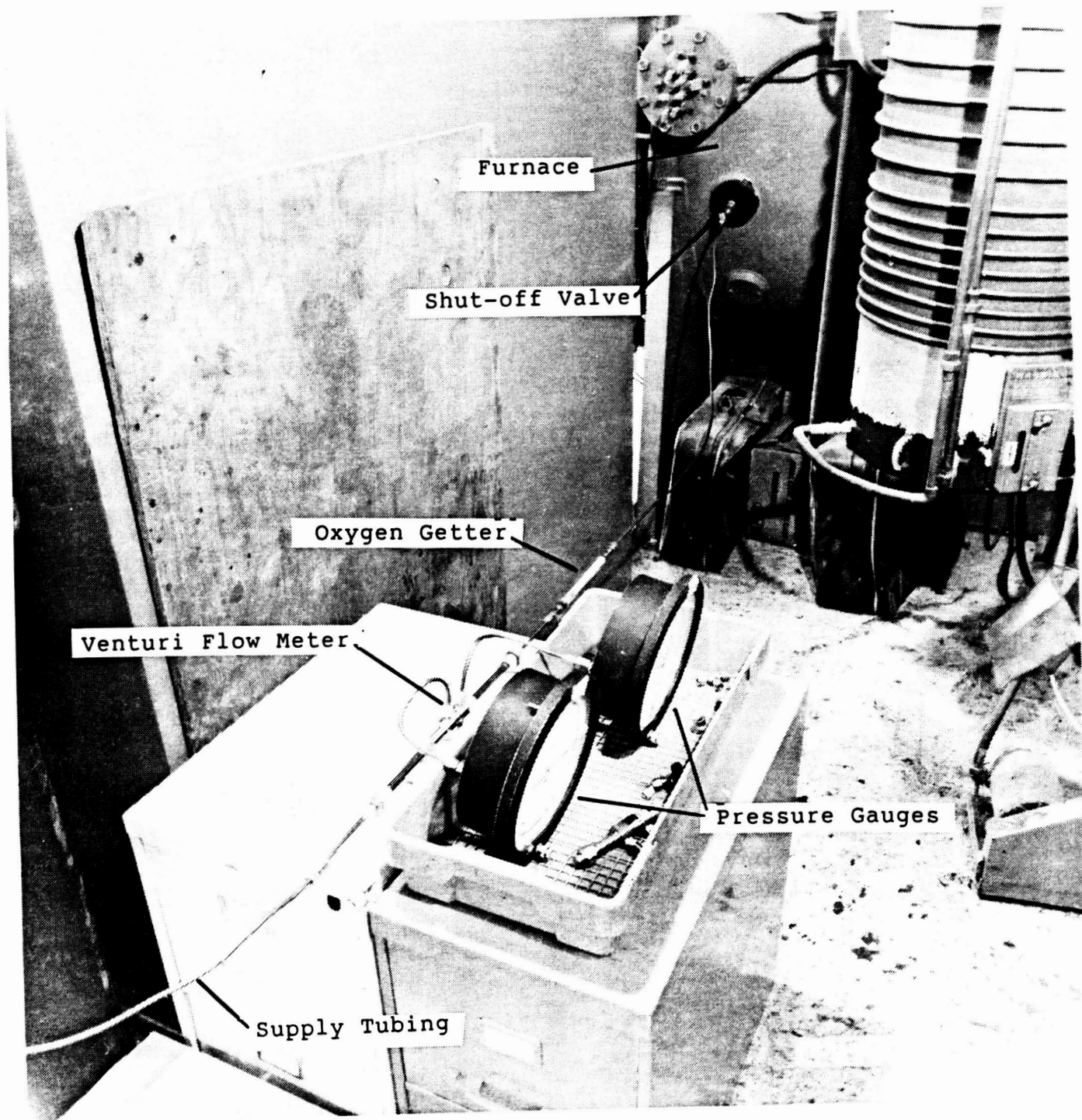


Figure 27 - GAS SUPPLY LINE

ORIGINAL PAGE  
BLACK AND WHITE PHOTOGRAPH

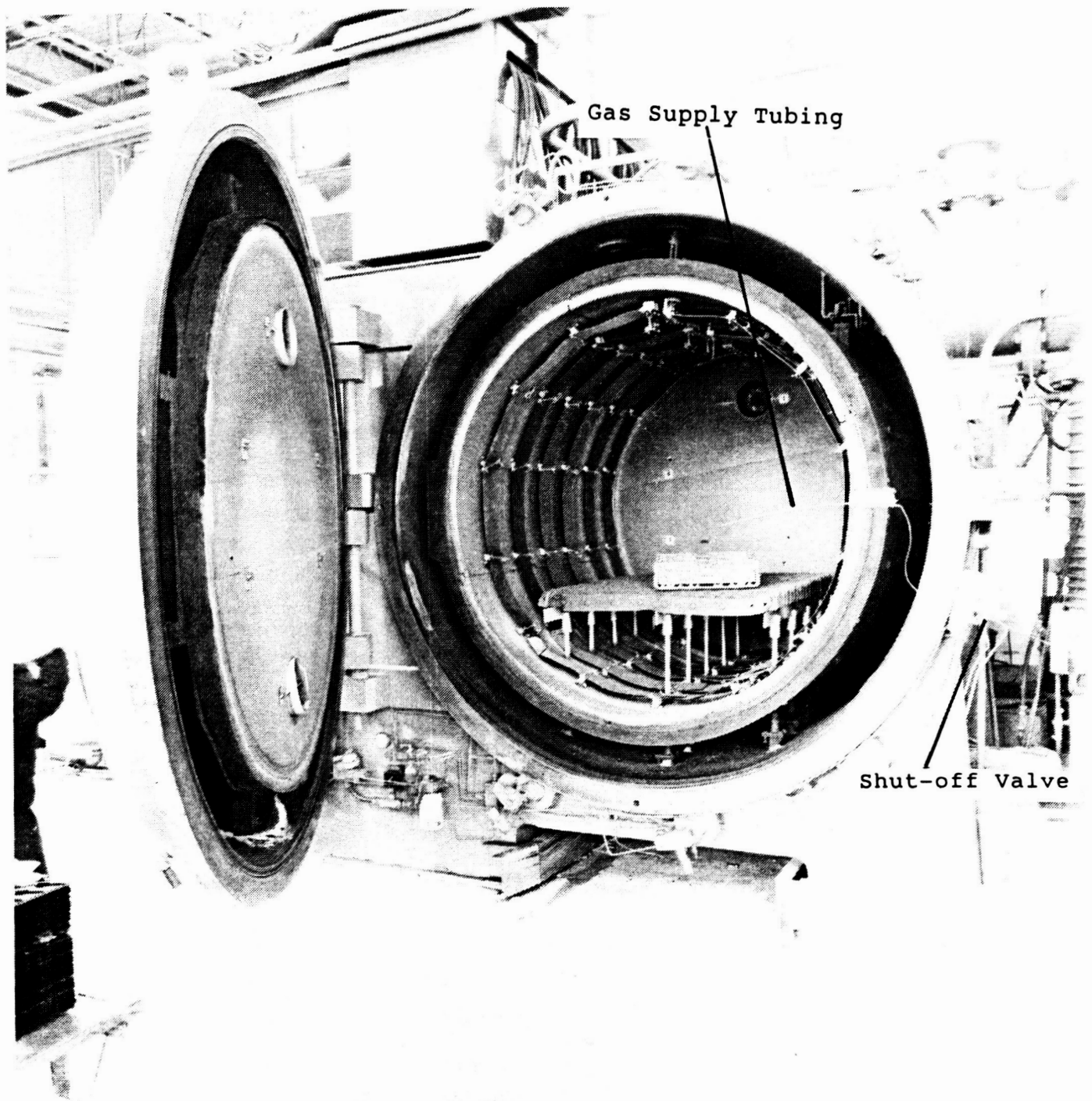


Figure 28 - VACUUM FURNACE

through the furnace wall to the tray holding the canisters. Finally, the gas flow is split into two gas injection tubes, as shown in Figure 29, where it enters the canisters. Blocks of nickel foam were also set in the tray in order to test the quality of the reducing atmosphere in the furnace. As an aside, a photograph of the control panel for the furnace, Figure 30, has been included.

The gas plumbing and the entire furnace were leak-checked with a helium leak detector by a vacuum furnace consultant. The consultant also provided guidance on the entire anneal and reduction process. All four canisters were processed at the same time. Gas inlet lines were fed into the two nickel-foam filled canisters, and the two empty canisters were placed at the back of the furnace. Process data, including temperature and pressure, were recorded and are included in Appendix B.

The furnace cycle, which is detailed in Appendix B, went as planned. When the temperature had fallen to 1255K (1800°F), the gas flow was started and adjusted to a mixture flow of 0.131 g/s (2.88E-04 LBM/S). This flow is about 24 times the necessary flow, but was the lowest setting at which the flow could be controlled due to internal leaks in the gas tank pressure regulator. During the reduction portion of the cycle, the furnace pressure was held at 75  $\mu$ m of Hg. After the reduction process was completed, the furnace was force-cooled with liquid nitrogen boil-off, and at 2:10 p.m. the canisters were removed from the oven. (The canisters were purged for five minutes with a flow of 0.19 g/s (4.09E-04 LBM/S) of the gas mixture to ensure that they were filled with inert gas.) The nickel-filled canisters were removed from the oven and capped immediately in special clamping fixtures as shown in Figure 31. The elastomeric seal on the temporary cap forms a leak-tight seal for small temperature differences. Thus, it was important that the canisters were allowed to cool to room temperature in the vacuum atmosphere before capping them. Figure 32 shows a canister that is clamped in a clamping fixture. Upon handling these canisters we noticed oxides coating the outer Inconel surfaces and the stainless steel tubing. Also, the furnace door had a 30 cm (1 ft) diameter darkened spot where impurity-laden gas had impinged on the door. Further inspection of the gas tubing showed that even the inner surface of the tubing was covered with a black oxide. This led us to believe that either the bottle of gas had excessive contaminants or air was leaking into the subatmospheric gas plumbing.

One of the nickel-filled canisters was inspected with a boro-scope, and as expected, the nickel foam had a gray, matte appearance, indicating that oxides had not been significantly reduced. The non-filled canisters seemed unaffected by the impurities issuing from the filled canisters, and thus were used as is. As an aside, another possible source of contaminants is the nickel foam itself since it is produced by using organic binders. However, these contaminants are not likely the only ones present since the tubing inner surface had an oxide coating over more than one meter (3 ft) of its length, indicating that contaminants were probably coming from the gas supply line.

Some apparatus changes were made to remedy this problem in the next furnace cycle. All plumbing was acetone cleansed and vapor degreased. All plumbing outside the furnace was maintained at super-atmospheric pressure to obviate the possibility of air leaking into the H<sub>2</sub>/Ar gas flow. The entire plumbing assembly was leak-checked with the "bubble-check" method to further preclude the chance of air ingress to the H<sub>2</sub>/Ar flow.

ORIGINAL PAGE  
BLACK AND WHITE PHOTOGRAPH

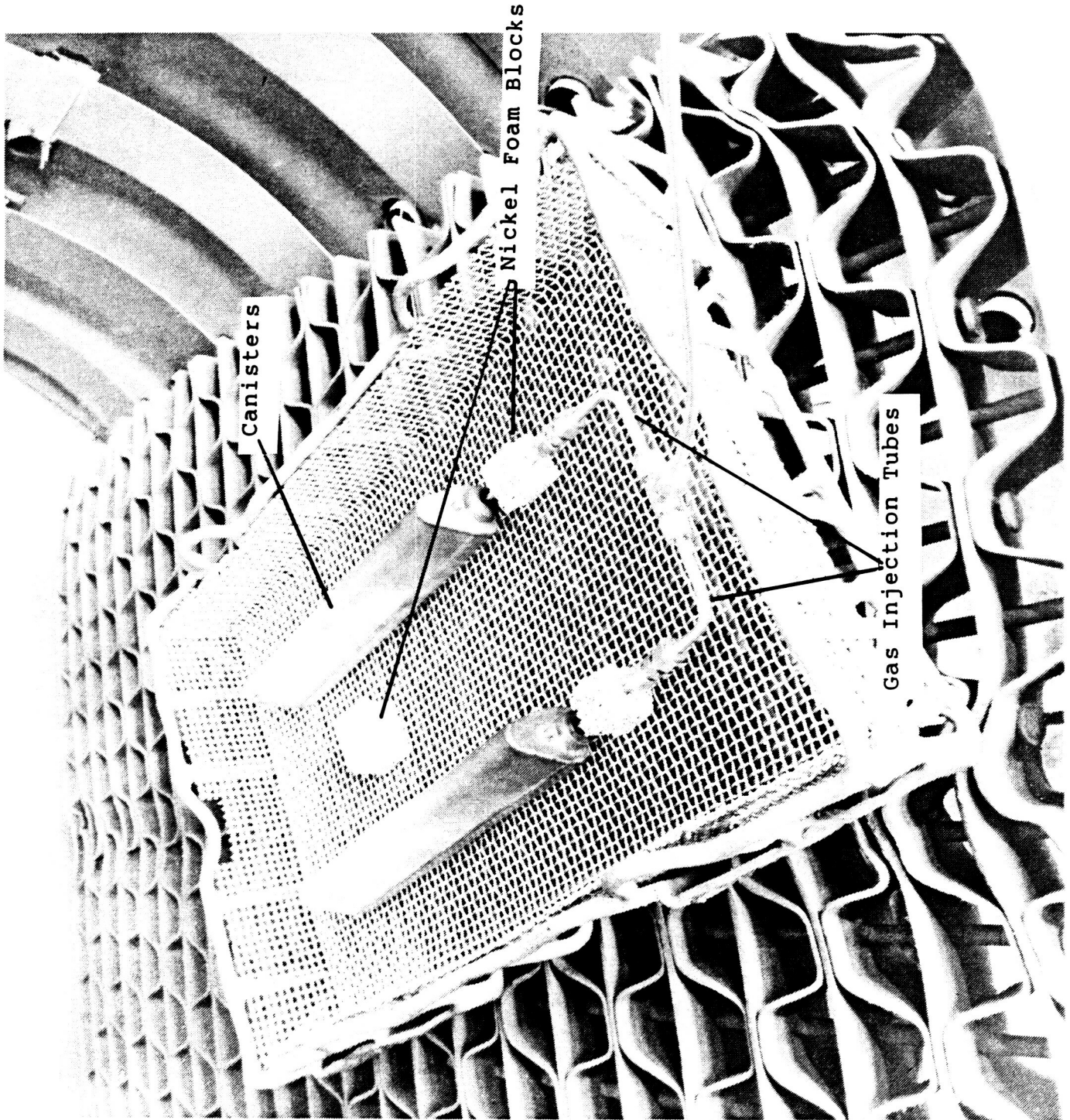


**Figure 29 - VIEW OF CANISTERS AND GAS PLUMBING IN FURNACE**



ORIGINAL PAGE  
BLACK AND WHITE PHOTOGRAPH

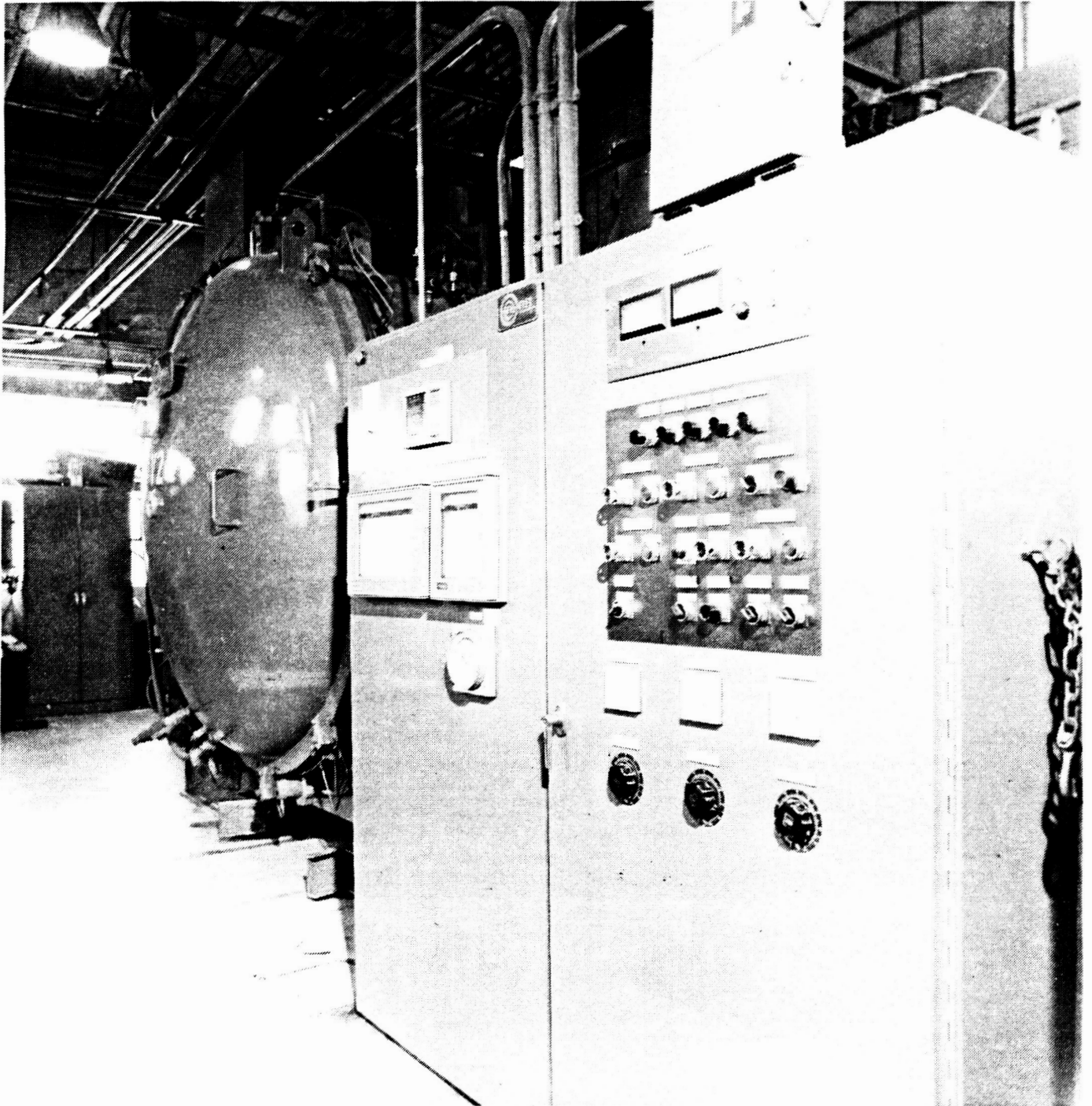


**Figure 30 - FURNACE CONTROL PANEL**

ORIGINAL PAGE  
BLACK AND WHITE PHOTOGRAPH

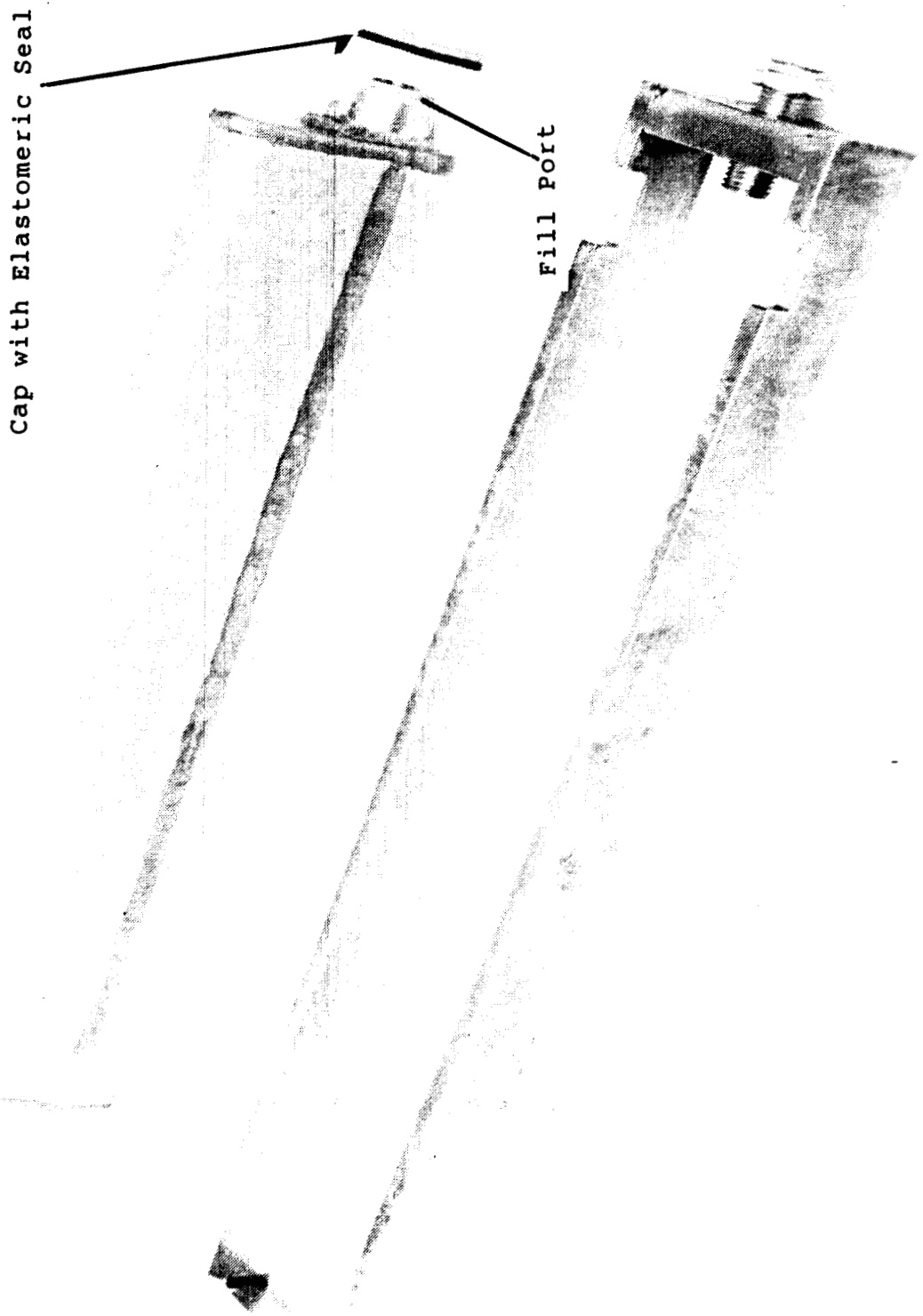
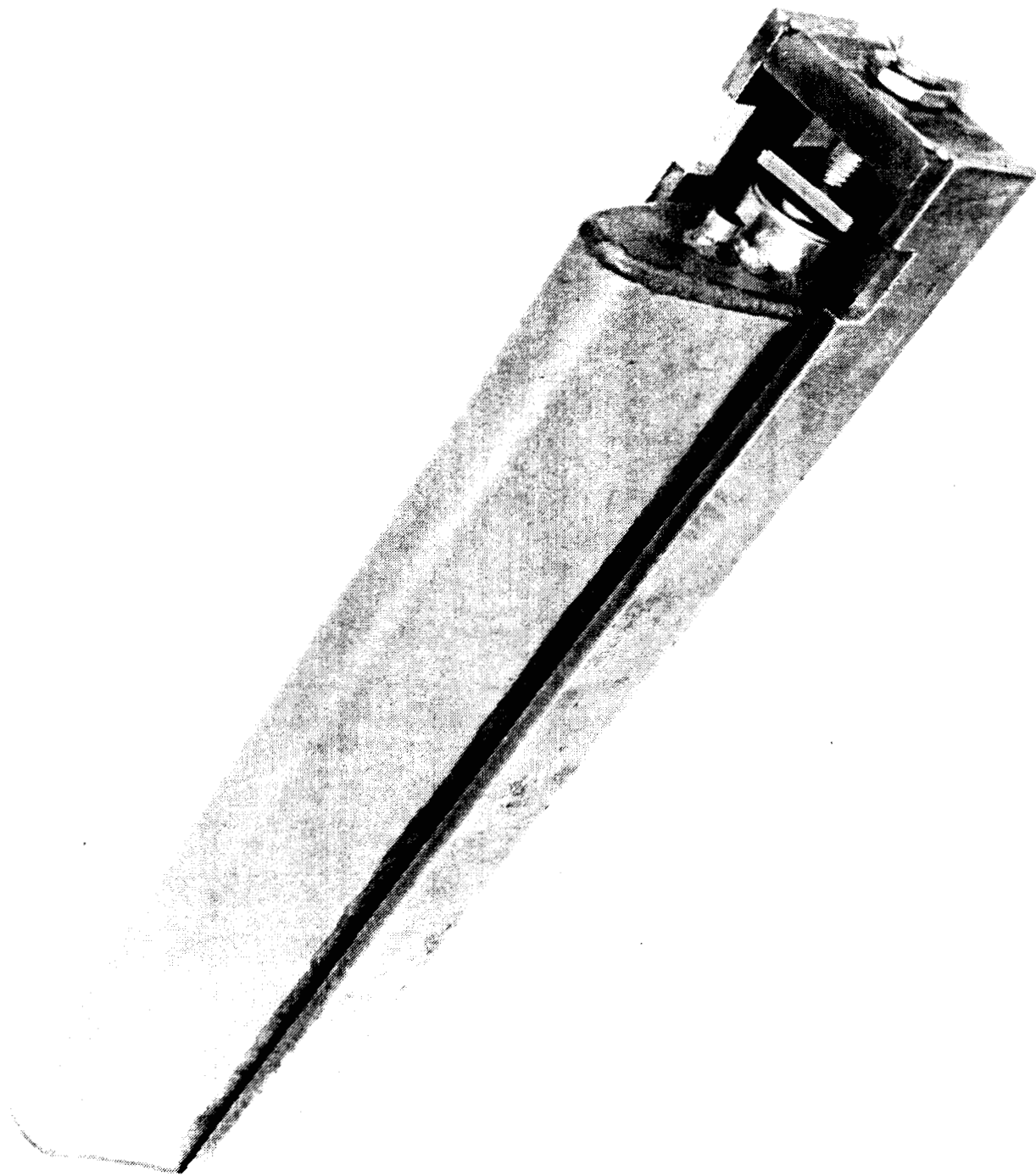


Figure 31 - CANISTER AND CLAMPING FIXTURE

ORIGINAL PAGE  
BLACK AND WHITE PHOTOGRAPH



**Figure 32 - CANISTER SECURED IN CLAMPING FIXTURE**

Finally, an "oxygen getter" cartridge was placed in the gas line to trap any O<sub>2</sub> that might have been in the gas flow. Two O<sub>2</sub> getters were expended in the first day due to air leaks. These leaks were discovered before an actual reduction run was attempted. On the second day pressure measurements showed that the getter caused a large pressure drop at the target mass flow rate, and thus would create a sub-atmospheric section in the external plumbing. Thus, the getter was used only for leak checking purposes and then was removed. Then further "bubble tests" were performed to assure leak tightness.

After this second reduction cycle, the gas injection tubing seemed much cleaner although some contaminants were present on the tubing. The decision was made to proceed with filling these two canisters with LiF salt for several reasons. First, the reduction process seemed to be at a point of diminishing returns. Also, thermal test results from a canister with a nickel foam insert would be useful even if oxides did remain on the foam, since the foam would at least provide thermal conductivity enhancement, and might also promote solidification farther from the cooling surface. Finally, no other oxide reduction process had been forwarded as more promising than the gas injection method being used.

#### 4.4 Filling Canisters

Canisters were filled with lithium fluoride (LiF) salt at NASA Lewis Research Center. Canister S/N 6, which did not contain nickel foam for thermal conductivity enhancement and void management, was the first canister filled with LiF. A detailed description of the fill procedures follows.

The canister was attached to the filling fixture, as shown in Figure 33. Powdered MoS<sub>2</sub> lubricant was used on all threaded bolts. A protective fill cap, as seen in Figure 34, was used to prevent molten LiF from spilling onto the closure cap weld area. The 575.9 g of LiF purchased from Cerac in 3 mm (1/8 in) vacuum fused chunks was added to the filling funnel. This mass of salt would theoretically give a 94.7 percent fill at 1172K (1650°F) per published density figures for LiF. The canister and fill fixture were placed in the vacuum furnace between the fixed controlling thermocouple and the door. Several other monitoring thermocouples were placed next to the canister and fill funnel.

The roughing pump was started at 11:00 a.m. and the cryopump (Helium at 12K) was engaged at 11:30 a.m. A residual gas analyzer (RGA) (mass spectrometer for masses 2 to 50) was started at 11:30 a.m. After pumping down to  $1 \times 10^{-5}$  Torr, heat was supplied at a low rate to dry the salt. Approximately 4 hours were required to reach the melting point of LiF 1121K (1558°F) and a vacuum level of  $1 \times 10^{-5}$  Torr was maintained once the salt reached 1073K (1472°F). Although LiF has a vapor pressure of 0.02 Torr at 1173K (1652°F), the vacuum gauge is in a cold section outside the furnace and the LiF would condense prior to reaching it.

Gases liberated during filling (RGA data) were comprised mainly of H<sub>2</sub>O initially, CO<sub>2</sub> during the range of 673-873K (752-1112°F) and roughly equal amounts of H<sub>2</sub>, H<sub>2</sub>O, N<sub>2</sub> and HF at 1173K (1652°F) although the amounts were very low ( $10^{-6}$  Torr range). Actual gas compositions can be calculated based on the total pressure and the partial pressures of the gases recorded by the RGA analyzer. The RGA data can be found in Appendix B.



ORIGINAL PAGE  
BLACK AND WHITE PHOTOGRAPH

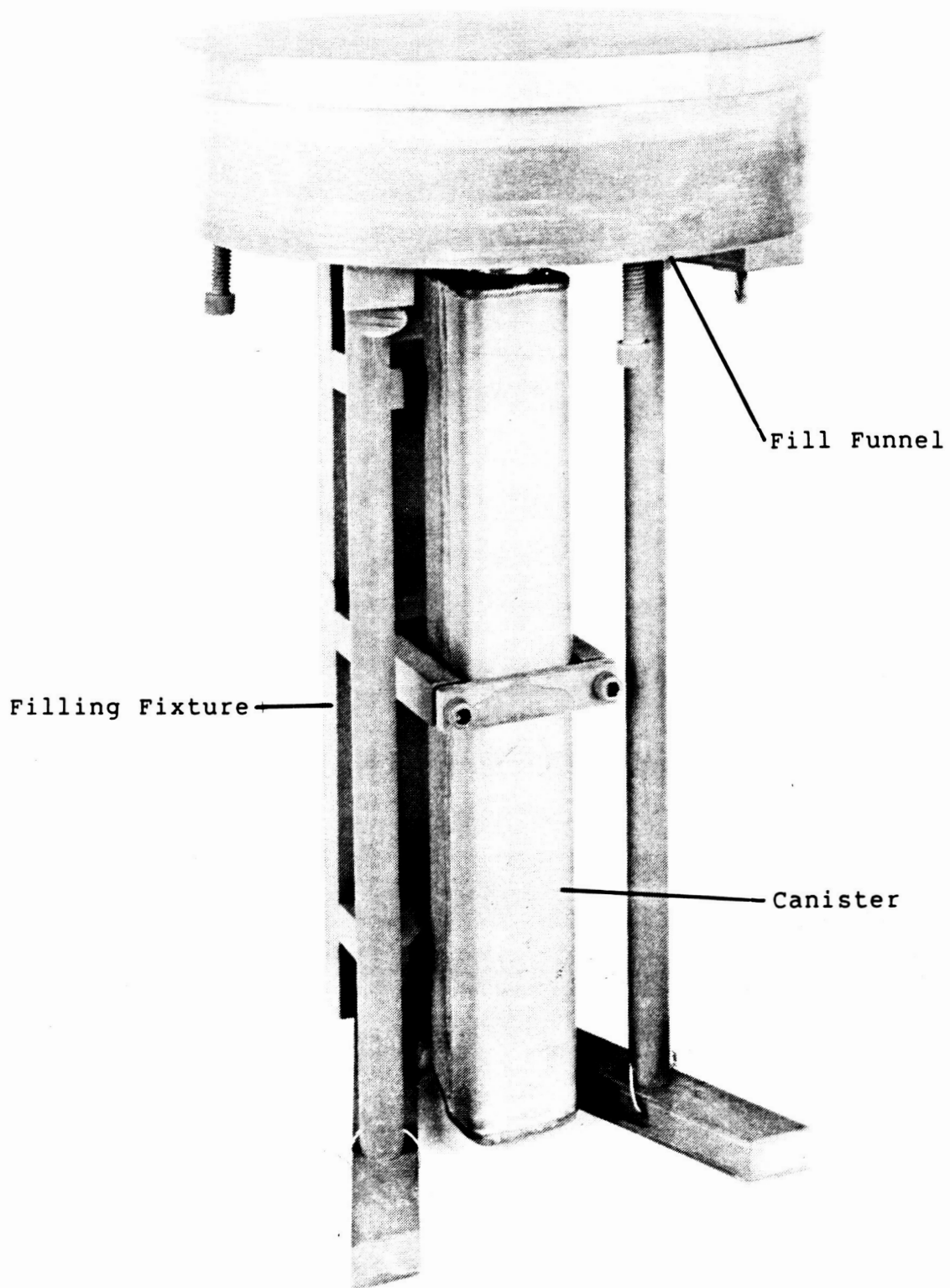


Figure 33 - CANISTER SECURED IN FILLING FIXTURE

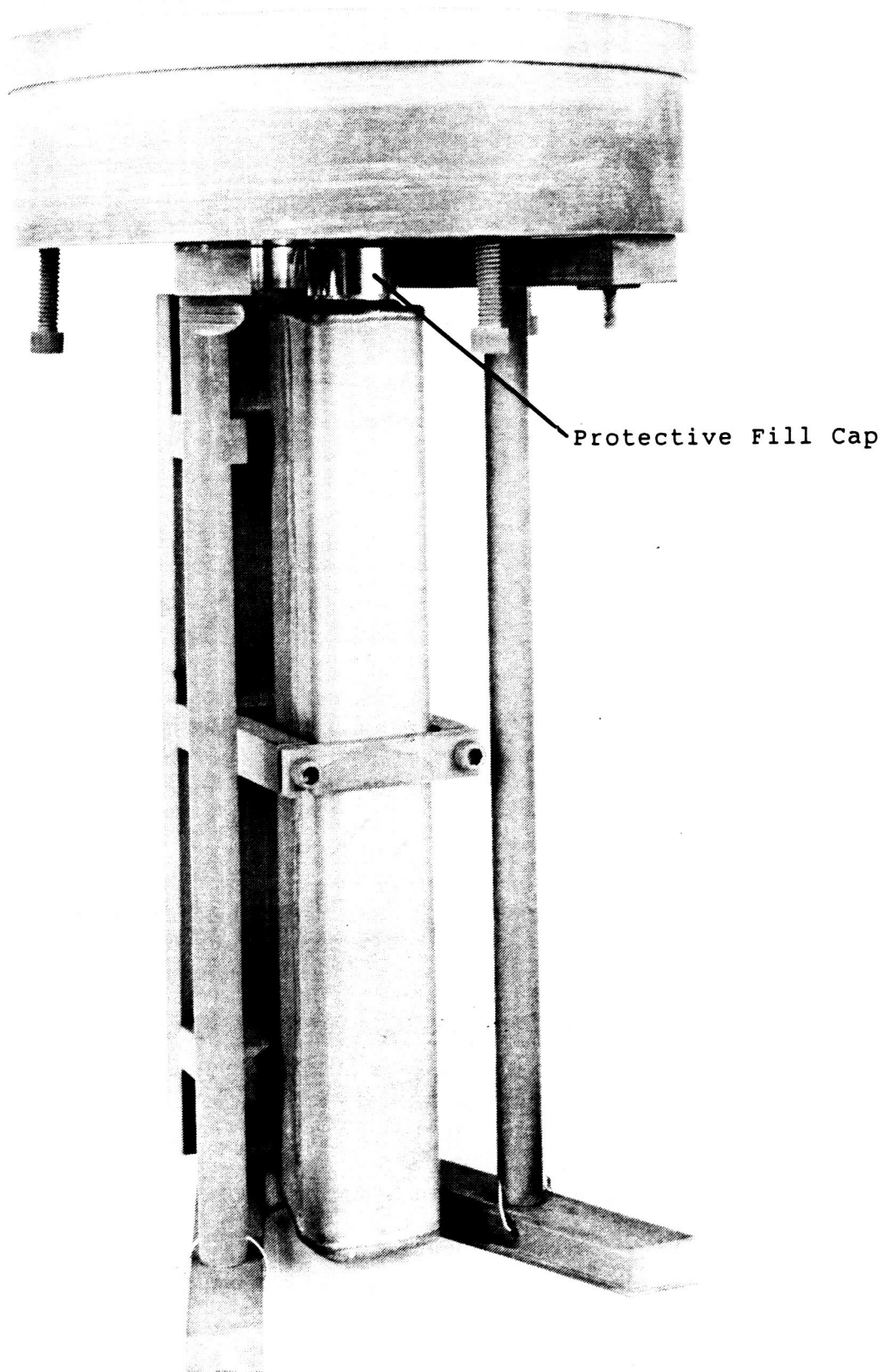


Figure 34 - CANISTER SECURED IN FILLING FIXTURE

During the filling operation the thermocouples were continuously monitored in order to detect if any salt flow from the filling funnel to the canister was occurring. During the 1st hour at 1173K (1652°F), no changes in the thermocouples were observed. However, the thermocouples were not physically attached to the hardware. To help ensure that complete filling would occur, the canister was held at 1173K (1652°F) for an additional 0.5 hours (1.5 hours total). The canister was then allowed to cool under a vacuum in the  $10^{-8}$  Torr range overnight.

After radiantly cooling overnight, the furnace was cooled with  $N_2$  gas and then opened. The exterior of the canister and filling fixture, in general, had a thin oxide coating over the exposed surfaces. A small amount of LiF remained in the fill funnel as a small frozen puddle covering the exit tube and small frozen droplets on the underside of the funnel lid.

The filling funnel was removed from the filling fixture and then the protective fill cap was removed from the canister. No salt or oxidation was evident on the weld area of the canister verifying that the protective fill cap worked. After removing the funnel, the canister was removed from the filling fixture. The ease with which the assembly screws turned indicated that the  $MoS_2$  powder was an excellent lubricating and anti-seizing compound. Immediately after exposing the canister to air, it was capped with a clamping fixture to prevent saturation of the LiF with water and oxygen.

Post-fill canister weight indicated a 92.7 percent fill (563.5 grams) at 1172K (1650°F), which was lower than the anticipated 94.7 percent. The 12.4 g of LiF lost in the filling process can probably be accounted for in the frozen puddle at bottom of fill funnel, the frozen droplets on underside of the fill funnel cover, and vaporization.

The canister was taken to the NASA LeRC weld shop for electron beam (EB) welding. However, the controller for the EB weld machine was not operational because it had just suffered an electronic component failure on the memory board. In order to reduce  $O_2$  and  $H_2O$  contamination of the LiF, the canister was stored in a vacuum chamber until the welder was repaired.

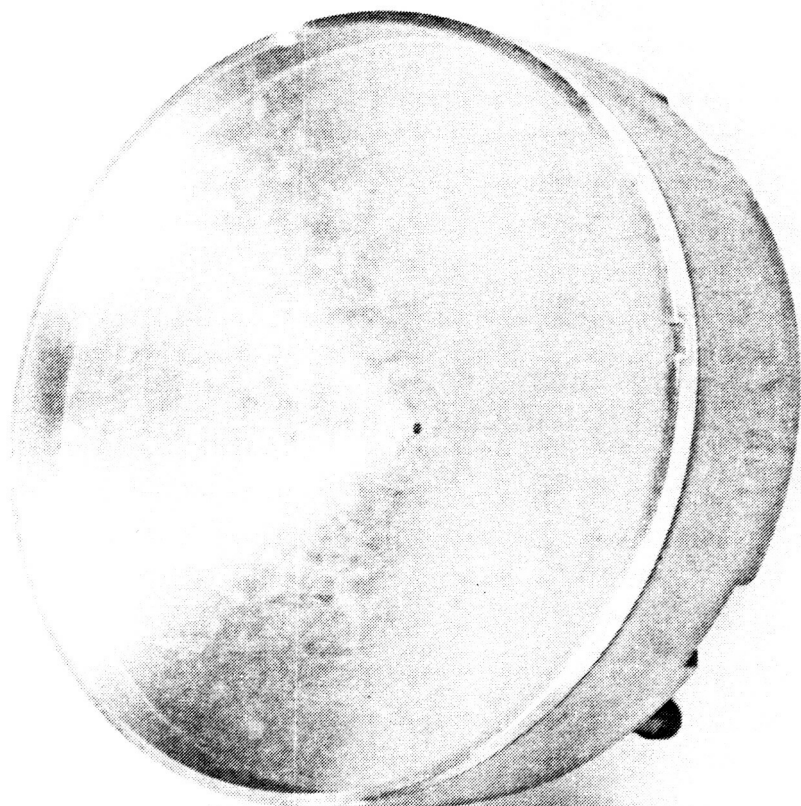
The fill funnel was returned to Sundstrand where it was cleaned and the funnel exit tube was enlarged. Figure 35 shows a view into the fill funnel and its lid. Note the LiF condensate on the lid. For the sake of reference, Figure 36, a view of the bottom of the fill funnel, has been included.

Canisters S/N 5 and S/N 7, which both contain nickel foam for thermal conductivity enhancement and void management, were filled during a later trip to NASA Lewis Research Center. The canisters and nickel foam had previously been heat treated in a dynamic reducing atmosphere to reduce the inherent nickel oxide on the nickel foam (refer to Section 4.3). The reduction process was used to promote wetting of the nickel foam by LiF. The detailed filling procedure and hardware used to fill these canisters with LiF were the same as that used on S/N 6.

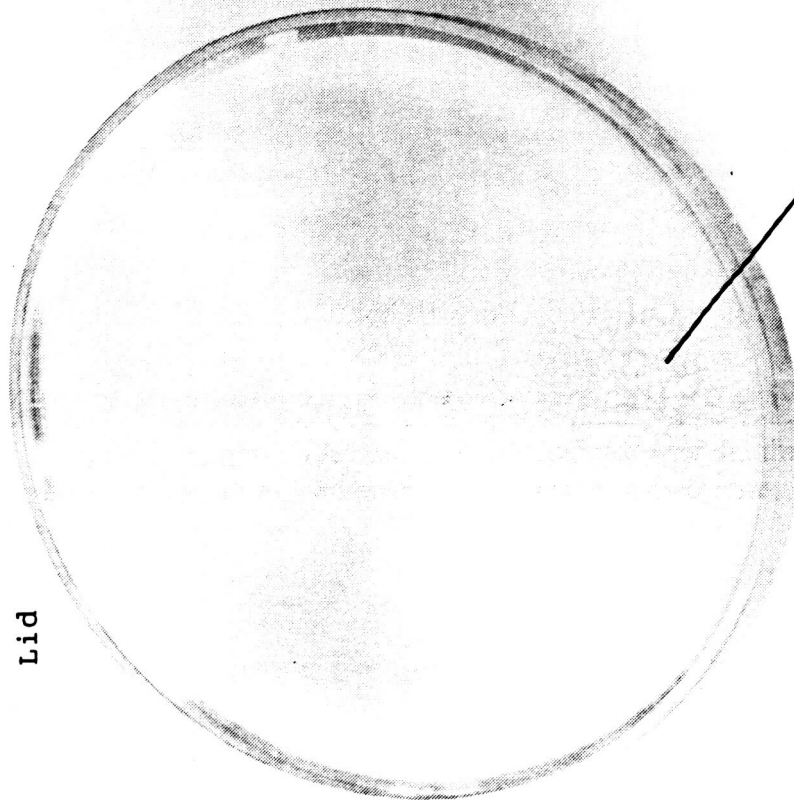
Canister S/N 7 was to be filled to achieve a 34.7 percent liquid volume at 1172K (1650°F). To compensate for salt losses which occur due to condensation on the fill funnel and volatilization, the actual target was a fill of 35.1 percent (10.4 g excess LiF). After filling, weight measurements show a 34.6 percent fill (200.6 grams) was achieved. (Only 3.2 grams of the salt had not flowed into the canister during filling.) It should be

ORIGINAL PAGE  
BLACK AND WHITE PHOTOGRAPH

Funnel



Lid



LiF Condensate

Figure 35 - VIEW INTO FILL FUNNEL

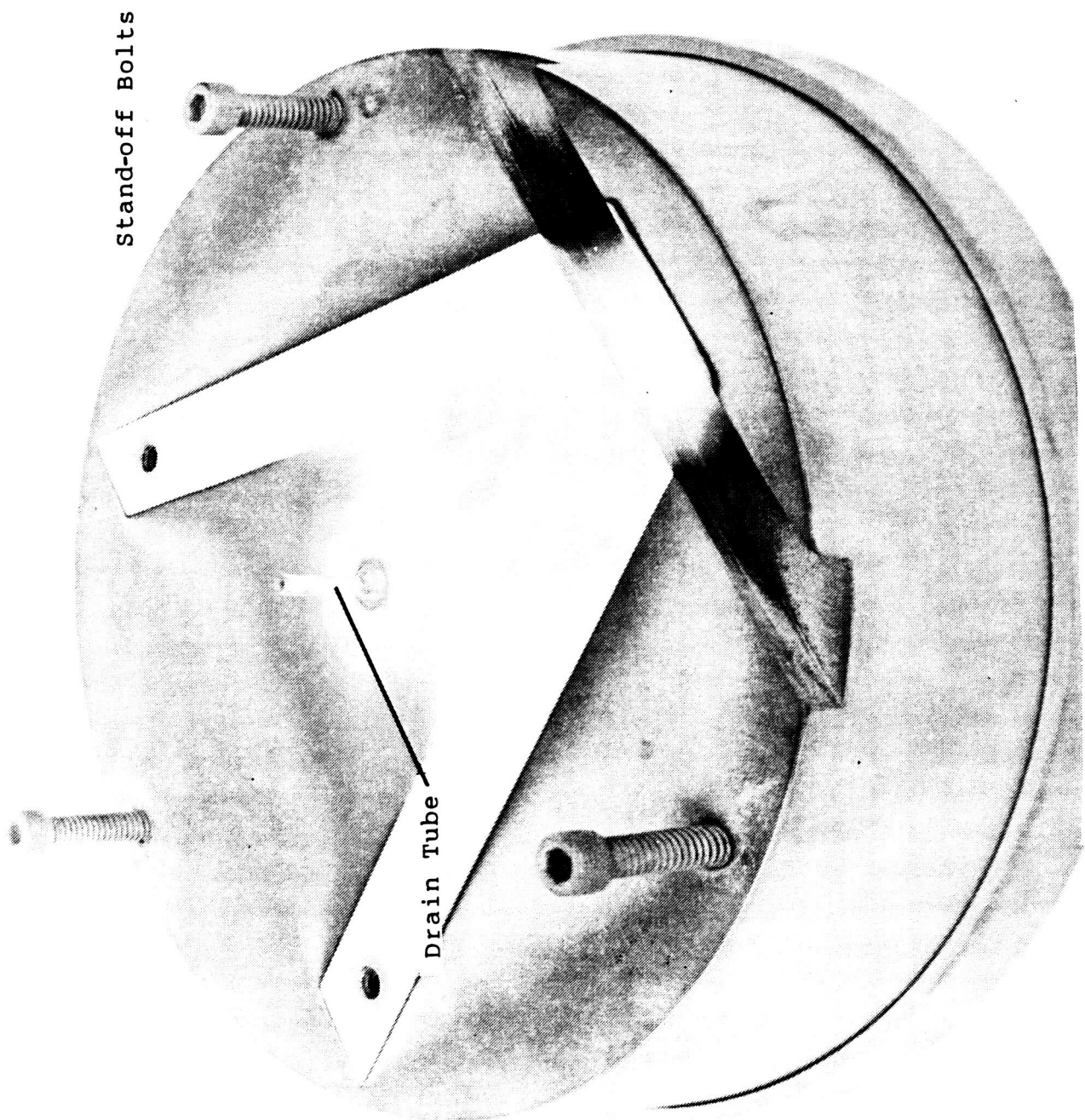


Figure 36 - VIEW OF BOTTOM SIDE OF FUNNEL

noted that it took approximately five minutes to secure the canister into the filling fixture and load the apparatus into the furnace, exposing the nickel foam to air during this time.

While removing the canister from the furnace the following day, it became evident that the fill tube was "bonded" to the canister by LiF which had wicked to fill the gap between the two parts. This bond was broken rather easily in a shear mode. However, the fill cap was bonded in a similar fashion and was quite difficult to loosen. This canister was not closure welded since it was to be inspected for wicking. Canister S/N 7 was sent to Bio-Imaging Research, Inc., for computed tomography analysis (CT scan), and then destructively sectioned to determine whether the salt had wetted the foam.

Canister S/N 5 was to be filled to achieve a 95 percent liquid volume at 1172K (1650°F). To compensate for salt losses, the actual target was a fill of 95.4 percent. After filling, weight measurements show a 91.7 percent fill (522.8 grams) was achieved. Examination of the canister revealed that some LiF had leaked out around the fill cap, down the canister, and onto the furnace tray. Although no salt was actually present on the outside of the canister, the hardware was slightly stained. The cause for the salt leakage is believed to be due to the fill funnel tube touching the canister and allowing salt to wick out. The fact that the canister is only 91.7 percent full should not affect the results of future tests. Canister S/N 5 was electron beam closure welded at NASA Lewis Research Center.

Notes from the filling procedures for all three canisters are included in Appendix B.

#### 4.5 Welding the Closure Caps

Two canisters, S/N's 5 and 6, were closure welded at the Electron Beam Welding facility at NASA Lewis Research Center. The closure caps were specially designed to preclude salt from solidifying in the fill port. A disassembled closure cap and canister are shown in Figure 37. Before either canister was welded, several sample welds were made on mock-ups of the weld joint. During initial attempts, problems experienced with misalignment between the weld and the joint were caused by residual magnetism in the fixturing chuck. Also, insufficient weld penetration caused by inadequate weld power was noted. These problems were corrected by using a non-magnetized holding fixture and by increasing the weld beam power. The weld beam specifications used in all subsequent welds were as follows:

Speed = 88.9 cm/min (35 inch/min)

Sharp Beam Focus, One Pass

Work Distance = 37.5 cm (14.75 inches)

Vacuum =  $4 * 10^{-5}$  Torr

Voltage = 55 kV

Current = 10 mA

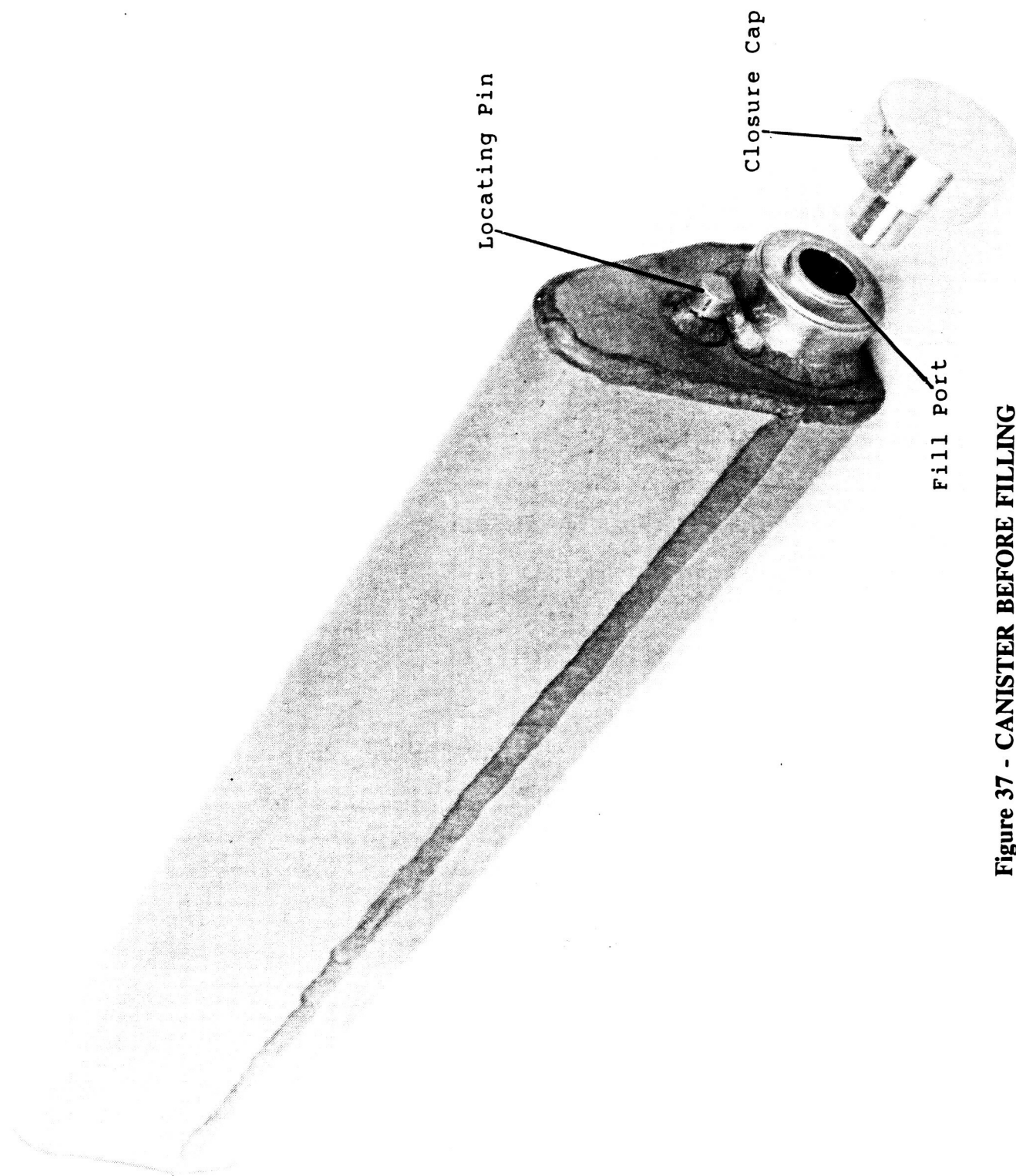


Figure 37 - CANISTER BEFORE FILLING



Weld samples were made immediately after each canister closure weld. These samples were made for verification of weld integrity. Figure 38 shows a canister that has been closure welded along with a sample weld. Cross sections of the weld samples are shown in Figures 39 and 40.

#### 4.6 Canister Insulation

In order to replicate the heat transfer conditions that the canister would experience in an integrated receiver design, the back and short side surfaces of the canister were insulated for some of the thermal cycle tests.

These are adiabatic surfaces in an actual receiver. Low thermal conductivity, 1366K (2000°F) temperature capability, and 2068 kPa (300 psi) compressive strength were the main requirements for this insulation. A ceramic foam made by Cotronics Corporation, Brooklyn, New York, with a thermal conductivity of 0.144 W/mK (0.083 Btu/hr/ft<sup>2</sup>/°F), 1922K (3000°F) temperature capability, and 4137 kPa (600 psi) compressive strength was chosen as an adequate insulation material. To achieve a thermal resistance 25 times greater on the insulated surfaces than that experienced on the uninsulated surface, the insulation thickness was set at 6.35 mm (0.25 inch). A drawing of the insulation is shown in Figure 41. In order to support the insulation and distribute clamping stresses, a trough was made of 0.127 mm (.005 inch) thick 316 stainless steel shim stock. Figure 42 shows the insulation inside of the stainless steel trough. Inconel wire was used to clamp the insulation to the canister as shown in Figure 43. As an aside, note that support wires run from various points on the frame to the thermocouple wires. Without these supports, the thermocouples were fatigued and broken by the vigorous bubbling action in the fluidized bed furnace.

#### 4.7 Thermocouple Attachment

Thermocouples were attached to the canisters to monitor temperatures during the thermal cycles. In an attempt to achieve intimate contact between the thermocouples and the canister, bare type K thermocouple wires were spot welded to the canister. However, it was difficult to provide strain relief for the wires, and they fatigued and broke due to the vigorous bubbling action in the fluidized bed furnace. To solve this problem, thermocouples with 1.59 mm (1/16 inch) inconel sheathing were affixed to the canister with small straps of stainless steel shim, as shown in Figure 44. The stainless steel shim was spot welded with a 70 Watt-second weld from a Weldmatic Model 1026C by Unitek Corporation, Monrovia, California. A 4.76 mm (3/16 inch) square piece of 1.59 mm (1/16 inch) thick ceramic felt insulation was placed over the thermocouple bead to ensure that the wall temperature, rather than the furnace temperature, was being read.

The thermocouples are located on the canister per the nomenclature given on Figure 45. From Figure 46 one can see how the thermocouples are arranged such that they do not cover much canister surface area, and also how they do not block the fluidized sand flow around the canister. The support wires mentioned in Section 4.6 are not in place for this photograph, but they must be used when testing due to the vigorous bubbling action in the furnace. Finally, note that the furnace temperature measurement is made by the thermocouple directly beneath the canister.



ORIGINAL PAGE  
BLACK AND WHITE PHOTOGRAPH

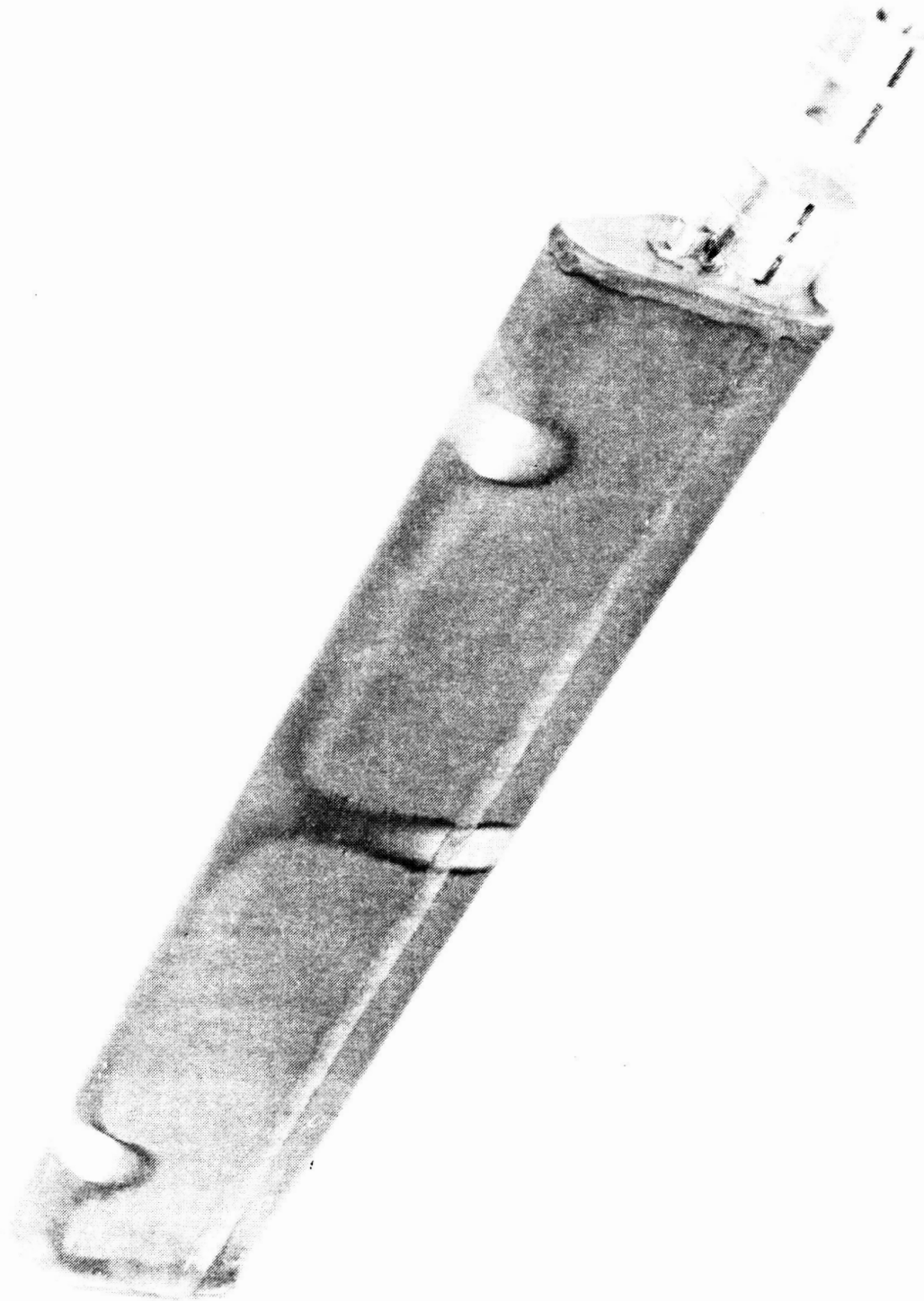


**Figure 38 - WELDED CANISTER ALONG WITH WELD SAMPLE**

ORIGINAL PAGE  
BLACK AND WHITE PHOTOGRAPH

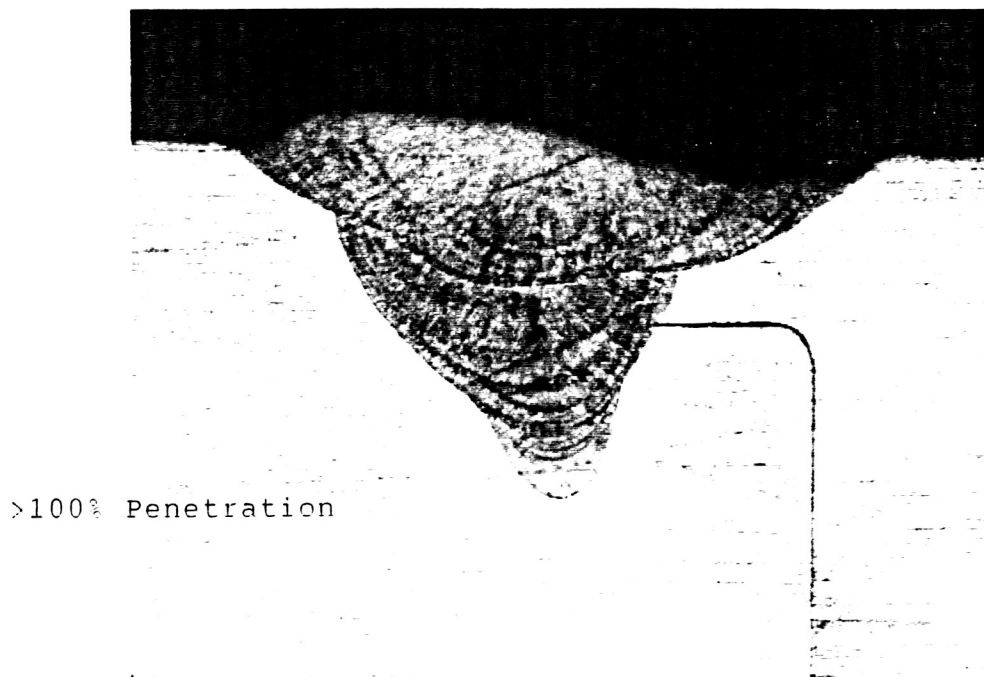
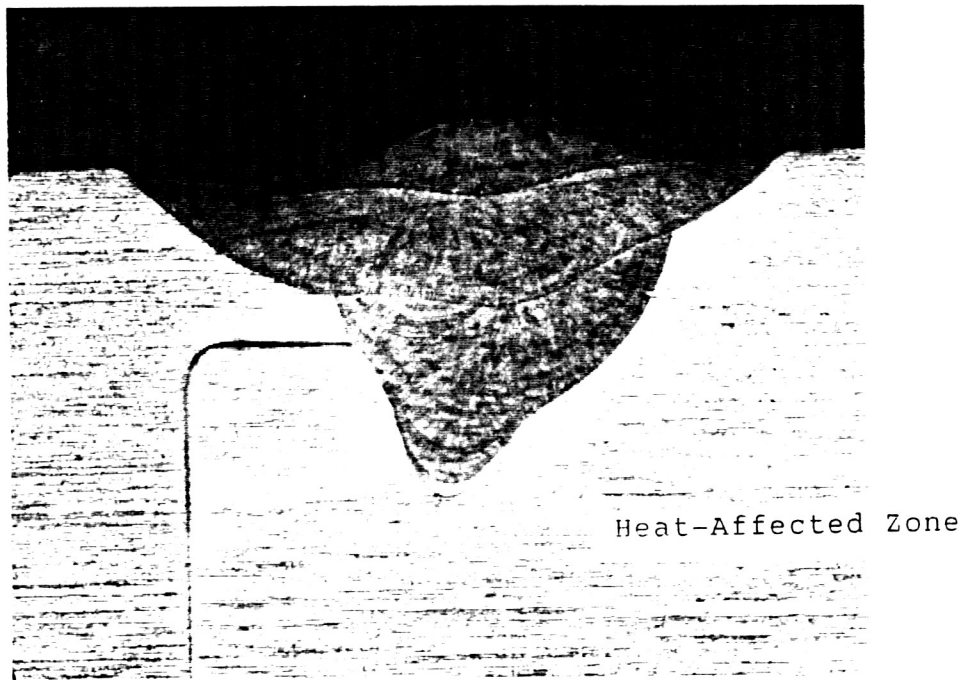


Figure 39 - CLOSURE CROSS-SECTION OF WELD SAMPLE FOR S/N 5,  
MAGNIFIED 32X, WELD JOINT IS IDENTIFIED AS 3 ON FIGURE 21

ORIGINAL PAGE  
BLACK AND WHITE PHOTOGRAPH

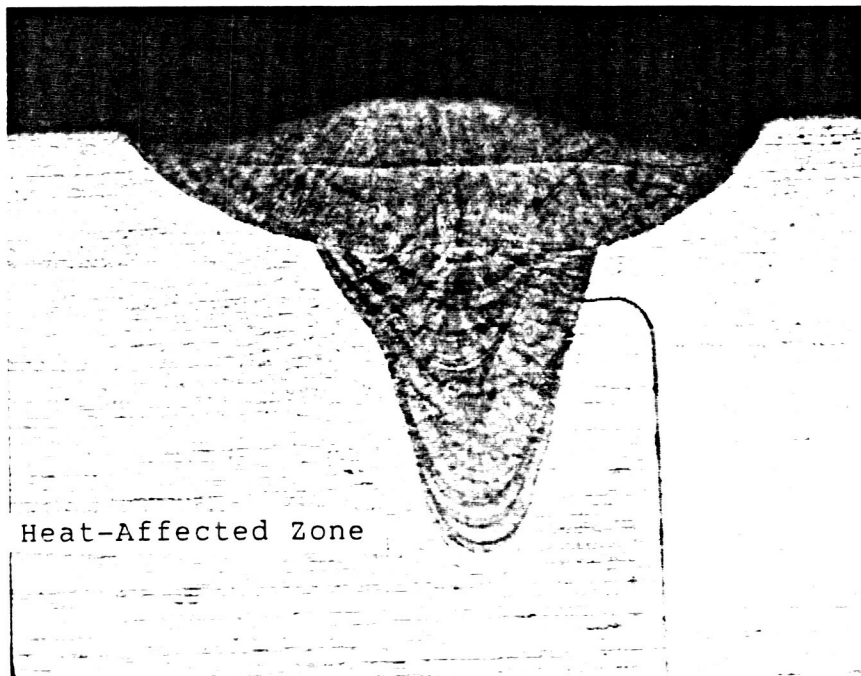
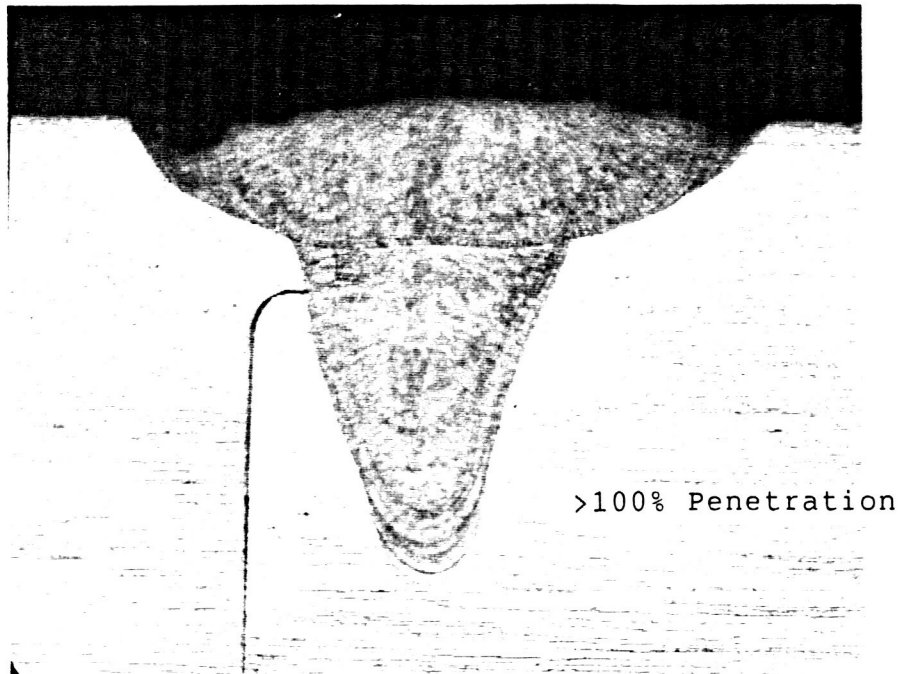
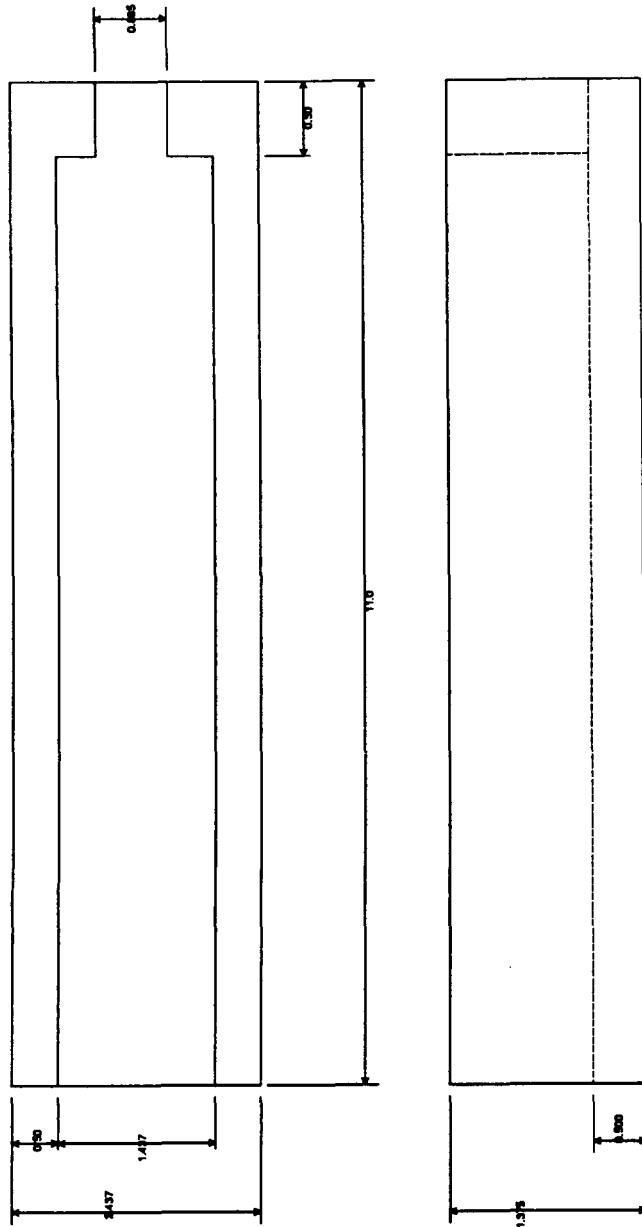


Figure 40 - CLOSURE CROSS-SECTION OF WELD SAMPLE FOR S/N 6,  
MAGNIFIED 32X, WELD JOINT IS SHOWN AS 3 ON FIGURE 21



Note: Dimensions in inches

Figure 41 - DRAWING OF CANISTER INSULATION

ORIGINAL PAGE  
BLACK AND WHITE PHOTOGRAPH

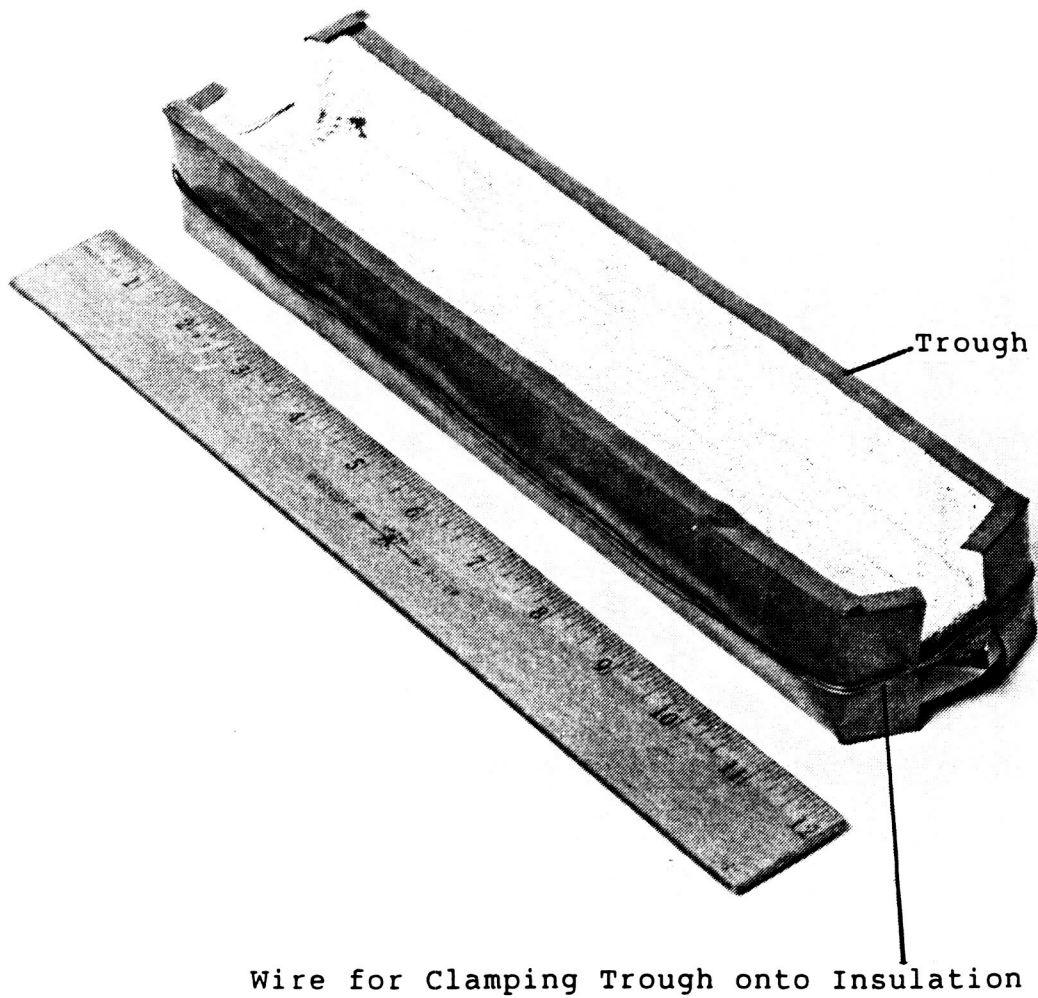


**Figure 42 - PICTURE OF INSULATION CONTAINED IN STAINLESS SHIM TROUGH**

ORIGINAL PAGE  
BLACK AND WHITE PHOTOGRAPH

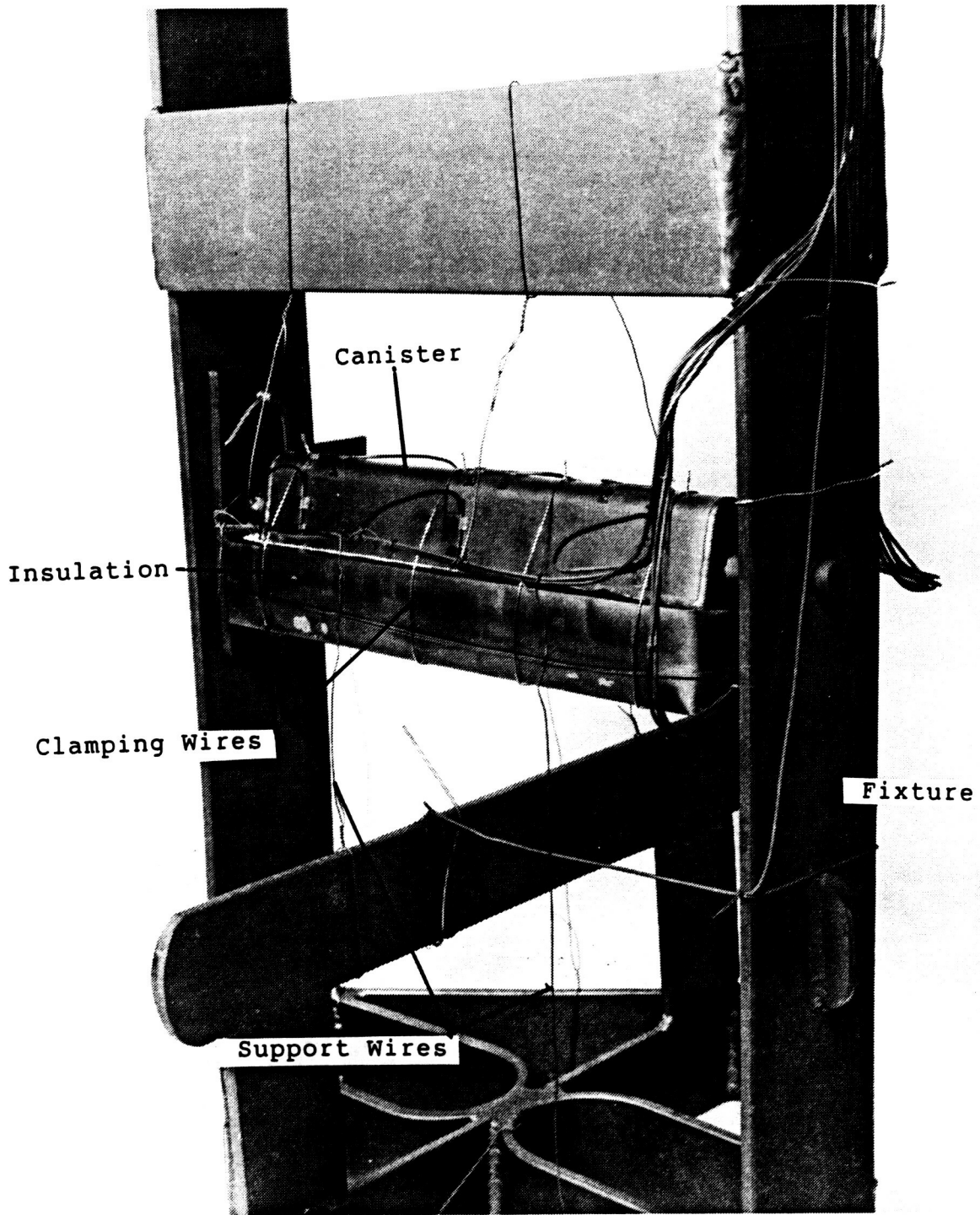
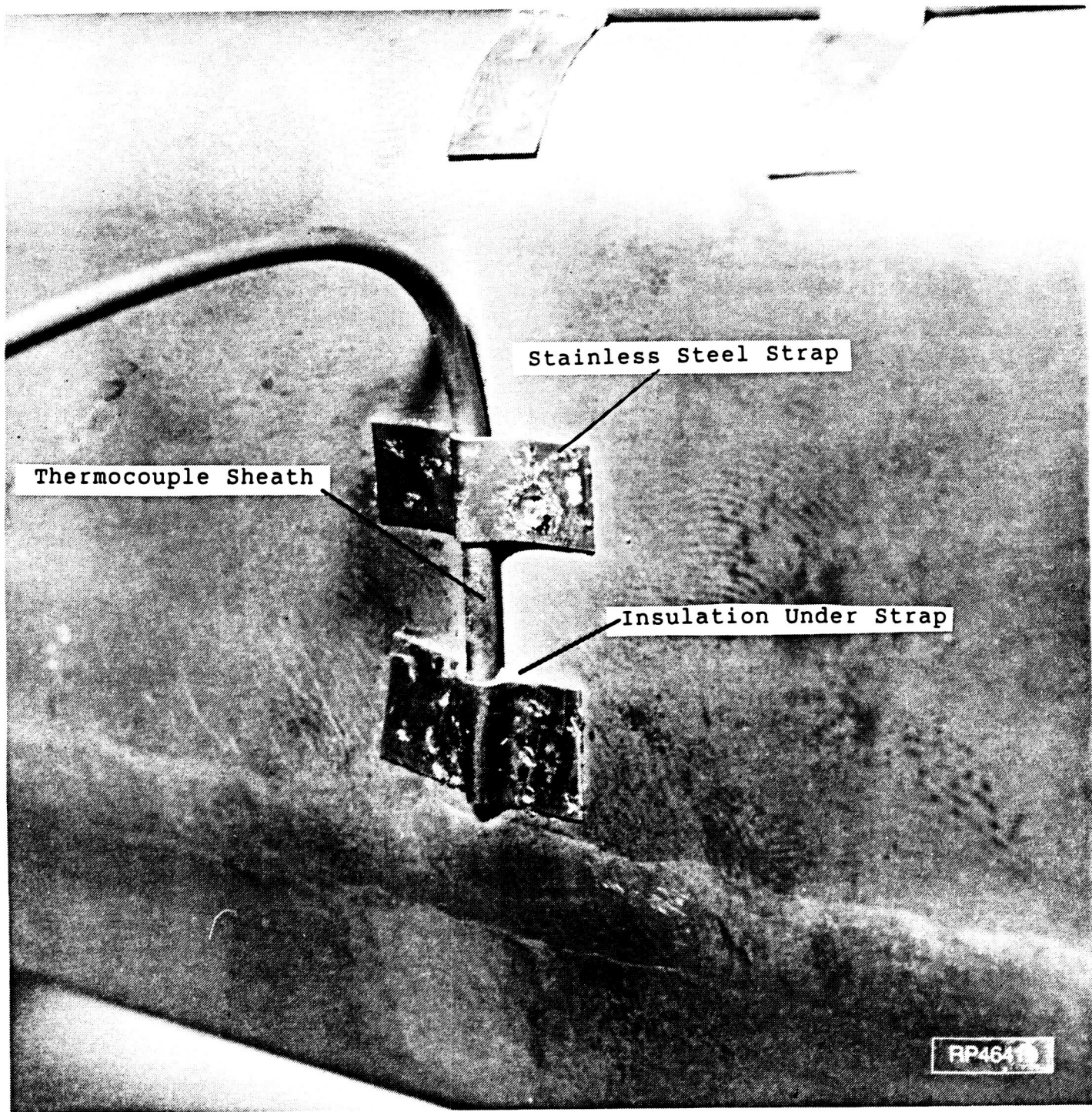


Figure 43 - PICTURE OF INSULATED CANISTER ON FURNACE FIXTURE



ORIGINAL PAGE  
BLACK AND WHITE PHOTOGRAPH



**Figure 44 - PICTURE OF THERMOCOUPLE ATTACHED TO CANISTER**

T1-3 WEDGE  
T4-6 RIGHT SIDE  
T7-9 LEFT SIDE  
T10-12 BOTTOM

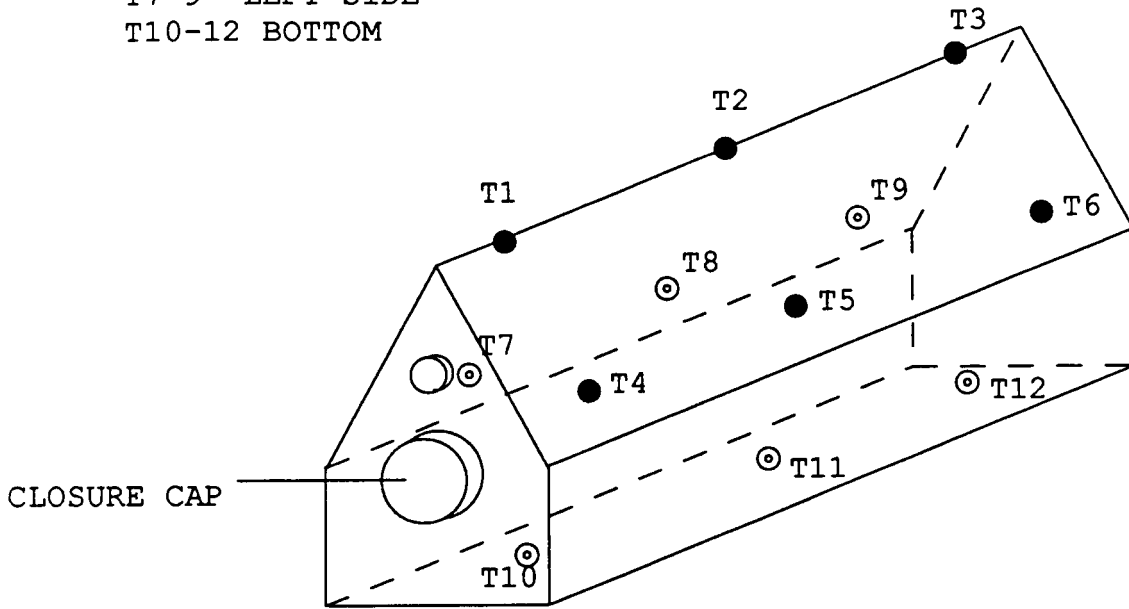


**Figure 45 - THERMOCOUPLE LOCATIONS ON CANISTERS**



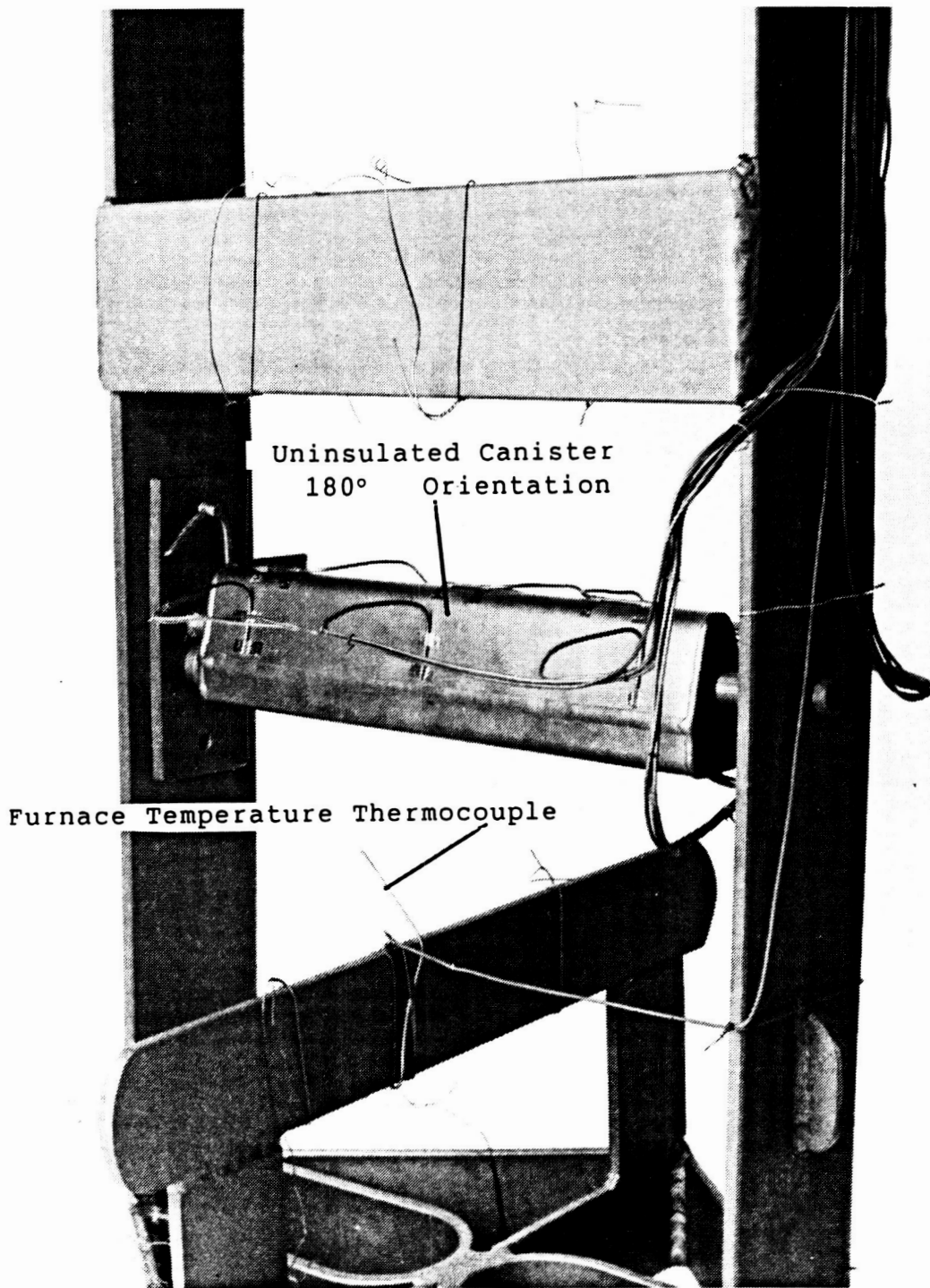


**Figure 46 - VIEW OF THERMOCOUPLE ARRANGEMENT ON CANISTER**

## 5.0 EXPERIMENTAL TEST PROGRAM

The Task 2 critical technology demonstration was a series of thermal cycling tests simulating a typical low earth orbit duty cycle on various canisters. The objectives of the test program were to determine the following canister characteristics:

1. effectiveness of the wedge geometry in preventing thermal ratcheting
2. performance (cycle  $\Delta T$ ) with insulated and uninsulated surfaces
3. performance (cycle  $\Delta T$ ) using thermal conductivity enhancement (TCE)
4. need for void control

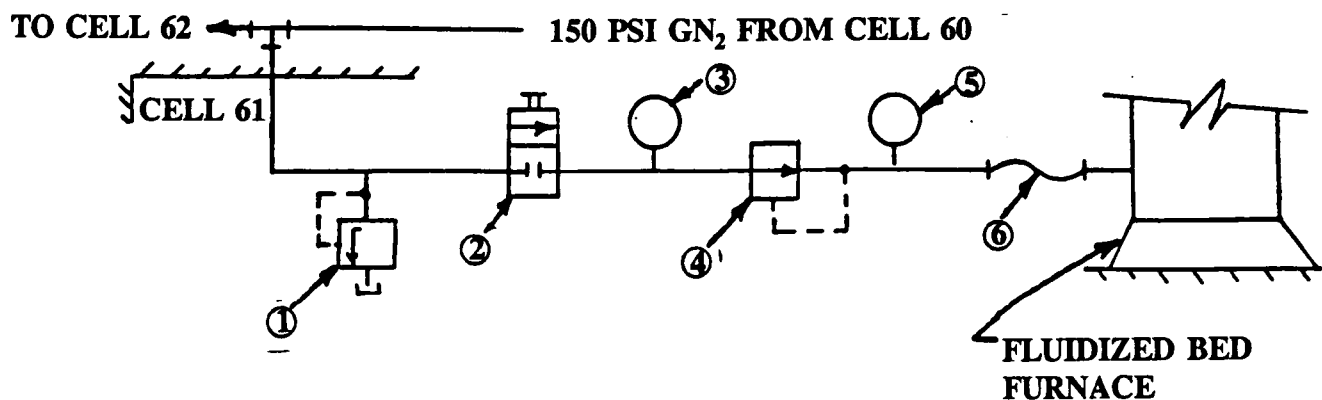
The demonstration technique was to perform a simulated orbital duty cycle (sunrise to sunset to sunrise) and monitor any change in the canister. Test measurement included deformation, checked by recording dimensions before and after each test, temperature data measured via thermocouples attached to the exterior surface of the canister, and internal void location, visualized with x-ray and computed tomography.

### 5.1 Test Facilities

The test facilities used are contained in Cell No. 61, a separately housed existing hazardous laboratory adjacent to Sundstrand's Plant 6 facility in Rockford, Illinois. This facility was previously used for endurance testing of LiOH filled canisters in 1985 and 1986 in support of the organic Rankine cycle option for Space Station Freedom solar dynamic power generation.

A fluidized bed furnace was chosen as the test bed for thermal cycle tests on canisters. The furnace, purchased from Fluidtherm Corporation, South Lyon, Michigan, has a 15 inch diameter retort. Gaseous nitrogen at ambient temperature enters the retort via the diffuser with inlet conditions of 34 kPa (5 psig), 294K (70°F), and 9.91 m<sup>3</sup>/hr (350 cubic feet per hour) as shown in the Figure 47, a schematic of the fluidized bed gaseous nitrogen supply. The hot gas was then collected in a furnace cover and vented outside the test cell as shown in Figure 48, which is a photograph of the furnace. The test cell was well ventilated to prevent a buildup of leaked nitrogen gas. The canister was held in a fixture as shown in Figure 49. Canisters were held in two orientations in the fixture, either with the wedge pointing up or the wedge pointing down.

A heat exchanger made of stainless steel tubing was added to the basic furnace design to provide cooling capability to replicate the eclipse portion of an orbit. Figure 50 shows a view down into the retort with the stainless steel cooling tubes immersed in the fluidized sand bed. The furnace controlling thermocouple is located in the well on the left hand side of the retort. A schematic of the nitrogen cooling gas supply is shown in Figure 51. A flow of 0.90 kg/min (1.98 LBM/min) of GN<sub>2</sub> at 103 kPa (15 psig) and 294K (70°F) is supplied to the cooling heat exchanger. Cooling gas flow was measured with a mass flow sensor.



- 1 PRESSURE RELIEF VALVE (SAFETY SETTING 200 PSIG)
- 2 HAND OPERATED SHUT OFF VALVE
- 3 0-200 PSI PRESSURE GAUGE
- 4 PRESSURE REGULATOR (SET AT 120 PSI)
- 5 0-200 PSI PRESSURE GAUGE
- 6 TRANSITION PIPING

A FLOWMETER FOR FLUIDIZED GAS (GN<sub>2</sub>) IS SUPPLIED AS PART OF FURNACE CONTROL PACKAGE.

Figure 47 - SCHEMATIC OF GASEOUS NITROGEN SUPPLY FOR FLUIDIZED BED

ORIGINAL PAGE  
BLACK AND WHITE PHOTOGRAPH

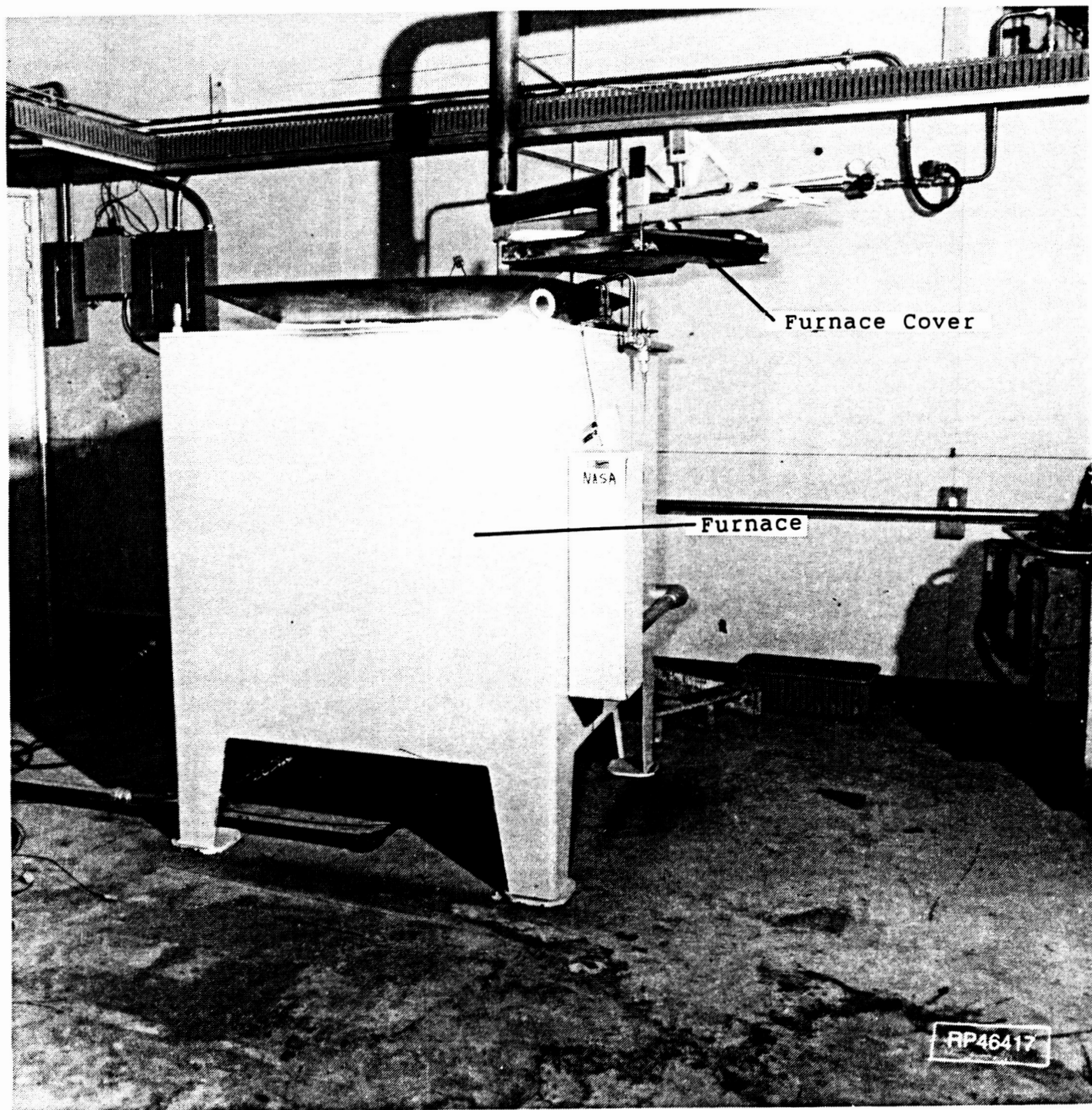


Figure 48 - PHOTOGRAPH OF FLUIDIZED BED FURNACE

ORIGINAL PAGE  
BLACK AND WHITE PHOTOGRAPH

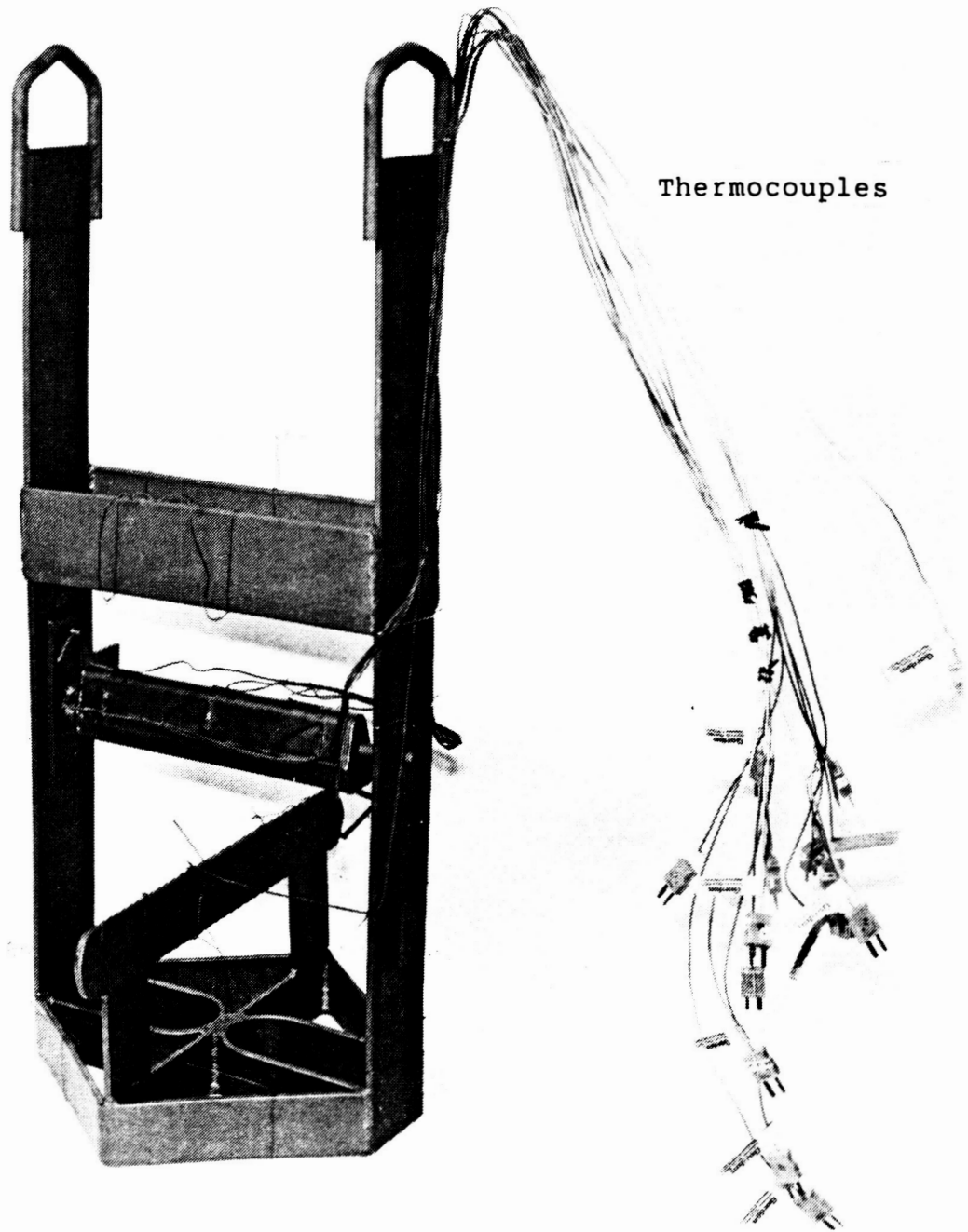


Figure 49 - PHOTOGRAPH OF CANISTER HELD IN FURNACE FIXTURE

ORIGINAL PAGE  
BLACK AND WHITE PHOTOGRAPH

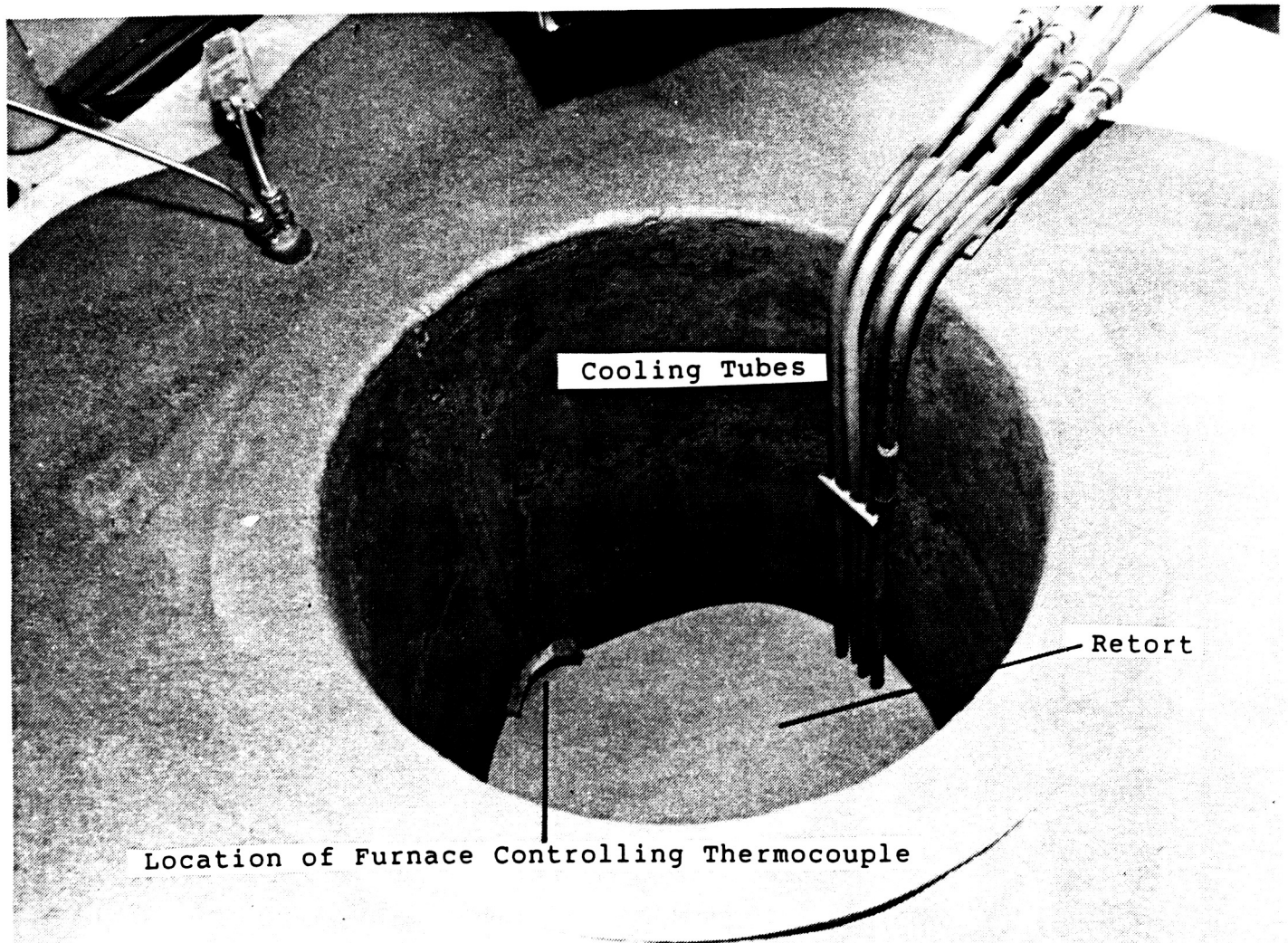


Figure 50 - VIEW DOWN INTO RETORT OF FURNACE



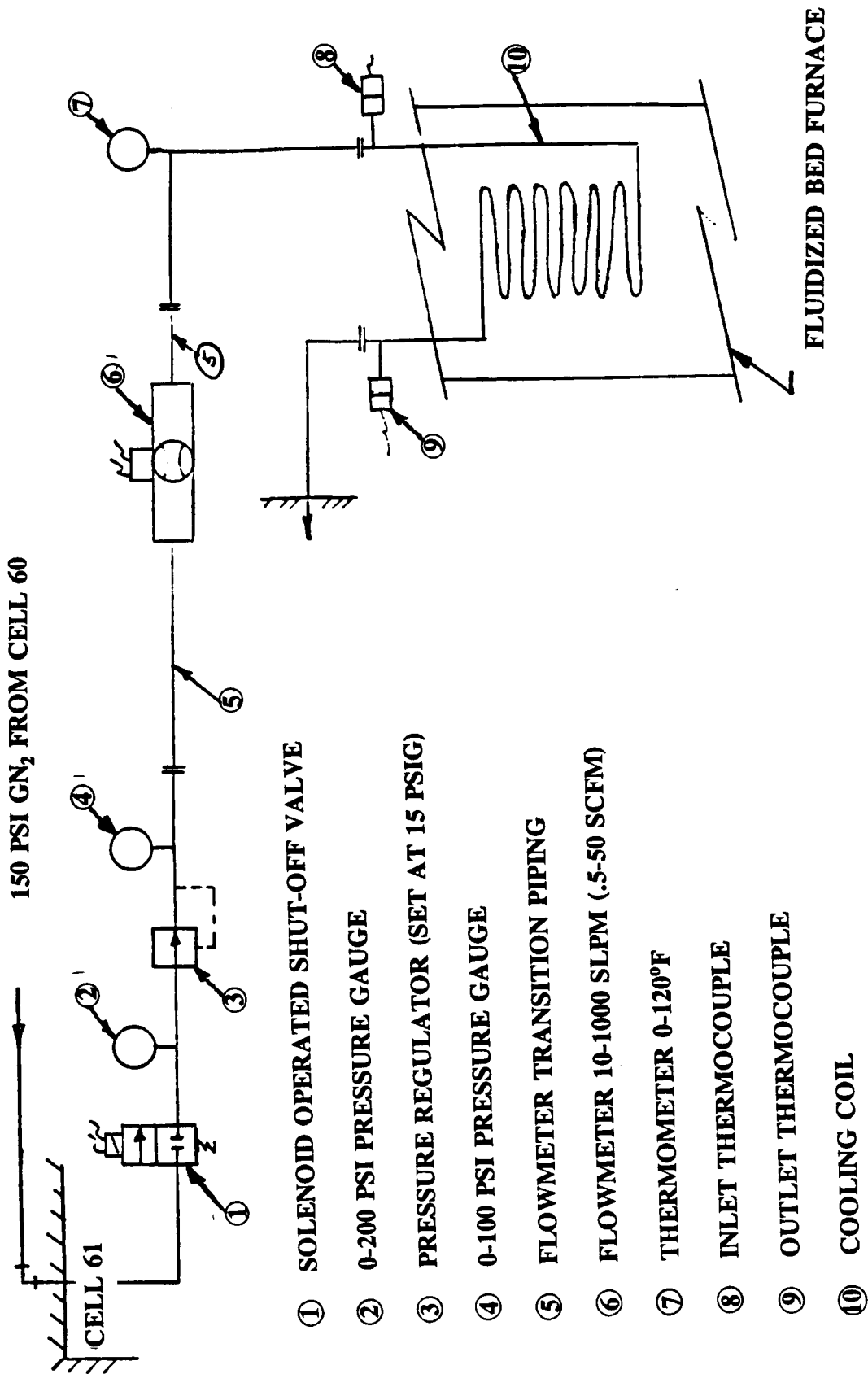


Figure 51 - SCHEMATIC OF NITROGEN COOLING GAS SUPPLY

The furnace control panel, shown in Figure 52, has safety features to shut down the furnace in the event the bed temperature becomes too high or if the fluidizing gas flow is too low to adequately fluidize the sand bed. A flow control valve was used to set the fluidizing gas flow. A digital controller made by LFE Corporation, Chesterland, Ohio, was used to control the temperature profiles. A Fluke data logger, to the right of the control panel in the photograph, was used to gather temperature, pressure, and flow data.

## 5.2 Test Plan

The following test plan was used.



ORIGINAL PAGE  
BLACK AND WHITE PHOTOGRAPH

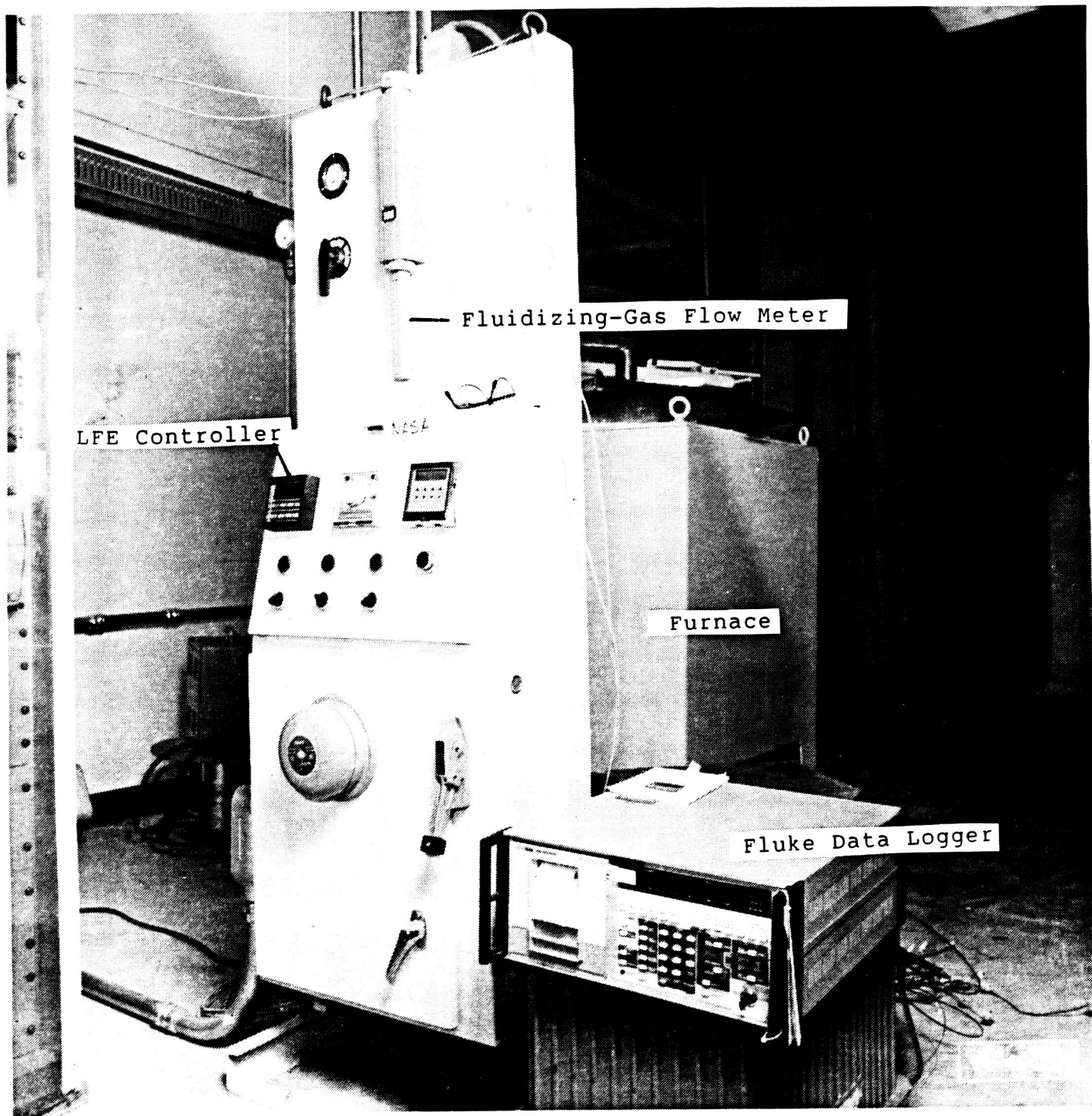


Figure 52 - FURNACE CONTROL PANEL

TEST PLAN

CANISTER NO.	TEST NO.	CANISTER ORIENTATION	TEST DESCRIPTIONS
S/N 007	1	N/A	Fill procedure checkout and LiF wicking test. This test is to checkout the liquid filling facility. A standard canister will be used. A secondary purpose is to determine the wicking capability of the thermal conductivity enhancement material, and how its presence affects the filling process. It is planned that this canister will only be filled to 30 percent of its volume. After the filling process is completed, the canister will be x-rayed, and the CT scans will be performed. Then it will be cut apart for visual inspection. Thus, correlation will be obtained between the x-ray, CT scans and visual methods of inspection.
S/N 006	2	180°	Canister No. 2 will be filled with LiF only, and the bottom and sides will be insulated with ceramic foam material that has low compressive strength in order that it will allow the canister to expand. Test No. 2 will be a checkout of the test facility with the test article installed. Previously, the test apparatus will have been checked out at the vendor's facility with a simulated canister installed in the holding fixture. After being filled while in the vertical orientation, all the salt will be concentrated at one end of the canister. To prevent any potential detrimental stress, the canister will be brought up to and through the melting process slowly. All thermocouples will be monitored. Heater power will be increased in small increments and then held until all thermocouples are reading the same, and for 10 minutes before another increase in power is made. The canister external temperature will be increased until it reaches 1172K (1650°F) in steady state conditions. The cooling coil valve will then be activated, and the canister will be cooled down to room temperature. A dimensional check of the canister will be performed before proceeding to an x-ray after Test No. 2.
S/N 006	3	180°	A single thermal cycle simulating a typical low earth orbit (LEO) duty cycle will be performed. Power will be increased slowly until the canister has stabilized at 1089K (1500°F). The 60 minute heating cycle will be conducted. A dimensional check will be performed after the test is completed. An x-ray and possibly a CT scan will be performed.
S/N 006	4	0°	Test No. 3 will be repeated with the orientation changed.
S/N 006	5	180°	Test No. 3 will be repeated in its entirety with insulation removed from the canister sides and bottom.
S/N 006	6	0°	Test No. 5 will be repeated with the orientation changed.
S/N 005	7	180°	Test No. 2 will be performed with canister S/N 005. This canister will be filled with nickel foam having 65 pores per inch, and the canister bottom and sides will be insulated.
S/N 005	8	180°	Test No. 3 will be performed on canister S/N 005.
S/N 005	9	0°	Test No. 4 will be performed on canister S/N 005.
S/N 005	10	180°	Test No. 5 will be performed on canister S/N 005.
S/N 005	11	0°	Test No. 6 will be performed on canister S/N 005.

### 5.3 Test Results

#### 5.3.1 Wicking Test

One of the canisters (S/N 7) with nickel foam thermal conductivity enhancement (TCE) was filled to the 34.6 percent liquid salt level (200.6 grams of LiF) and used for wicking tests. The object of the wicking test was to determine whether the nickel foam would wick the liquid LiF. Since the canister was filled in a vertical orientation, the LiF was free to wick up to 16.5 cm (6.5 inches) above the liquid level. Later, computed tomography (CT) images of the canister were produced at Bio-Imaging Research, Inc., of Lincolnshire, Illinois, to determine the wicking ability of the nickel foam.

The wicking test canister was destructively inspected to determine the validity of the computed tomography (CT) images. As expected, the CT images were accurate representations of actual canister cross sections. Figure 53 shows six sections from the cross-sectioned canister while Figures 54, 55, 56, and 57 show close-up photographs of cross sections at 2.54, 5.08, 7.62, and 10.16 cm (1.0, 2.0, 3.0, and 4.0 inches) from the bottom, respectively. For the sake of comparison, CT images of these same four sections are shown in Figures 58, 59, 60, and 61. At the 12.7 cm (5.0 inch) section of the canister, some salt is present along the canister wall. Either LiF vapor condensed along the wall or some liquid LiF did wick between the foam and the canister wall. Only a trace of LiF was found along the wall at the 15.24 cm (6.0 inch) cross section. As an aside, the LiF solidified into a very regular crystal pattern along the canister walls. Also, an X-ray photograph of the canister shown in Figure 62 for reference, reveals little about the void location.

The nickel foam did not show any signs of mechanical distortion from the single thermal cycle it experienced. Note that the void formed at the center of the canister because the salt froze first on the walls of the canister. Also, the purpose of the hole in the foam was to facilitate the flow of the salt into the canister during the fill process. However, the large gap between the nickel foam and the canister walls was a revelation from the CT images. This gap was such a significant thermal resistance that it might have offset most of the conductivity augmentation of the nickel foam. This gap, which of course was undesirable, was the result of oversights in the manufacturing process.

#### 5.3.2 Thermal Cycle Tests

It was originally planned that one canister test cycle would require a 1 1/2 hour time period; one hour of heating followed by 1/2 hour of cooling. The GN<sub>2</sub> fluidizing gas was supplied continuously and the GN<sub>2</sub> cooling was supplied only during the 1/2 hour cooling period. The cycle was automated after the fluidized gas supply valve was manually opened and the furnace was activated.

Two canisters, S/N's 5 and 6, were cycled thermally in the fluidized bed furnace to determine the effects of thermal conductivity enhancement, canister orientation, and surface insulation. The canisters were subjected to furnace temperature profiles which replicated a worst case low earth orbit with a temperature variation from 977K (1300°F) to 1244K (1780°F). The cycles took approximately 130 minutes, which is longer than the desired 90 minutes. However, the ramp rates exceeded the expected ramp rates during the phase change portions of the cycle, and since mechanical stresses are greatest during the

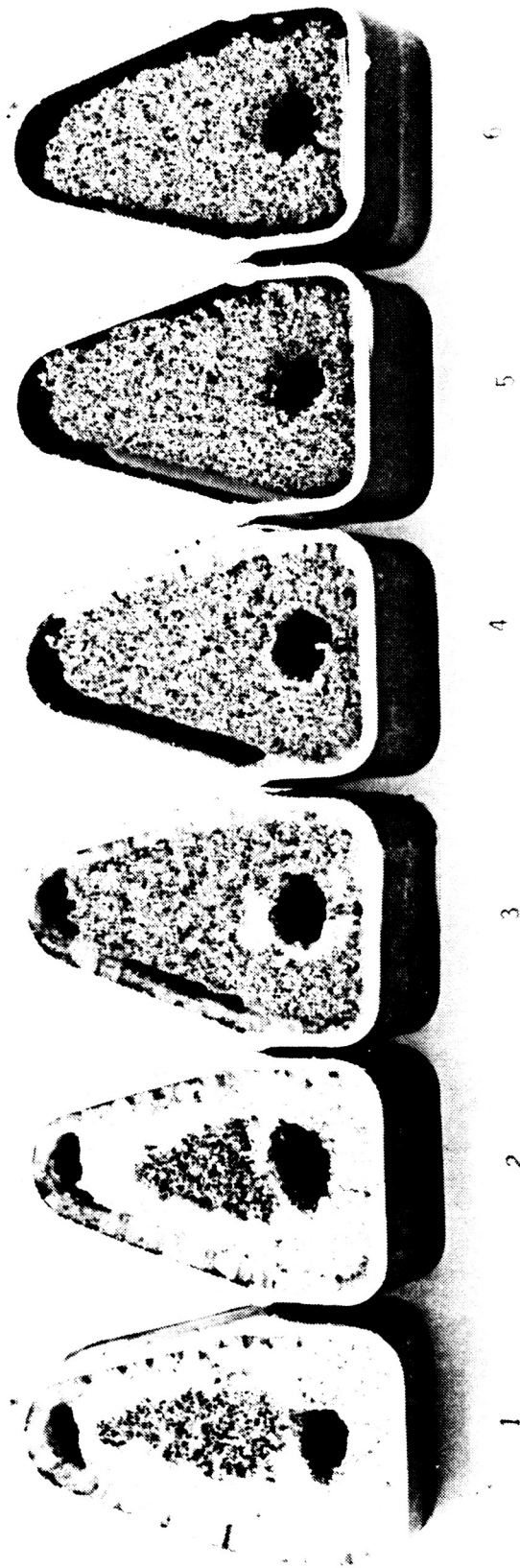
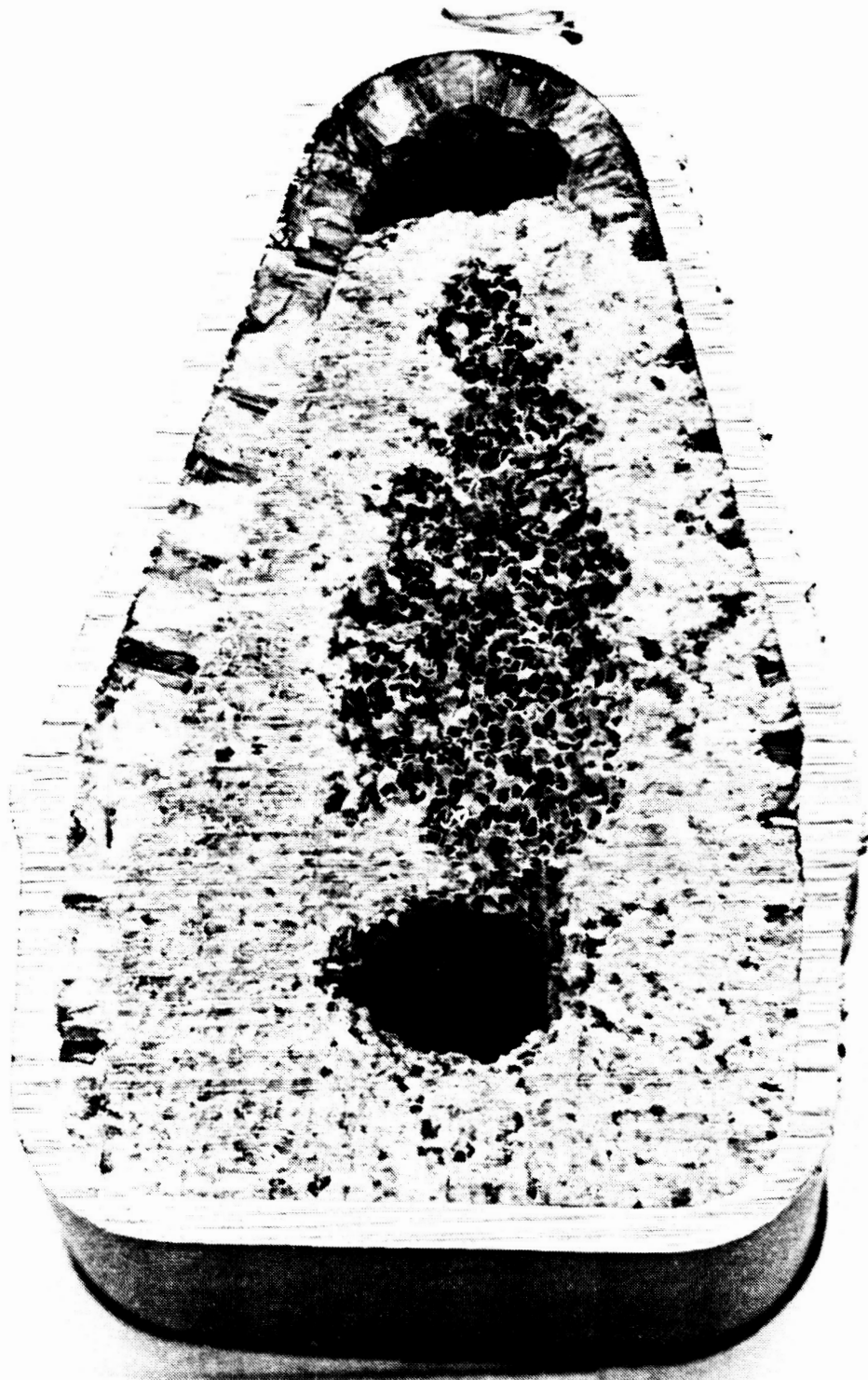


Figure 53 - PHOTOGRAPH OF SIX SECTIONS FROM WICKING TEST CANISTER RP46884

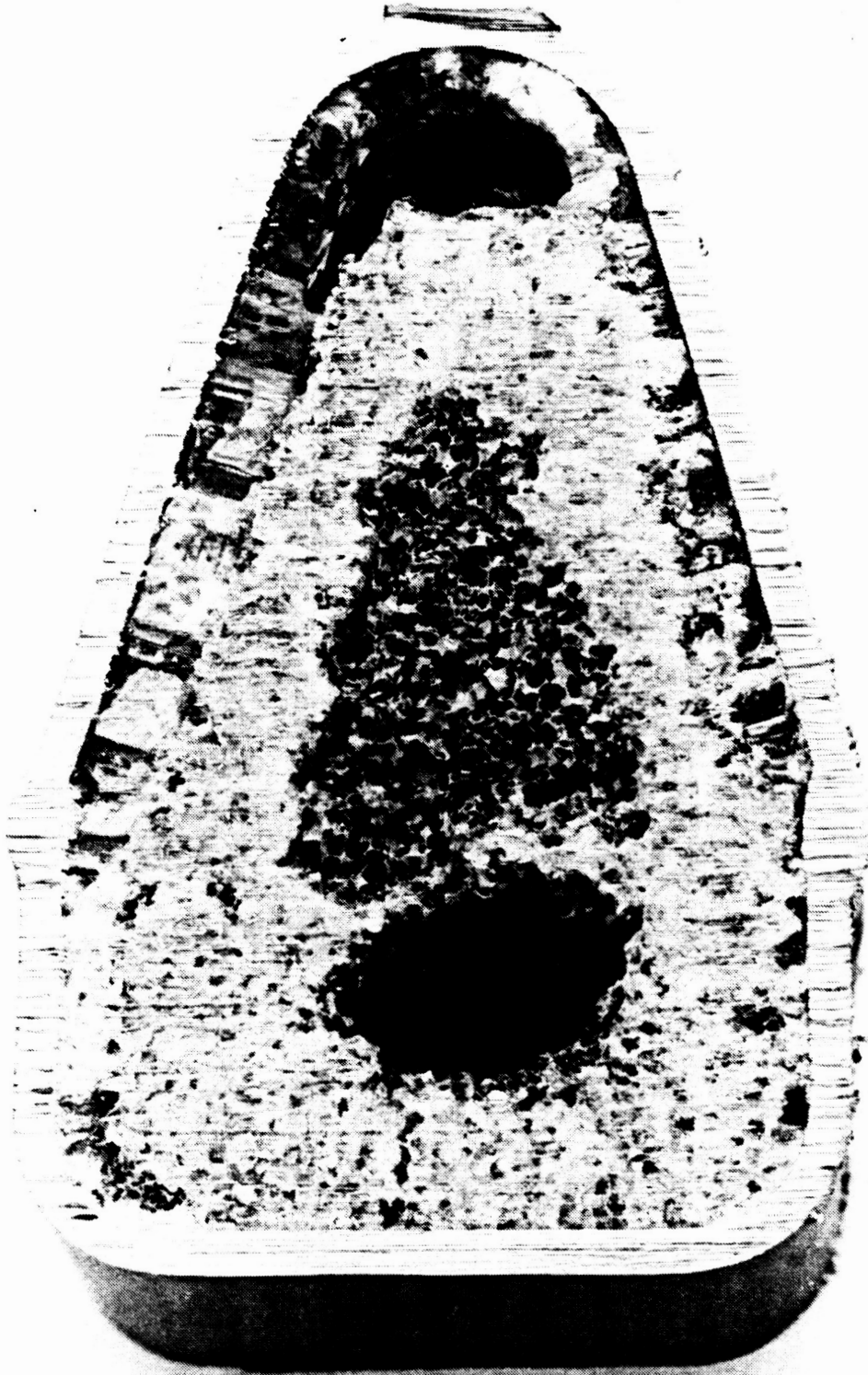
ORIGINAL PAGE  
BLACK AND WHITE PHOTOGRAPH



1

Figure 54 - PHOTOGRAPH OF SECTION 1.0 INCH FROM BOTTOM OF CANISTER

ORIGINAL PAGE  
BLACK AND WHITE PHOTOGRAPH



2

Figure 55 - PHOTOGRAPH OF SECTION 2.0 INCHES FROM BOTTOM OF CANISTER



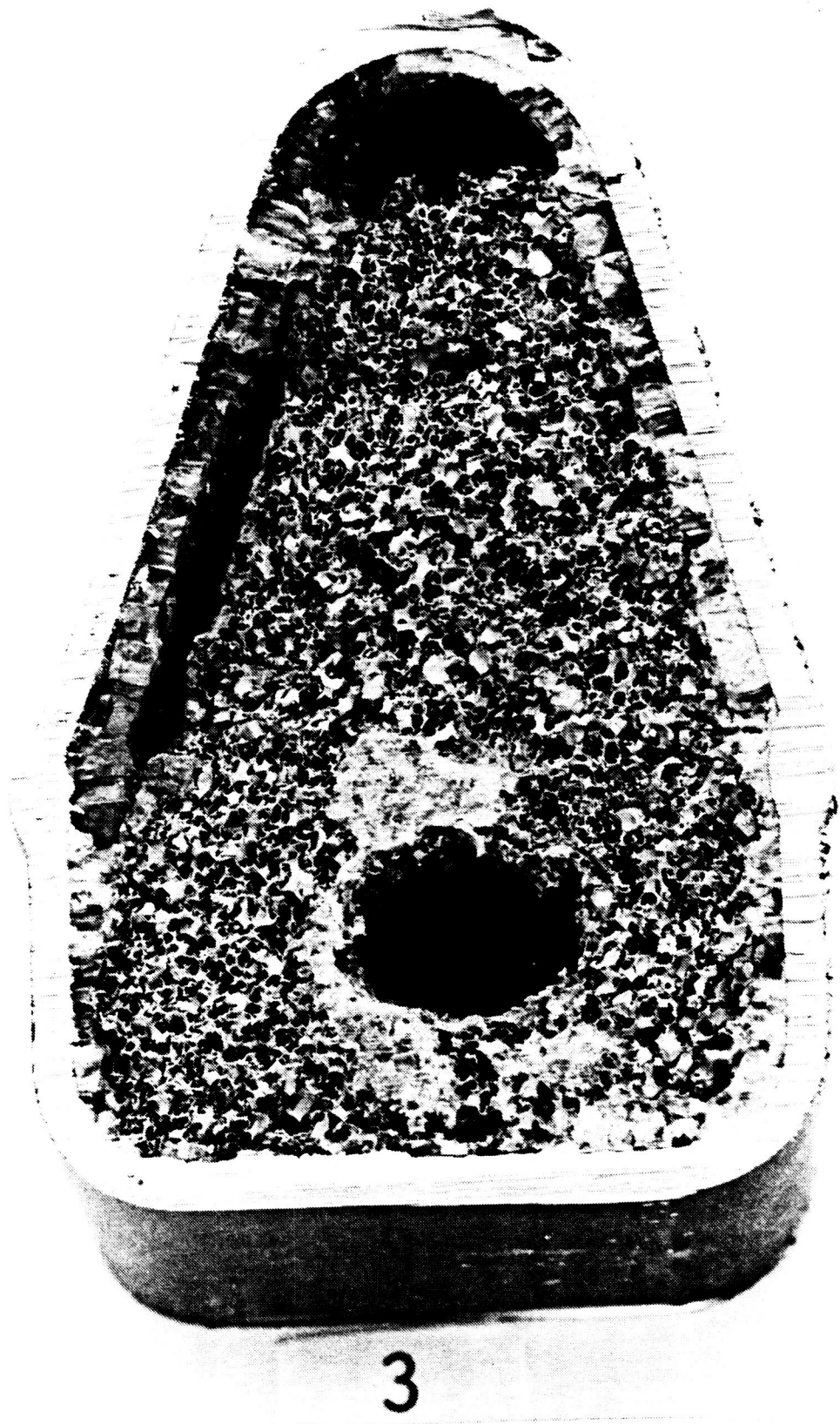
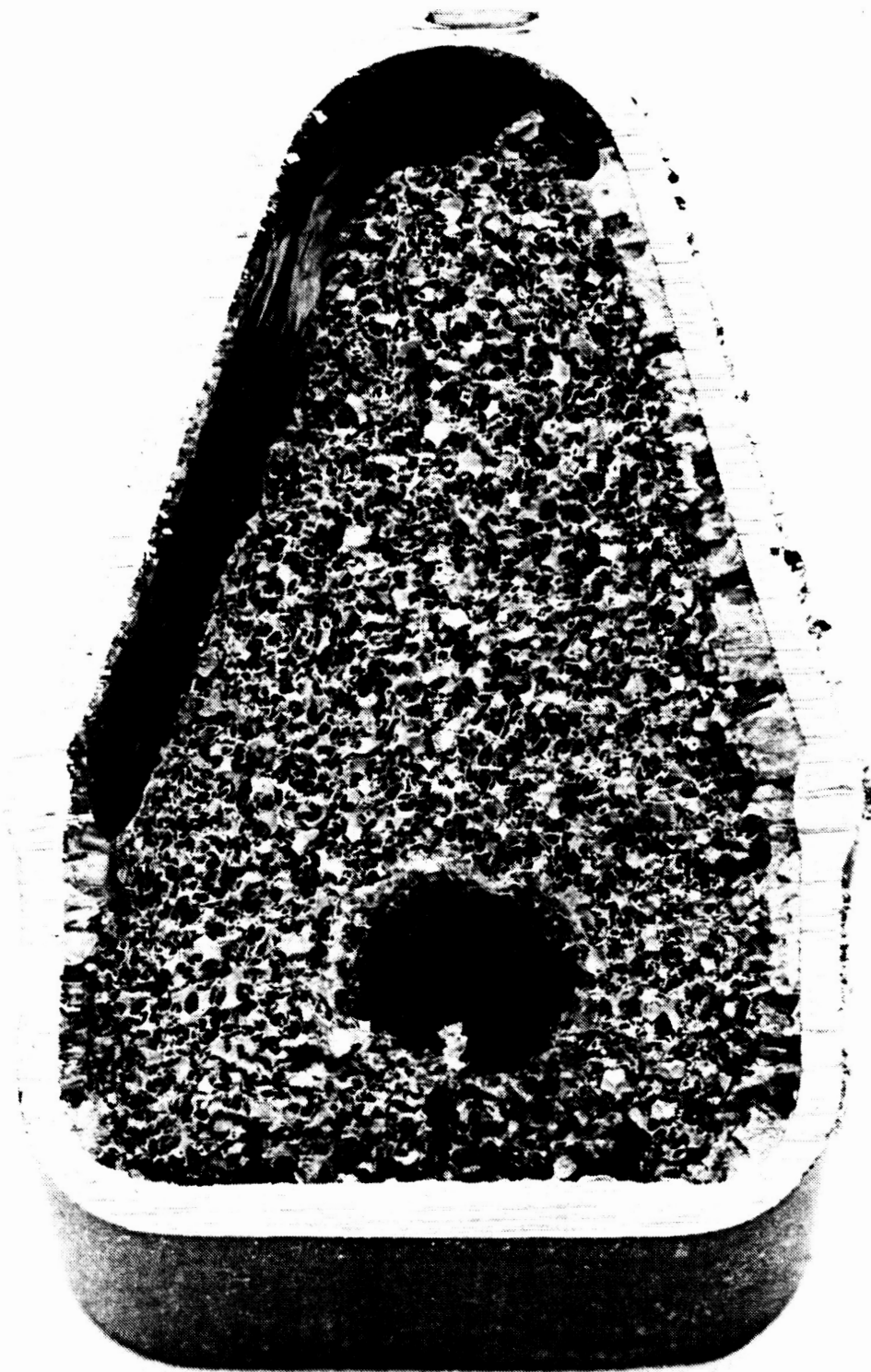


Figure 56 - PHOTOGRAPH OF SECTION 3.0 INCHES FROM BOTTOM OF CANISTER

ORIGINAL PAGE  
BLACK AND WHITE PHOTOGRAPH



4

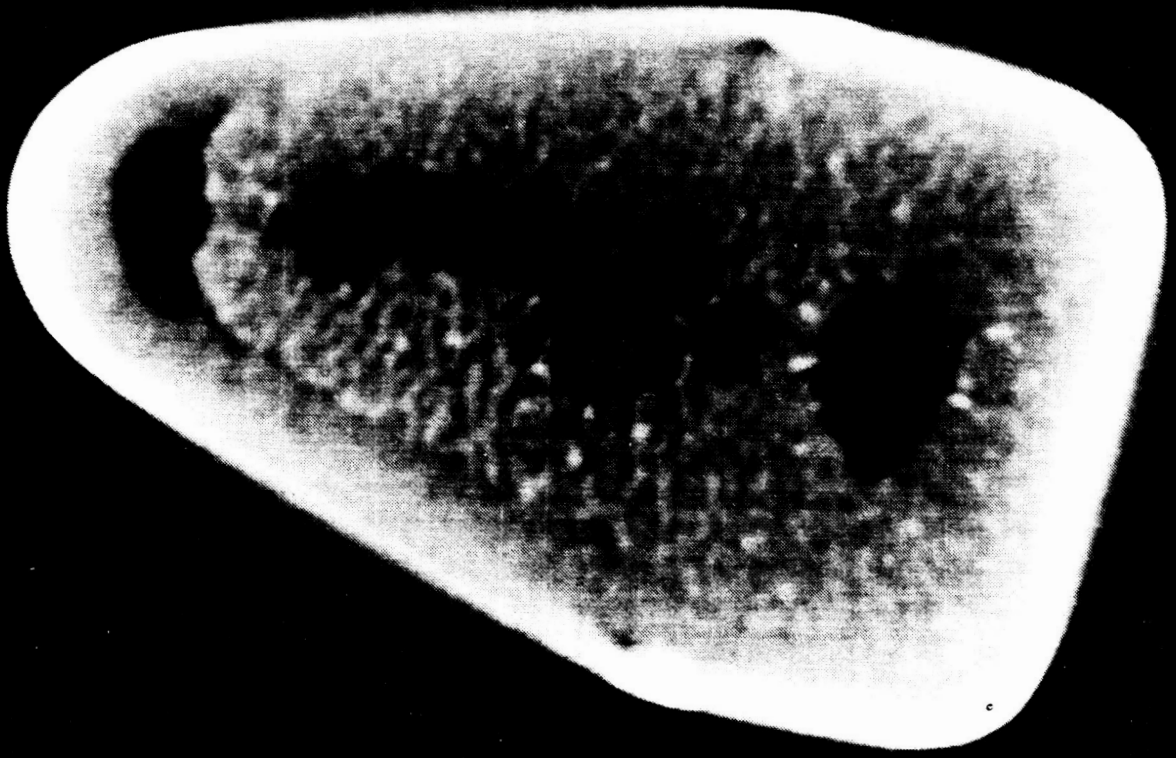
Figure 57 - PHOTOGRAPH OF SECTION 4.0 INCHES FROM BOTTOM OF CANISTER



0005:IMG  
2/23/91

Figure 58 - CT IMAGE OF SECTION 1.0 INCH FROM BOTTOM OF CANISTER

Matrix X  
Vscale 9.99  
Hscale 9.99  
Pscale 9.99  
Window  
Level 9999  
Width 9999  
R O I  
Length  
Cursor X 256  
Y 256  
Data  
Angle 0  
Size X 3  
Y 3  
\*Statistics\*  
Area  
Mean  
StdDv  
Min  
Max



RP46886

0010.IMG  
02/23/91

Figure 59 - CT IMAGE OF SECTION 2.0 INCHES FROM BOTTOM OF CANISTER

Matrix  
X  
Uscale 9.99  
Hscale 9.99  
Pscale 9.99

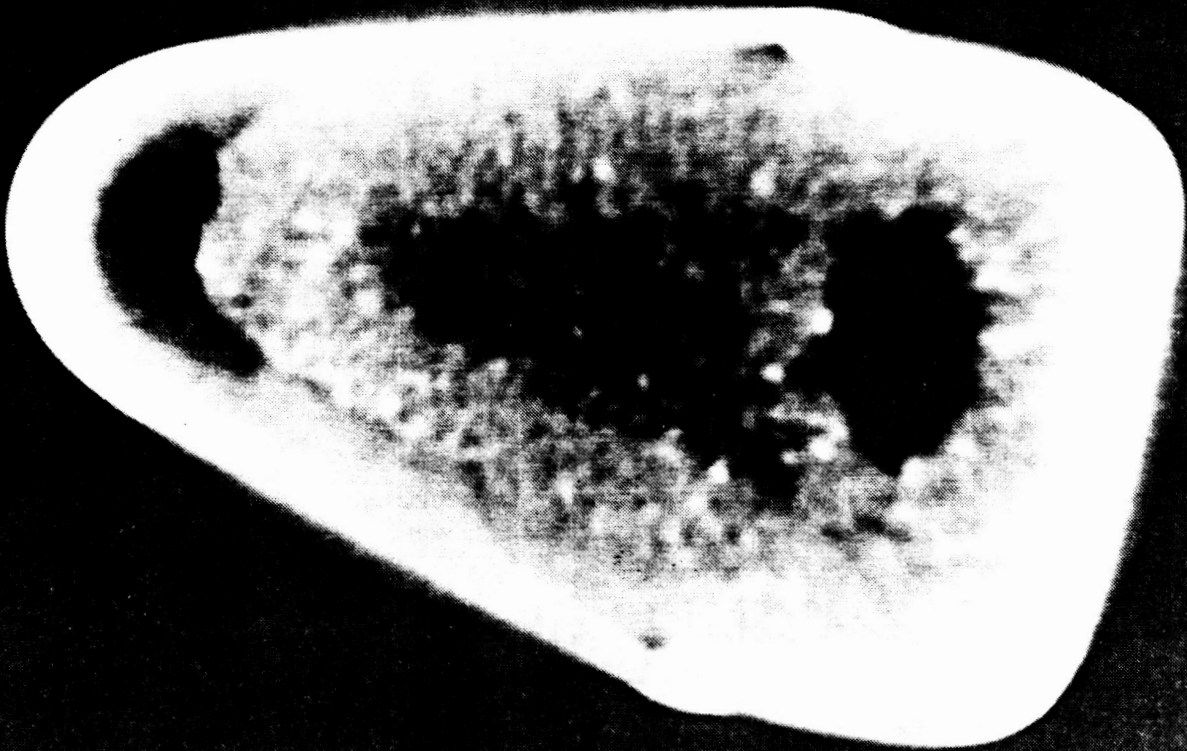
Window

Level 9999  
Width 9999

R O I  
Length  
Cursor X 256  
Y 256

Data  
Angle 0  
Size X 3  
Y 3

\*Statistics\*  
Area  
Mean  
Stddv  
Min  
Max



RP46887

0015:IMG  
02/23/91

Figure 60 - CT IMAGE OF SECTION 3.0 INCHES FROM BOTTOM OF CANISTER

Matrix

X

Uscale 9.99  
Hscale 9.99  
Pscale 9.99

Window

Level 9999  
Width 9999

R O I

.Length  
Cursor X 256  
Y 256

Data

Angle 0  
Size X 3  
Y 3

\*Statistics\*

Area

Mean

StdDv

Min

Max



RP46889

0020:IMG  
02/23/91

Matrix  
K

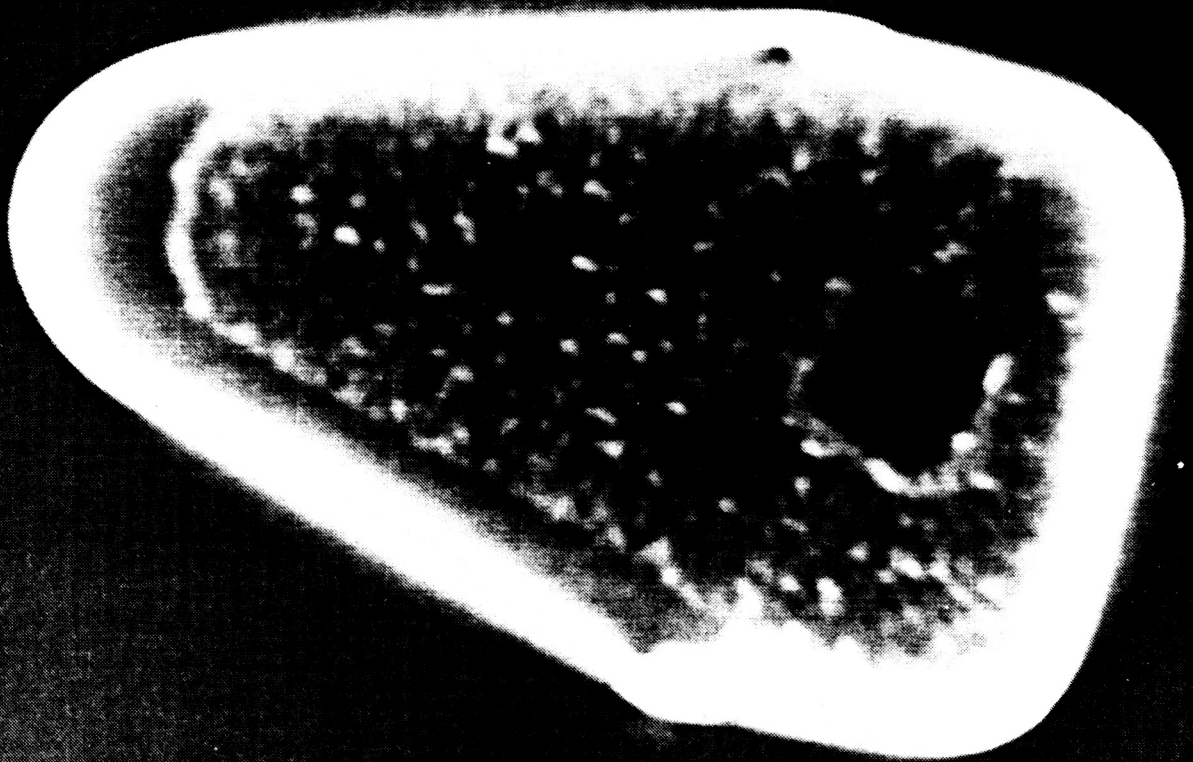
Uscale 9.99  
Hscale 9.99  
Pscale 9.99

Level 1409  
Width 2816



RP46888

Figure 61 - CT IMAGE OF SECTION 4.0 INCHES FROM BOTTOM OF CANISTER



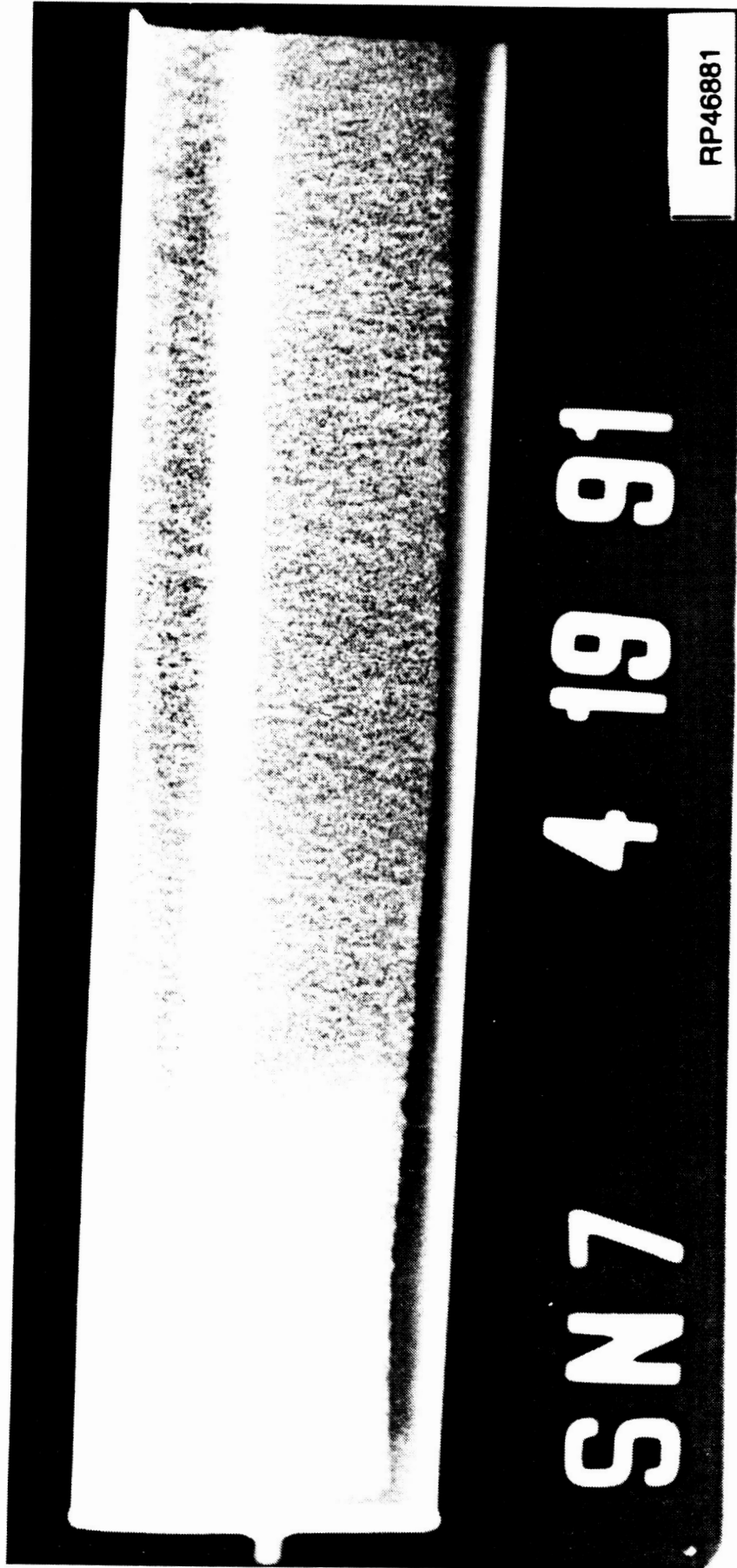


Figure 62 - X-RAY OF SIDE VIEW OF WICKING TEST CANISTER

phase change, this cycle was conservative from a stand point of stressing the canister. A comparison between a more realistic thermal cycle, which would have a temperature variation from 1089K (1500°F) to 1144K (1600°F), and the test cycle is shown in Figure 63. From the figure, one can see that the test cycle temperature ramp rate was 3.3K (6°F) per minute as opposed to 0.6-1.1K (1-2°F) expected in a more realistic cycle.

Canister S/N 6, which did not contain a nickel foam insert, was tested first. First, test point #2 was performed by following the "slow melt" temperature profile, shown on Figure 63. The purpose of test point #2 was to re-position the salt from its vertical fill orientation to a horizontal orientation for the remainder of the test points. Insulation was affixed to the canister back and sides for this test, and the wedge was pointed upward (180 degree orientation). Dimensional inspection and an X-ray photograph verified that the canister had not been damaged during this test. Several thermocouples broke loose from the canister during test point #2 due to the vigorous bubbling action of the fluidized bed.

Thus, the cable-sheathed thermocouples were replaced with inconel tubing-sheathed thermocouples. These new thermocouples were not fused to the canister wall like the original thermocouples, but temperature data indicated that they did have intimate enough contact with the canister since they gave reasonable readings of the wall temperatures. Additional support wires were used to minimize movement of the thermocouple assemblies. At this point the canister was ready for thermal cycling.

The first true thermal cycle to be performed was test point #3 in which canister S/N 6 was oriented with the wedge pointing upward (180 degree radial orientation), and the back wall was insulated. After the canister had been affixed in the holding fixture, the fixture was lowered into the furnace assuring that the canister was covered with sand. Furnace power was turned on and the furnace temperature increased from room temperature to 1244K (1780°F) over the course of about four hours. Then the temperature was held at the 1244K (1780°F) level for 30 minutes to allow the lithium fluoride to melt completely. After the high temperature dwell, the furnace controller turned on the cooling gas to simulate the eclipse portion of the orbit.

Temperature data from this test, which is plotted as a function of time in Figure 64, showed a strong inflection in the phase change region (1121K, 1558°F), especially in the back wall thermocouples. Note that the back wall thermocouple data are plotted as "B's", side wall data denoted as "S's", wedge data as "W's", and furnace data as "F's." The furnace temperature fell approximately 33K (60°F) during the high temperature dwell due to a controller error, as can be seen from this plot. Also, note that two of the wedge thermocouples and two of the side wall thermocouples broke loose during this test. Since it is difficult to differentiate data from the various canister locations in this plot, plots of average temperatures for the wedge, side walls, and back wall were made. Figure 65 is a plot of average temperatures for the second repetition of test point #3. (Note that the reference in the title to test 3-2 refers to the second repetition of test point #3.) From this plot one can see that the back wall temperatures lagged farthest behind the furnace temperature. This was the expected behavior since the insulation kept the LiF salt frozen longer on the back wall. Side wall temperatures also lagged far behind the furnace temperature due to the fact that insulation covered the lower portion of the side walls.



**Figure 63 - AVERAGE FURNACE TEMPERATURE PROFILE COMPARISONS**

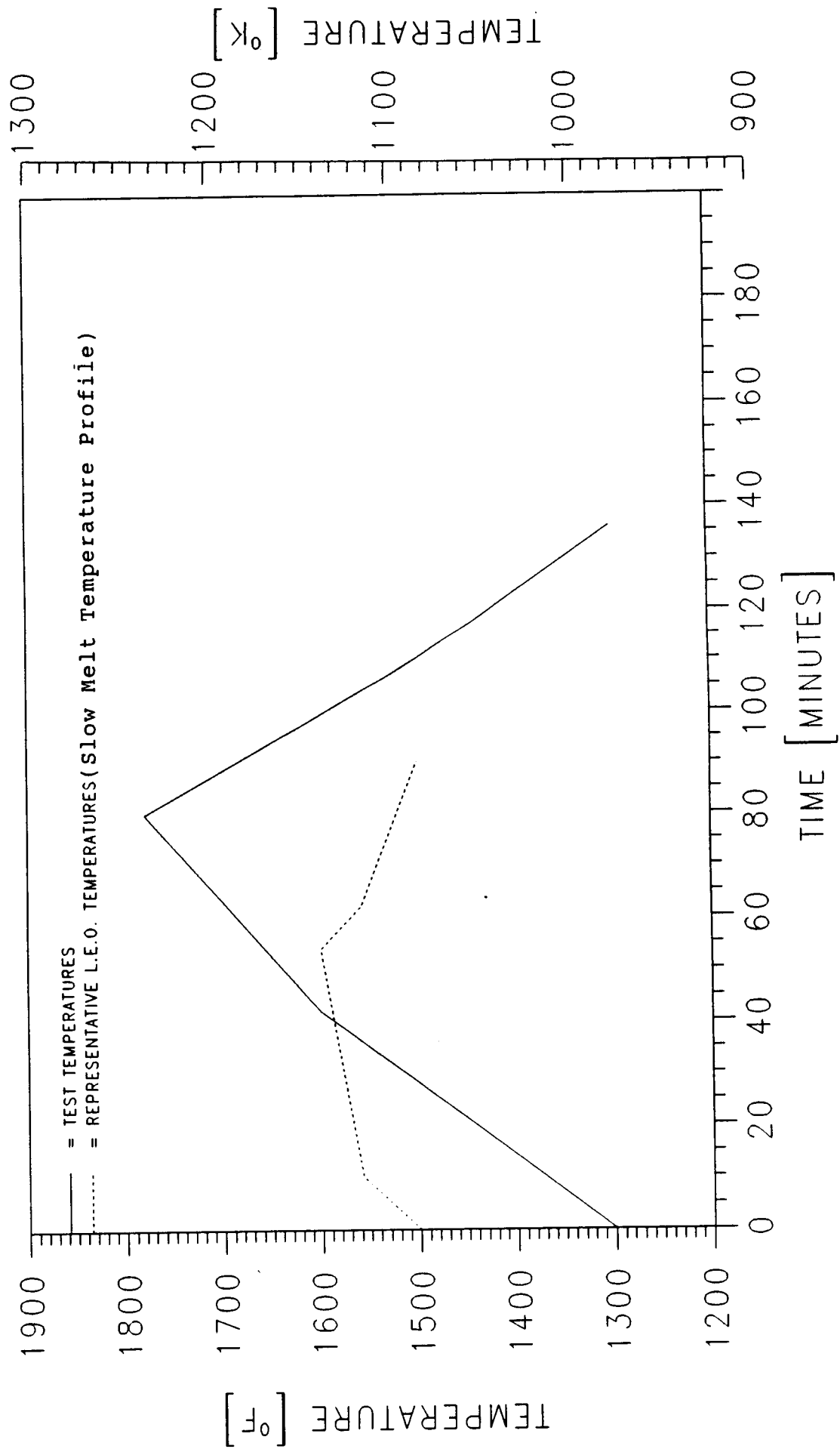
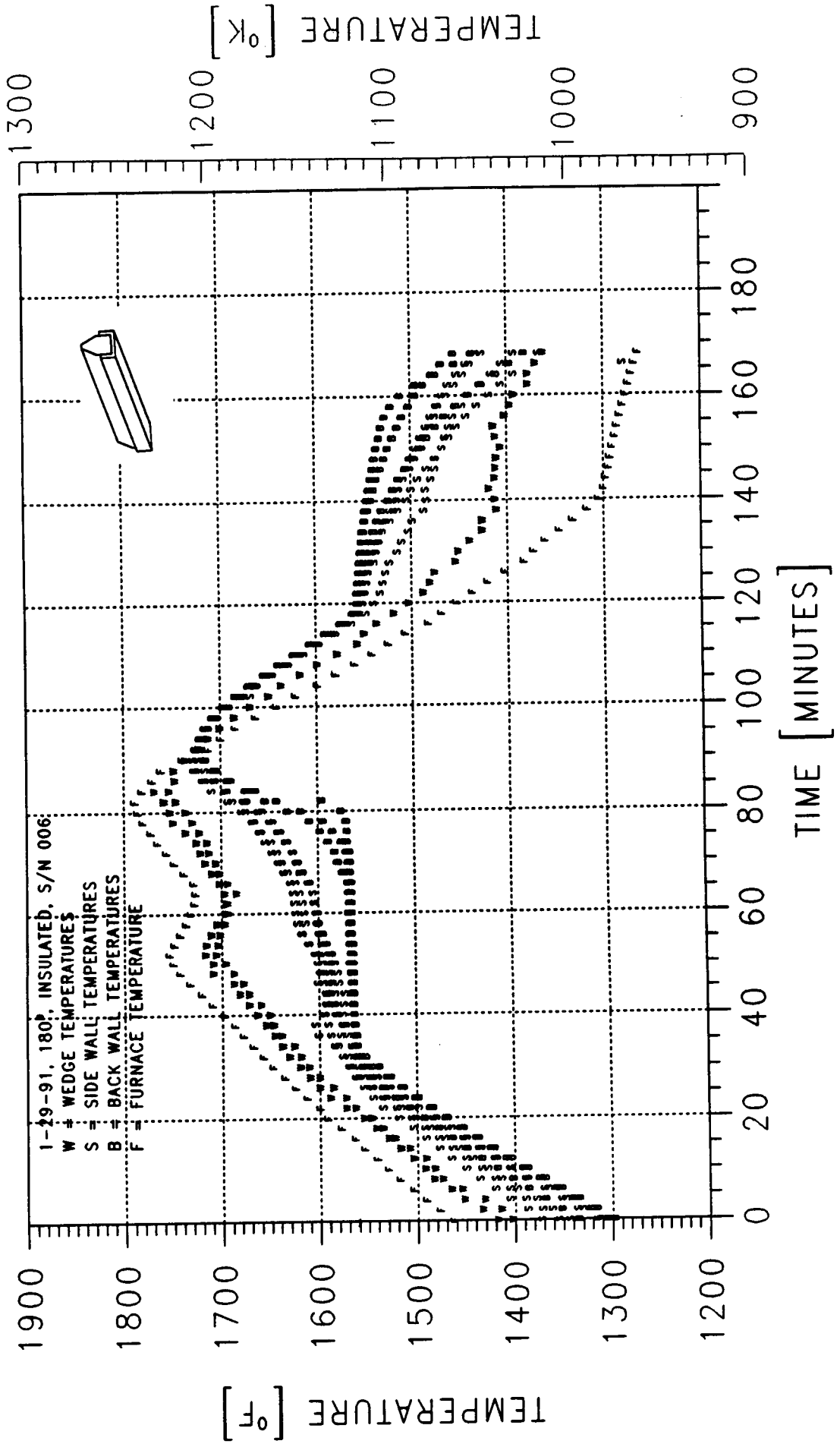
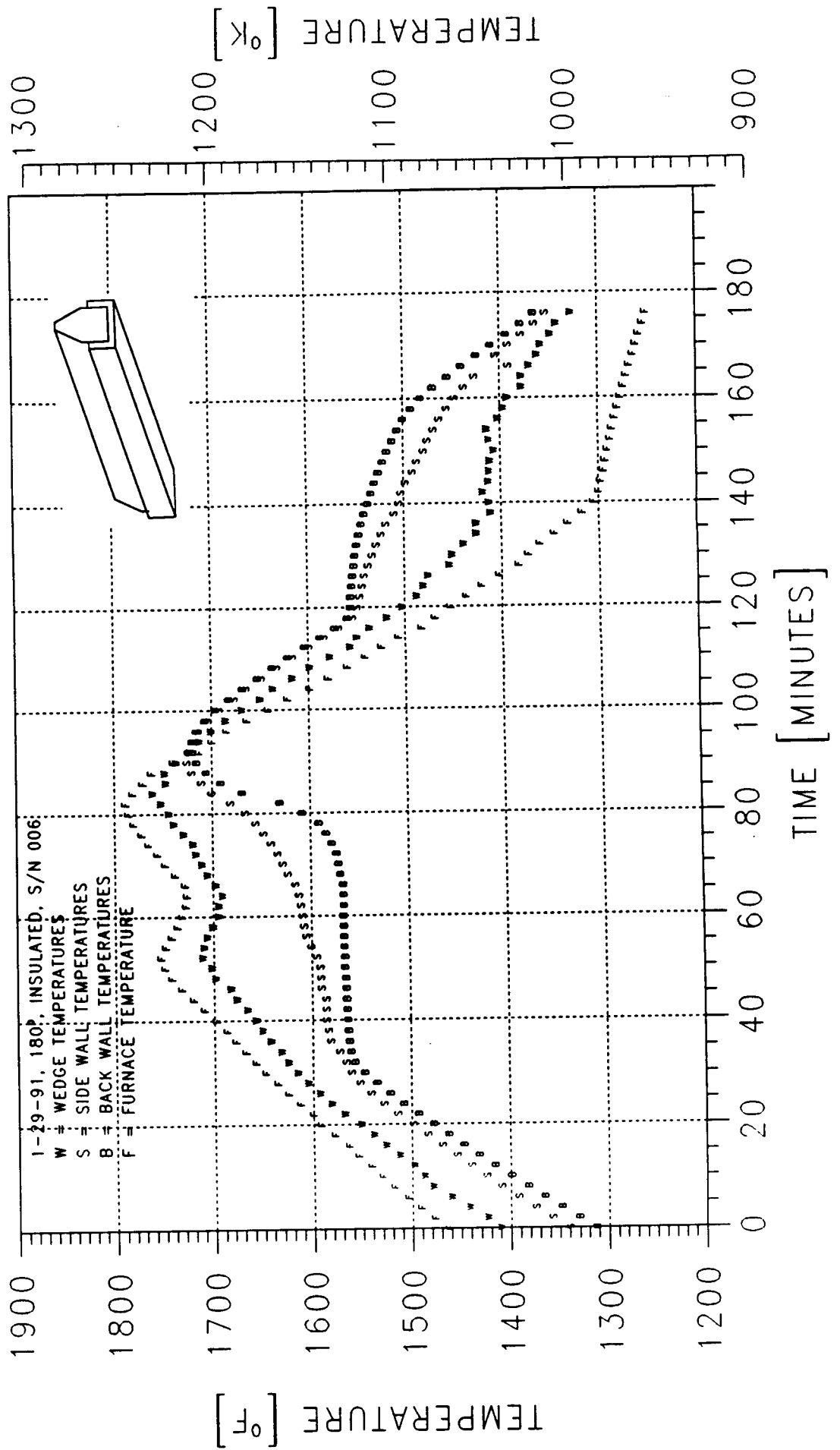


Figure 64 - TEMPERATURE PROFILES: TEST NO. 3-2





**Figure 65 - AVERAGE TEMPERATURE PROFILES: TEST NO. 3-2**



Wedge temperatures, on the other hand, followed the furnace temperature rather closely. Note that similar trends have been observed in independent canister thermal investigations.

The canister was allowed to cool overnight and then removed from the furnace. After the insulation had been removed, dimensional inspections were made and the canister was X-rayed. Results from the dimensional inspections and X-ray photography will be discussed in Sections 5.3.3 and 5.3.4, respectively. Then, broken thermocouples were replaced, the insulation was re-attached to the canister, and the canister was mounted on the furnace fixture again. These basic procedures were followed for all subsequent tests. It is noteworthy that thermocouple failure rates were lower for subsequent tests due to improved attachment methods.

Test point #4 was performed with the S/N 006 canister wedge pointing downward and the back surface insulated. Data from the first repetition was neglected since the lithium fluoride needed to be melted from the 180 degree orientation to the 0 degree orientation. Average temperatures from the second repetition of test point #4, called Test No. 4-2, are shown in Figure 66. As expected, the back surface temperature follows the furnace temperature more closely, although it lags a small amount due to the insulation. The back and wedge surfaces show predictable phase change inflections, although it is interesting to note that the wedge temperature does not show as much of a deflection upon freezing as it did during melting.

Since the lithium fluoride had frozen when the canister was held in the 0 degree orientation during test condition #4, test point #6 was performed next. The canister was left at the 0 degree orientation and the insulation was removed. From Figure 67, one can see that the back wall temperature followed the furnace temperature much more closely during the melt, although it lags the furnace temperature more during the freeze portion of the cycle. Also note that the wedge temperature profile for this test closely resembles the profile for test 4-2. Finally, the high temperature dwell time was reduced simply to expedite the test. In all subsequent tests in which the canister was uninsulated, the high temperature dwell time was reduced or deleted. This was done because the entire canister surface area was participating in heat transfer, lessening the time required to change the phase of the LiF mass.

For the next test, test point #5, the canister was rotated to a 180 degree orientation and was left uninsulated. Figure 68, a plot of average temperature profiles for test 5-1, shows an exchange between the back wall and wedge temperature profiles as compared to test 6-1. As expected, the back wall temperature shows the larger inflection in the melt region. For the sake of comparison, test condition #5 was repeated, and the results of this second repetition are shown in Figure 69. The two plots match very well, especially in the melt region.

After these tests on S/N 6 were completed, the canister with the nickel foam insert, S/N 5 was readied for testing. New thermocouples were attached, the canister was mounted on the furnace fixture with the wedge facing upward (180 degree orientation), and the insulation was affixed to the canister. During the first repetition of test point 8, the furnace fixture accidentally tilted 6 degrees off horizontal. The average temperatures from

Figure 66 - AVERAGE TEMPERATURE PROFILES: TEST NO. 4-2

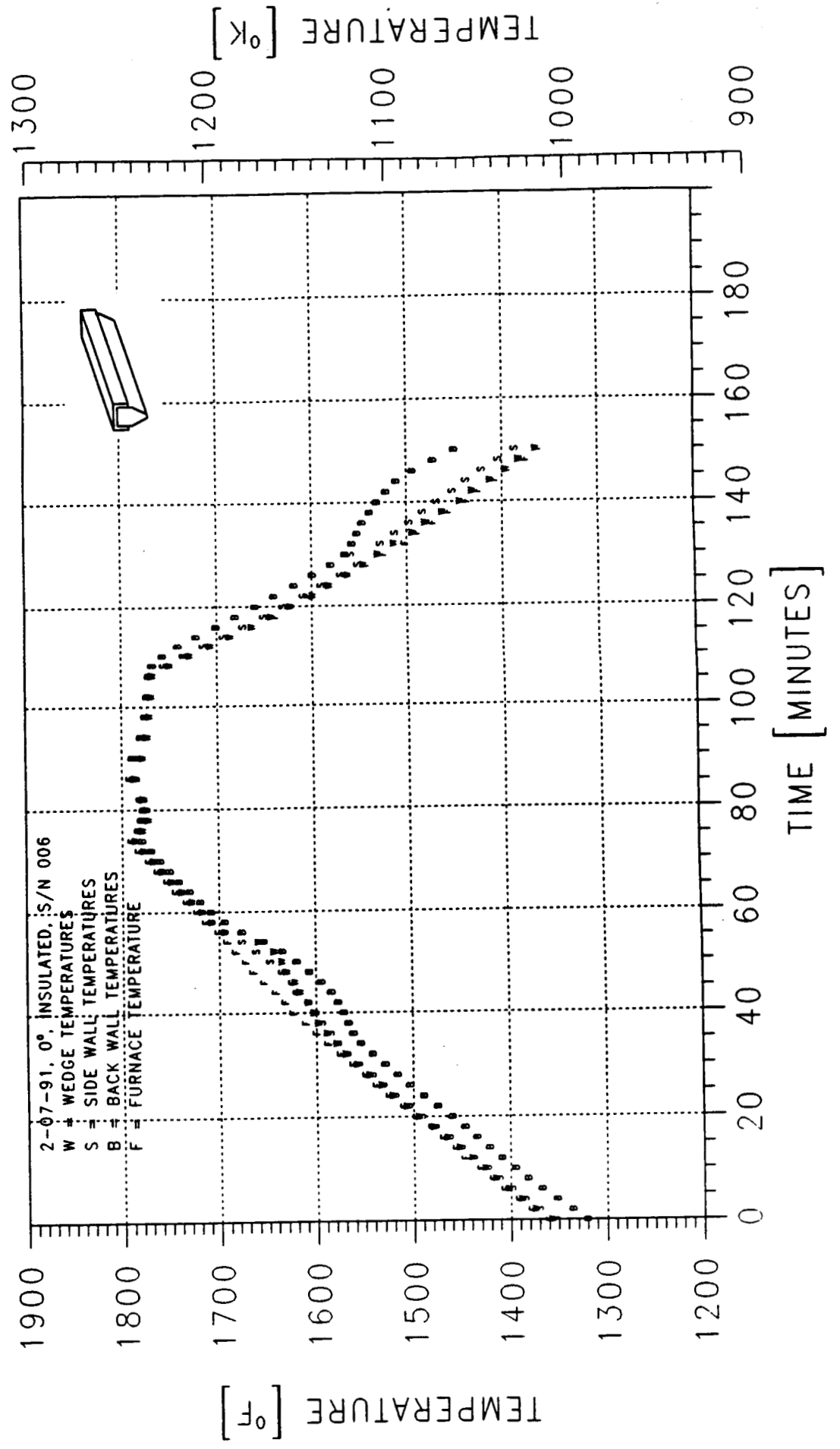


Figure 67 - AVERAGE TEMPERATURE PROFILES: TEST NO. 6-1

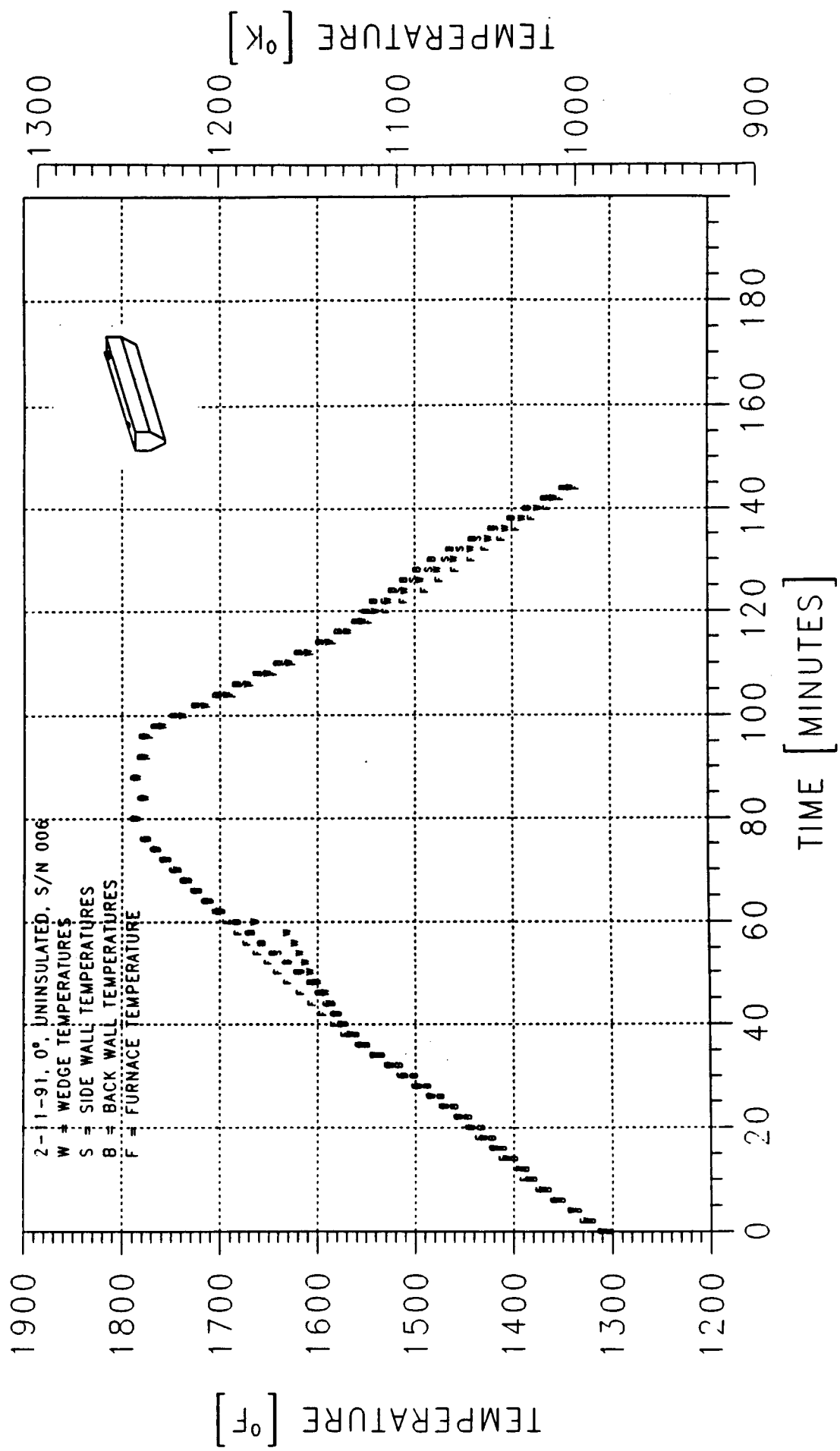
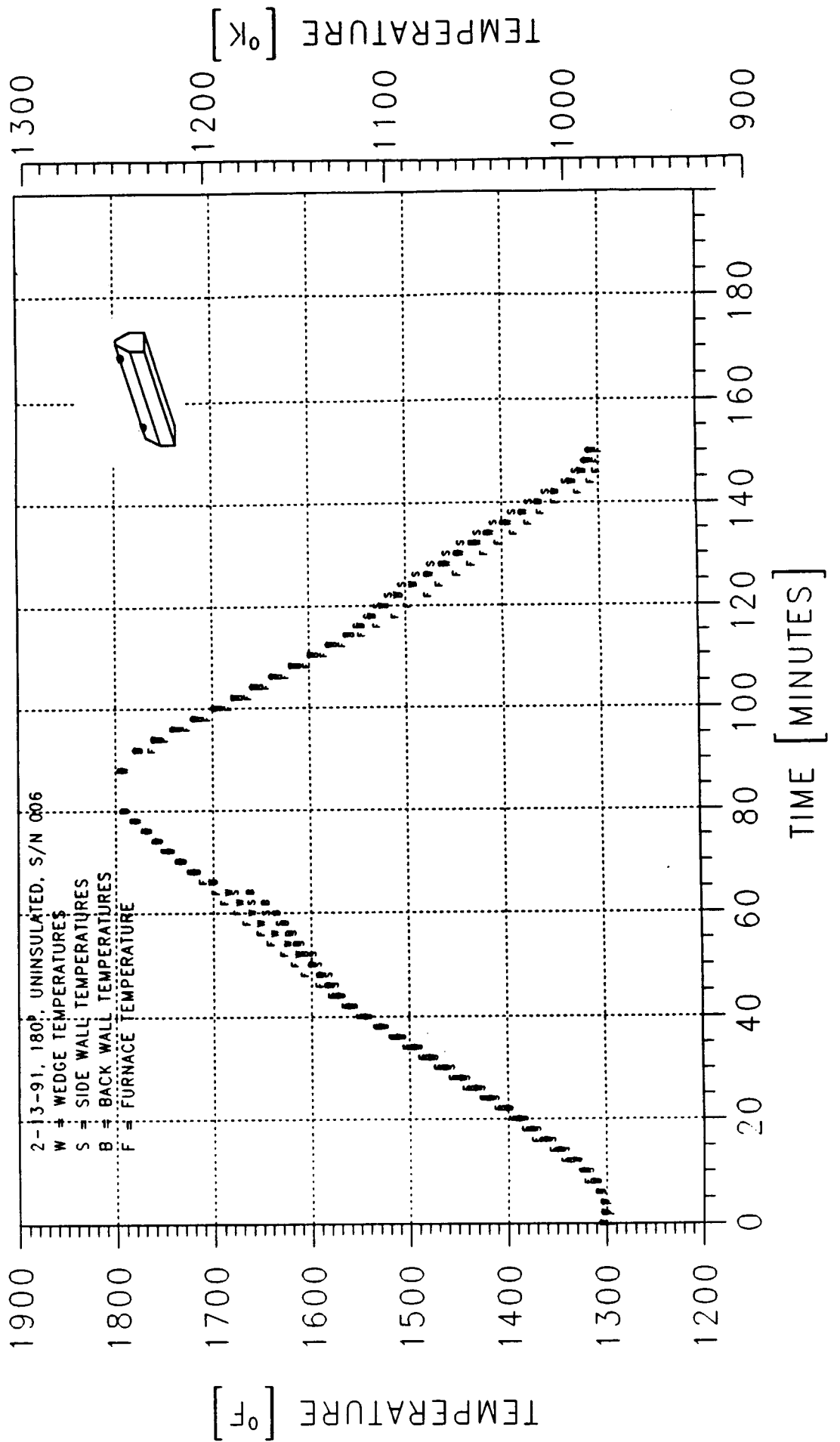


Figure 68 - AVERAGE TEMPERATURE PROFILES: TEST NO. 5-1



**Figure 69 - AVERAGE TEMPERATURE PROFILES: TEST NO. 5-2**

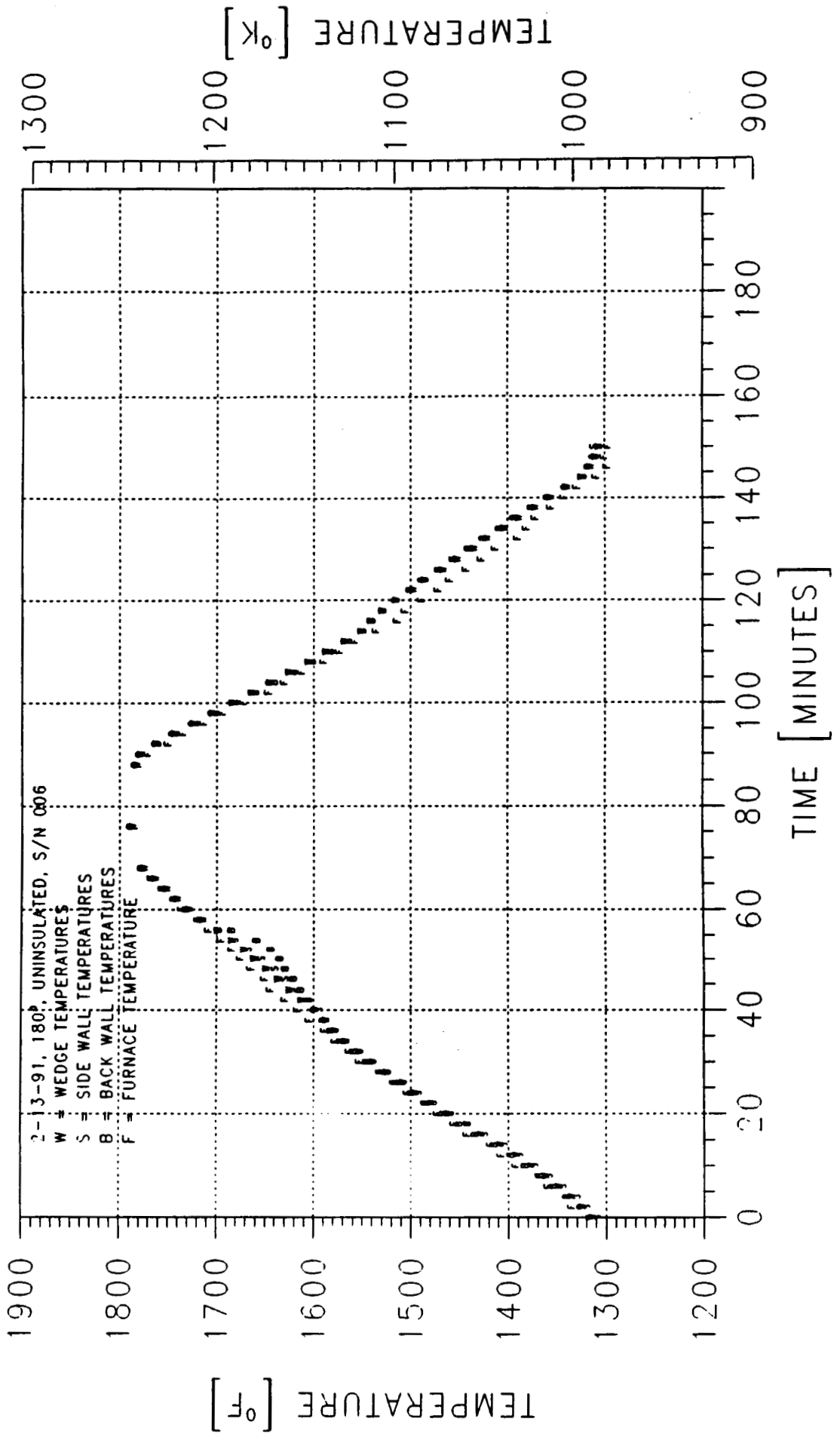
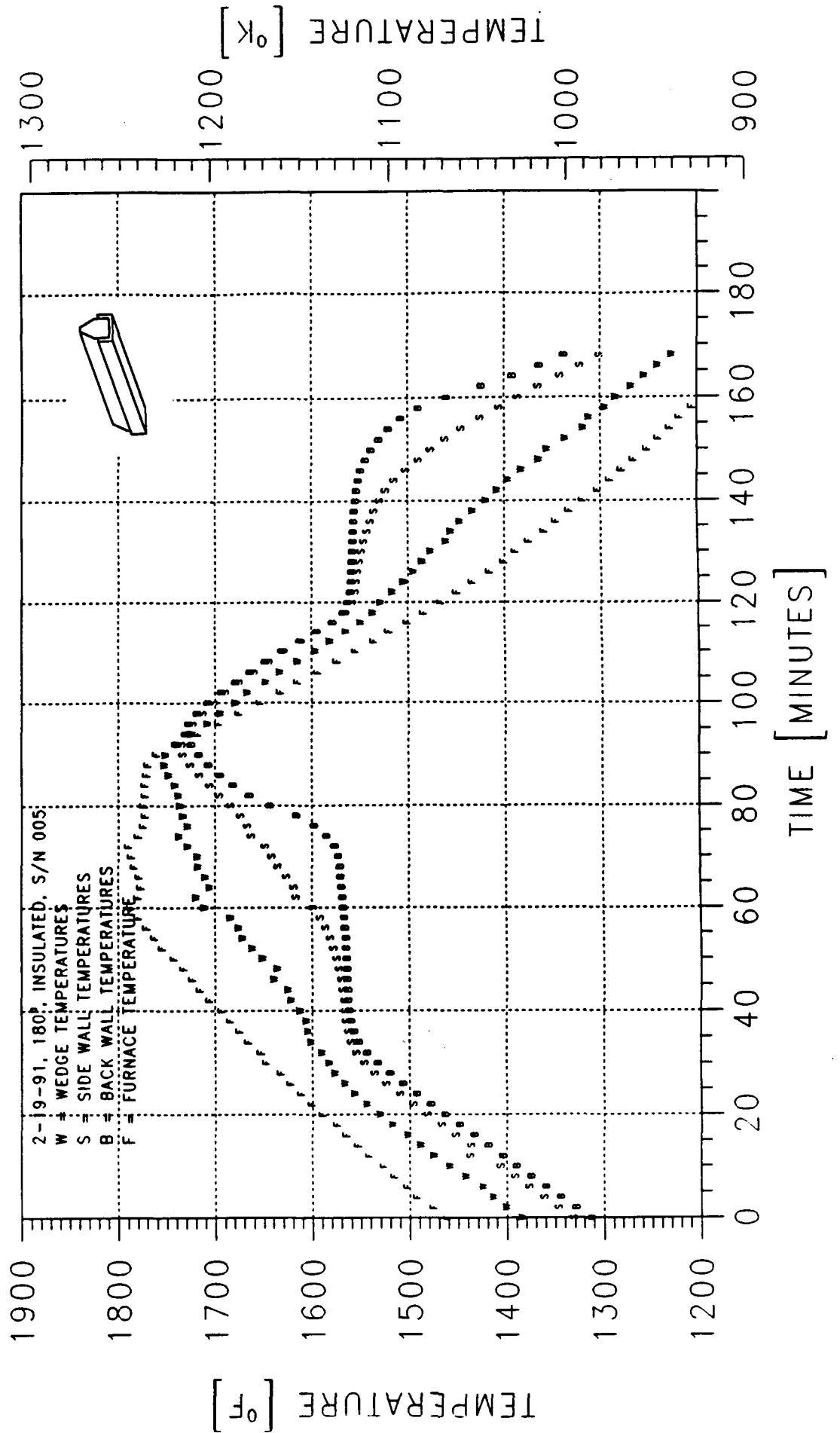


Figure 70 - AVERAGE TEMPERATURE PROFILES: TEST NO. 8-1 (TILTED 6°)



this test are shown in Figure 70. Another two repetitions of test condition #8 were executed, and average temperatures from test #8-3 are shown on Figure 71. By comparing the two figures, one can see little difference between the two cases.

The canister was rotated to a 0 degree orientation for test point #9. As expected, the wedge temperature profile has a slight inflection in the phase change regions, as shown in Figure 72 and the back wall temperatures lag behind the furnace temperatures due to the insulation. High temperature soak data was not plotted since the canister was nearly isothermal.

To prepare for test condition #11, the insulation was removed from the canister, and the radial orientation was left at 0 degree. From Figure 73, one can see slight inflections in the wedge and side wall temperatures during the phase changes, and the back wall temperatures follow the wedge temperatures more closely since the insulation was removed.

Finally, the canister was rotated to a 180 degree orientation, and test condition #10 was executed. Average temperatures from test #10-2, shown in Figure 74, had predictable temperature trends with the back wall temperatures displaying the greatest phase change temperature lag.

One of the main goals of the test program was to determine whether or not the nickel foam insert in canister S/N 5 provided significant thermal conductivity enhancement. To assess the conductivity enhancement, comparisons were made between the temperature profiles of the canister with the nickel foam insert, S/N 5, and the canister without an insert, S/N 6. The comparisons were made between test points which had identical canister orientations and insulation conditions. For instance, test points #3 and #8 both had 180 degree canister orientation and back wall insulation.

Figure 75 shows a comparison between back wall temperature results from tests #3 and #8. The top plot shows average temperature data for the back wall and furnace for both tests. It is obvious that the profiles are out of phase with respect to time but that they otherwise display similar trends. From the middle plot one can see the temperature difference between the furnace and back wall for both canisters. Once again, the profiles follow similar trends, especially in the phase change region. However, one notable difference between the two profiles can be seen in this plot. The temperature difference between the insulated back wall and the furnace was greater for S/N 5, the canister with the nickel foam insert. For instance, during thaw the maximum  $\Delta T$  between the furnace and the back wall was 124K (224°F) for S/N 5 while the maximum  $\Delta T$  for S/N 6 was 105K (189°F). During freeze, the maximum  $\Delta T$  was 167K (301°F) for S/N 5 while the maximum  $\Delta T$  for S/N 6 was 130K (234°F). The probable cause of the larger  $\Delta T$ 's in S/N 5 was the nickel foam, which acted as a radiant receptor surface. The pure LiF in S/N 6, on the other hand, was a good transmitter of radiant flux and passed more of the heat to the back wall where it was absorbed. These results were expected based on the results of Jaworske, et. al. [12].

The difference between the two profiles in the middle plot at the end of the thermal cycle can be attributed to differences in the final portion of the furnace temperature profiles. Finally, the maximum temperature difference between any two thermocouples on the back of a given canister is shown in the lower plot. Once again, both profiles follow the same



Figure 71 - AVERAGE TEMPERATURE PROFILES: TEST NO. 8-3

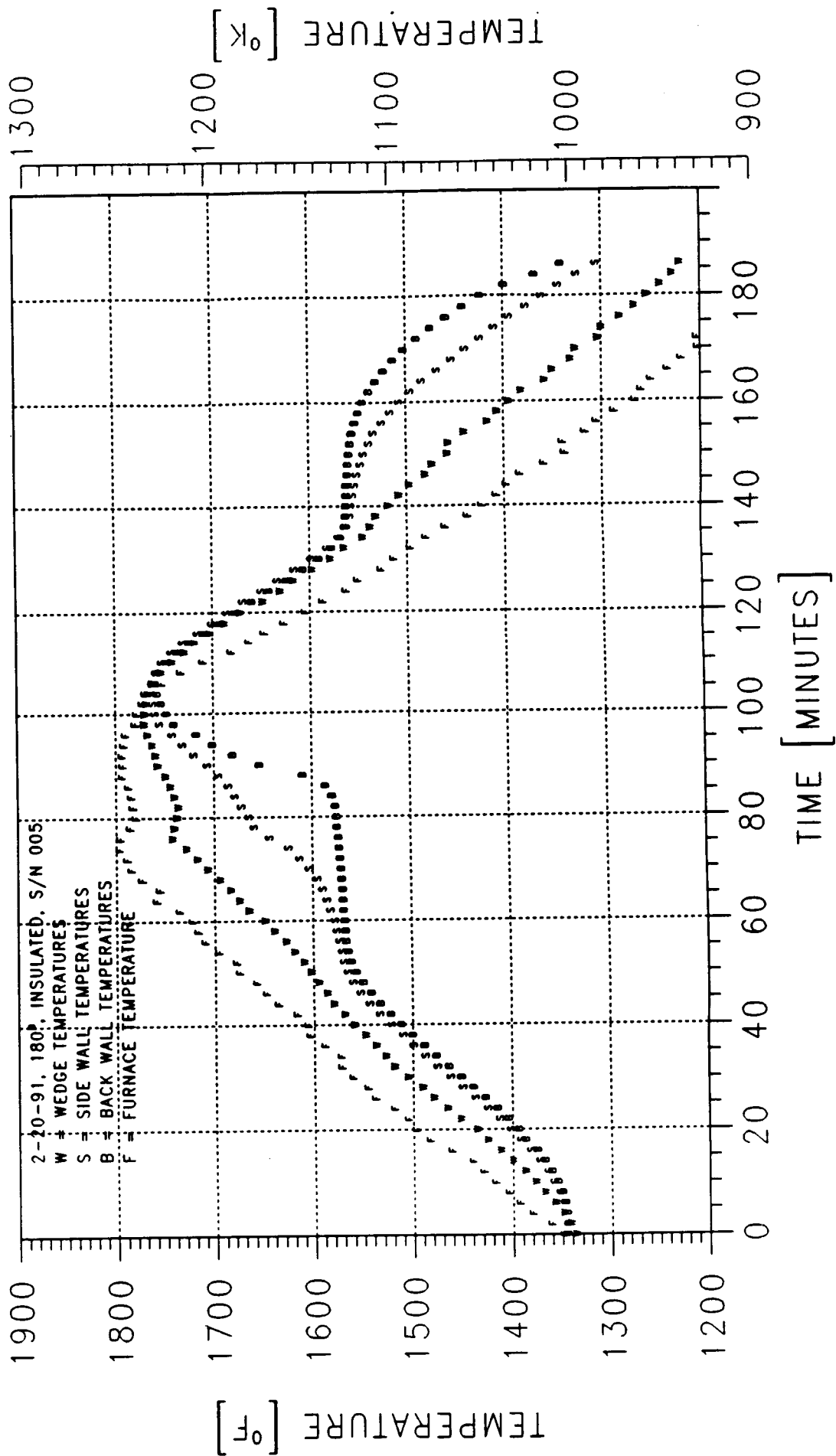


Figure 72 - AVERAGE TEMPERATURE PROFILES: TEST NO. 9-2

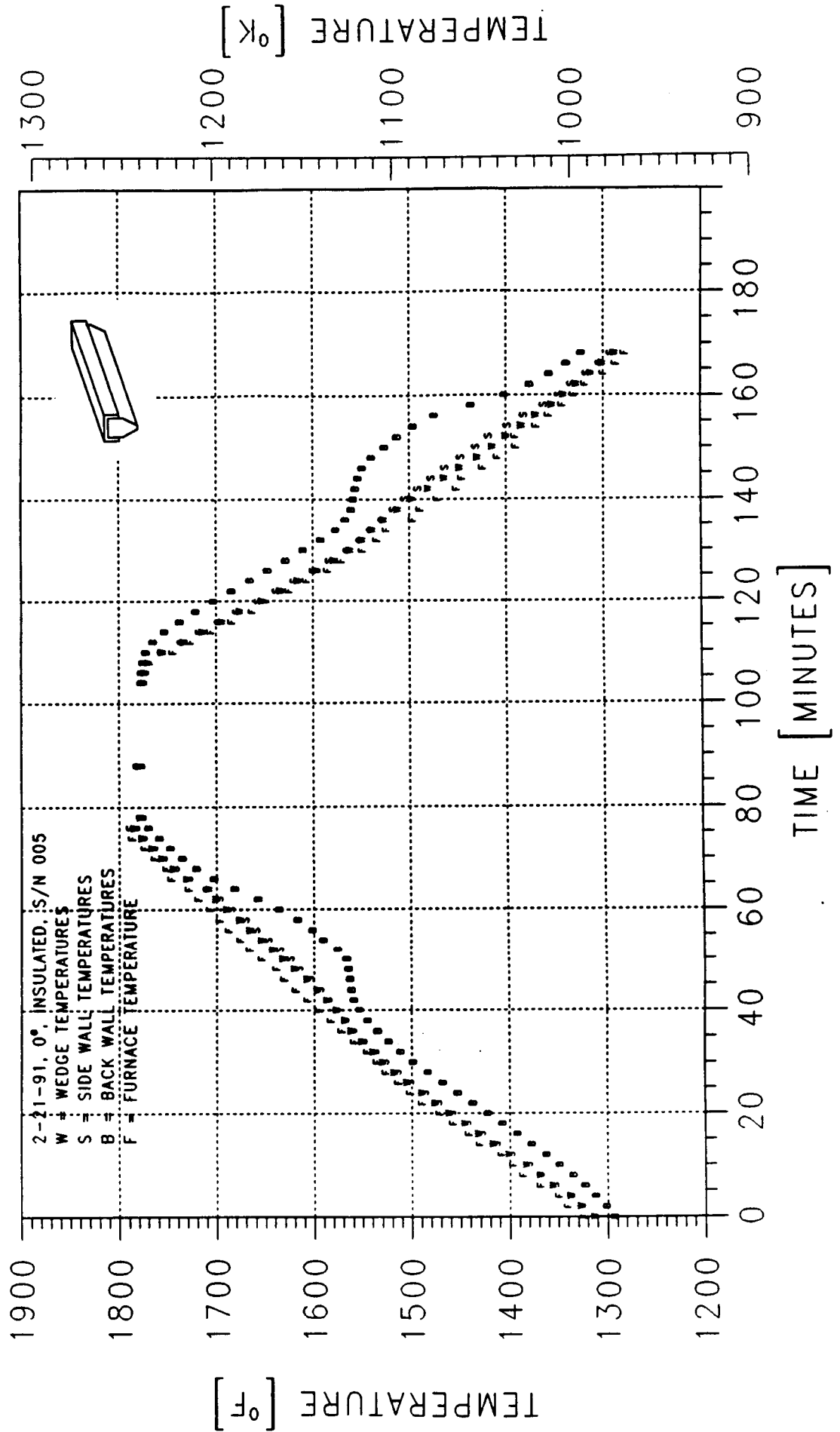


Figure 73 - AVERAGE TEMPERATURE PROFILES: TEST NO. 11-1

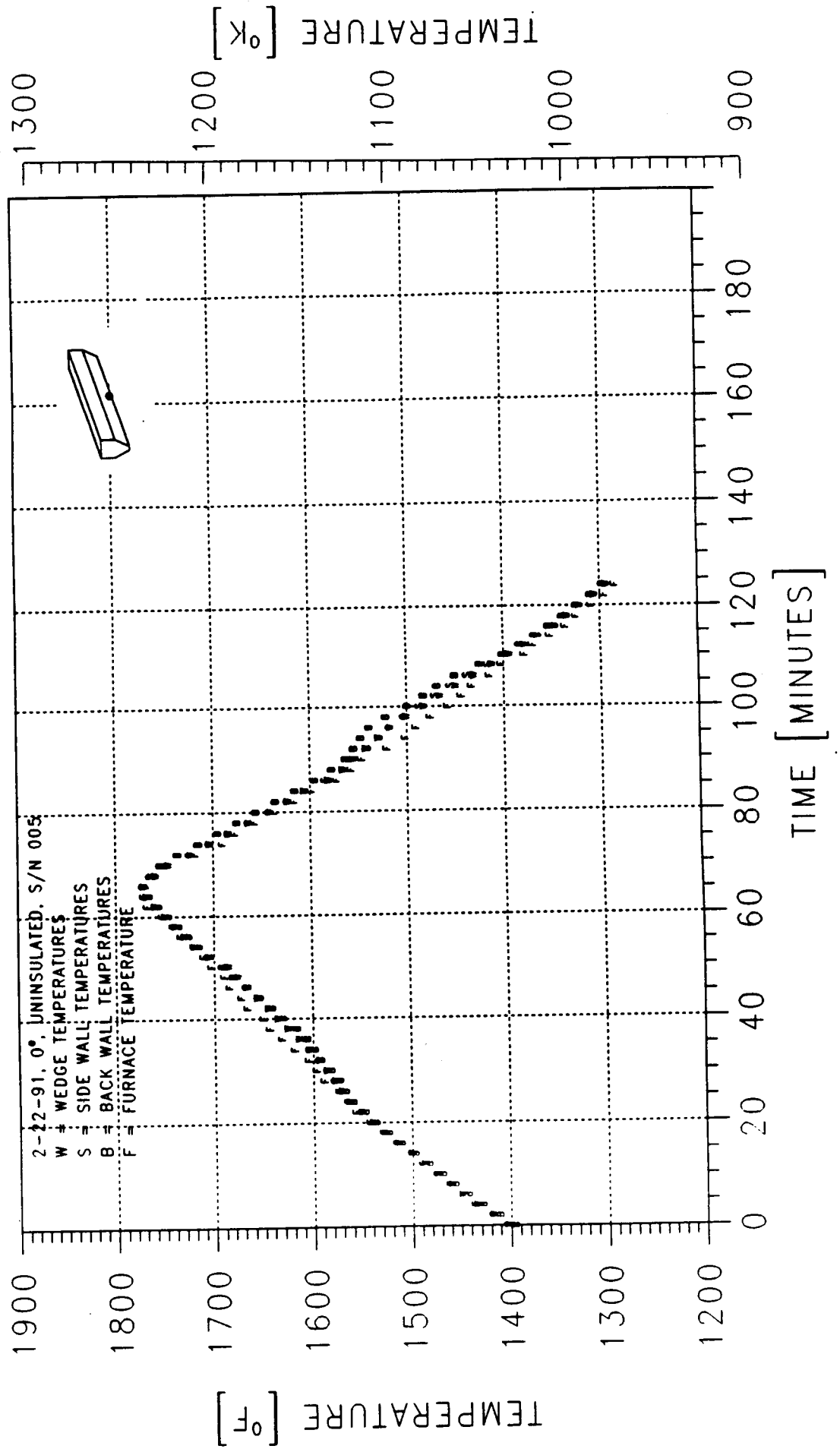


Figure 74 - AVERAGE TEMPERATURE PROFILES: TEST NO. 10-2

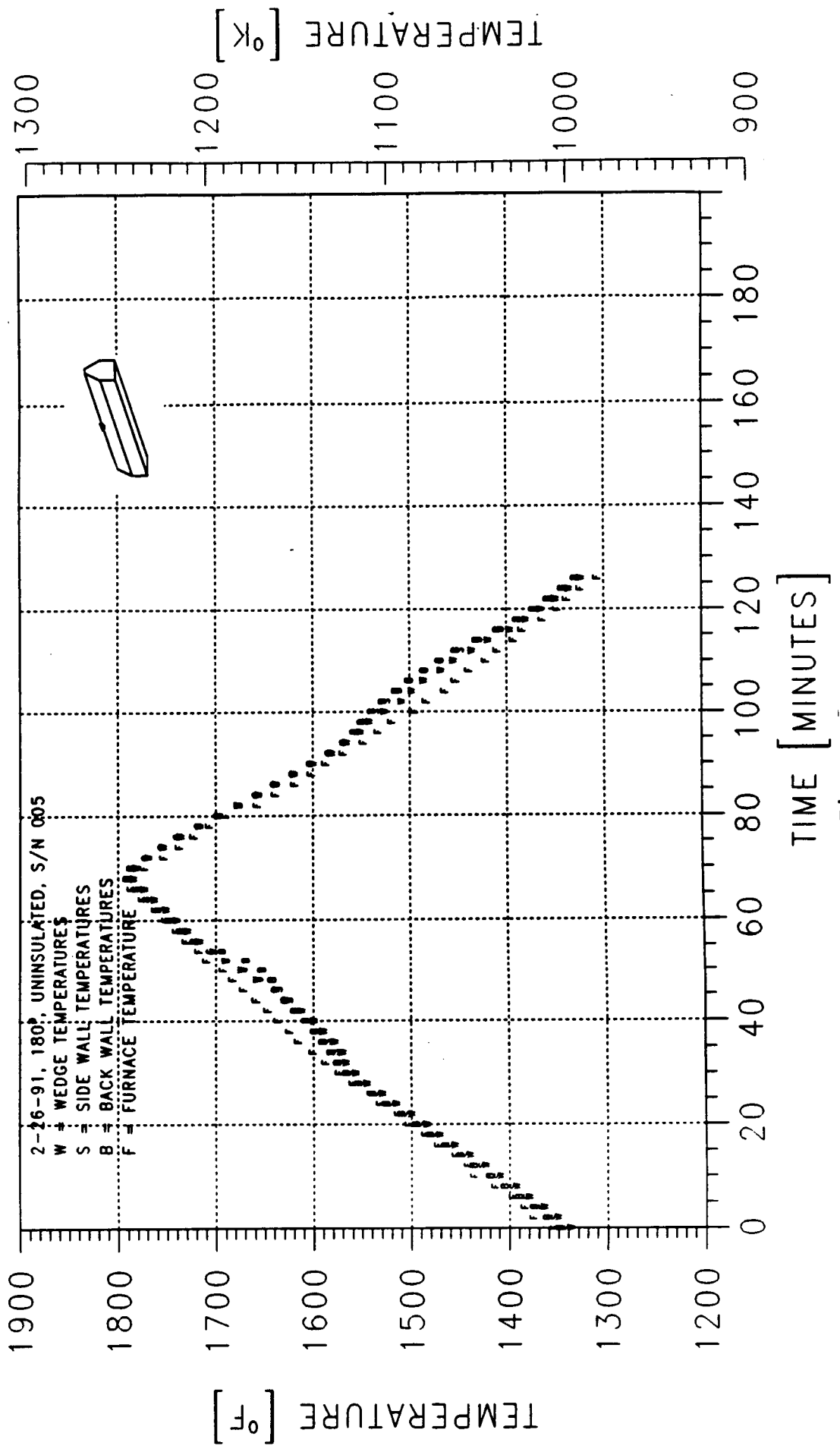
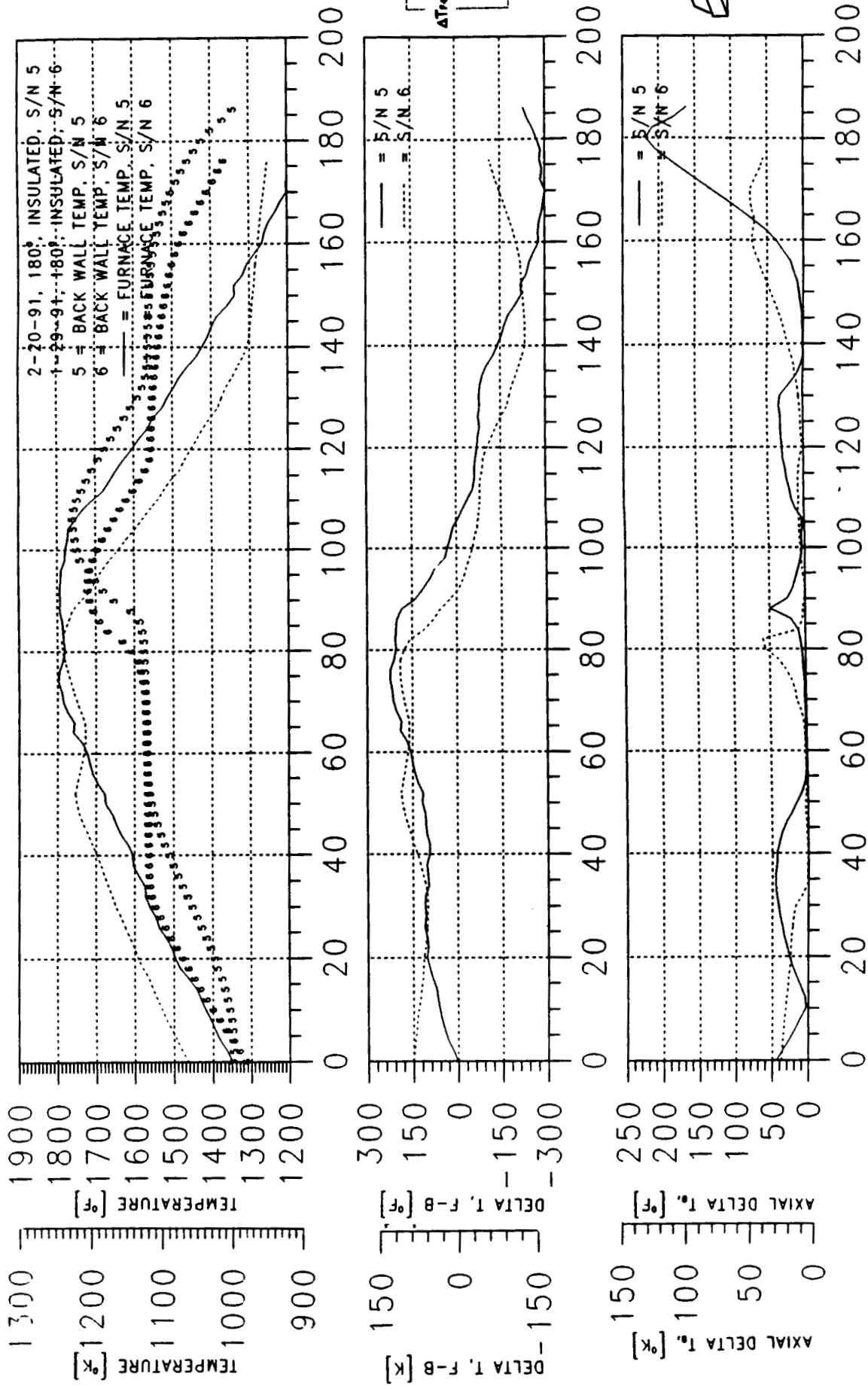


Figure 75 - COMPARISONS OF BACK WALL TEMPERATURES, TESTS 3-2 AND 8-3

[S/N 5 HAS NICKEL FOAM, S/N 6 DOES NOT]



general trends with the exception of the end portion of the profiles. Sketches on the right hand side of Figure 75 illustrate the thermocouple locations as well as the canister orientation and insulation status.

Comparisons of canister wedge temperatures for tests #3 and #8 are shown in Figure 76. The furnace to wedge temperature difference curves shown in the middle plot match well while the axial gradients shown on the lower plot differ slightly, as much as 33K (60°F), from one canister to the other. Two of the three thermocouples on the wedge of canister S/N 6 broke midway through the test which explains why the axial temperature gradient fell to zero at that time.

Tests #4 and #9, in which the canisters had a 0 degree orientation and insulation on the back surface, are compared in the next two figures. Back wall temperatures are compared in Figure 77. Furnace to back wall temperature difference profiles show the same trends observed in Figure 75. Once again, the canister with nickel foam had larger furnace to canister  $\Delta T$ 's. During the thaw, the maximum  $\Delta T$  between the furnace and the insulated back wall was 50K (90°F) for S/N 5 while the maximum  $\Delta T$  for S/N 6 was 33K (59°F). During freeze, the maximum  $\Delta T$  for S/N 5 was 76K (136°F) while the maximum  $\Delta T$  for S/N 6 was 57K (103°F). The nickel foam probably acted as a resistance to radiant heat flow and thus caused larger  $\Delta T$ 's. The axial temperature difference profiles, shown in the lower plot, match fairly well too.

Wedge temperature trends are compared in Figure 78. The furnace to wedge temperature differences are small in magnitude for each canister, and the profiles match each other well. Although the axial temperature difference profiles show some inconsistencies, the greatest magnitude of the difference between the canisters is only 25K (45°F).

The next two tests to be compared, tests #5 and #10, had 180 degree canister orientation and no insulation on the back surface. From Figure 79, a comparison of back wall temperatures, one can see that all of the profiles match well. This favorable match can be partially attributed to the fact that the canister was not insulated and thus had more heat transfer area and lower temperature differences. Likewise, the wedge temperature comparisons shown in Figure 80 show little difference in the profiles from one canister to the other.

Finally, tests #6 and #11, in which the canister was oriented at 0 degree and was uninsulated, are compared in the next two figures. Back wall temperature comparisons, shown in Figure 81, exhibit close matches between the two canisters. Similarly, wedge temperature comparisons shown in Figure 82 match fairly well.

Another set of comparison plots, Figures 83 and 84, were made to assess the repeatability of the test results from tests #5-1 and #5-2. As can be seen from these figures, the profiles are nearly identical. Likewise, Figures 85 and 86, which compare tests #8-1 and #8-3 performed on canister S/N 6, show profiles nearly indistinguishable from each other.

Figure 76 - COMPARISONS OF WEDGE TEMPERATURES, TESTS 3-2 AND 8-3

[S/N 5 HAS NICKEL FOAM, S/N 6 DOES NOT]

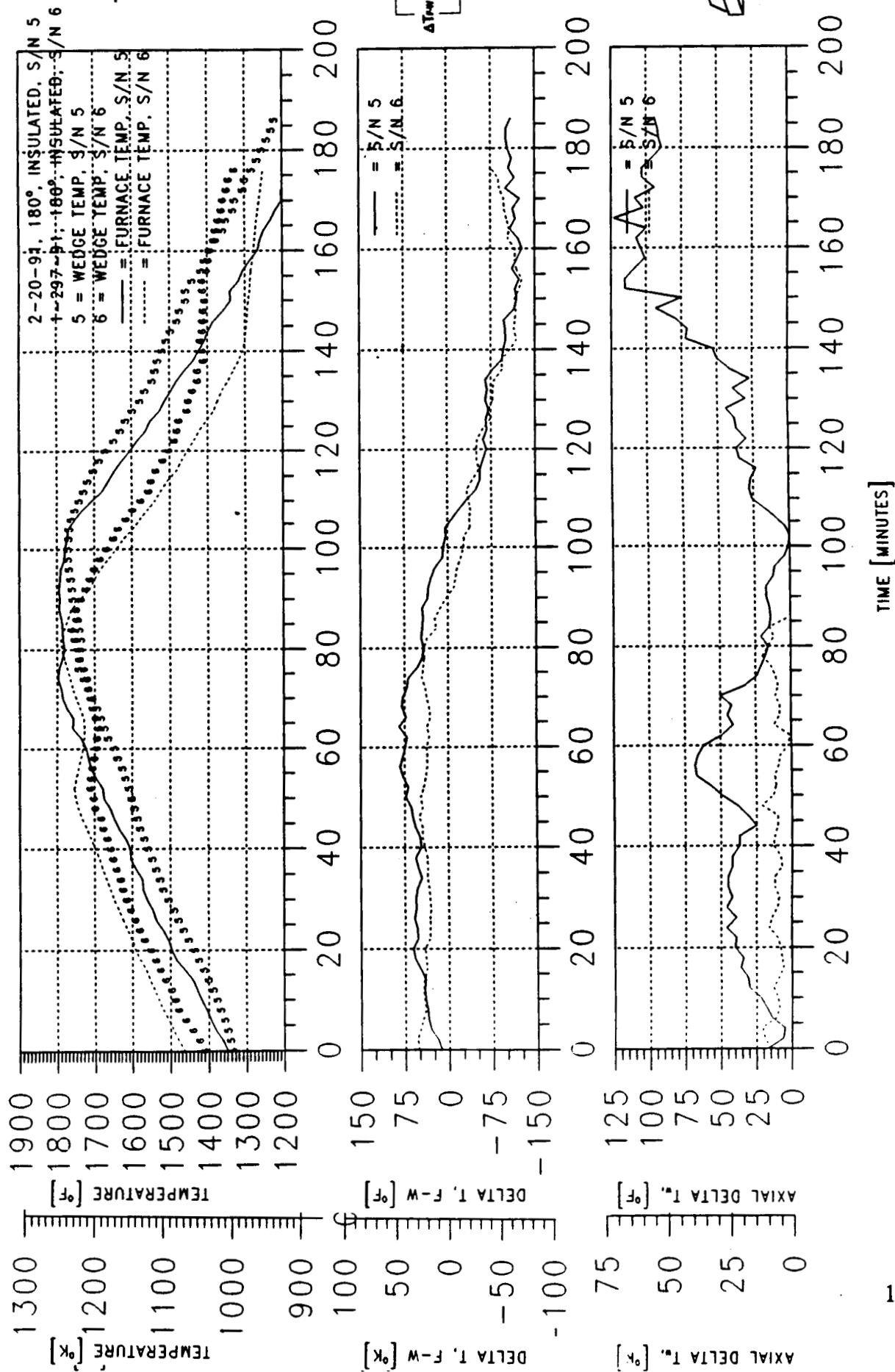


Figure 77 - COMPARISONS OF BACK WALL TEMPERATURES, TESTS 4-2 AND 9-2

[S/N 5 HAS NICKEL FOAM, S/N 6 DOES NOT]

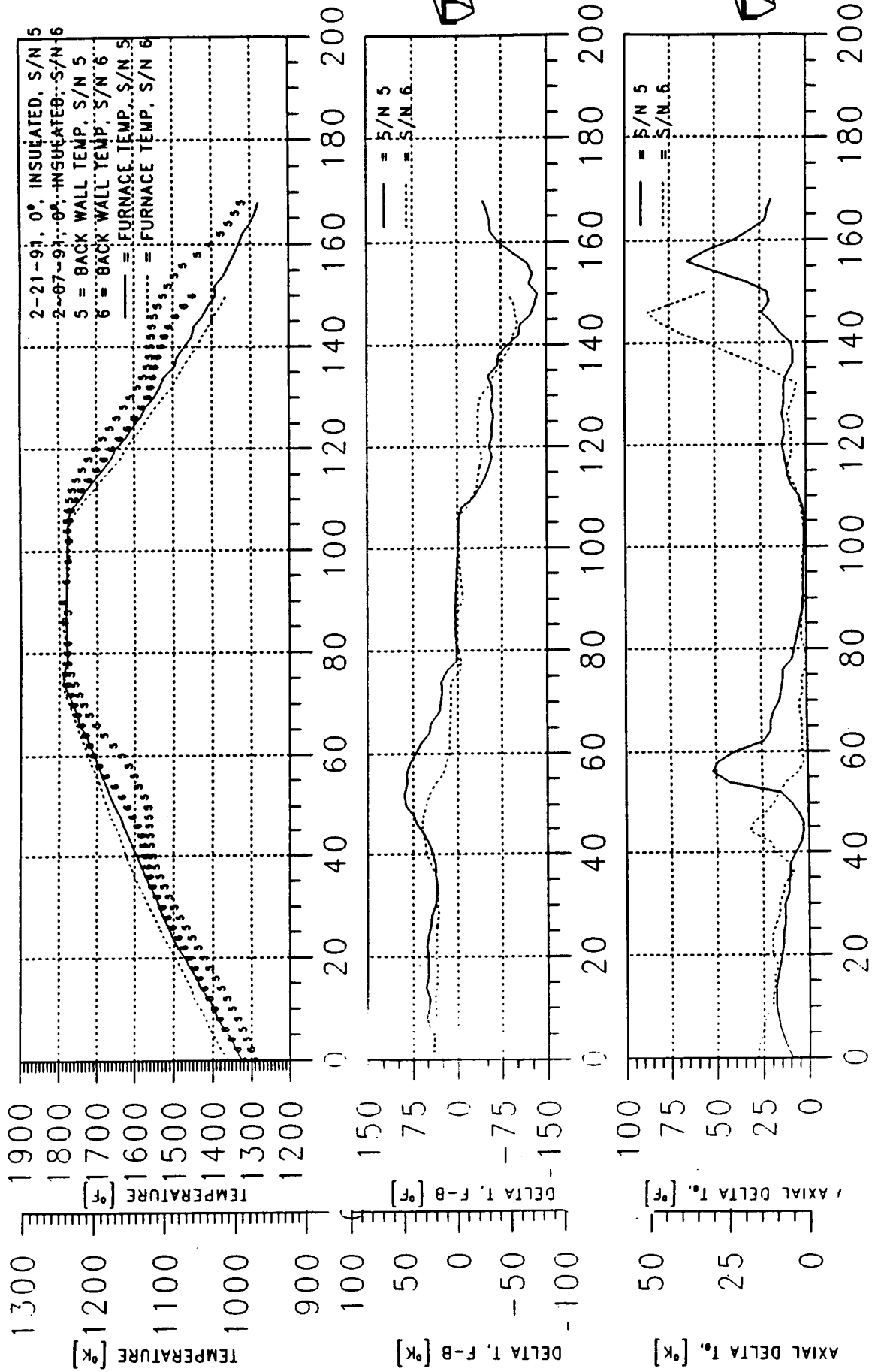




Figure 78 - COMPARISONS OF WEDGE TEMPERATURES, TESTS 4-2 AND 9-2

[S/N 5 HAS NICKEL FOAM, S/N 6 DOES NOT]

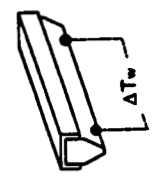
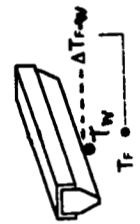
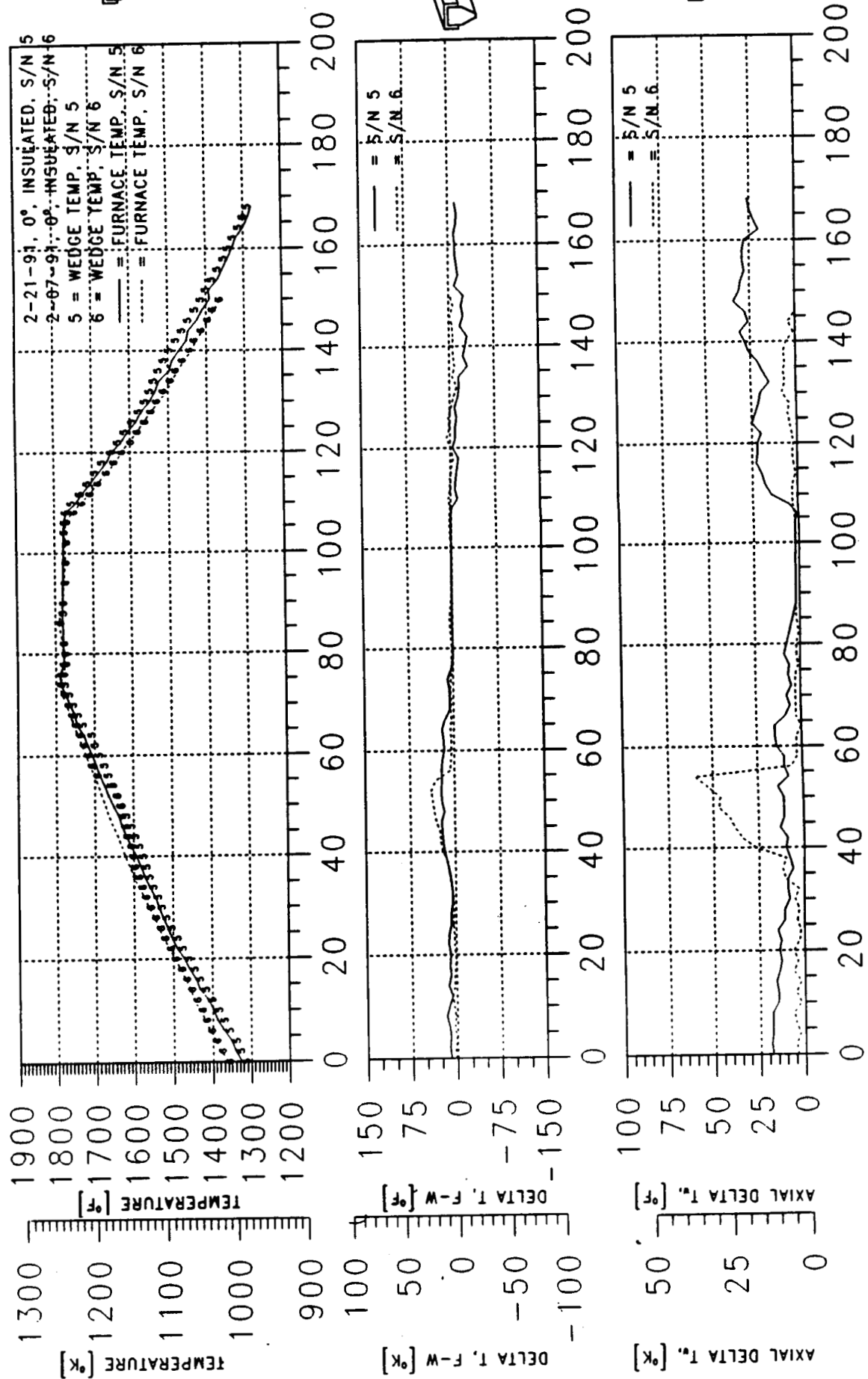


Figure 79 - COMPARISONS OF BACK WALL TEMPERATURES, TESTS 5-1 AND 10-2

[S/N 5 HAS NICKEL FOAM, S/N 6 DOES NOT]

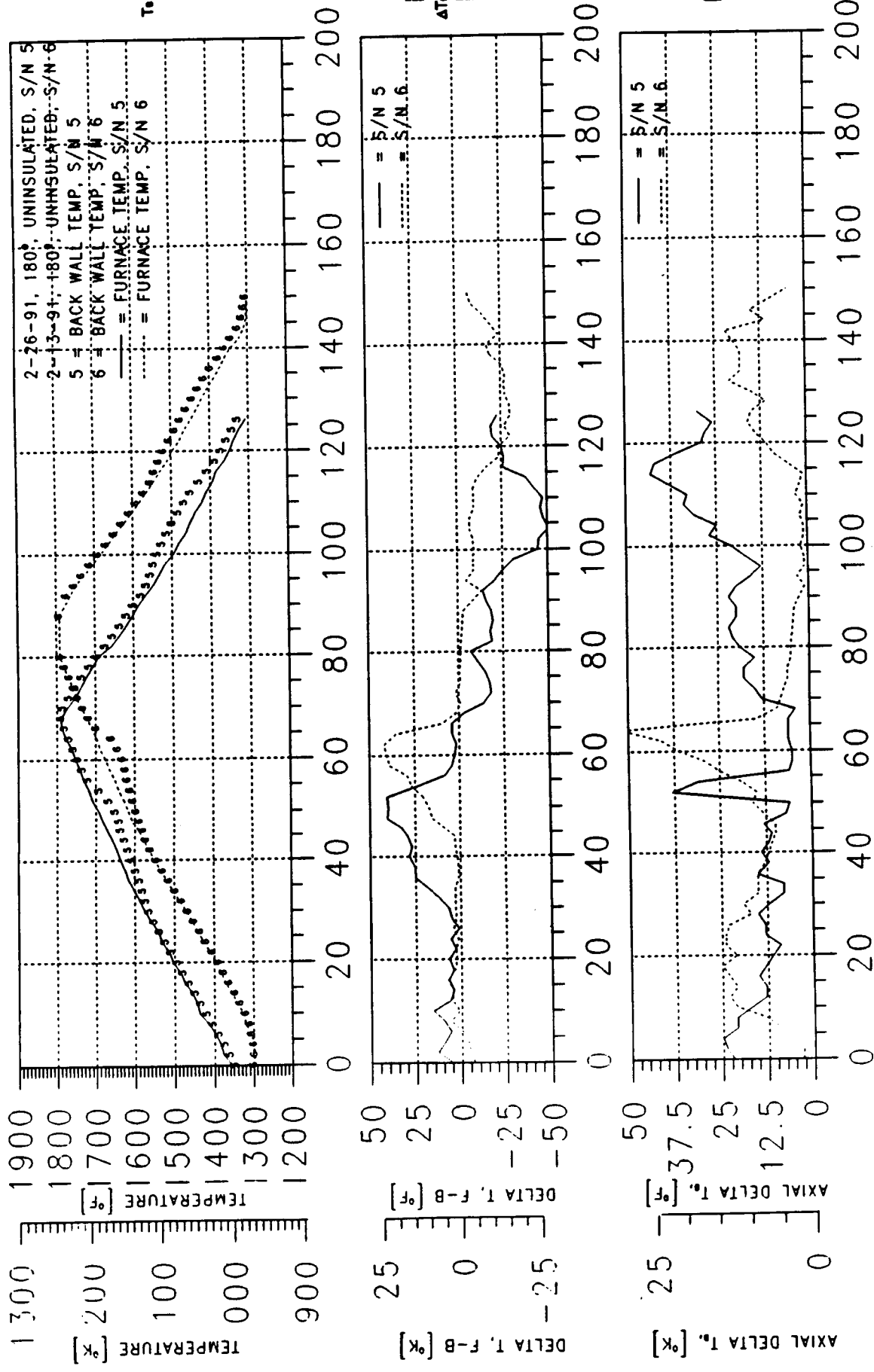


Figure 80 - COMPARISONS OF WEDGE TEMPERATURES, TESTS 5-1 AND 10-2

[S/N 5 HAS NICKEL FOAM, S/N 6 DOES NOT]

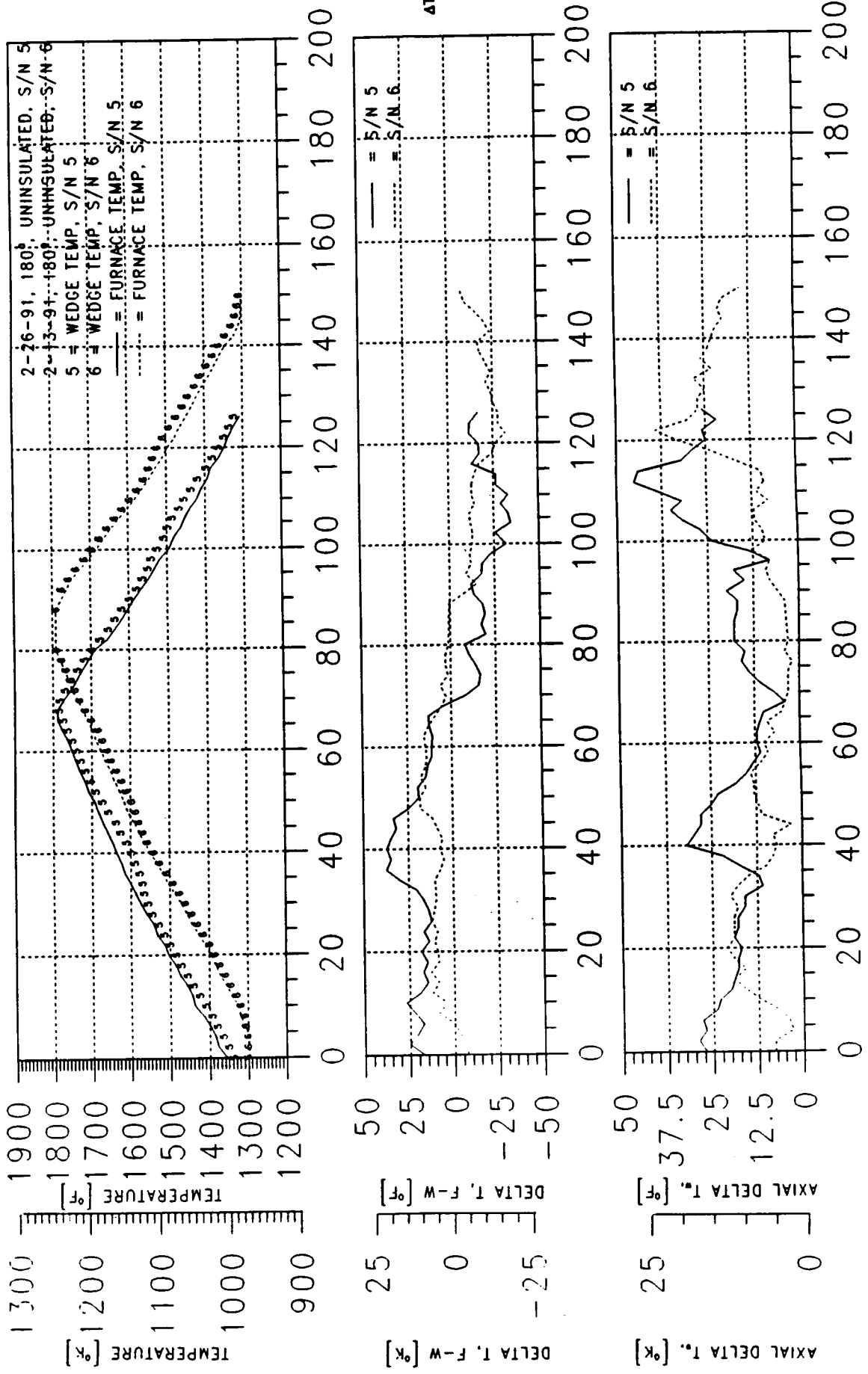


Figure 81 - COMPARISONS OF BACK WALL TEMPERATURES, TESTS 6-1 AND 11-1

[S/N 5 HAS NICKEL FOAM, S/N 6 DOES NOT]

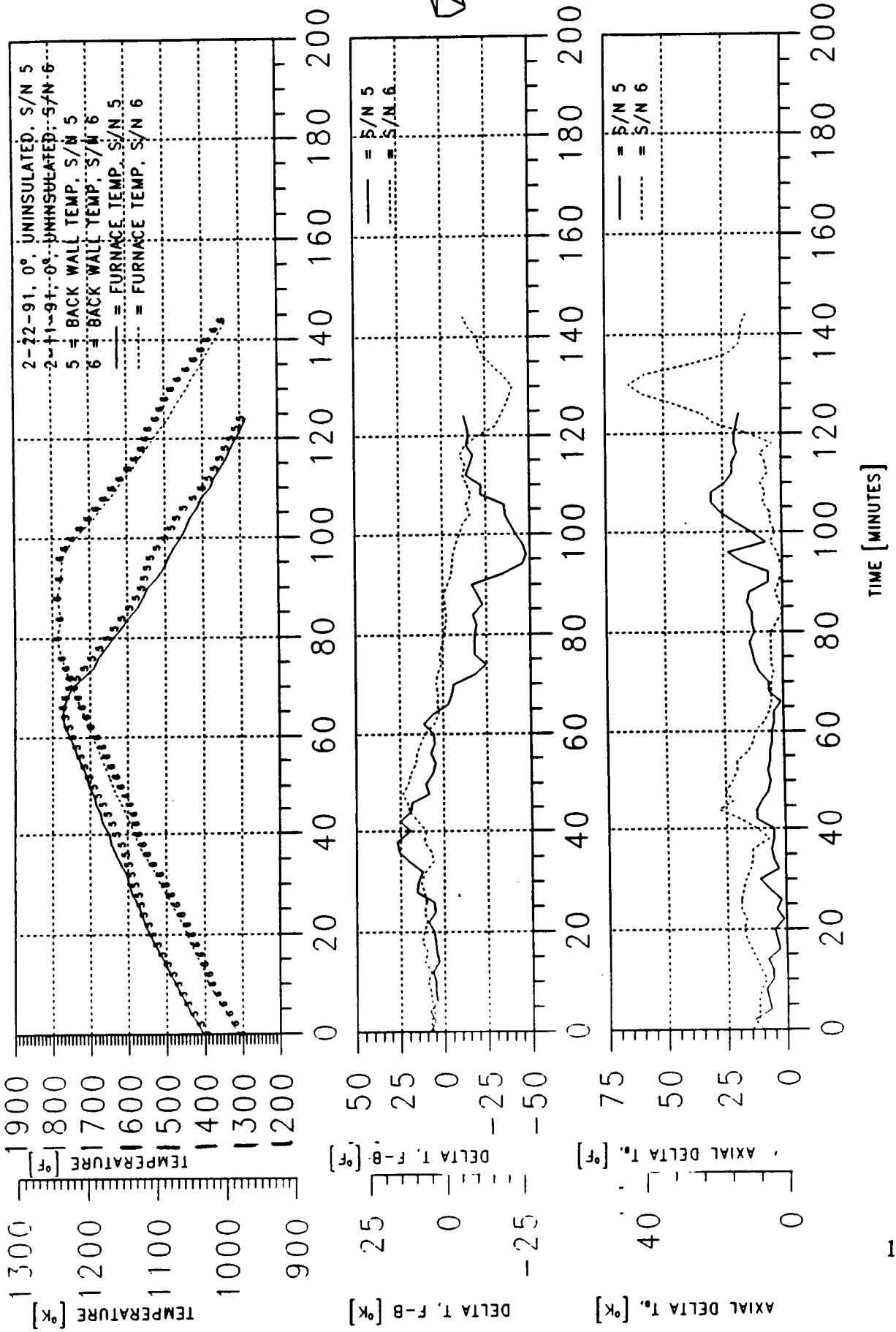


Figure 82 - COMPARISONS OF WEDGE TEMPERATURES, TESTS 6-1 AND 11-1

[S/N 5 HAS NICKEL FOAM, S/N 6 DOES NOT]

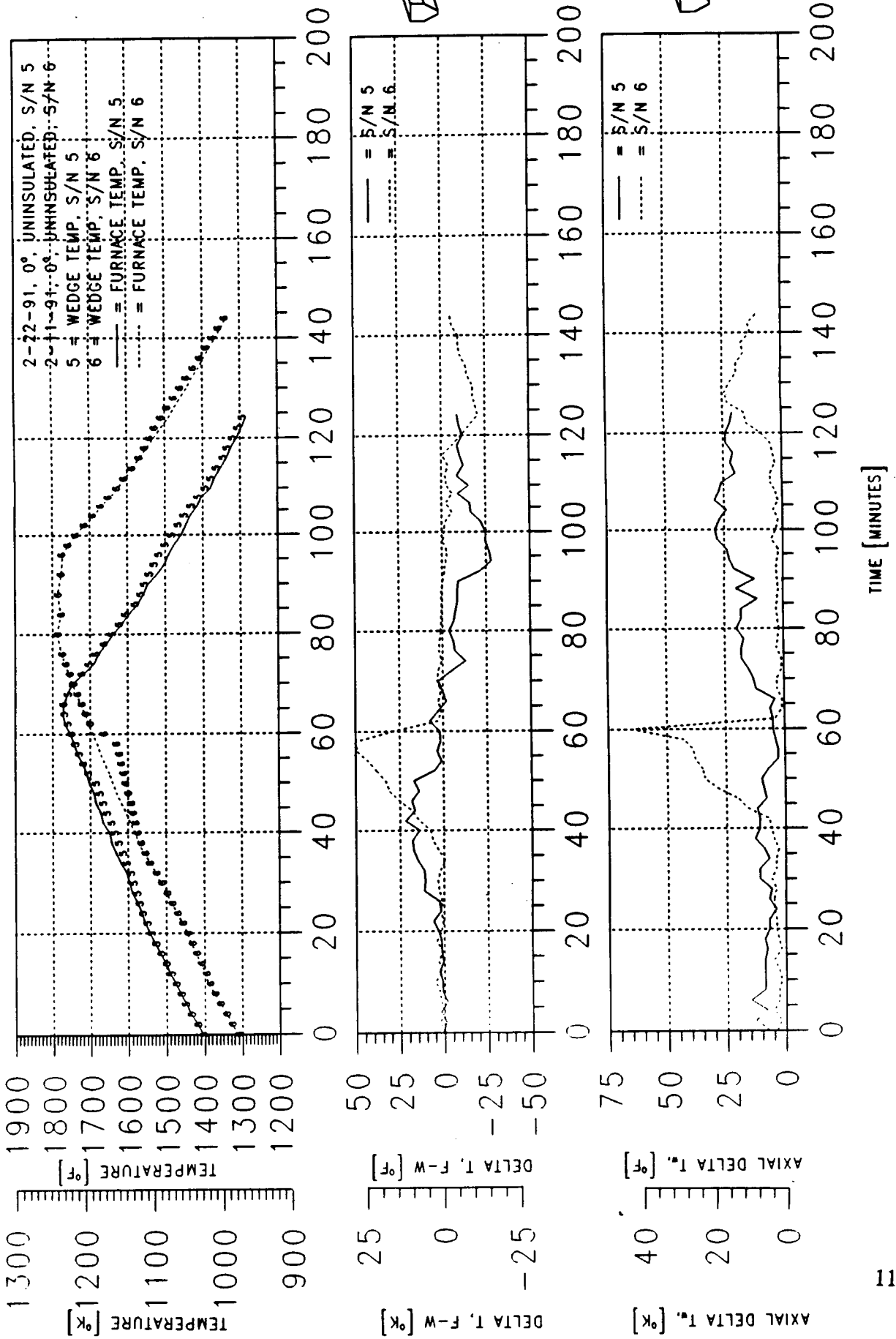


Figure 83 - COMPARISONS OF BACK WALL TEMPERATURES, TESTS 5-1 AND 5-2

[S/N 6 DOES NOT HAVE NICKEL FOAM INSERT]

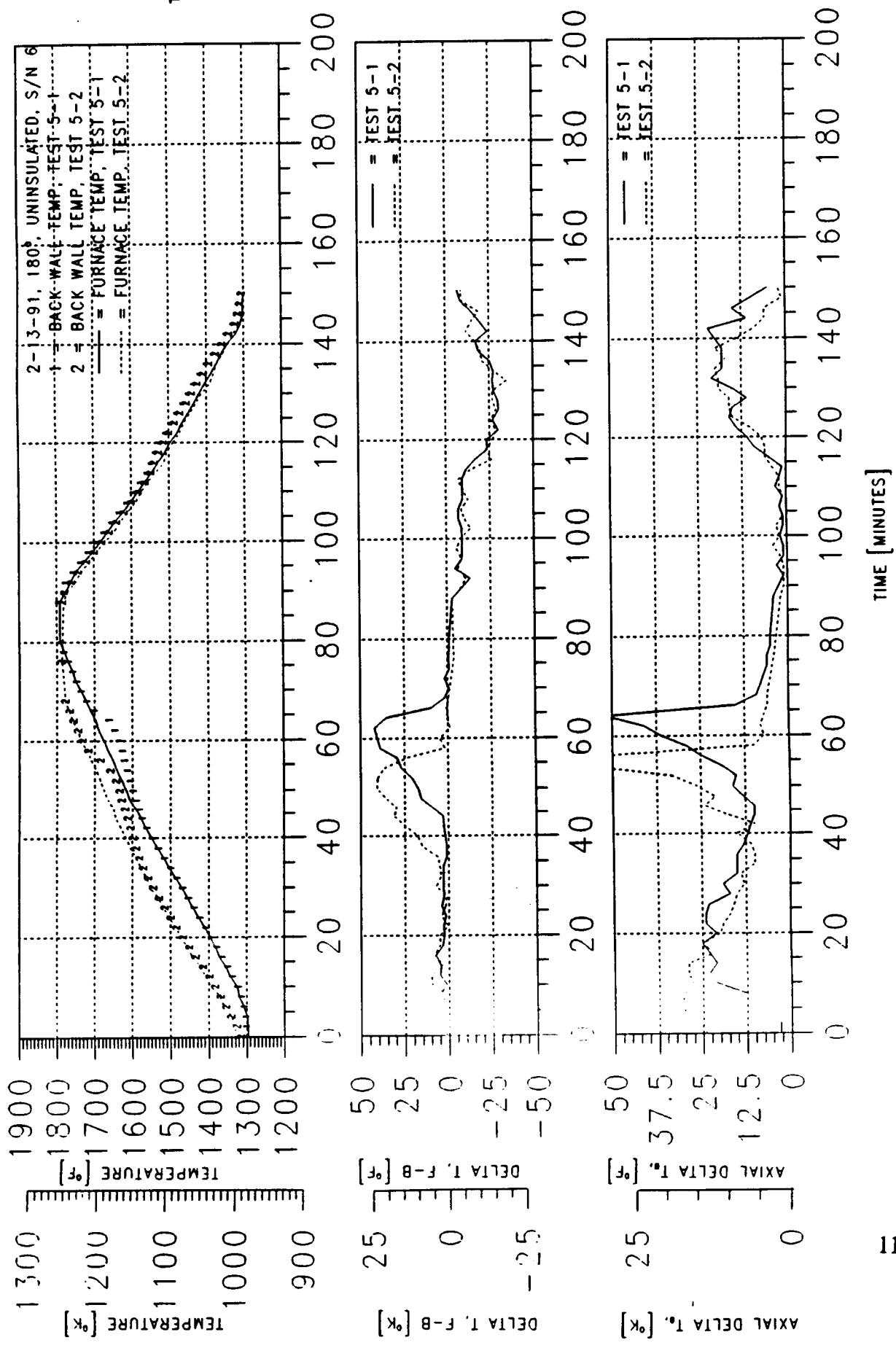


Figure 84 - COMPARISONS OF WEDGE TEMPERATURES, TESTS 5-1 AND 5-2

[S/N 6 DOES NOT HAVE NICKEL FOAM INSERT]

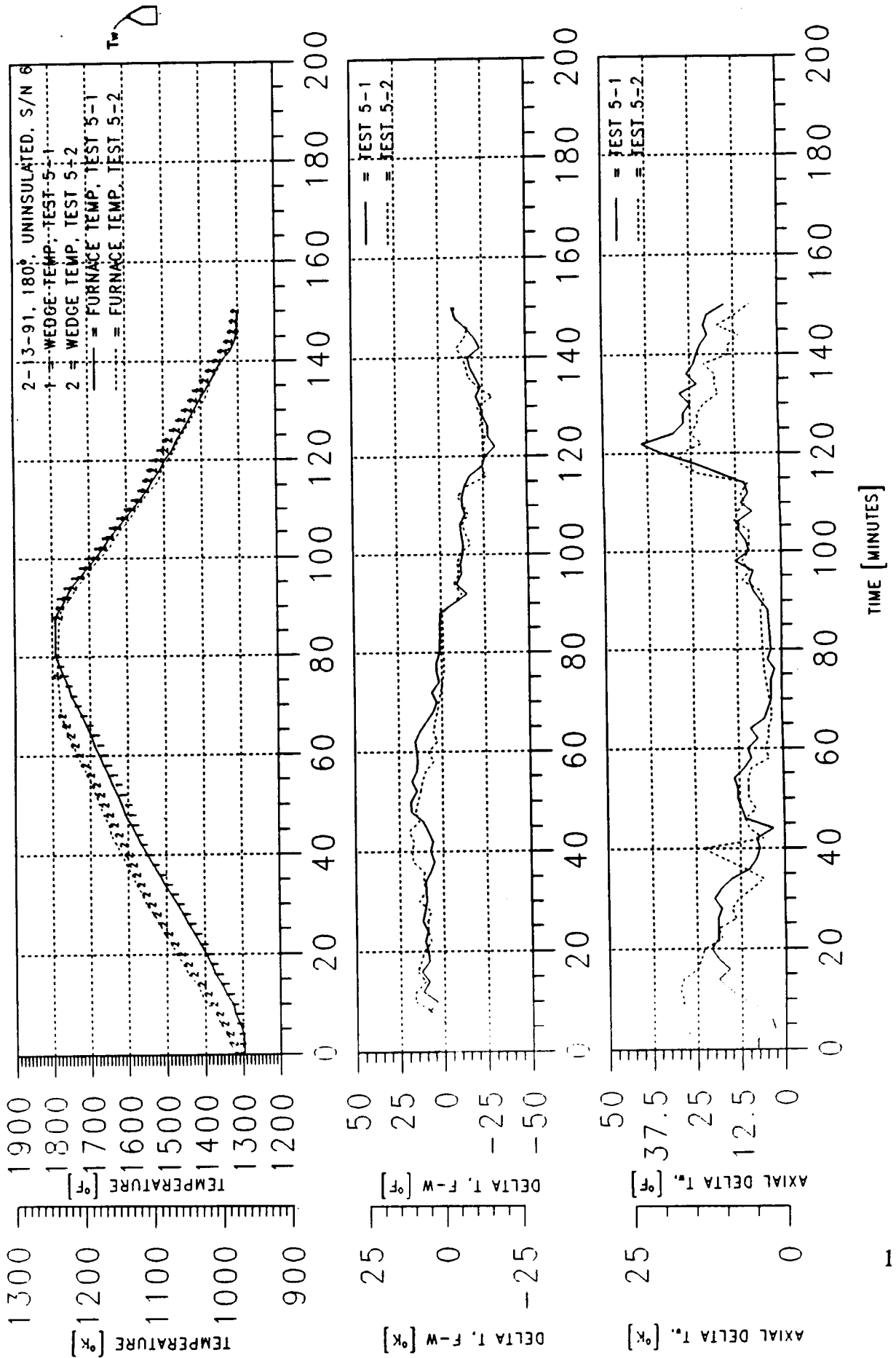
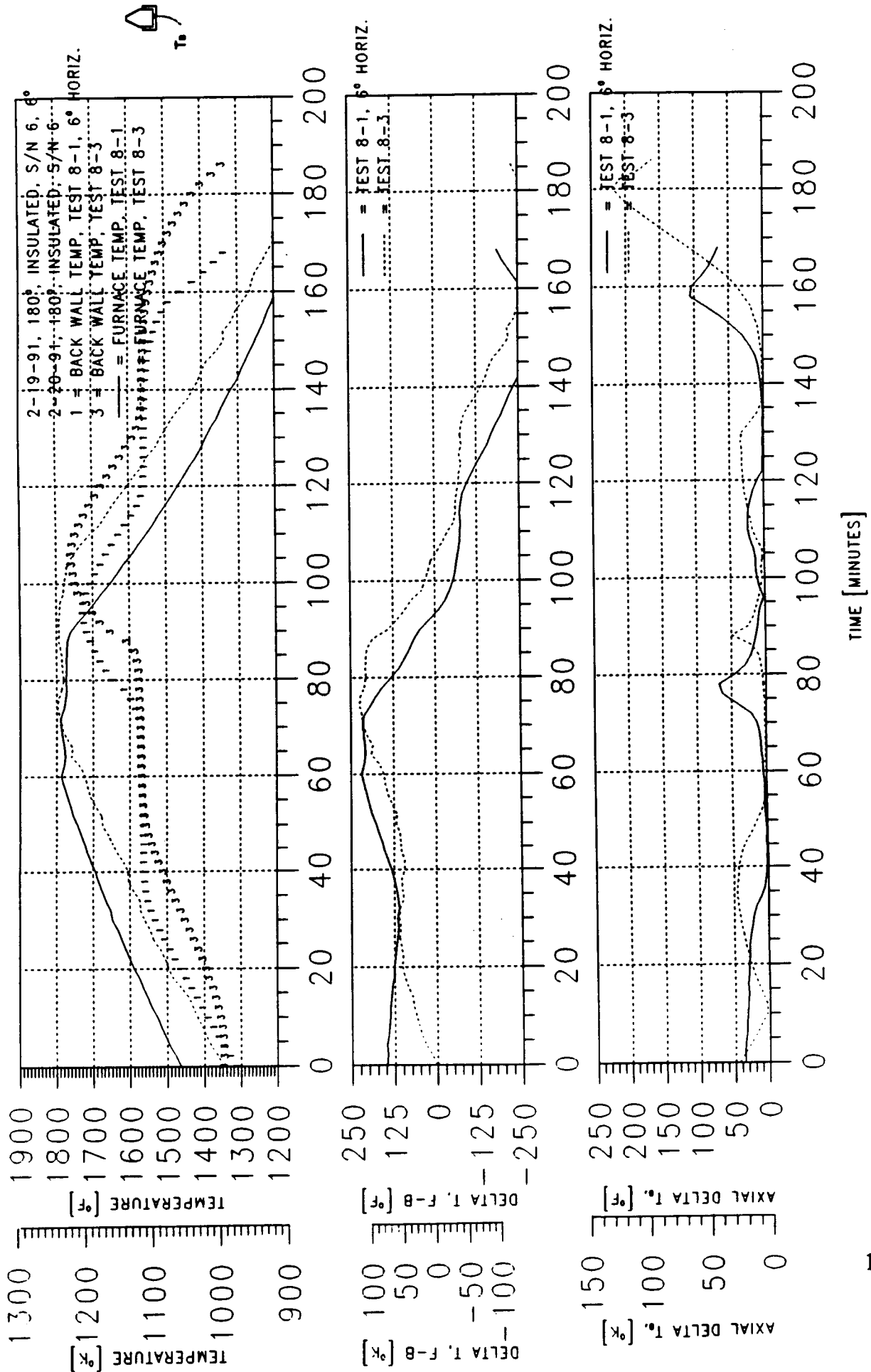


Figure 85 - COMPARISONS OF BACK WALL TEMPERATURES, TESTS 8-1 AND 8-3

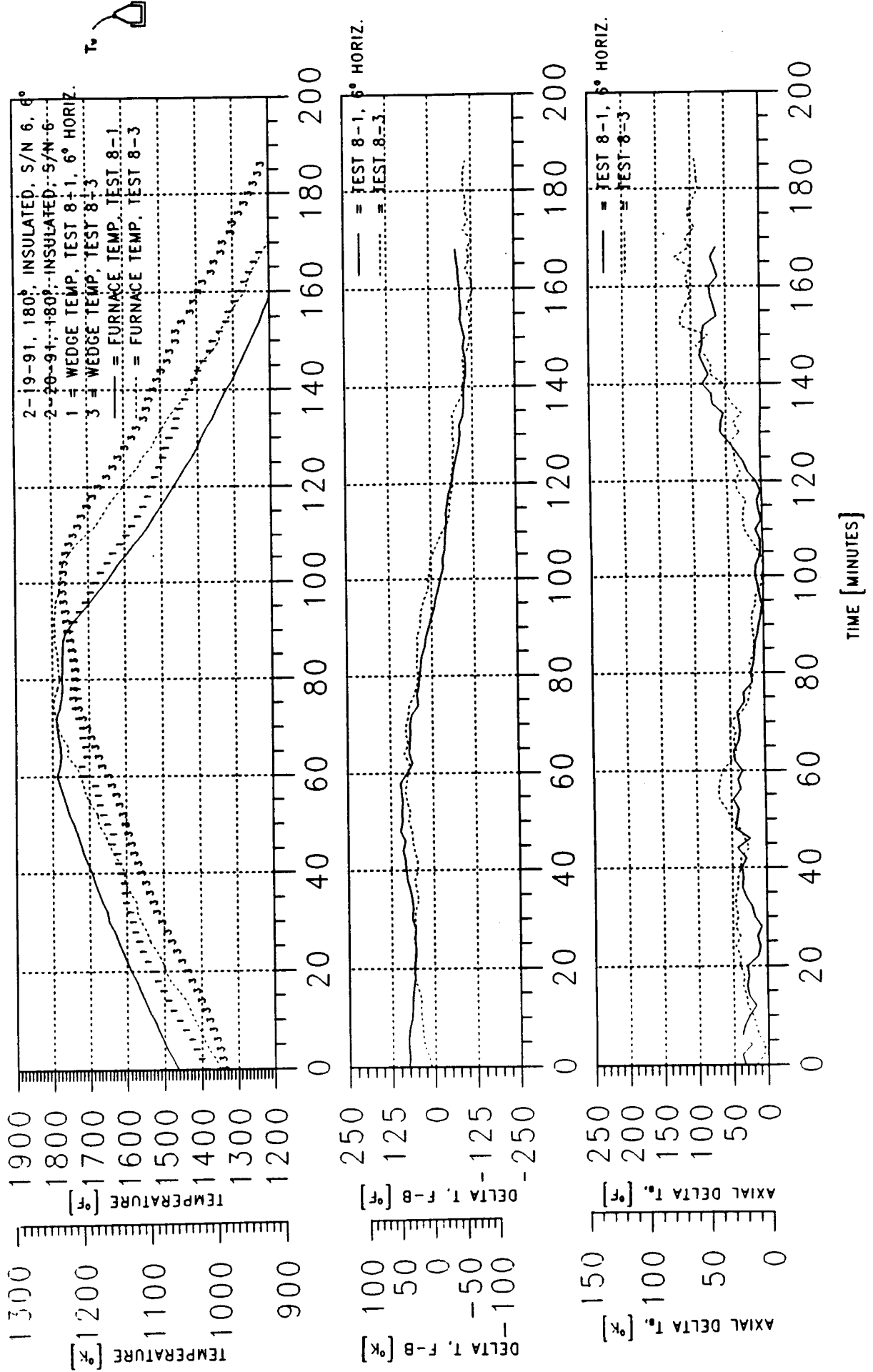
[S/N 6 DOES NOT HAVE NICKEL FOAM INSERT]





**Figure 86 - COMPARISONS OF WEDGE TEMPERATURES, TESTS 8-1 AND 8-3**

[S/N 6 DOES NOT HAVE NICKEL FOAM INSERT]



The only measurable impact of the nickel foam was seen when the back and short sides of the canister were insulated. In tests with insulation, the furnace to back side  $\Delta T$  was smaller when nickel foam was not present, probably as a result of the high transmissivity of the pure LiF. In tests without insulation, the impacts of the nickel foam are visible but quite small in magnitude. In fact, one could argue that the profiles match each other fairly well.

Several possible explanations can be made for the near match between the temperature profiles of the two canisters. First, it is possible that the nickel foam provided less thermal conductivity enhancement than predicted. The predicted values for the enhanced thermal conductivity ranged from 2.20 to 5.31 W/m-K (1.27 to 3.07 Btu/hr-ft- $^{\circ}$ F), compared to the liquid LiF conductivity of 1.73K (1.0 Btu/hr-ft- $^{\circ}$ F) [7]. Furthermore, a gap existed between the nickel foam and the canister wall adding a significant resistance to the heat flow. Thus, comparisons between the temperature profiles of the canister with TCE to the one without could differ by only 2.8K (5 $^{\circ}$ F), and that value could be smaller due to the poor fit of the TCE in the canister. Finally, buoyancy-driven natural convection could have significantly increased the conductance, in the canister without the nickel foam insert, to the extent that it surpassed the conductance augmentation of the insert. It is difficult to tell whether or not other convection mechanisms, such as surface tension and g-jitter, would produce the same trends in a micro-gravity environment [13]. In fact, just as the foam probably inhibited buoyancy-driven convection in a one-g environment, it might likewise inhibit surface tension-driven convection in a micro-gravity environment since the foam cell diameter, 0.38 mm (0.015 inch), is less than the Benard-cell diameter by at least an order of magnitude. On the other hand, LiF is practically transparent to radiant heat transfer and thus might heat faster with the aid of receptor surfaces dispersed throughout the salt, as nickel foam provides. Thus, no generalizations can be extrapolated from these tests. Instead, one can only conclude that the canisters perform approximately the same in a one-g environment both with and without the TCE utilized. One cannot predict, on the basis of these experiments, that a larger volume percentage of TCE in micro-gravity conditions will increase the conductance.

All temperature data is tabulated in Appendix C. For each test point there is a table of the raw data followed by a table of the averaged data. Finally, a plot of the raw data for each test point is also included in the Appendix C.

### 5.3.3 Dimension Data

Dimension data on the canisters were gathered throughout the fabrication and test program. Measurements were made with a dial indicator at ten datum locations along the canisters' five faces. A canister is shown mounted in the inspection fixture in Figure 87. The nomenclature used for the five faces is illustrated in Figure 88. Also, the use of the dial indicator with the inspection fixture is illustrated in the figure. Thermocouples attached to the canisters complicated the process of positioning the canisters in the inspection fixture as shown in Figure 89. Although the accuracy of the measurement process was on the order of  $\pm 0.076$  mm ( $\pm .003$  inch) due to surface irregularities and positioning inaccuracies, the procedure was useful in detecting trends in the dimension changes.

ORIGINAL PAGE  
BLACK AND WHITE PHOTOGRAPH

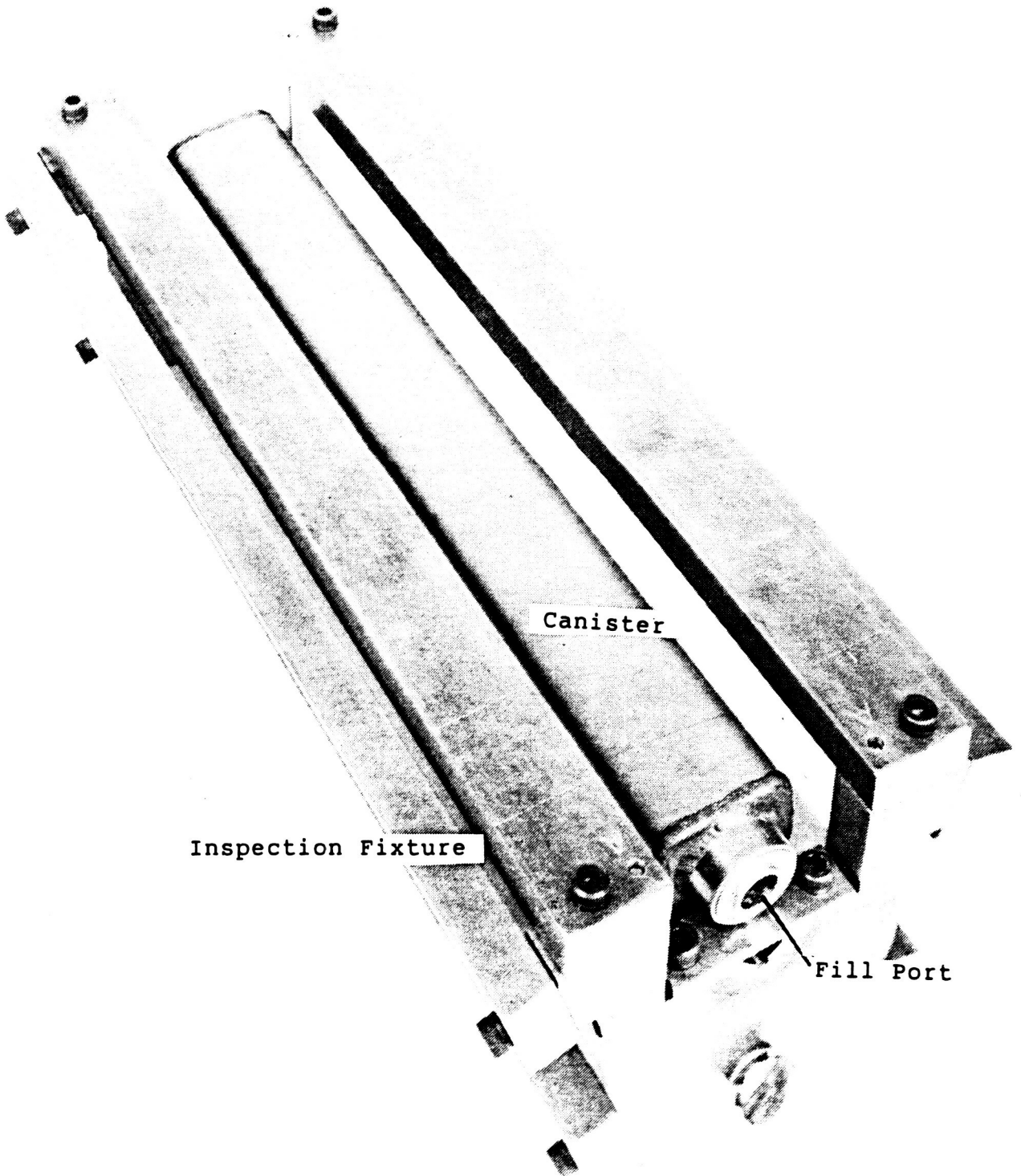


**Figure 87 - CANISTER MOUNTED IN INSPECTION FIXTURE**

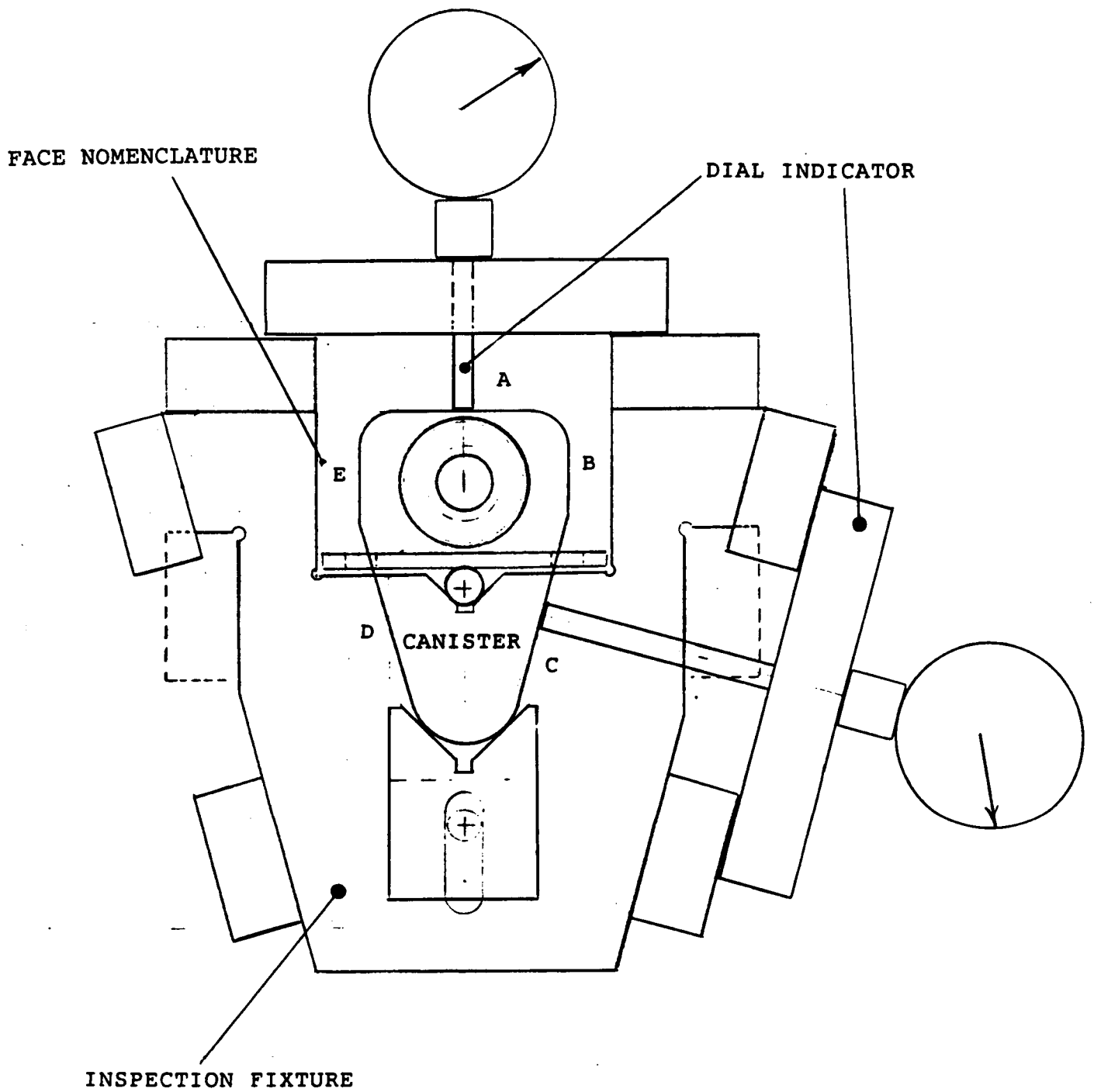
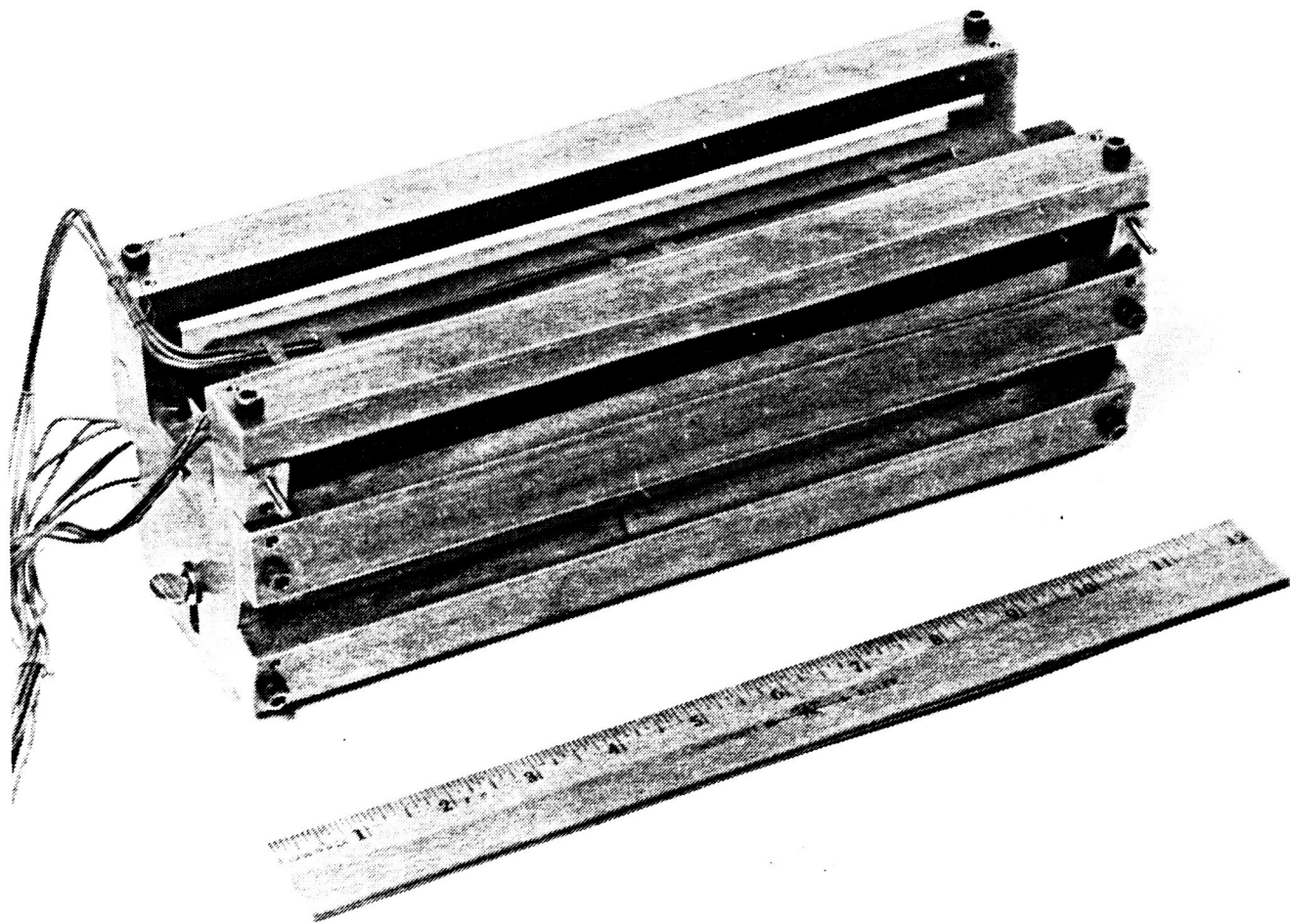


Figure 88 - NOMENCLATURE OF CANISTER FACES

ORIGINAL PAGE  
BLACK AND WHITE PHOTOGRAPH



**Figure 89 - PHOTOGRAPH SHOWING FIXTURING DIFFICULTIES PRESENTED BY THERMOCOUPLES ATTACHED TO THE CANISTER**

Overall, dimension changes over the course of the program were well within acceptable limits. The maximum dimension change at any location was 0.58 mm (0.023 inch) experienced on canister S/N 5 while the largest change was 0.56 mm (0.022 inch) on S/N 6. Dimension changes for S/N 5 are illustrated in Figure 90. The top plot, which shows the dimension measurements along the length of the canister on all five surfaces, indicates that the canister started with an initial dimension spread of 0.53 mm (0.021 inches). After nine thermal cycles, the range of the dimensions was 1.02 mm (0.040 inch) as shown on the middle plot. The maximum difference between any location's initial and final measurements, illustrated in the lower plot, was 0.58 mm (0.023 inch). From this plot one can see that there was a contraction in the sides of the canister, faces "B" through "E," while there was a slight expansion in face "A," the back surface of the canister.

The same basic trends were observed with canister S/N 6, the canister without the nickel foam insert. From the top plot on Figure 91, it is evident that the range in dimensions, before filling, was 0.79 mm (0.031 inch). After ten thermal cycles, the spread in dimensions equalled 1.07 mm (0.042 inch) as shown in the middle plot. Finally, the lower plot shows that the maximum difference between any location's initial and final measurements was 0.56 mm (0.022 inch). Once again, there was a contraction in faces "B" through "E," while face "A" experienced a slight expansion.

Since the dimensions did change over the course of the test program, a check was performed to determine whether the changes occurred initially or if the changes were progressive. Thus, comparisons were made between measurements made before the canisters were heat treated to those made after they were filled. Figure 92 illustrates the fact that canister S/N 5 dimensions did change after filling although the maximum change at any location was only 0.36 mm (0.014 inch). Note that surfaces "B" and "E" expanded whereas they had contracted after nine cycles.

Canister S/N 6 had larger dimension changes, as shown in Figure 93, with a maximum change of 0.64 mm (0.025 inch). It is interesting to note that the largest dimension changes were at the anti-fill end of the canister, datum locations five through ten. This could possibly be due to the fact that this end of the canister was facing downward during the fill process and could have been more highly stressed as the salt froze. This theory is substantiated by the fact that the sides contracted instead of expanding. However, the only explanation for the fact that this trend was not observed on S/N 5 is that the Ni foam might have wicked the salt and distributed the stress over the length of the canister. Finally, Figure 94 further illustrates the dimension changes at any location as a function of the number of thermal cycles. The plots show that a large portion of the dimension changes occurs during the heat treat cycles, especially in S/N 6.

Based on these findings, it seems that the dimension changes could be progressive in nature, but one could make an equally convincing argument that the changes are simply due to initial stress relief and, thus, not progressive. The canisters need to accumulate more thermal cycles before any conclusions can be reached regarding the cause of dimension changes.

Dimension data is tabulated in Appendix C.

Figure 90 - CANISTER WITH TCE DISTORTION COMPARISONS

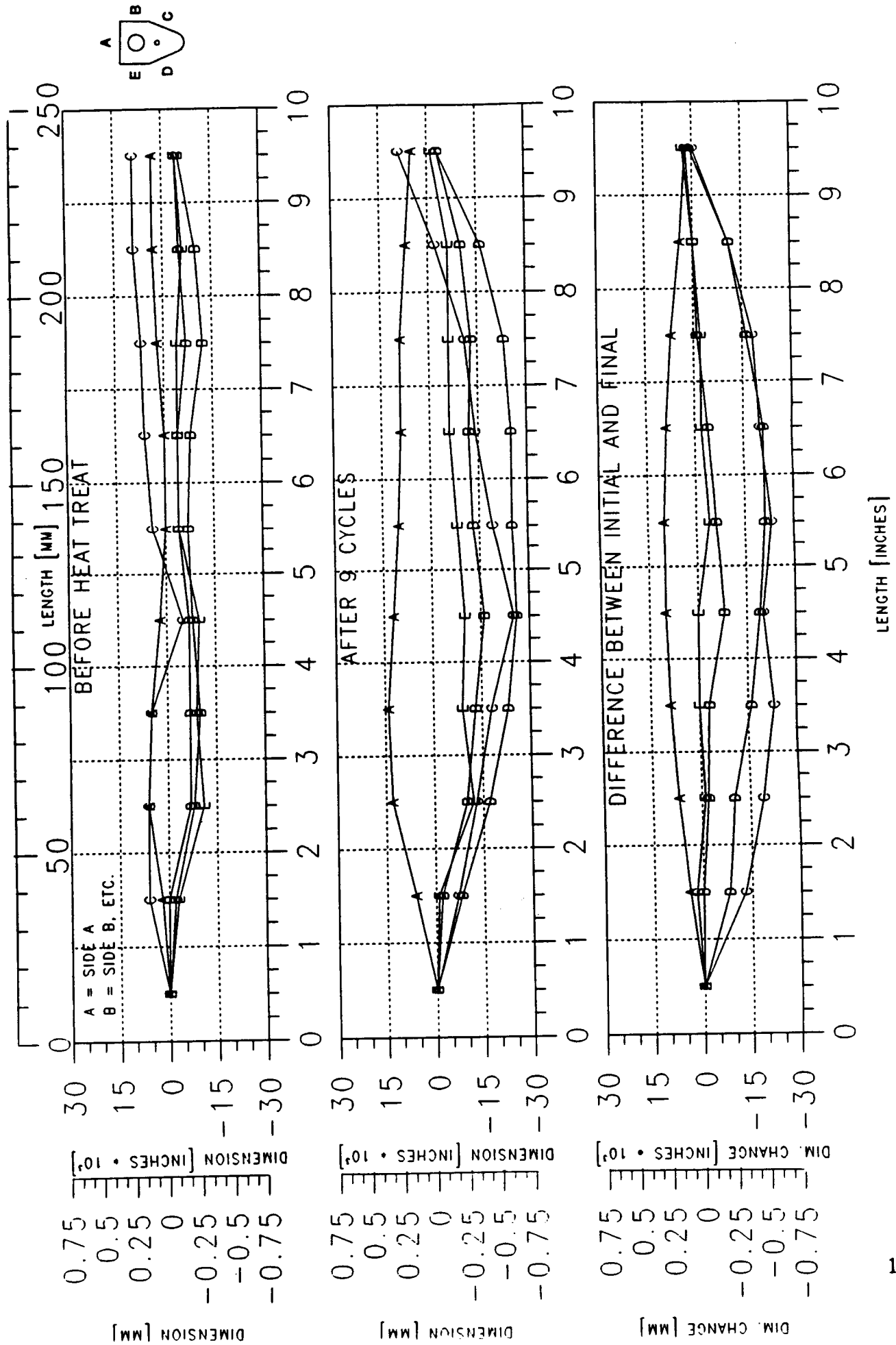


Figure 91 - CANISTER S/N 6 DISTORTION COMPARISONS

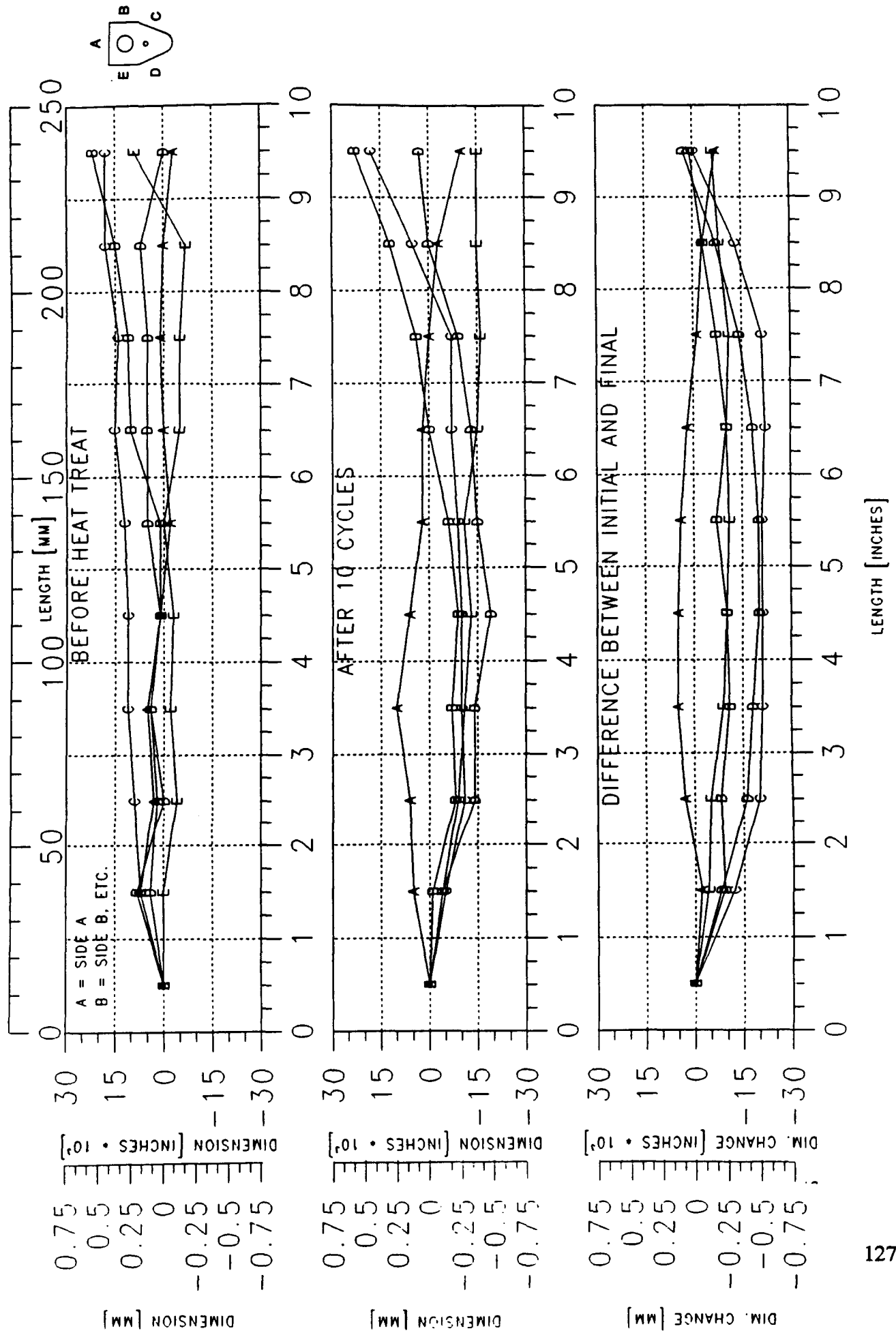




Figure 92 - CANISTER S/N 5 DISTORTION COMPARISONS

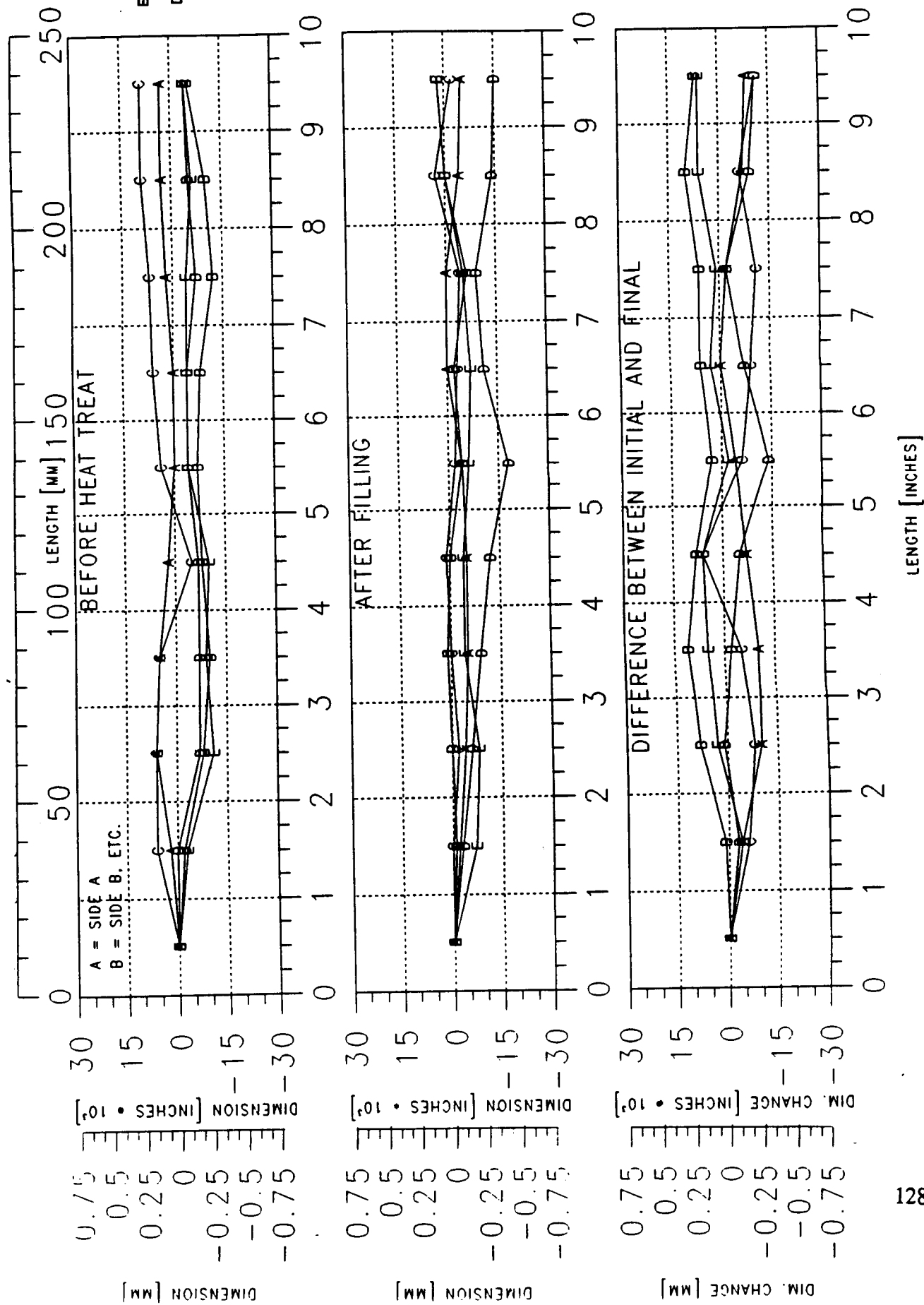
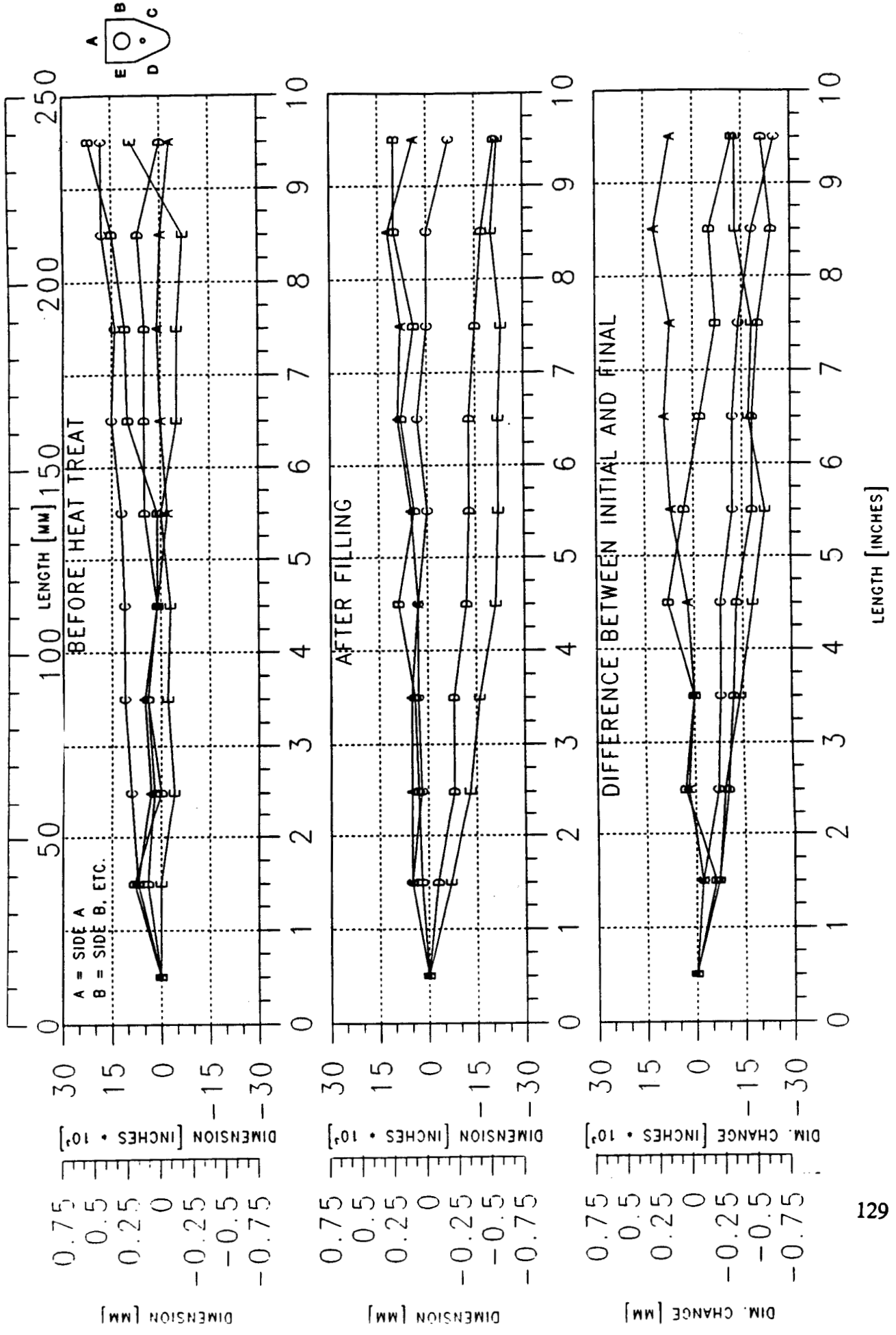
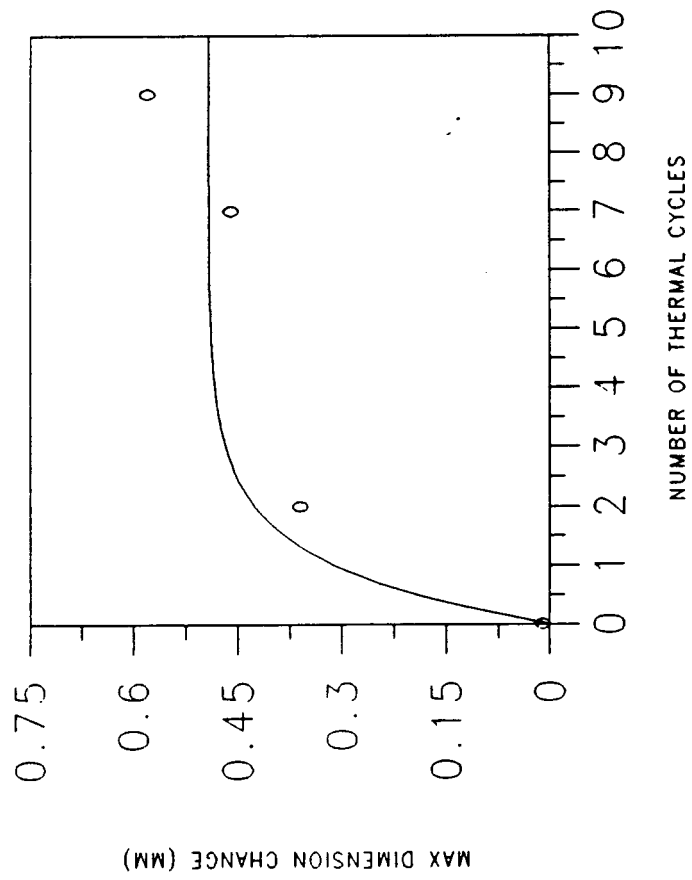


Figure 93 - CANISTER S/N 6 DISTORTION COMPARISONS



S/N 5 DIMENSION CHANGES



S/N 6 DIMENSION CHANGES

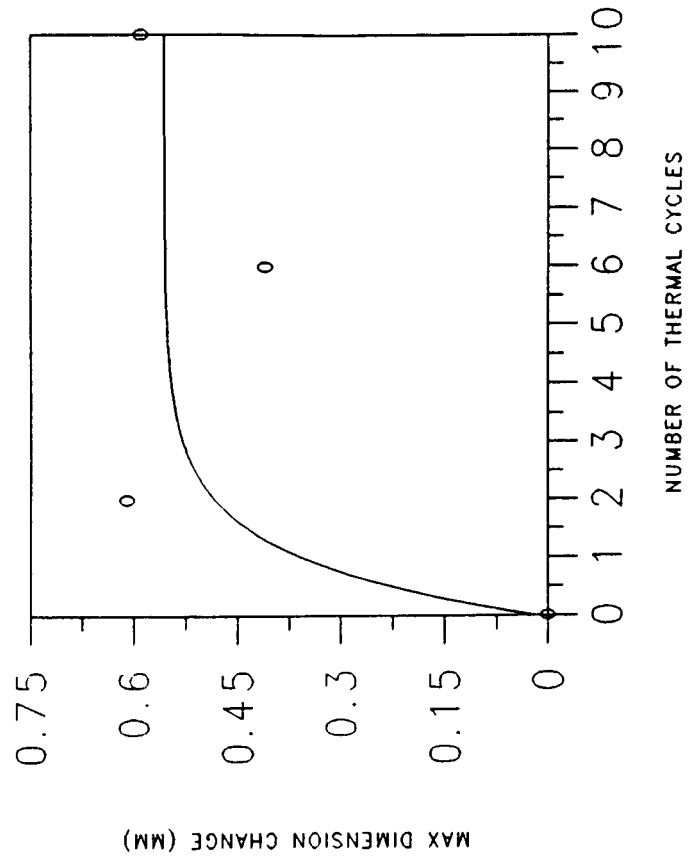


Figure 94 - PLOTS OF MAXIMUM DIMENSION CHANGES

#### 5.3.4 X-ray Data

X-ray photographs were taken of the canisters throughout the thermal cycling program. The purpose of the photographs was to locate the voids in the canisters. Figure 95 shows the two canisters used in the thermal cycles, S/N 5 and 6, after they had been filled. A cone shaped void is easily seen in the canister without the nickel foam insert, S/N 6, while it cannot be discerned as easily in S/N 5. Note that the canisters were filled in a vertical orientation. Also, the vertical white lines in both canisters are weld joints.

Figure 96 shows the frozen LiF profile after test condition #3-2, the test performed on canister S/N 6 in which the canister wedge was pointing upward and the back and short sides of the canister were insulated. As expected, the salt froze on the back surface of the canister, due to gravity, as well as on the ends of the canister because they were not insulated. Figure 97 shows the same canister after it had been tested with the wedge pointing down (0 degree orientation) and uninsulated. Finally, Figure 98 shows the canister after test #5-2 in which the canister had been uninsulated in the 180 degree orientation. The small mound of salt near the right end could be due to the extended heat transfer surface that the fill cap provided at that end.

Figure 99 shows the canister with the nickel foam insert, S/N 5, after test #8-3, in which the canister had been insulated and in the 180 degree orientation. Unfortunately, it is difficult to discern void regions from those with solid LiF in this photograph. However, it is clear that a large gap exists between the nickel foam insert and the canister wall and that the insert fell to the bottom surface, the back surface in this test, due to gravity. Likewise, when the canister had been tested in the 0 degree orientation in test #9-2, the insert drifted down to the wedge due to gravity, as shown in Figure 100. Finally, Figure 101 shows the canister after test #10-2 in which the canister was uninsulated and held at a 180 degree orientation.

Also, note that the small cracks present in the frozen LiF provided a communication path between the melting salt and the void space when heating from room temperature. However, tests by Raj and Whittenberger indicated that stress relief cracks were not as likely to be present at elevated temperatures [2].

From these photographs one can conclude that X-ray is a satisfactory non-destructive inspection technique for canisters without TCE. The photographs show predictable solid LiF profiles and cracks in the LiF.

## 6.0 SUMMARY OF RESULTS

Two thermal energy storage canisters designed for use in an Advanced Brayton Heat Receiver were tested in one g to determine thermal performance with and without thermal conductivity enhancement materials and to investigate distortion due to thermal cycling. The only measurable impact of the nickel foam was seen when the back and short sides of the canister were insulated. In tests with insulation, the furnace to back side  $\Delta T$  was larger in the canister with the nickel foam insert, probably due to the radiant absorptivity of the nickel. However, the differences in the temperature profiles of the two canisters

Nickel Foam Insert

Void

SN 005

SN 006

Figure 95 - X-RAY OF SIDE VIEWS OF THERMAL TEST CANISTERS

RP46885

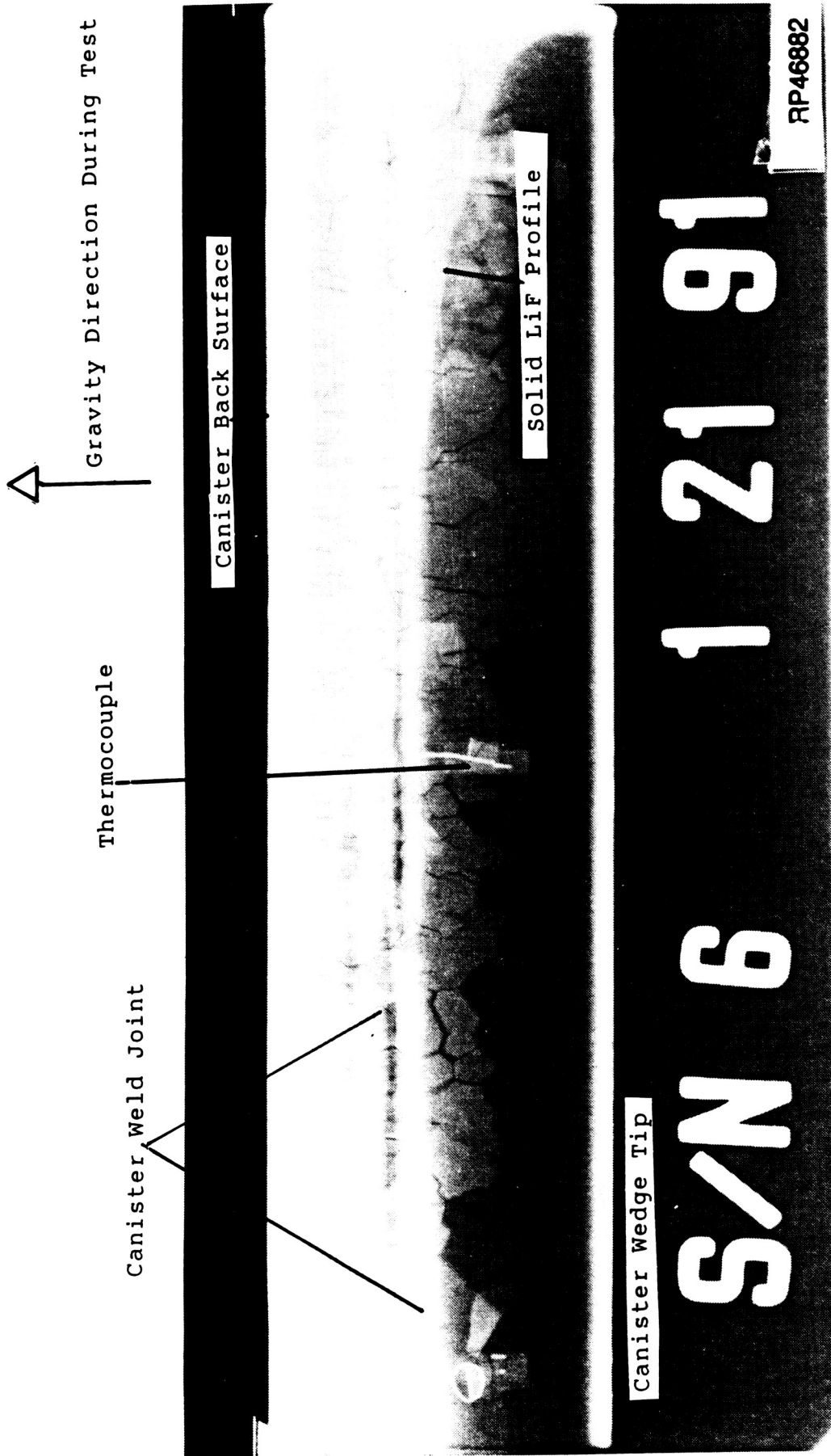


Figure 96 - X-RAY OF CANISTER WITHOUT TCE, WITH INSULATION

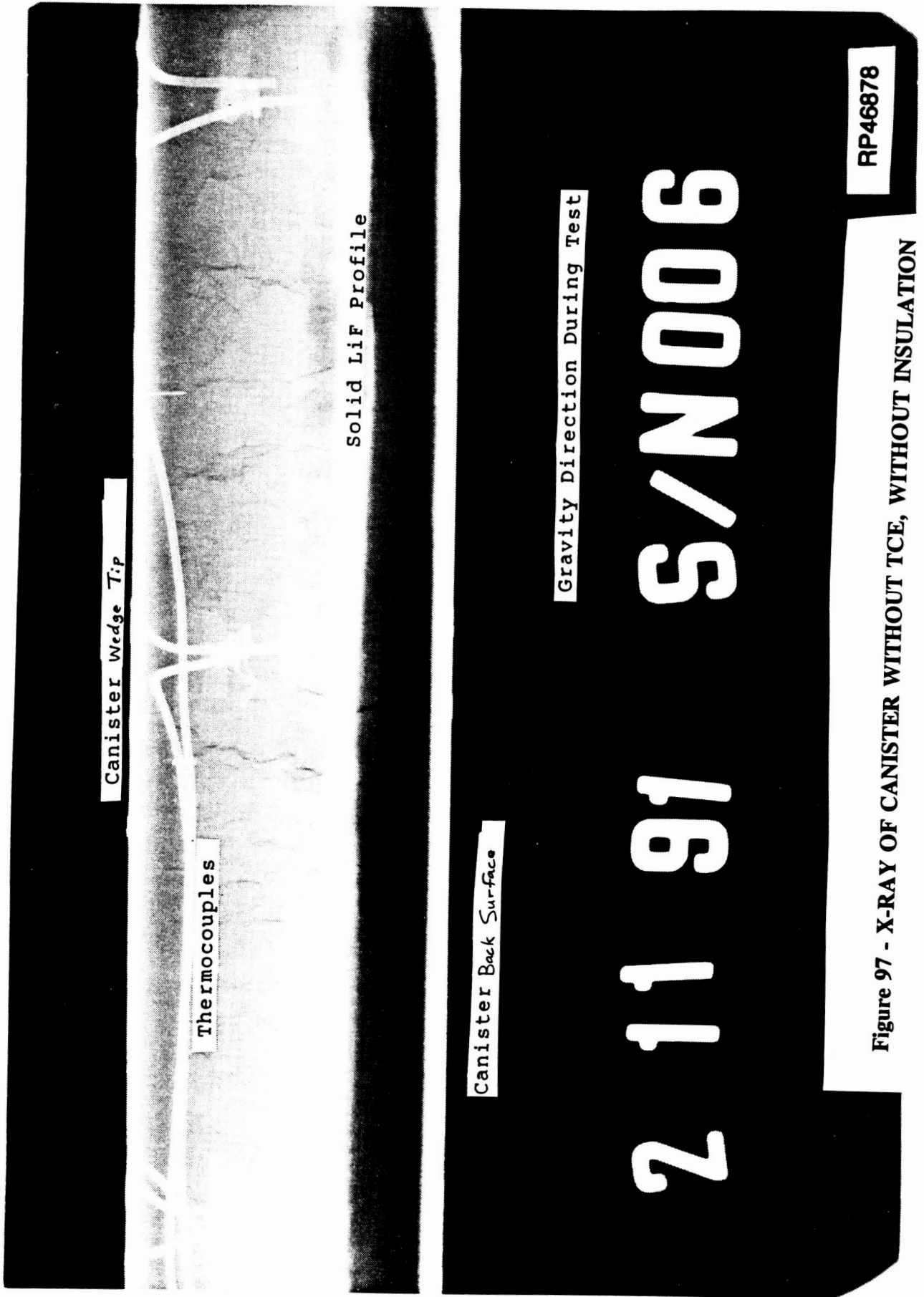
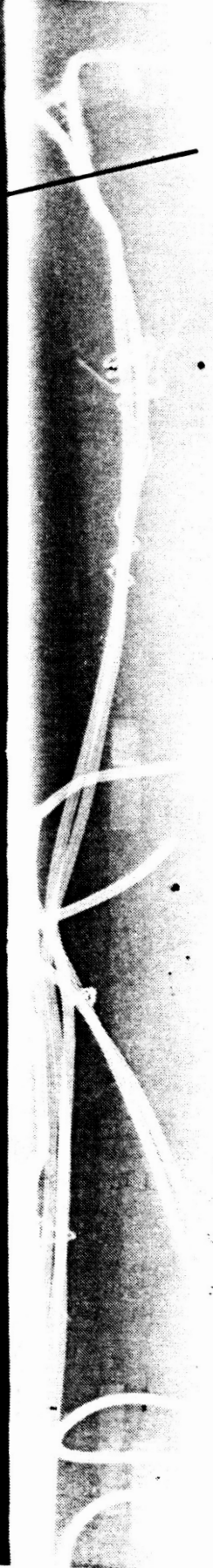


Figure 97 - X-RAY OF CANISTER WITHOUT TCE, WITHOUT INSULATION

Gravity Direction During Test

Small Mound of LiF



Solid LiF Profile

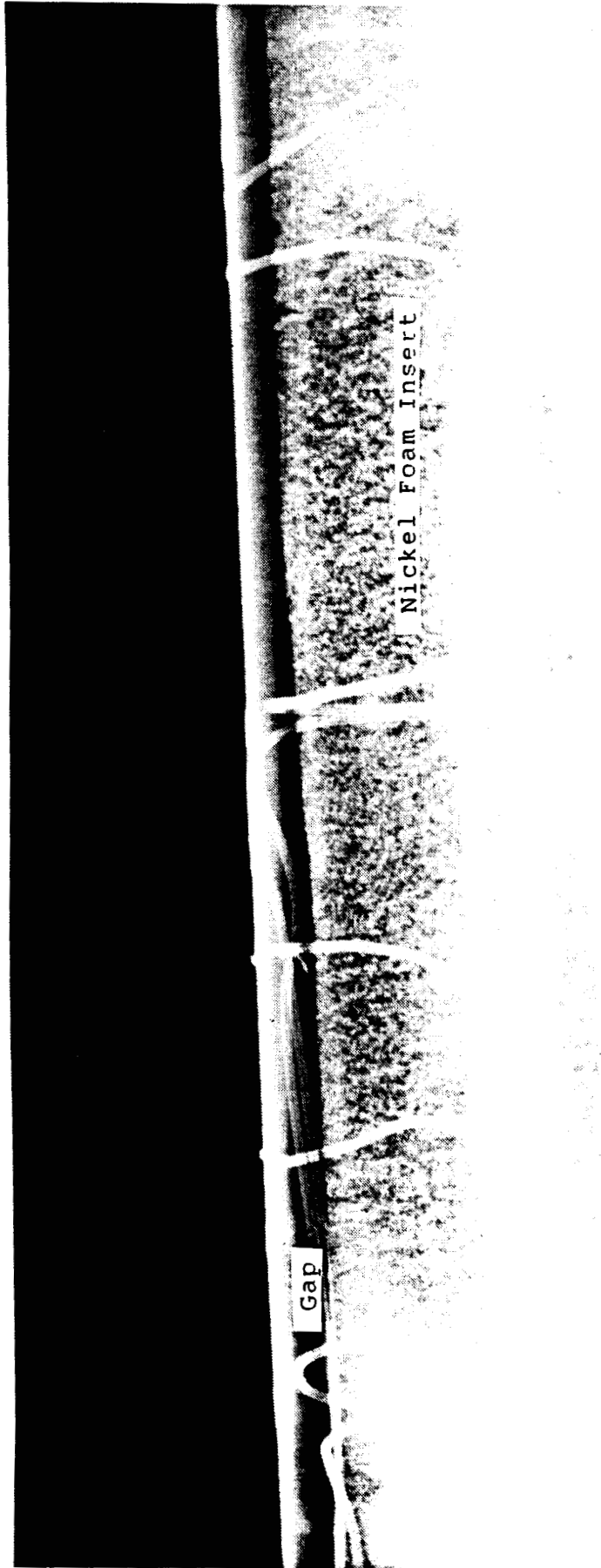
Canister Back Surface

Figure 98 - X-RAY OF CANISTER WITHOUT TCE, WITHOUT INSULATION

SN 6 2 21 91

RP46880





Gap

Nickel Foam Insert

Canister Back Surface

Gravity Direction During Test

SN 5 2 21 91

Figure 99 - X-RAY OF CANISTER WITH TCE, WITH INSULATION

RP46879

Gravity Direction During Test

Nickel Foam Insert

Gap

Canister Back Surface

SN 5 2 22 91

Figure 100 - X-RAY OF CANISTER WITH TCE, WITH INSULATION

RP46983



Gravity Direction During Test

5 91

N 5

Canister Back Surface

Gap

RP46884

Figure 101 - X-RAY OF CANISTER WITH TCE, WITHOUT INSULATION

were small, and in many cases the profiles match each other fairly well. There are several possible explanations for these near matches including 1) natural convection effects which offset the thermal conductivity enhancement, 2) the use of parallel heat flow thermal conductivity enhancement predictions instead of series or empirical methods (5.31 W/m-K for the parallel model versus 2.20 for empirical and 1.73 for liquid LiF), 3) large gap between the canister wall and TCE insert, or 4) inadequate resolution in instrumentation. It is noteworthy that the canisters maintained mechanical integrity, having dimension changes within acceptable limits, in spite of the rigorous temperature profiles. Also, temperature profiles and void locations were predictable and repeatable. Since removal of oxides from the nickel TCE material is essential for good wicking performance, the nickel oxide reduction technique needs to be refined. Finally, computed tomography was verified as an accurate non-destructive inspection technique.

## **7.0 RECOMMENDED STUDY AND DEVELOPMENT PLAN**

### **7.1 Critical Technology Experiments**

Experience gained from these critical technology experiments has shown that further tests and studies would be beneficial to learn more about TES canisters and their integration into a heat receiver. One possibility would be to build a heat pipe module consisting of a heat pipe, TES canister, and a gas heat exchanger. Tests with this module would address heat pipe start-up, adiabatic surface isothermality, material compatibility, and canister mechanical integrity.

Another potential test would be additional thermal cycling of the canister to learn more about the nature of the dimension changes. With test data gathered to date, one cannot determine whether or not dimension changes are progressive in nature. Since canisters could fail during this type of test, it should be performed after the canisters have been used for other tests, as a risk mitigation measure. While doing the thermal cycling, heat transfer coefficient data could be gathered in order to make rough estimates of heat transfer rates.

It might be desirable to attach insulation directly to the back and short sides of canisters in an integrated heat receiver. Thus, some development will be required to select a satisfactory material and associated attachment process.

Refinements could be made to the nickel oxide reduction process, for instance the use of a hydrogen furnace, in order to improve the wicking ability of the nickel foam. Simple tests with foam in a beaker of LiF could be used to assess the success of various nickel oxide reduction techniques.

Finally, further studies could be performed to assess the impact of TCE on temperature variations. An indepth analytical study could be performed to learn about the effects of TCE on all modes of heat transfer. Then this analysis could be compared to transient test data gathered on small capsules dipped in a high temperature brine bath or fluidized bed.

## **7.2 Brayton Heat Receiver Preliminary Design**

### **7.2.1 Preliminary Thermal Analysis**

As part of the heat receiver design process, thermal analysis will be performed on the following components: Brayton working gas tube heat exchangers, TES canisters, heat pipe, receptor surface, aperture, and back plate. In addition, analysis will be performed to address the issues of thermal conductivity enhancement and heat pipe transient performance. Also, further analysis of the radiant heat transfer through the frozen LiF is necessary. Specifically, transmissivity values will be incorporated into the thermal analysis of heat transfer inside the canisters. Finally, thermal studies will be performed to assure that canister insulation is sufficient to provide TES void control.

### **7.2.2 Preliminary Structural Analysis**

Standard stress analysis will be performed on the heat pipes and TES canisters, gas tubes, aperture plate, and back plate. Additional analysis will be required to address stress issues associated with differential thermal expansion between canister and insulation, canister fixturing in an integrated receiver, gas tube interfaces with the receiver, and receptor surface stresses induced by axial temperature gradients.

### **7.2.3 Preliminary Fabrication Plan**

A detailed fabrication plan will be developed to address construction of the canisters, filling of the canisters, assembly into heat pipe sections, integrating of sections into a receiver, and filling the heat pipes with sodium. Experience gained from experimentation will dictate the best method for insulating the canisters. Aperture and back plate fabrication plans will be developed based on the materials selected and the impact of receiver assembly stresses. Special attention will be given to stresses induced in heat pipe sections as they are joined together to form the receiver. Also, a detailed fabrication and start-up plan will be developed to assure that sodium is present on the receptor surfaces before a solar orbit test is performed.

## REFERENCES

1. M. Olszewski and M. Siman-Tov, "Development of Encapsulated Lithium Hydride Thermal Energy Storage," presented at 24th IECEC in Washington, DC, August 7-12, 1989.
2. S. V. Raj and J. D. Whittenberger, "The Mechanical Properties of Fluoride Salts at Elevated Temperatures," published at 8th International Conference on the Strength of Metals and Alloys, Tampere, Finland, August 22-26, 1988.
3. J. Daniel Whittenberger, "Tensile Properties of HA 230 and HA 188 After 400 and 2500 Hour Exposures to  $\text{LiF-22CaF}_2$  and Vacuum at 1093K," *Journal of Material Engineering*, June, 1989.
4. D. T. Baurgette, "Evaporation of Iron-, Nickel- and Colbalt-Base Alloys at 760 to 980C in High Vacuum," ORNL-3677, Oak Ridge National Laboratory, November, 1964.
5. L. M. Sedgwick, "Solar Dynamic Heat Receiver Technology Final Report," NASA-CR-187040, January, 1991.
6. Roger A. Crane, "Thermal Evaluation of Advanced Solar Dynamic Heat Pipe Receivers Performance," NASA CR-185117, 1989.
7. W. J. Mantle and W. S. Chang, "Effective Thermal Conductivity of Sintered Metal Fibers," 24th IECEC in Washington, DC, August 1989.
8. R. L. Gay, et. al., "Tests of Heat Transfer Enhancement For Thermal Energy Storage Canisters," 23rd IECEC, Denver, CO, August 1988.
9. Timothy R. Knowles, "Metal/Phase Change Material Composite Thermal Storage Materials," AIAA 22nd Thermophysics Conference Paper AIAA-87-1489.
10. R. A. Gnadt, "Filling Heat Storage Tubes For Solar Brayton Cycle Heat Receiver With Lithium Fluoride," ORNL-TM-2732, Oak Ridge National Laboratory, July 1970.
11. Arthur Fraas, Engineering Evaluation of Energy Systems, McGraw-Hill Book Company, 1982.
12. D. A. Jaworske and W. D. Perry, "Void Control in the Crystallization of Lithium Fluoride," Eighth Symposium on Space Power Systems, Albuquerque, NM, 1991.
13. Philomena G. Grodzka and Tommy C. Bannister, "Natural Convection in Low-g Environments," AIAA 12th Aerospace Sciences Meeting, Washington, D.C.

**APPENDIX A**

**SAFETY INFORMATION**

**Introductory Note:**

Following is a set of studies performed on the safety of testing TES canisters.



APPENDIX A

SUNDSTRAND AVIATION  
MEMO

To: A. Munn

MSE89/653

From: M. Brege <sup>MB</sup>

Date: 10/18/89

Subject: Safety of Canister Testing in a  
Fluidized Bed. Advanced Brayton  
Cycle Receiver

Copies: R. Waxler 742RW6  
G. Zwiefelhofer 742RW6  
O. Briles 789

Rupturing of a canister during test in a fluidized bed will result in LiF and possibly lithium or sodium (if tested) to come into contact with sand at -1600°F. The fluidized bed is an open system with a low flow of GN<sub>2</sub> flowing through it.

Provided below is a summary of several safety aspects that were considered if a canister rupture occurs. Specific details and references are attached.

MB:vl

Advanced Brayton Cycle Receiver  
"Safety Summary"

A. Vapor Pressure

1. LiF @ 1600°F = 0.0149 mm Hg ( $2.9 \times 10^{-4}$  psia)
2. Lithium @ 1617°F = 10 mm Hg (0.2 psia)
3. Sodium @ 1638°F = 760 mm Hg (14.7 psia)

Comments

- a. LiF vapor will condense in air to form a dust.  
LiF is relatively non-toxic (see data sheet).
- b. Lithium and sodium vapors will react upon contact with air. Vapors will not be contained or accumulate and therefore only a series of small reactions (if any) should occur.

---

Keywords: Safety, LiF, Lithium, Sodium, Brayton Cycle Receiver, Canister

B. Hydrogen Generation

- Worse case, assumes 100% reaction

1. Lithium (18.2 g) = 2.6 g H<sub>2</sub> (1 ft<sup>3</sup> @ STP)
2. Sodium (30.4 g) = 2.6 g H<sub>2</sub> (1 ft<sup>3</sup> @ STP)

Comments

- a. 2.6 g H<sub>2</sub> if ignited is equivalent to ~0.18 lbs. TNT.
- b. Reaction mechanism will probably be from vapors of the alkali metal with H<sub>2</sub>O in atmosphere, which will result in many small reactions (if any) instead of one significant reaction.

C. Compatibility with Sand (Al<sub>2</sub>O<sub>3</sub>)

1. LiF with Al<sub>2</sub>O<sub>3</sub>

- No potential problems indicated.

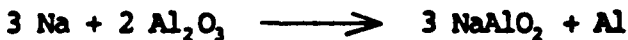
2. Lithium with Al<sub>2</sub>O<sub>3</sub>

- Free energy of formation of Li<sub>2</sub>O and Al<sub>2</sub>O<sub>3</sub> are identical indicating either no reaction or only an equilibrium type reaction will occur. If an equilibrium reaction does occur, it will be slow and non-violent.



3. Sodium with Al<sub>2</sub>O<sub>3</sub>

- Free energy of formation of Al<sub>2</sub>O<sub>3</sub> is greater than Na<sub>2</sub>O indicating no reaction will occur. However, reports state that complex compounds (i.e. NaAlO<sub>2</sub>) can form. These types of reactions are nonviolent.





**LITHIUM CORPORATION OF AMERICA**  
A SUBSIDIARY OF GULF RESOURCES & CHEMICAL CORPORATION

ORIGINATOR:  
DISTRIBUTION:

	THIS	REPLACES
FILE:	1500-416	
DATE:	9/23/77	
PAGE:	4 OF 6	OF

## 5.0 SAFETY - OSHA

### 5.1 Hazard Analysis

Lithium Fluoride is non-combustible and relatively non-toxic.

The physiological properties of lithium fluoride reside in the lithium and the fluorine content but the low solubility in water limits its activity. For guinea pigs the lethal dose has been reported to be 200 mg/kg [Simonin, C. rend. Soc. biol. 124, 133 (1937) ]. For higher animals the toxicity of lithium fluoride is believed to be low. Fluorine does not cause chronic toxicity. The chronic effects of fluorides as normally encountered would be limited to fluorosis due to an increased fluorine content in the bones and is mostly observed in animals. In man, fluorosis occurs only after exposure to large quantities of fluorides over a period of many years. Clinical fluorosis can be detected by x-ray examination. This clinical syndrome represents a change in bone structure but is almost never disabling. [Ref: Public Health Report 73, 721-746 (1958)].

### 5.2 Safety Precautions

Although lithium fluoride is considered to be non-hazardous in general handling, it is advisable to avoid excessive exposure. When dusty conditions are encountered, a dust mask should be worn. Gloves and aprons are optional and normally not required.

### 5.3 Treatment and Antidotes

As indicated above, lithium fluoride does not cause acute or chronic toxicity. However, it is recommended that normal good hygienic practices be observed. Hands should be washed before coffee breaks, meals and at the end of the shift.

As with any chemical, ingestion should be avoided. If a significant quantity of lithium fluoride is inadvertently swallowed, induce vomiting. Refer to a physician.

**SAFETY****A. Vapor Pressure****LiF:**

1600°F = 0.0149 mm Hg

1700°F = 0.0527 mm Hg

1800°F = 0.1623 mm Hg

**Lithium:**

1522°F = 5 mm Hg

1617°F = 10 mm Hg

1724°F = 20 mm Hg

**Sodium:**

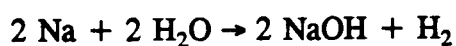
1513°F = 400 mm Hg

1638°F = 760 mm Hg

## HYDROGEN GENERATION

Note: Worse Case Scenario

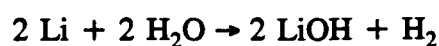
### A. Sodium



$$30.4 \text{ g Na} \times \frac{\text{mol}}{23.0 \text{ g}} \times \frac{2 \text{ mol H}_2}{2 \text{ mol Na}} \times \frac{2.0 \text{ g H}_2}{\text{mol}} = 2.6 \text{ g H}_2$$

$$2.6 \text{ g} \times \frac{\text{lbm}}{454 \text{ g}} \times \frac{\text{lbm-mol}}{2 \text{ lbm}} \times \frac{359 \text{ ft}^3}{\text{lbm-mol}} = 1.0 \text{ ft}^3 \text{ H}_2 @ \text{ STP}$$

### B. Lithium

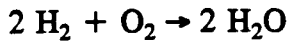


$$18.2 \text{ g Li} \times \frac{\text{mol}}{6.9 \text{ g}} \times \frac{1 \text{ mol H}_2}{2 \text{ mol Li}} \times \frac{2.0 \text{ g H}_2}{\text{mol H}_2} = 2.6 \text{ g H}_2$$

$$2.6 \text{ g H}_2 \times \frac{\text{lbm}}{454 \text{ g}} \times \frac{\text{lbm-mol}}{2 \text{ lbm}} \times \frac{359 \text{ ft}^3}{\text{lbm-mol}} = 1.0 \text{ ft}^3 \text{ H}_2 @ \text{ STP}$$

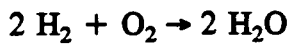
## HYDROGEN GENERATION (CONTINUED)

### TNT Equivalent



$$H_f \quad 0 \quad 0 \quad 2 (-59.4) @ 1520^\circ\text{F}$$

$$\Delta H_f = -118.8 \text{ kcal/mol}$$



$$2.6 \text{ g (0.0057 lbm)}$$

$$2.6 \text{ g H}_2 \times \frac{\text{mol}}{2 \text{ g}} \times \frac{2 \text{ mol H}_2\text{O}}{2 \text{ mol H}_2} = 1.3 \text{ mol H}_2\text{O (23.4 g) (0.052 lbm)}$$

$$1.3 \text{ mol H}_2\text{O} \times \frac{118.8 \text{ kcal}}{\text{mol}} \times \frac{1000 \text{ cal}}{\text{kcal}} \times \frac{3.97 \times 10^{-3} \text{ BTU}}{\text{cal}} = 613 \text{ BTU}$$

$$\text{H}_2 \rightarrow \frac{613 \text{ BTU}}{0.0057 \text{ lbm}} = 107,500 \frac{\text{BTU}}{\text{lbm H}_2}$$

$$\text{TNT} \rightarrow 2,054 \frac{\text{BTU}}{\text{lbm TNT}}$$

$$0.0057 \text{ lbm H}_2 \times \frac{107,500 \text{ BTU}}{\text{lbm H}_2} \times \frac{\text{lbm TNT}}{2,054 \text{ BTU}} = 0.3 \text{ lbm TNT (Equivalent)}$$

Or

B.  $0.25 \text{ lbs H}_2 = 7.80 \text{ lbm TNT (SCEPS Calc.)}$

$$0.0057 \text{ lbs H}_2 \times \frac{7.82 \text{ H}_2\text{O TNT}}{0.25 \text{ lbs H}_2} = 0.18 \text{ lbs TNT}$$

Or

C.  $1.75 \text{ lbs Li} = 7.22 \text{ lbs TNT}$

$$18.2 \text{ g Li} \times \frac{\text{lb}}{454 \text{ g}} \times \frac{7.72 \text{ lbs TNT}}{1.75 \text{ lbs Li}} = 0.18 \text{ lbs TNT}$$

Will assume SCEPS calculation is correct.

## II. Technical Discussion

### A. Test Materials

Titanium-stabilized type 321 stainless steel was utilized for these tests. This selection was based on the prior test results and other work (Ref. 5) which indicated that titanium stabilization of the containment material eliminated carbon mass transfer. Analyses of the starting material are given in Table 1.

Table 1. Analyses of starting materials

Element	Content, %	
	Sheet stock	Tubing
Chromium	17.35	17.60
Copper	0.22	0.10
Manganese	1.62	1.51
Molybdenum	0.32	<0.20
Nickel	11.20	10.50
Silicon	0.72	0.75
Titanium	0.47	0.48
Carbon	0.08	0.04
Hydrogen	1 part/10 <sup>6</sup>	11 parts/10 <sup>6</sup>
Nitrogen	0.010	0.030
Oxygen	0.006	0.011
Phosphorous	0.018	0.021
Sulphur	0.005	0.021

Lithium and potassium were used in these tests because they had been shown to be more aggressive than cesium or rubidium. Typical analyses of the liquid metals are given in Table 2.

Flow stream gettering agents were selected on the basis of their oxide stability (Table 3) and nitride stability (Table 4). The gettering elements selected were beryllium, hafnium, samarium, titanium, thorium, yttrium, and zirconium. Data shown in Table 3 indicate beryllium, samarium, thorium, and yttrium oxides are more stable at all temperatures of interest than lithium oxide. Hafnium and zirconium oxides are more stable at elevated temperatures (1760°F) than lithium oxide but not more stable at 1150°F. Titanium oxide is indicated to be less stable than lithium oxide at both temperatures. The uncertainty in the accuracy of the free energies of formation presented, together with the closeness of the relative stabilities, indicates the possibility that relative

Table 2. Typical analyses of lithium and potassium metals

Element	Content, parts/10 <sup>6</sup>	
	Lithium	Potassium
Iron	20	20
Boron	~100	<10
Cadmium	—	25
Manganese	1	3
Aluminum	20	5
Magnesium	35	5
Copper	3	10
Chromium	2	<5
Silicon	<0.1%	<25
Nickel	~400	5

\*Content of other elements was below limits of detection.

Table 3. Free energies of formation of oxides

Compound	Oxide stability,* kcal/g atom of oxygen	
	900°K (1150°F)	1200°K (1780°F)
K <sub>2</sub> O	-54	-37
Li <sub>2</sub> O	-114	-105
Na <sub>2</sub> O	-69	-58
BaO	-122	-113
1/2 HfO <sub>2</sub>	-112	-105
2/3 Sm <sub>2</sub> O <sub>3</sub>	-124	-118
2/3 ThO <sub>2</sub>	-126	-119
TiO	-103	-97
1/3 Ta <sub>2</sub> O <sub>5</sub>	-101	-95
2/3 Y <sub>2</sub> O <sub>3</sub>	-118	-111
2/3 ZrO <sub>2</sub>	-110	-109
1/3 Al <sub>2</sub> O <sub>3</sub>	-111	-103
1/3 Cr <sub>2</sub> O <sub>3</sub>	-72	-64
FeO	-49	-45
1/3 Fe <sub>3</sub> O <sub>4</sub>	-47	-41
NiO	-37	-31
MnO	-76	-71
MgO	-120	-112
1/2 SiO <sub>2</sub>	-85	-79

\*Data from Cochrane, J. P., Corrections to the Data on Theoretical Metallurgy, Bureau of Mines Bulletin 342, U. S. Government Printing Office, Washington, 1934.

APPENDIX Z


OFFICE MEMORANDUM

December 21, 1989  
FS89-201

TO: Gary Heidenreich/741A6

cc: M. Brege/789-6  
R. Waxler/742RW6

FROM:

  
Al Munn/994-6

SUBJECT: NASA Advanced Brayton Heat Exchanger

I have reviewed the material submitted to be by Mark Brege and yourself and, based on that information and my understanding of this project, offer the following recommendations and requirements.

- a) Precautions must be taken to ensure employees and other persons cannot and do not come in contact with this operation during test. The temperatures of the surface will become very hot.
- b) The canisters to be tested are filled and welded outside Sundstrand.
- c) Adequate general ventilation must be provided to the cell to ensure no excessive build-up of N<sub>2</sub> gas so as to present a threat to employees monitoring the test and to remove excessive heat build-up.
- d) Adequate ventilation must be provided to the cell and/or stand to eliminate the build-up of hydrogen should the canister rupture under test.
- e) The test is to be conducted in either cells 61 or 62 at Plant 6. Keep in mind that both cells are equipped with deluge-type sprinkler systems for fire protection. Cell 62 is also equipped with a CO<sub>2</sub> total flood system which is designed to trip prior to activation of the sprinkler system.
- f) If nitrogen is to be supplied by cylinders, they must be secured in place with proper flow rate regulation. Bottles not in use must also be secured with caps in place. If from a bulk source, proper regulation of flow must be maintained.

I would recommend that your systems safety person also review the project. Our primary interest is in protecting employees and facilities and the test stand and article is secondary. Project system safety people are more attuned to test stand and article safety.

If you have any questions please feel free to call me at X6934.

AM:cw



Based on these studies, the risks associated with the TES canister tests seem relatively low.

**APPENDIX B**

**NICKEL OXIDE REDUCTION AND CANISTER FILLING PROCEDURES**



TO:	W. Greenlee	DATE:	October 3, 1990
FROM:	M. Schneider	MEMO NO.:	RM90/1941.MGS
SUBJECT:	Canister Heat Treat Results	CC:	T. Bland S. Downing L. Suit R. Mokadam
REFERENCE:	EWR No. 39766 Charge No. L632-003		G. Heidenreich/430D6 M. Brege/789-6 O. Briles/789-6
SUBJECT FILE:	4.2.4.4		

Two weeks of preparations for heat treat of Advanced Receiver canisters culminated on Wednesday, September 20, 1990 at Progressive Steel Treating, Inc. with actual processing of the parts. This report will document the preparations and results.

The furnace was vacuum baked for one day to remove impurities and was plumbed with a gas inlet line to allow introduction of an argon/5 percent hydrogen mixture for the reduction process. The plumbing schematic is shown in Figure 26, page 47. The gas plumbing and the entire furnace was leak-checked with a helium leak detector by John Olsen, a vacuum furnace consultant hired regularly by Progressive. John also provided guidance on the entire anneal and reduction process. All four canisters were processed at the same time. Gas inlet lines were fed into the two Nickel-filled canisters, and the two empty canisters were placed at the back of the furnace. Process data, including temperature and pressure, were recorded by Mark Brege, and this data is included in Table 1. The furnace cycle (detailed in memo number RM90/1896.MGS) went as planned. When the temperature had fallen to 1800°F (at 11:45 a.m.), the gas flow was commenced and controlled to a flow of 2.88E-04 LBM/S (mixture flow rate). This flow is about 24 times the necessary flow, but was the lowest setting at which the flow could be controlled due to internal leaks in the gas tank pressure regulator. During the reduction portion of the cycle, the furnace pressure was held at 75  $\mu$ m of Hg. After the reduction process was completed, the furnace was force-cooled with liquid nitrogen boil-off, and at 2:10 p.m. the canisters were removed from the oven (the canisters were purged for five minutes with a flow of 4.09E-04 LBM/S to ensure that they were filled with inert gas). The Nickel-filled canisters were removed from the oven and capped immediately. Upon handling these canisters, we noticed oxides coating the outer Inconel surfaces and the stainless steel tubing. Also, the furnace door had a 1.0 foot diameter darkened spot where impurity-laden gas had impinged on the door. Further inspection of the gas tubing showed that even the inside diameter of the tubing was covered with a black oxide. This led us to believe that either the bottle of gas had excessive contaminants or air was leaking into the gas plumbing (the gas pressure in this tubing was subatmospheric). To remedy this problem, an ultra-high purity grade of gas will be used, and an orifice will be added to the plumbing to assure superatmospheric pressure in the tubing outside the furnace.

Keywords:	EWR No. 39766	Subject File No. 4.2.4.4	Subject Advanced Receiver	General Heat Treat	General Canister
-----------	------------------	-----------------------------	---------------------------------	--------------------------	---------------------

Memorandum to W. Greenlee  
October 3, 1990  
Page Two

One of the Nickel-filled canisters was inspected with a boro-scope, and as expected, the Nickel foam had a gray, matte appearance, indicating that oxides had not been significantly reduced. The non-filled canisters seemed unaffected by the impurities issuing from the filled canisters, and thus will be used as is. As an aside, another possible source of contaminants is the Nickel foam itself since it is produced by using organic binders. However, these contaminants are not likely the only ones present since the tubing inside diameter had an oxide coating over several feet of its length.

A venturi flow coefficient versus pressure ratio curve is shown in Figure 2 for the .040 inch meter used in this project.

Attachments  
MGS:lo

0.040 INCH VENTURI PRESSURE VS FLOW COEFFICIENTS

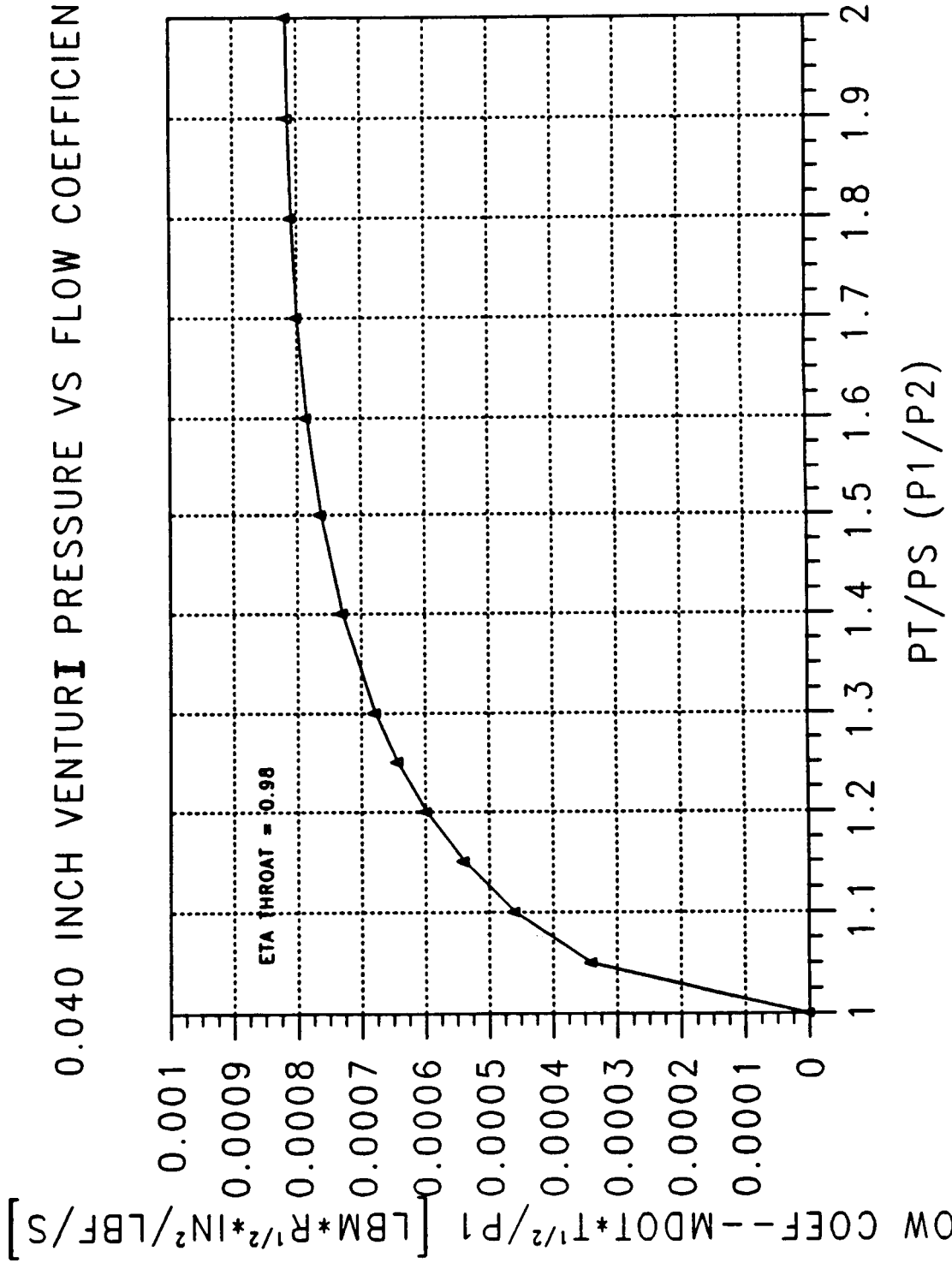


Figure 2



TO: W. Greenlee  
 FROM: M. Schneider *M.S.*  
 SUBJECT: Reduction Treatment of Canisters  
 REFERENCE: EWR No. 39766  
 Charge No. L632-003  
 SUBJECT FILE: 4.2.4.4

DATE: October 24, 1990  
 MEMO NO.: RM90/1980.MGS  
 CC: T. Bland  
 R. Mokadam  
 M. Brege/789-6  
 G. Heidenreich/430D6  
 S. Downing  
 R. Mokadam  
 L. Suit

Mark Brege and I made another attempt at reduction treating the foam filled canisters at Progressive Steel Treating on October 18, 1990. Although the process went smoothly, the 3/16" gas supply tubes were covered with a thin oxide or contaminant layer. Contaminants in the foam itself are the suspected cause.

Some apparatus changes were made to effect these results. All plumbing was acetone cleansed and vapor degreased. All plumbing outside the furnace was maintained at super atmospheric pressure to obviate the possibility of air leaking into the H<sub>2</sub>/Ar gas flow. The entire plumbing assembly was leak-checked with the "bubble-check" method to further preclude the chance of air ingress to the H<sub>2</sub>/Ar flow. Finally, an "O<sub>2</sub> getter" was placed in the gas line in order to trap any O<sub>2</sub> that might have been in the gas flow. Two O<sub>2</sub> getters were spent in the first day due to air leaks. (These leaks were discovered before an actual reduction run was attempted.) On the second day we discovered that the getter caused a large pressure drop, and thus would create a sub-atmospheric section in the external plumbing. Thus, the getter was used only for leak checking purposes and then was removed. Then further "bubble tests" were performed to assure leak tightness.

The decision was made to proceed with filling these two canisters with LiF salt for the following reasons:

1. We felt that we were at a point of diminishing returns with regard to removing oxides and other contaminants from the foam.
2. Thermal test results from a foam-filled canister would be useful even if oxides did remain on the foam, since the foam would at least provide thermal conductivity enhancement, and might also promote solidification farther from the cooling surface.
3. We do not have another well-defined reduction process to use if we want to make another attempt at oxide reduction.

MGS:lo

Keywords:	EWR No. 39766	Subject File No. 4.2.4.4	Subject Advanced Receiver	General Reduction Process	General Canisters
-----------	------------------	-----------------------------	---------------------------------	---------------------------------	----------------------



TO: W. Greenlee  
FROM: M. Schneider *MSS*  
SUBJECT: Trip Report - Filling Canister  
at NASA LeRC  
REFERENCE: EWR No. 39766  
Charge No. L632-003  
SUBJECT FILE: 4.2.4.3

DATE: October 3, 1990  
MEMO NO.: RM90/1944.MGS  
CC: S. Downing  
T. Bland  
L. Suit  
R. Mokadam  
G. Heidenreich/430D6  
M. Brege/789-6  
R. Reynolds/995JM6

Attendees:

Mark Brege - Sundstrand  
Gary Heidenreich - Sundstrand  
Mike Schneider - Sundstrand  
Miles Dustin - NASA LeRC  
Jim Mierzejewski - NASA LeRC  
Subramaniam V. Raj - NASA LeRC  
Dan Whittenberg - NASA LeRC  
Scott Richter - Sverdrup

Mark Brege, Gary Heidenreich and I flew to Cleveland on the evening of Monday, September 24, 1990 and met with NASA personnel on Tuesday morning to fill a canister with Lithium Fluoride salt. We chose to fill a canister which was not filled with nickel foam since the reduction process at Progressive Steel, Inc. had not satisfactorily removed the oxides from the nickel (refer to memorandum number RM90/1941.MGS for a detailed discussion of the reduction process at Progressive).

We immediately prepared the canister for filling by bolting it into the filling fixture and filling the funnel with 575.9 grams of LiF which would yield a 94.7 percent fill at 1650°F. We raised the furnace temperature to 900°C and dwelled at this temperature for 1.5 hours. Then we allowed the canister to radiantly cool overnight in a vacuum atmosphere. While removing the canister from the furnace the next morning, we noticed that a black film (possibly carbon) was coating the outside of the canister and the furnace surfaces. Also, we noticed that a small portion of the LiF (12.4 grams) had not flowed into the canister, but rather had both remained as condensate in the funnel and vaporized. The funnel will be returned to Sundstrand to quantify the relative amounts of condensation and vaporization. Also, the funnel exit tube will be analyzed and enlarged if necessary to facilitate drainage from the funnel. It should be noted that the fill caps worked quite well in keeping the salt away from the weld joint. A detailed report on the fill procedure and the oven temperature/pressure schedule is contained in a report by Mark Brege (memorandum number MSE90/575).

Keywords:	EWR No. 39766	Subject File No. 4.2.4.3	Subject Advanced Receiver	General Lithium Fluoride	General Filling Canister
-----------	------------------	-----------------------------	---------------------------------	--------------------------------	--------------------------------

Memorandum to W. Greenlee  
October 3, 1990  
Page Two

Dan Whittenberg, the furnace operator, was very accommodating, staying late with us on Tuesday evening to fill the canister and coming in early the next day to cool the parts down quickly. Also, one of his colleagues, Subramaniam V. Raj, who is characterizing LiF mechanical properties, was also helpful as he supplied me with literature he had generated and collected on LiF-22 percent  $\text{CaF}_2$  Hypereutectics and LiF single crystal properties. All in all, the fill process went rather smoothly, and we will cap and test this particular canister.

The canister was then taken to the Electron Beam Weld (EBW) facility to be capped, but the controller for the weld machine had broken down due to a component failure on the memory board. However, the Operator, Jim Mierzejewski, had already fixtured a spare canister onto the welding turntable and had adjusted its position to reduce axial and radial run outs at the weld joint area to .001 and .005 inch, respectively. Thus, when the controller is repaired (approximately October 5, 1990), the filled canister can be welded immediately. Presently, the filled canister is being held in a room temperature, vacuum environment. We reviewed photographs of the weld samples which Jim had made earlier, and he agreed that penetration was inadequate. Also, he said that misalignment was due to magnetism in a holding chuck. Thus with higher power and demagnetized parts, we feel that weld quality can be greatly improved. Welding is addressed in detail in memorandum number RM90/1942.MGS.

Gary and Miles discussed the fact that I would be assuming program responsibilities and Miles seemed satisfied with our effort to continue supporting the program. Having met Miles, the other NASA personnel and Scott Richter, a contracted Sverdrup employee who is working on the collector and receiver, I feel the working arrangement will be a positive one. Overall, the NASA facilities seem clean and more than adequate to complete the job.

MGS:lo



SUNDSTRAND AVIATION  
MEMO

To: O. Briles

MSE90/575

From: M. Brege *ms.*

Date: 9/28/90

Subject: Trip Report to NASA LeRC,  
September 24-26, Fill TES Canister  
with LiF  
EWR 39766 L632-003

Copies: M. Schneider  
B. Greenlee  
G. Heidenreich  
W. Leeming  
D. Reynolds

Attendees: Mark Brege - Sundstrand  
Mike Schneider - Sundstrand  
Gary Heidenreich - Sundstrand (1 day)  
Miles Dustin - NASA LeRC (Program Manager)  
Dan Whittenberg - NASA LeRC (Furnace Operator)  
Jim Mierzejewski - NASA LeRC (EB Welder)  
Scott Richter - Sverdrup (Helper)

Canister 006 (no nickel foam for thermally conductivity enhancement/void management) was filled with LiF at NASA LeRC. The procedure used is as follows.

The canister was attached to the filling fixture and powdered MoS<sub>2</sub> was used on all threaded bolts. 575.9 g of LiF (Cerac, vacuum fused, ~1/8" chunks) was added to the filling funnel. This mass of salt would theoretically give a 94.7% fill at 1650°F if the density of LiF recorded in the literature is correct. The canister and fill fixture were placed in the vacuum furnace between the fixed controlling thermocouple and the door.

The roughing pump was started at 11:00 AM and the cryopump (He at -12°K) was engaged at 11:30 AM. A residual gas analyzer (mass spectrometer for masses 2 to 50) was started at ~11:30 AM. After pumping down to  $1 \times 10^{-5}$  Torr, heat was supplied at a low rate to dry the salt. Approximately 4 hours were required to reach the melting point of LiF (847°C) and a vacuum level of  $\sim 1 \times 10^{-5}$  was maintained once the salt reached 800°C. Although LiF has a vapor pressure of ~0.02 Torr at 900°C, the vacuum gauge is in a cold section outside the furnace and the LiF would condense prior to reaching it.

Gases liberated during filling (RGA data) were comprised mainly of H<sub>2</sub>O initially, CO<sub>2</sub> during the range of 400-600°C and roughly equal amounts of H<sub>2</sub>, H<sub>2</sub>O, N<sub>2</sub> and HF at 900°C although the amounts were very low ( $10^{-6}$  Torr range). Actual gas compositions can be calculated based on the total pressure and the partial pressures of the gases recorded by the RGA analyzer. The RGA data is in the possession of the writer.

---

Keywords: Brayton Cycle, LiF, Canister, Fill, TES, Trip Report

During the filling operation the thermocouples were continuously monitored in order to detect if any salt flow from the filling funnel to the canister was occurring. During the 1st hour at 900°C, no changes in the thermocouples were observed. However, all persons present believed the salt was melting and flowing but no temperature fluctuations were occurring because the thermocouples were not physically attached (just in close proximity) to the hardware. To help ensure complete filling would occur, the canister was held at 900°C for an additional 0.5 hours (1.5 hours total). The canister was then allowed to cool under vacuum ( $10^{-8}$  Torr range) overnight.

The furnace was cooled with  $N_2$  in the morning and then opened. The exterior of the canister and filling fixture, in general, had a thin coating (probably an oxide) over the exposed surfaces. The interior of the filling funnel indicated a good fill except for a small frozen puddle of LiF at the fill tube and small frozen droplets on the underside of the filling funnel lid which appear to have been formed by condensing LiF vapor.

The filling funnel was removed (easily) from the filling fixture and then the protective cap was removed (easily) from the canister. The weld area of the canister was in perfect condition (no salt or oxidation) verifying that the protective cap works. The canister was then removed (easily) from the filling fixture. The ease at which the assemblies came apart shows that the  $MoS_2$  powder was an excellent lubricating and anti-seizing compound.

The canister was weighed and the results indicate a 92.7% fill (94.7% fill projected) at 1650°F. The 12.4 g of LiF lost in the filling were caused by the following phenomena:

1. Frozen puddle at bottom of fill funnel.
2. Frozen droplets on underside of fill funnel cover.
3. Volatilization of LiF due to its vapor pressure and vacuum level.

The salt puddle and droplets will be weighed to access how much salt was lost to volatilization and to better understand how to make a more complete fill next time. Also, the fill tube may be enlarged to make sure a puddle does not form next time. The filling funnel will be sent to Sundstrand for cleaning and evaluation.

The canister was taken to the NASA LeRC weld shop for EB welding. However, the EB weld machine had just suffered some type of hardware problem (probably a bad electronic board). NASA LeRC is now in the process of trying to fix the EB weld machine. The canister is currently being stored in a vacuum chamber to reduce  $O_2$  and  $H_2O$  contamination of the LiF.

Notes from the filling procedure are attached.

MAB:vl

FILL CANISTER 006 AT NASA LEWIS RESEARCH CENTER

Salt Mass: Canister 006

- Assume: 1. Volume = 340.7 cm<sup>3</sup>  
 2. 97 percent full at 1800°F

$$\rho_{\text{LiF}} @ 1800^\circ\text{F} (1256 \text{ K}) = 1.7429 \text{ g/cm}^3$$

$$97 \text{ percent full } (340.7 \text{ cm}^3) \times 1.7429 \text{ g/cm}^3 = 576 \text{ g LiF}$$

$$\text{Check at } 1650^\circ\text{F}; \rho = 1.7846 \text{ g/cm}^3$$

$$576 \text{ g LiF} \times \frac{\text{cm}^3}{1.7846 \text{ g}} = 322.8 \text{ cm}^3$$

$$\frac{322.8 \text{ cm}^3}{340.7 \text{ cm}^3} \times 100\% = 94.7\% \text{ full @ } 1650^\circ\text{F}$$

$$\text{Salt weight} = 330.91 + 245.01 = 575.92 \text{ g}$$

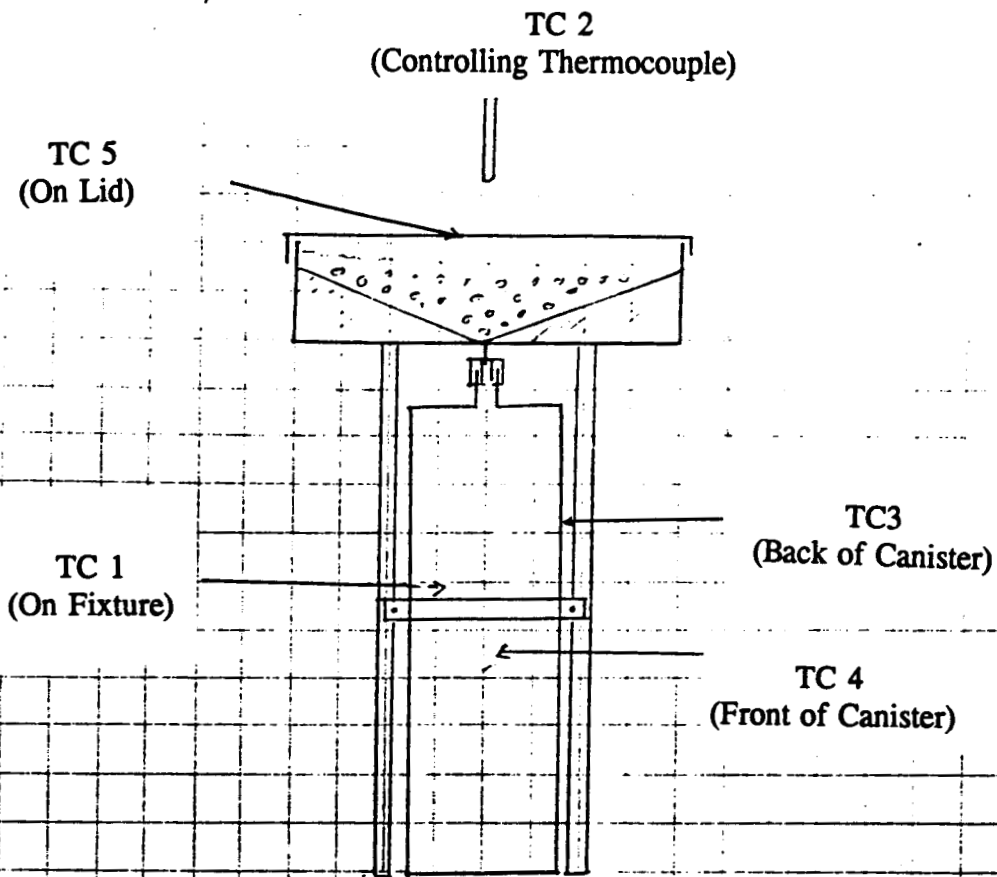
$$\text{Weight of canister} + \text{salt} = 1185.9 \text{ g}$$

$$\text{Weight of canister} = 622.3 \text{ g}$$

$$\text{Weight of salt} = 563.6 \text{ g}$$

Approximately 92.7 percent full at 1650°F

9/25/91



**Note:** None of the thermocouples were directly in contact with the canister or fill fixture. Only laying as close as physically possible.



TO: W. Greenlee  
 FROM: M. Schneider *MJS*  
 SUBJECT: Trip Report - Filling Canisters at NASA LeRC  
 REFERENCE: EWR No. 39766  
 Charge No. L632-003  
 SUBJECT FILE: 4.2.4.3

DATE: October 31, 1990  
 MEMO NO.: RM90/1998.MGS  
 CC: S. Downing  
 T. Bland  
 R. Grennan/741F6  
 R. Mokadam  
 L. Suit  
 K. Weber/741F6  
 P. Westhoff/741F6  
 G. Heidenreich/430D6  
 M. Brege/789-6  
 R. Reynolds/995JM6

Attendees:

- Mark Brege - Sundstrand
- Mike Schneider - Sundstrand
- Miles Dustin - NASA LeRC
- Ted Mroz - NASA LeRC
- Ron Sovie - NASA LeRC
- Dan Whittenberg - NASA LeRC
- Scott Richter - Sverdrup

Mark Brege and I travelled to Cleveland, Ohio on Monday evening, October 23, 1990 to fill two canisters for the Advanced Receiver program. On October 24, 1990, we filled canister S/N 007, the "wicking test canister," with 203.8 grams of LiF which is 34.7 percent liquid volume fill at 1650°F. It should be noted that it took approximately five minutes to secure the canister into the filling fixture and load the apparatus into the furnace, exposing the nickel foam to air during this time. The furnace cycle included a one hour dwell at 900°C to allow the liquid salt to flow into the canister.

While removing the canister from the furnace on October 25, 1990, we noticed that the fill tube was "bonded" to the canister by LiF which had wicked to fill the gap between the two parts, and this bond was broken rather easily in a shear mode. However, the fill cap was bonded in a similar fashion and was quite difficult to loosen. Only 3.2 grams of the salt had not flowed into the canister during filling. This canister was not welded since it will be inspected for wicking.

The fill process was repeated on the next canister, S/N 005, with an initial charge of 543.93 grams, and a 900°C dwell time of 1.5 hour. Again, the funnel tube stuck to the fill cap, but was removed rather easily. Also, when removing the apparatus from the oven, we noticed that some liquid salt had flowed over the outside of the canister. Post-fill canister weight was 1316.4 grams indicating that 21.1 grams had not flowed into the canister. This will yield a 91.7 percent volume fill at 1650°F.

Keywords:	EWR No. 39766	Subject File No. 4.2.4.3	Subject Advanced Receiver	General Filling Canister	General Trip Report
-----------	------------------	-----------------------------	---------------------------------	--------------------------------	------------------------

Memorandum to W. Greenlee  
October 31, 1990  
Page Two

The canister will be electron beam welded the week of October 29, 1990 and will be shipped to Sundstrand along with canister S/N 006 the fill fixture, funnel, LiF, and other miscellaneous hardware.

Miles Dustin seemed to agree that we were following the right course in filling the foam filled canisters in spite of the results of the reduction process. Also, Ted Mroz indicated that the Naval Research Center personnel had visited this week and that they might be interested in applying Brayton Advanced Receiver technology to future Naval Satellites. Finally, Miles said we should consider submitting a paper for the IECEC Conference.

MGS:lo

SUNDSTRAND AVIATION  
MEMO

To: O. Briles

MSE90/635

From: M. Brege *MB*

Date: 10/31/90

Subject: Trip Report to NASA LeRC,  
October 23-26, Fill TES  
Canisters with LiF  
EWR 39766 L632-003

Copies: W. Leeming 789  
D. Reynolds 995  
L. Hughes 789  
M. Schneider 741A  
B. Greenlee 741A  
G. Heidenreich 430D

Reference: Trip Report to NASA LeRC; MSE90/575.

Attendees: Mark Brege - Sundstrand  
Mike Schneider - Sundstrand  
Miles Dustin - NASA LeRC (Program Manager)  
Dan Whittenberg - NASA LeRC (Furnace Operator)

Canisters 005 and 007 (both contain nickel foam for thermally conductivity enhancement/void management) were filled at NASA LeRC. The canisters and nickel foam had previously been heat treated in a dynamic reducing atmosphere to reduce the inherent nickel oxide on the nickel foam (Memo No: RM90/1980.MGS). The reduction process was used to promote wetting of the nickel foam by LiF. The detailed filling procedure and hardware used to fill the canisters with LiF has been documented in the memo MSE90/575 which describes the filling of canister 006.

Canister 005 was to be filled 33.3% full (@ 1650°F). To compensate for salt losses (salt loss to volatilization and condensation on the fill funnel), the actual target was a fill of 35.1% (10.4 g excess LiF). After filling, weight measurements show a 34.6% fill was achieved. Canister 005 will be returned to Sundstrand, then sent out for x-ray analysis (CAT scan) and then destructively sectioned to determine whether any wetting of the foam by the salt has occurred.

Canister 007 was to be filled 95% full (@ 1650°F). To compensate for salt losses, the actual target was a fill of 95.4%. After filling, weight measurements show a 91.7% fill was achieved. Examination of the canister revealed that some LiF had leaked out around the fill cap, down the canister and onto the furnace tray. Although no salt was actually present (LiF had volatilized), the hardware was slightly stained. The cause for the salt leakage is believed to be due to the fill funnel tube touching the canister and allowing salt to wick out. The fact that the canister is only 91.7% full should not affect the results of our future tests. Canister 007 will be EB welded at NASA LeRC and returned to Sundstrand.

Notes from the filling procedure are attached.

MAB:vl  
Attachment

---

Keywords: Canister, Receiver, TES, Receiver, NASA, LiF

Canister = 007

$V = 325.1 \text{ cm}^3$

$\rho = 1.7846 \text{ g/cm}^3 @ 1650^\circ\text{F}$

Assume: 331 full @ 1650°F

$$\text{Salt} = 1/3 (325.1 \text{ cm}^3) \times \frac{1.7846 \text{ g}}{\text{cm}^3} = \frac{1.93.4 \text{ g} + 10.4 \text{ g excess}}{205.8 \text{ g}}$$

Weight of salt = 203.77

Weight of canister + LiF = 976.3

Weight of canister = 775.7 g

Weight of LiF = 200.6

\_\_\_\_\_ Lost 3.2 g of LiF

#### Actual Fill

$$200.6 \text{ g} \times \frac{\text{cm}^3}{1.7846 \text{ g}} = 112.4 \text{ cm}^3$$

$$\frac{112.4 \text{ cm}^3}{325.1 \text{ cm}^3} \times 100\% = 34.6\% \text{ fill (@ } 1650^\circ\text{F)}$$

Target = 35.1%

Actually target = 33.31% + 1.81% excess



Canister = 005

$$V = 319.6 \text{ cm}^3$$

$$\rho = 1.7846 \text{ g/cm}^3 @ 1650^\circ\text{F}$$

$$\text{Salt} = 95\% (319.6 \text{ cm}^3) \times \frac{1.7846 \text{ g}}{\text{cm}^3} = 541.84 \text{ g}$$

Note: Add 2 g excess salt, approximately 543.84 g salt

LiF

$$351.27 + 192.66 = 543.93 \text{ actual}$$

$$\text{Weight of salt} + \text{canister} = 1316.4$$

$$\text{Weight of canister} = 793.6$$

$$\text{Weight of salt} = 522.8 \text{ g}$$

\_\_\_\_\_ Lost 21.1 g of LiF

Actual Fill

$$522.8 \text{ g} \times \frac{\text{cm}^3}{1.7846 \text{ g}} = 293.0 \text{ cm}^3$$

$$\frac{293.0 \text{ cm}^3}{319.6 \text{ cm}^3} \times 100\% | 91.7\% \text{ fill (@ } 1650^\circ\text{F)}$$

Target = 95% fill

Actually target = 95% + 0.4% excess

NAME \_\_\_\_\_

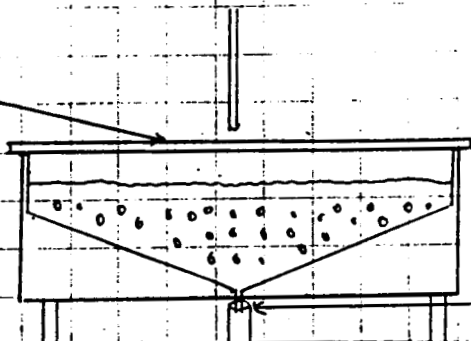
CONTRACT \_\_\_\_\_

MODEL \_\_\_\_\_

10/24/96

TC 2 - "Over Temp"

TC 5 - On Lid



TC 4 - Weld Joint

TC 3 - Wedge of Canister  
at the Bracket

TC 1 - Side of Canister  
(Controlling TC)

**APPENDIX C**

**TEST DATA**

THE FIRST LINE OF DATA INDICATES THE ORDER AND QUANTITY OF CHANNELS AT EACH CANISTER LOCATION. FOR INSTANCE, THIS DATA SET CONTAINS 89 POINTS COMPRISED OF 2 WEDGE CHANNELS, 5 SIDE WALL CHANNELS, AND 3 BACK WALL CHANNELS. THE FIRST COLUMN IS THE TIME IN MINUTES. ALL TEMPERATURES ARE IN DEGREES FAHRENHEIT. A '0000' VALUE IN THE MIDDLE OF A DATA SET INDICATES THAT THE THERMOCOUPLE BROKE DURING THE TEST. RAW DATA FOR THIS TEST POINT IS GIVEN ON THE NEXT TWO PAGES WHILE AVERAGE DATA IS GIVEN ON THE FOLLOWING TWO PAGES. DATA FROM ALL TEST POINTS ARE GIVEN IN CHRONOLOGICAL ORDER IN THIS APPENDIX.

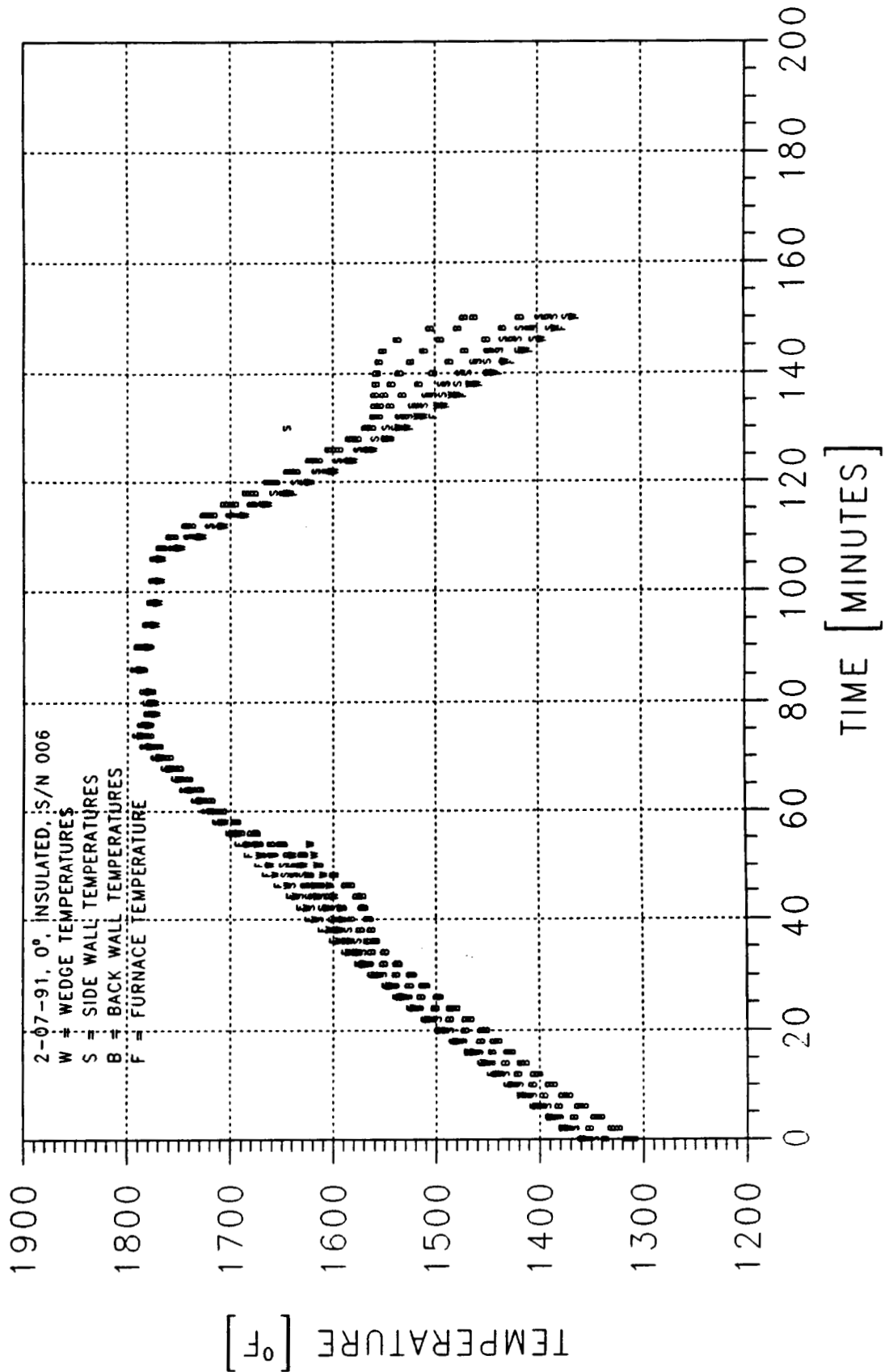
TEST #	TIME	TEMPERATURE	...
1	00	...	...
2	01	...	...
3	02	...	...
...	...	...	...
89	...	...	...







# TEMPERATURE PROFILES: TEST NO. 4-2

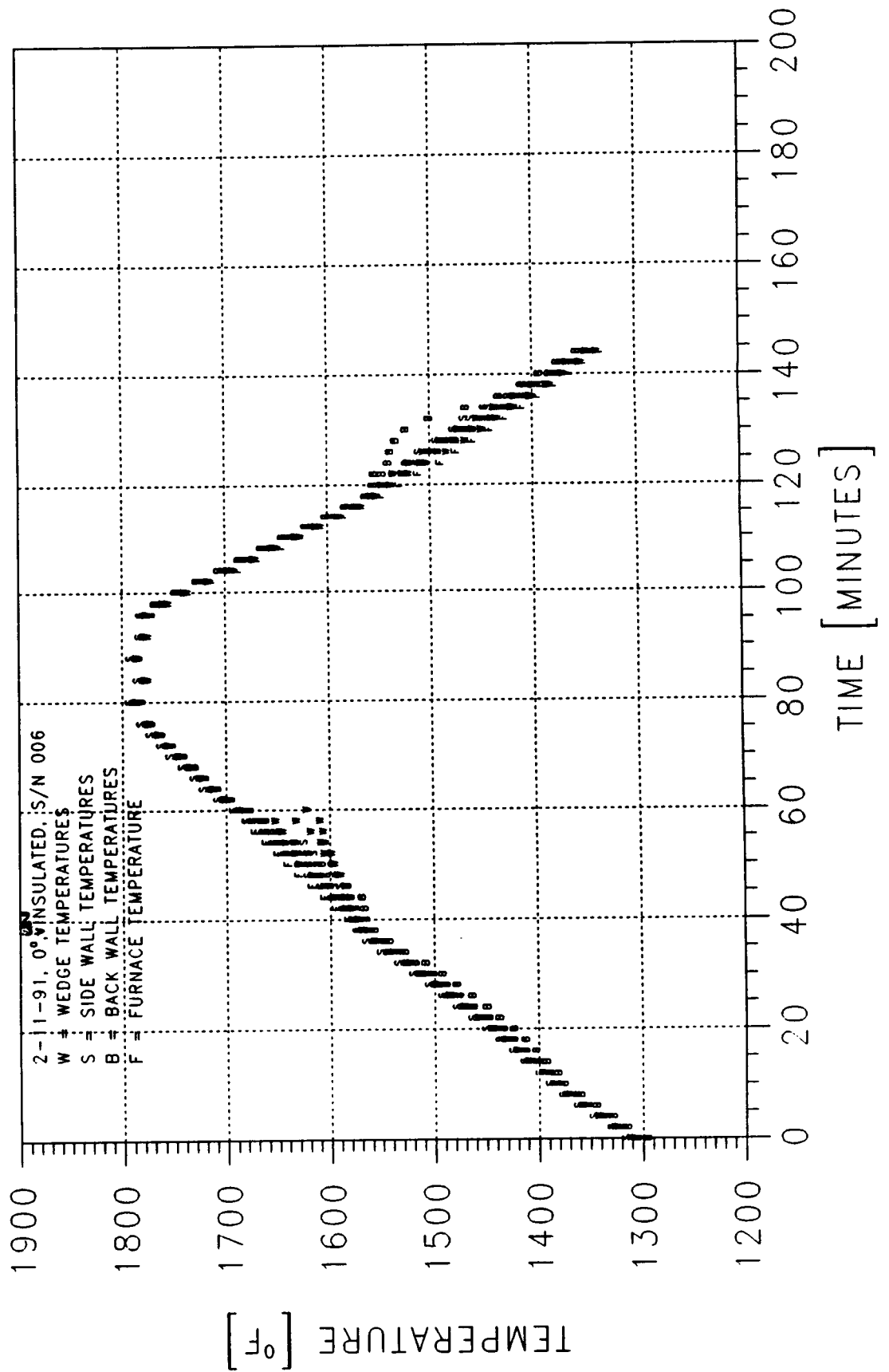








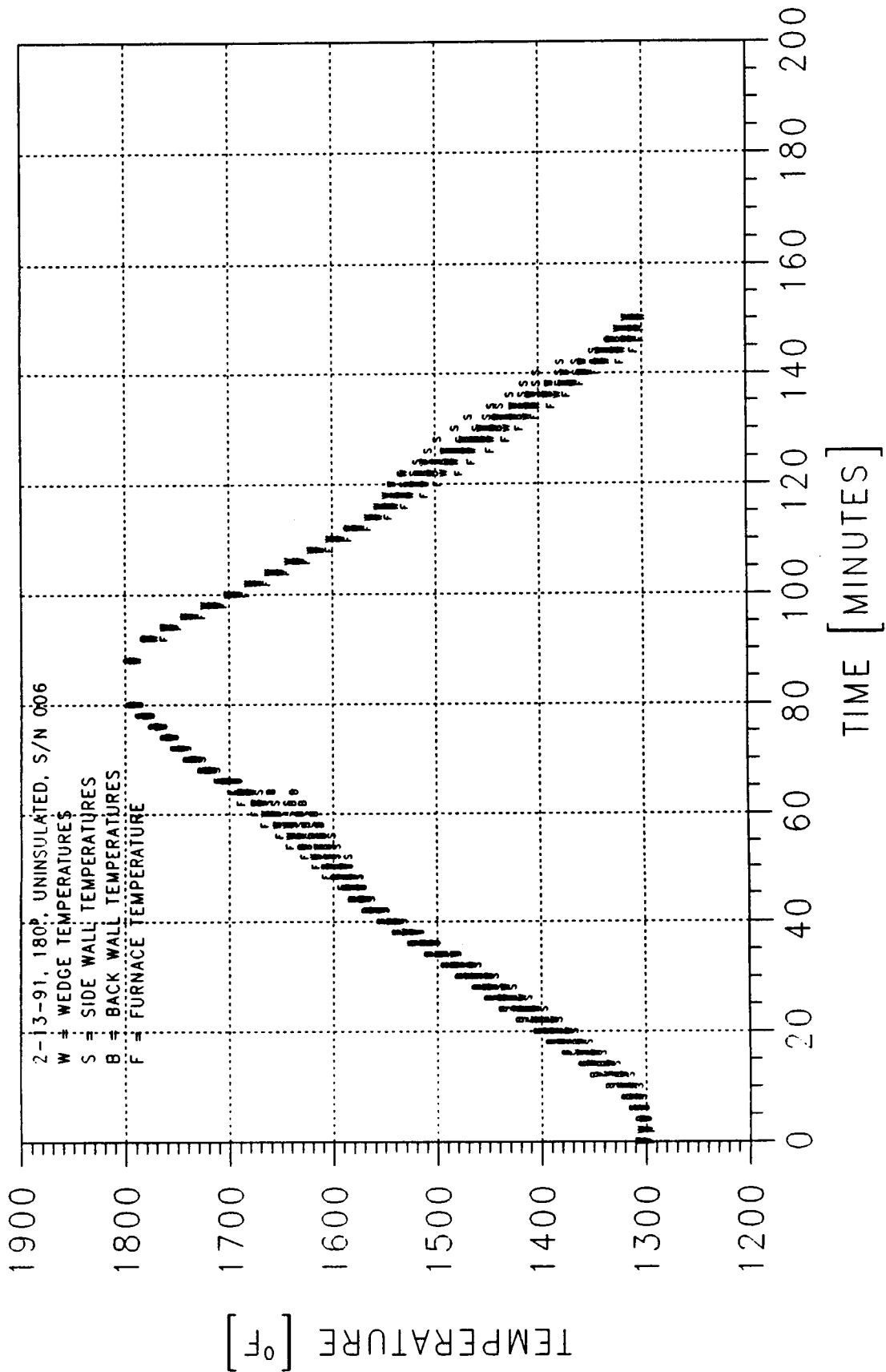
TEMPERATURE PROFILES: TEST NO. 6-1







TEMPERATURE PROFILES: TEST NO. 5-1

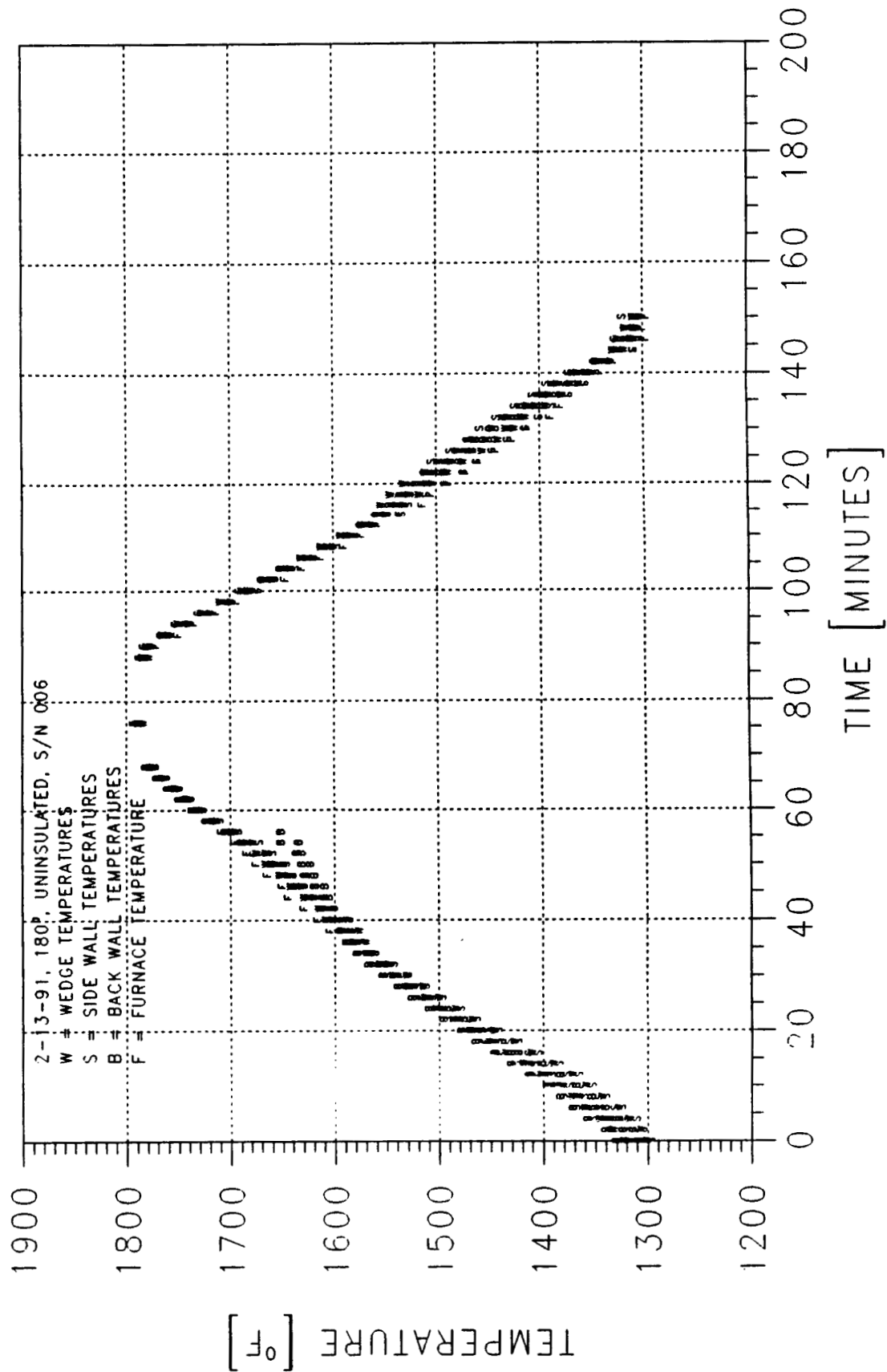








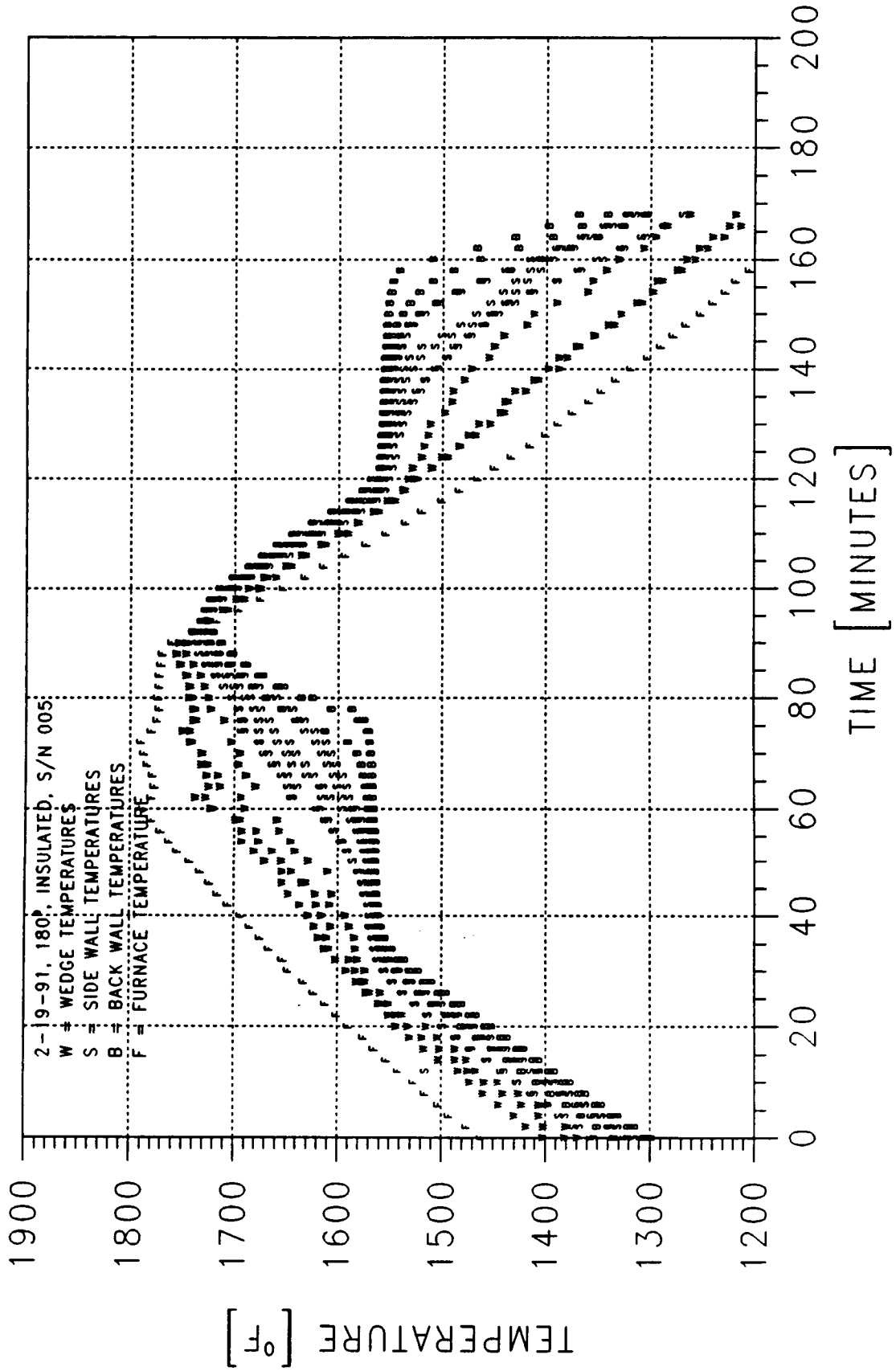
# TEMPERATURE PROFILES: TEST NO. 5-2







TEMPERATURE PROFILES: TEST NO. 8-1 (TILTED 6°)









000000000000  
.....  
000000000000  
000000000000  
000000000000  
000000000000

000000000000  
.....  
000000000000  
000000000000  
000000000000  
000000000000

000000000000  
.....  
000000000000  
000000000000  
000000000000  
000000000000

000000000000  
.....  
000000000000  
000000000000  
000000000000  
000000000000

000000000000  
.....  
000000000000  
000000000000  
000000000000  
000000000000

000000000000  
.....  
000000000000  
000000000000  
000000000000  
000000000000

000000000000  
.....  
000000000000  
000000000000  
000000000000  
000000000000

000000000000  
.....  
000000000000  
000000000000  
000000000000  
000000000000

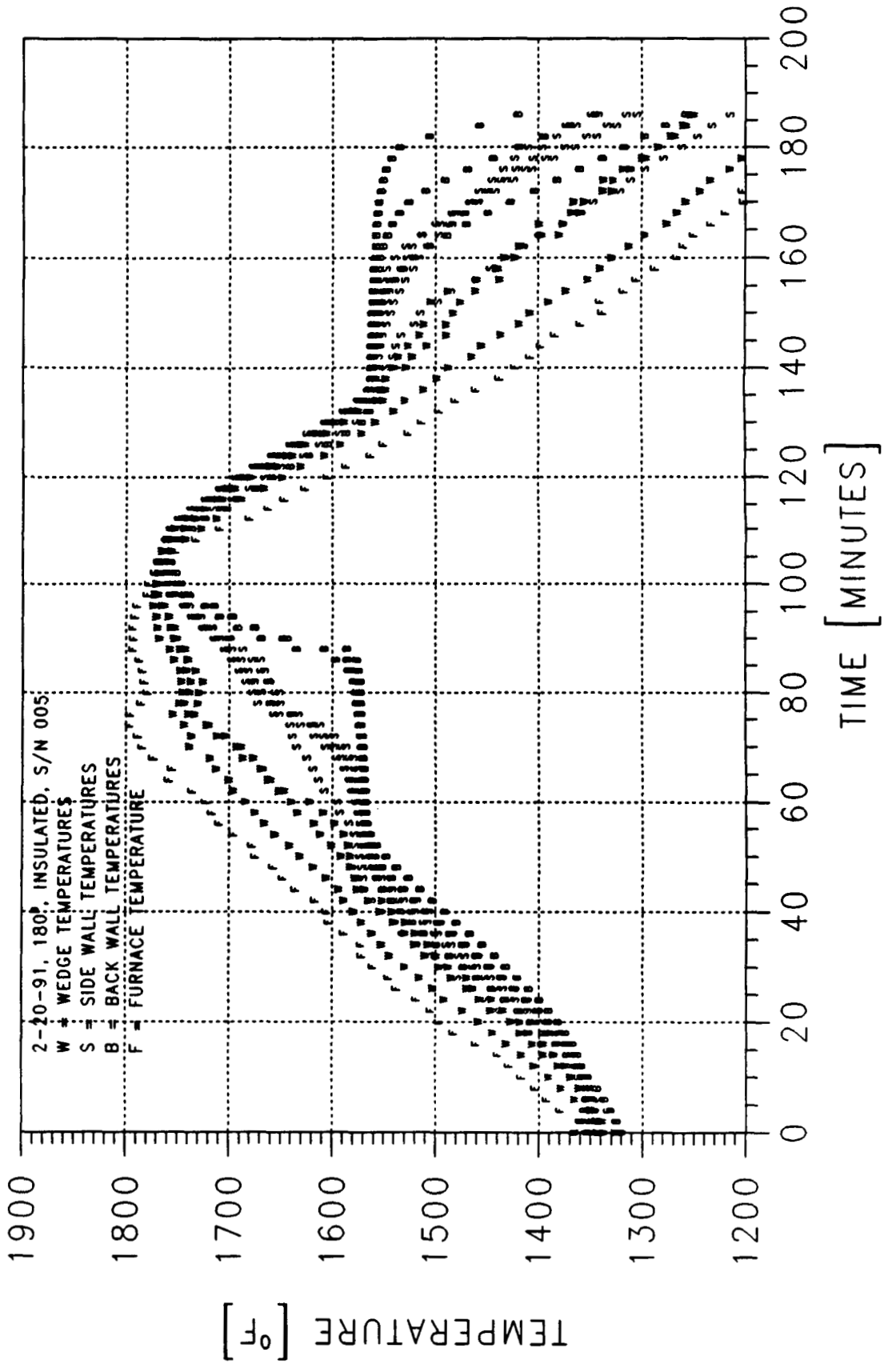
000000000000  
.....  
000000000000  
000000000000  
000000000000  
000000000000

000000000000  
.....  
000000000000  
000000000000  
000000000000  
000000000000

000000000000  
.....  
000000000000  
000000000000  
000000000000  
000000000000



# TEMPERATURE PROFILES: TEST NO. 8-3



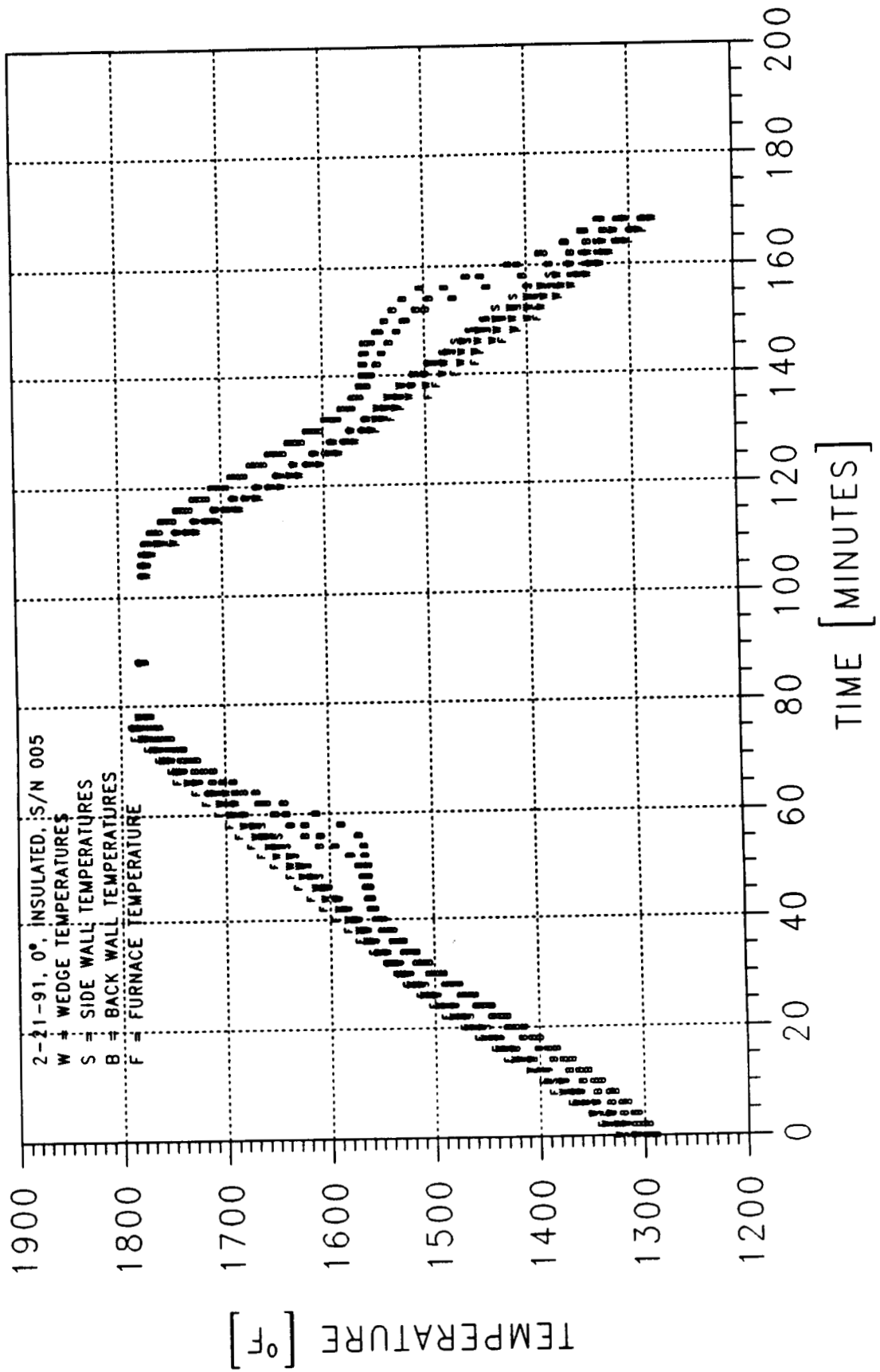








TEMPERATURE PROFILES: TEST NO. 9-2



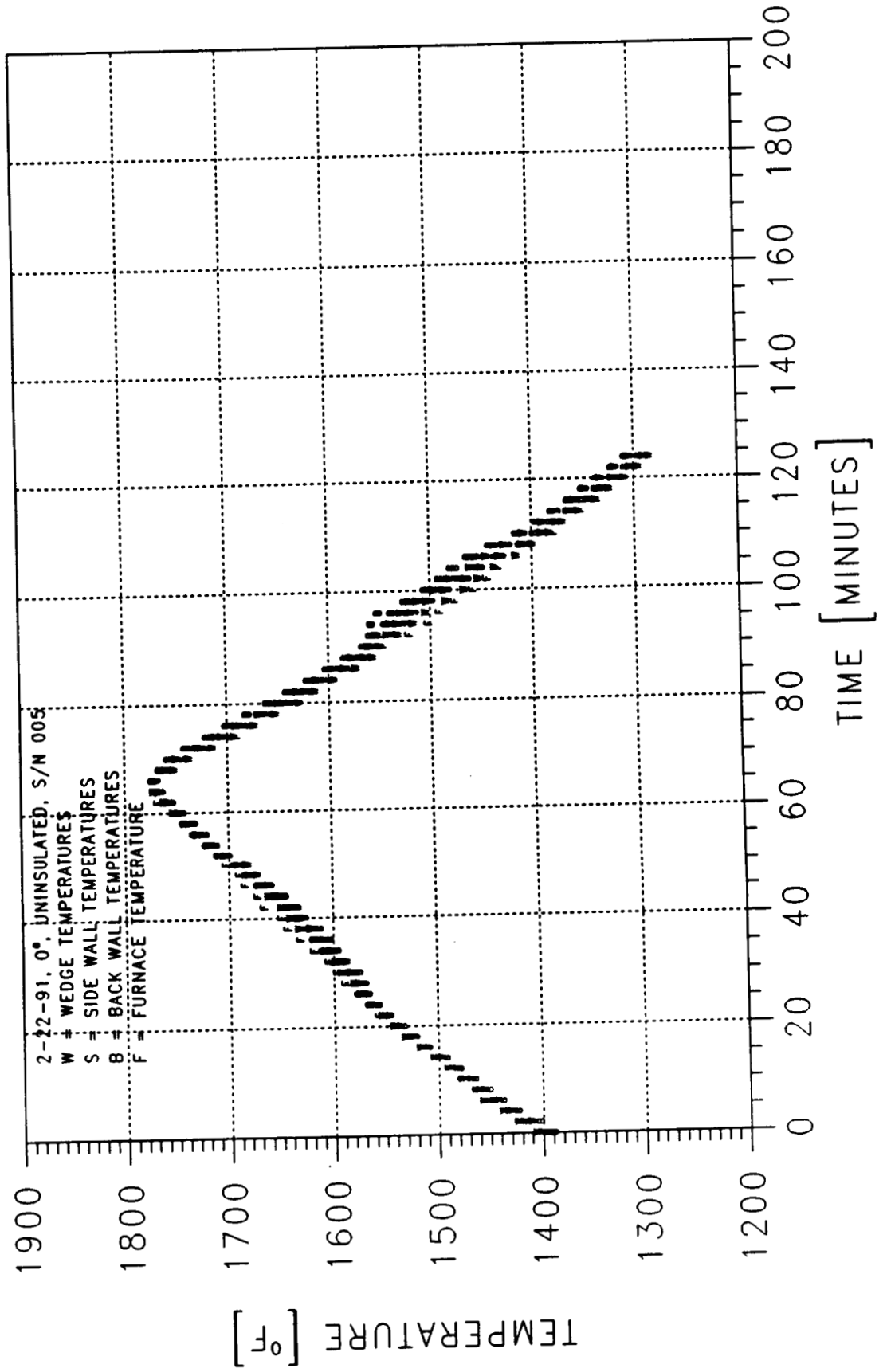






168.0 1289.0 -11.0 26.0 1292.7 -14.7 25.0 1322.7 -44.7 19.0 1278.0

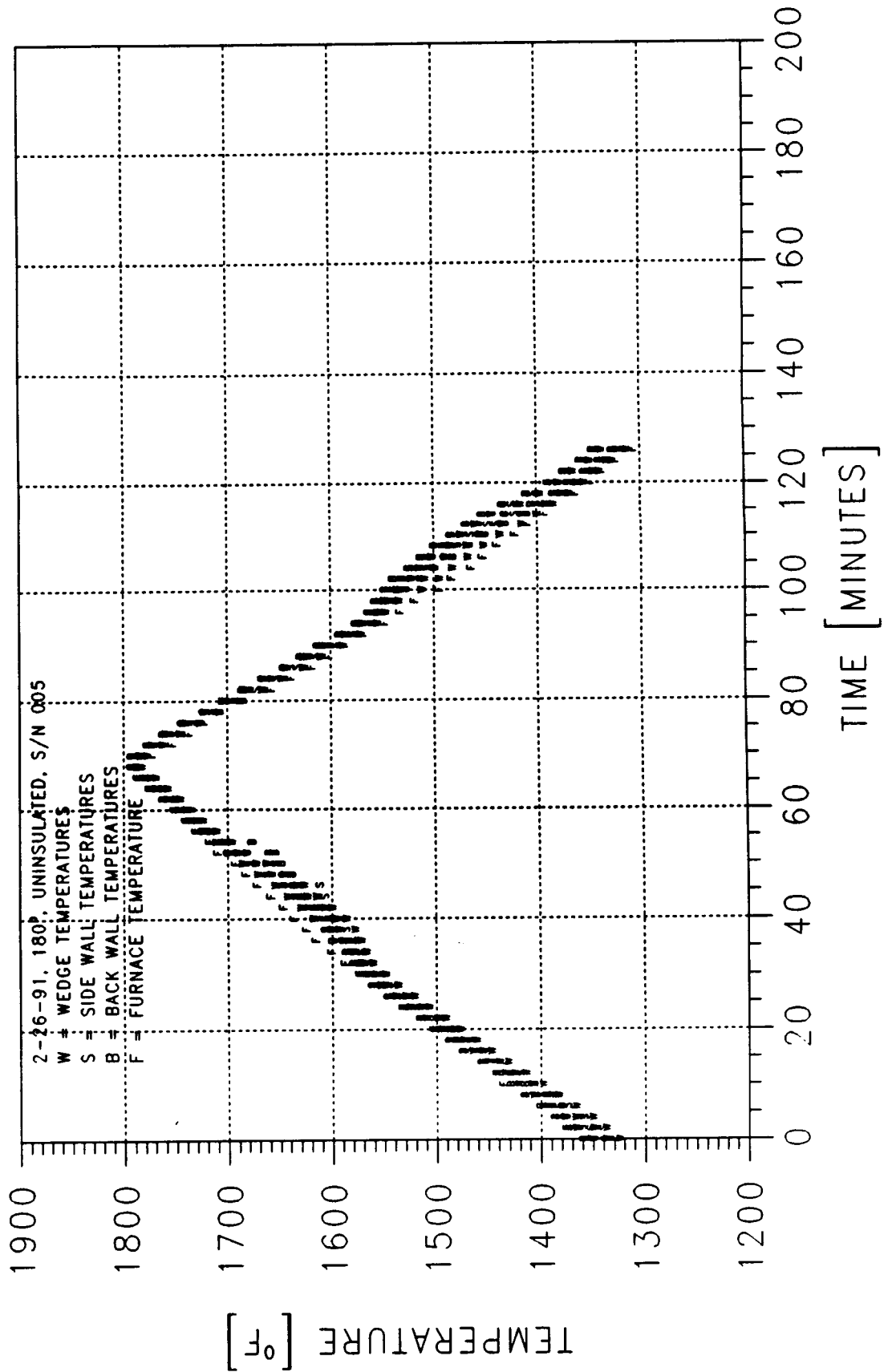
# TEMPERATURE PROFILES: TEST NO. 11-1







TEMPERATURE PROFILES: TEST NO. 10-2







**CANISTER DIMENSION CHANGE MEASUREMENTS**



Dimension Change  
 (From before heat treat to after 9-10 cycles)

3/6/91

Inch · 10<sup>-3</sup>

		Length Datum									
Surface I.D.	1	2	3	4	5	6	7	8	9	10	
A	0	4	7	9	10	10	9	7	4	2	
B	0	0	-2	-3	-8	-6	-4	-1	0	2	
S/N 5 C	0	-13	-19	-23	-20	-23	-20	-18	-11	0	
D	0	-8	-10	-16	-19	-21	-21	-1.6	-11	1	
E	0	2	-1	0	0	-4	-2	-2	0	3	

$$\sum_i |X_i| = 372 \quad \bar{X} = 7.44$$

A	0	-2	3	5	5	4	2	-1	-3	-7
B	0	-9	-8	-11	-10	-7	-10	-7	-3	+1
S/N 6 C	0	-12	-20	-21	-21	-21	-22	-21	-13	+0
D	0	-8	-16	-18	-20	-20	-18	-14	-7	+3
E	0	-4	-5	-9	-10	-11	-10	-11	-8	-6

$$\sum_i |X_i| = 447 \quad \bar{X}_i = 8.94$$

Dimension Change  
(From before heat treat to after filling)

4/11/91

Inch · 10<sup>-3</sup>

		Length Datum									
Surface I.D.	1	2	3	4	5	6	7	8	9	10	
S/N 5	A	0	-4	-10	-10	-7	-4	0	-2	-7	-8
	B	0	+1	+8	+11	8	3	6	6	10	7
	C	0	-6	-8	-5	6	-6	-9	-11	-6	-11
	D	0	-3	1	-2	-5	-14	-7	-2	-9	-11
	E	0	-4	3	5	6	-2	3	1	6	6

$$\sum_i |X_i| = 270 \quad \bar{X} = 5.40$$

S/N 6	A	0	-2	2	0	2	7	9	7	12	7
	B	0	-6	3	0	8	3	-2	-7	-5	-12
	C	0	-2	-7	-8	-8	-12	-12	-14	-18	-25
	D	0	-7	-10	-12	-13	-18	-18	-20	-24	-21
	E	0	-7	-9	-14	-18	-22	-17	-18	-13	-13

$$\sum_i |X_i| = 474 \quad \bar{X} = 9.48$$

**Dimension Change**  
**(Before heat treat to after 6 cycles, before 4-2)**

6/18/91

Inch · 10<sup>-3</sup>

		Length Datum									
Surface I.D.	1	2	3	4	5	6	7	8	9	10	
S/N 6	A	0	+3	8	2	10	7	6	5	2	-1
	B	0	-5	-1	-8	-4	-1	-6	-4	-1	1
	C	0	-9	-7	-14	-15	-5	-7	-7	-8	3
	D	0	-8	-12	-14	-16	-16	-15	-12	-7	2
	E	0	-2	-4	-5	-6	-6	-5	-5	-3	-1

After 7 cycles (after 9-1)

S/N 5	A	0	3	9	10	11	11	9	6	4	2
	B	0	0	-3	-2	-3	-4	-4	0	0	2
	C	0	-14	-14	-17	-11	-18	-15	-13	-6	2
	D	0	-3	-8	-12	-13	-13	-4	-10	-3	3
	E	0	-2	-3	-3	-6	-6	-4	-3	-1	3

**Before Heat Treat  
8/23/90**

Inch · 10<sup>-3</sup>

		Datum Point at 1/1000 inch									
Serial #	Surface I.D.	1	2	3	4	5	6	7	8	9	10
0004	A	0	5	2	3	-3	-4	-3	-3	-4	-9
	B	0	5	2	3	2	3	8	10	15	23
	C	0	6	8	11	11	12	15	12	17	17
	D	0	3	1	4	-1	5	5	4	8	1
	E	0	1	-5	-2	-6	0	-5	-5	-6	-7
0005	A	0	2	6	5	2	0	0	2	3	3
	B	0	-2	-8	-10	-8	-7	-8	-12	-10	-5
	C	0	6	6	5	-5	4	6	7	9	9
	D	0	0	-7	-7	-7	-4	-4	-7	-5	-4
	E	0	-3	-11	-9	-10	-4	-4	-4	-6	-4
0006	A	0	7	3	5	1	-2	0	1	0	-3
	B	0	8	0	4	1	1	10	11	15	22
	C	0	7	9	11	11	12	15	14	18	18
	D	0	4	2	4	1	5	5	5	7	0
	E	0	0	-4	-2	-3	0	-5	-5	-7	-9
0007	A	0	2	3	3	3	5	10	13	14	13
	B	0	-8	-11	-13	-20	-23	-20	-28	-25	-22
	C	0	-8	-13	-16	-18	-20	-22	-27	-25	-27
	D	0	-3	-5	-1	3	10	14	14	20	18
	E	0	-9	-4	-7	-10	-11	-17	-17	-18	-20

Use a dial depth micrometer (3/4 x 2 1/2" base). Locate mike centered on window and scribed graduations of fixture.

After Heat Treat

9/20/90

Inch · 10<sup>-3</sup>

		Datum Point at 1/1000 inch									
Serial #	Surface I.D.	1	2	3	4	5	6	7	8	9	10
0004	A	0	1	2	4	8	15	19	22	24	24
	B	Could not check clamp inway.									
	C	0	-3	-9	-9	-10	-7	-6	-6	-3	-4
	D	0	-12	-11	-19	-27	-28	-36	-33	-26	-20
	E	Could not check clamp inway.									
0006	A	0	7	3	4	0	-2	0	0	0	-4
	B										
	C	0	8	9	11	11	13	15	14	18	19
	D	0	3	1	3	1	4	4	4	6	1
	E										
0004 After Zoning Surface A	A	0	-2	-3	-3	-3	2	4	4	3	0
	C	0	-4	-7	-6	-7	-5	-4	-5	0	-1
	D	0	-9	-17	-20	-23	-34	-30	-28	-18	-10
0007	C	0	-9	-11	-10	-11	-12	-13	-17	-15	-17
	D	0	-5	-5	-3	1	5	8	7	10	10
	A	0	0	-0	-2	-2	0	2	6	6	3
0005	A	0	0	5	5	1	0	0	1	2	2
	C	0	2	5	4	-7	4	6	7	9	7
	D	0	1	-2	-2	-2	0	-1	-4	-4	-2

Location #1 is at fill tube end. Had difficulty loading #0007 properly in the checking fixture. By shifting the position of the non-fill end, numbers very close to those prior to heat treat can be achieved.

**Advanced Brayton Heat Receiver Canister**

**Surface Distortion Measurements After Filling**

1/2/91

Inch • 10<sup>-3</sup>

Serial #	Surface Letter	Datum Location Reference									
		1	2	3	4	5	6	7	8	9	10
0005	A	0	-2	-4	-5	-5	-4	0	0	-4	-5
	B	0	-1	0	+1	0	-4	-2	-6	0	+2
	C	0	0	-2	0	+1	-2	-3	-4	+3	-2
	D	0	-3	-6	-9	-12	-18	-11	-9	-14	-15
	E	0	-7	-8	-4	-4	-6	-7	-5	0	+2
0006	A	0	+5	+5	+5	+3	+5	+9	+8	+12	+4
	B	0	+2	+3	+4	+9	+4	+8	+4	+10	+10
	C	0	+5	+2	+3	+3	0	+3	0	0	-7
	D	0	-3	-8	-8	-12	-13	-13	-15	-17	-21
	E	0	-7	-13	-16	-21	-22	-22	-23	-20	-22

Advanced Brayton Heat Receiver Canister

Surface Distortion Measurements

S/N: 006

Test No. 3-1 and 3-2

Date: 1/23/91 and 1/29/91

Inch · 10<sup>-3</sup>

Serial #	Surface Letter	Axial Location No.									
		1	2	3	4	5	6	7	8	9	10
006 Test 3-1	A		0	+1	+1	0	+2	+10	10	15	4
	B	0	2	2	2	8	-2	6	2	8	10
	C	0	5	1	1	1	-1	2	-3	-2	-5
	D	0	-4	-12	-13	-15	-15	-16	-17	-15	-19
	E	0	-7	-15	-15	-23	-27	-24	-27	-22	-24
006 Test 3-2	A	0	+10	+7	+11	+8	+4	4	3	3	-3
	B	0	2	-1	-3	-3	1	4	7	14	23
	C	0	6	5	9	4	6	9	11	15	25
	D	0	-15	-8	-6	-7	-5	-6	-3	1	4
	E	0	-2	-7	-6	-8	-7	-9	-9	-9	-10

Advanced Brayton Heat Receiver Canister

Surface Distortion Measurements

S/N: 006

Test No. 4-2

Date: 2/11/91

Inch · 10<sup>-3</sup>

Serial #	Surface Letter	Axial Location No.									
		1	2	3	4	5	6	7	8	9	10
006 Test 4-2	A	0	10	11	7	11	5	6	6	2	-4
	B	0	3	-1	-4	-3	0	4	7	14	23
	C	0	-2	2	-3	-4	7	8	7	10	+21
	D	0	-4	-10	-10	-15	-11	-10	-7	0	+2
	E	0	-2	-8	-7	-9	-6	-10	-10	-10	-10
006 Test 6-1	A	0	6	6	9	6	1	2	1	-3	-10
	B	0	-2	-3	-7	-7	-3	0	+4	1	21
	C	0	-3	-3	-6	-6	-4	-3	-1	+1	+8
	D	0	-3	-10	-10	-12	-11	-9	-6	+1	+3
	E	0	-2	-8	-6	-7	-6	-8	-10	-10	-9



Advanced Brayton Heat Receiver Canister

Surface Distortion Measurements

S/N: 006 & 005

Test No. 5-2 & 7-1

Date: 2/19/91

Inch · 10<sup>-3</sup>

Serial #	Surface Letter	Axial Location No.									
		1	2	3	4	5	6	7	8	9	10
006 Test 5-2	A	0	5	6	10	6	2	2	0	-3	-10
	B	0	-1	-8	-7	-9	-6	0	4	12	23
	C	0	-5	-11	-10	-10	-9	-7	-7	5	18
	D	0	-4	-14	-14	-19	-15	-13	-9	0	+3
	E	0	-4	-9	-11	-13	-11	-15	-16	-15	-15
005 Test 7-1	A	0	3	8	9	6	4	3	4	5	5
	B	0	-3	-8	-9	-9	-9	-8	-11	-10	-5
	C	0	1	-1	-1	-6	-2	1	4	7	9
	D	0	2	4	1	-4	-3	-4	-3	-6	-8
	E	0	-3	-11	-8	-10	-6	-5	-8	-7	-6

Advanced Brayton Heat Receiver Canister

Surface Distortion Measurements

S/N: 005

Test No. 8-3

Date: 2/21/91 & 2/22/91

Inch · 10<sup>-3</sup>

Serial #	Surface Letter	Axial Location No.									
		1	2	3	4	5	6	7	8	9	10
005 Test 8-3	A	0	2	10	11	8	4	4	5	4	4
	B	0	-5	-11	-11	-11	-10	-10	-13	-9	-3
	C	0	-2	-2	-8	-15	-7	-5	0	5	8
	D	0	-3	-14	-12	-8	-6	-11	-9	-9	0
	E	0	-2	-10	-8	-10	-6	-4	-4	-5	-1
005 Test 9-1	A	0	5	15	15	13	11	9	8	7	5
	B	0	-2	-11	-12	-11	-11	-12	-12	-10	-3
	C	0	-8	-8	-12	-16	-14	-9	-6	3	11
	D	0	-3	-15	-19	-20	-17	-8	-17	-8	-1
	E	0	-5	-14	-12	-16	-10	-8	-7	-7	-1

Advanced Brayton Heat Receiver Canister

Surface Distortion Measurements

S/N: 005

Test No. 10-2 & 11-1

Date: 2/26/91

Inch · 10<sup>-3</sup>

Serial #	Surface Letter	Axial Location No.									
		1	2	3	4	5	6	7	8	9	10
005 Test 11-1	A	0	6	13	16	13	12	10	9	7	4
	B	0	-4	-11	-11	-12	-11	-12	-12	-9	-4
	C	0	-11	-10	-15	-20	-18	-13	-7	-2	+10
	D	0	-5	-12	-18	-17	-16	-14	-22	-12	-3
	E	0	-3	-10	-9	-10	-7	-5	-5	-5	-1
005 Test 10-2	A	0	6	13	14	12	10	9	9	7	5
	B	0	-2	-10	-13	-16	-13	-12	-13	-10	-3
	C	0	-7	-13	-18	-25	-19	-14	-11	-2	+9
	D	0	-8	-17	-23	-26	-25	-25	-23	-16	-3
	E	0	-1	-12	-9	-10	-8	-6	-6	-6	-1

1. Report No. NASA CR-189045		2. Government Accession No.		3. Recipient's Catalog No.	
4. Title and Subtitle Analysis, Design, and Experimental Results for Lightweight Space Heat Receiver Canisters				5. Report Date March 1992	
				6. Performing Organization Code	
7. Author(s) Michael G. Schneider Mark A. Brege Gary R. Heidenreich				8. Performing Organization Report No. AER 3562	
				10. Work Unit No.	
9. Performing Organization Name and Address Sundstrand Corporation 4747 Harrison Avenue Rockford, IL 61125-7002				11. Contract or Grant No. NAS3-25554	
				13. Type of Report and Period Covered Interim Report, 7/89-7/91	
12. Sponsoring Agency Name and Address National Aeronautics and Space Administration Lewis Research Center Cleveland, OH 44135-3191				14. Sponsoring Agency Code	
15. Supplementary Notes Project Manager, Miles Dustin, Power Technology Division, NASA Lewis Research Center					
16. Abstract  Critical technology experiments have been performed on thermal energy storage modules in support of the Brayton Advanced Heat Receiver program. The modules are wedge-shaped canisters designed to minimize the mechanical stresses in the canisters that occur during the phase change of the lithium fluoride phase change material. Nickel foam inserts in some of the canisters were used to provide thermal conductivity enhancement and to distribute the void volume throughout the canister. The canisters were filled with lithium fluoride and closure welded at NASA Lewis Research Center. Two canisters, one with a nickel foam insert, the other without an insert, were thermally cycled in various orientations in a fluidized bed furnace at Sundstrand. The only measurable impact of the nickel foam was seen when the back and short sides of the canister were insulated to simulate operation in the advanced receiver design. In tests with insulation, the furnace to back side $\Delta T$ was larger in the canister with the nickel foam insert, probably due to the radiant absorptivity of the nickel. However, the differences in the temperature profiles of the two canisters were small, and in many cases the profiles matched each other fairly well. Computed Tomography (CT) was successfully used to non-destructively demarcate void locations in the canisters. Finally, canister dimensional stability, which was measured throughout the thermal cycling test program with an inspection fixture was satisfactory with a maximum change of 0.635 mm (.025 inch).					
17. Key Words (Suggested by Author(s)) Heat receiver Phase change material Thermal energy storage Lithium fluoride Brayton advanced heat receiver			18. Distribution Statement Unclassified - Unlimited		
19. Security Classif. (of this report) Unclassified		20. Security Classif. (of this page) Unclassified		21. No of pages 218	22. Price* A10